INVESTIGATION INTO THE ELECTROCATALYTIC HYDROGENATION OF PYROLYSIS BIOOIL:ECONOMIC, LIFE CYCLE AND KINETIC ANALYSIS

By

Sabyasachi Das

A DISSERTATION

Submitted to
Michigan State University
in partial fulfillment of the requirements
for the degree of

Chemical Engineering – Doctor of Philosophy

2020

ABSTRACT

INVESTIGATION INTO THE ELECTROCATALYTIC HYDROGENATION OF PYROLYSIS BIO-OIL: ECONOMIC, LIFE CYCLE AND KINETIC ANALYSIS

By

Sabyasachi Das

Rising concerns about the environmental impacts of fossil transportation fuels have motivated the development of alternative sources of energy that are renewable and environment-friendly. Biomass-derived liquid hydrocarbon fuels, offer an immediate "drop-in" alternative for displacing petroleum-derived transportation fuels, owing to their ability to use existing infrastructure. However, biomass, as an energy source is disadvantaged in terms of carbon and energy content. The Billion Ton Report 2016 predicts 1.3 billion tonnes of harvestable biomass in the U.S. by 2030. The carbon and energy content of this amount of biomass is not sufficient to support the demands of the U.S. transportation sector alone. Furthermore, traditional bioenergy systems like cellulosic fermentations to ethanol (CE), lose 1/3rd of the biomass carbon as CO₂ and fail to utilize lignin (~40% of biomass energy) for fuel production. This calls for biomass conversion technologies that retain most of the biomass carbon and efficiently capture the inherent biomass energy in the produced liquid fuels. This can be achieved via fast pyrolysis that can convert all biomass (including lignin) to predominantly liquid bio-oil. However, this bio-oil is unstable, due to the presence of reactive functional groups. This fact combined with its low energy content makes it unfit as a fuel or a stable intermediate. In this regard, electrocatalytic hydrogenation (ECH) can harness renewable electricity from solar/wind farms and sufficiently hydrogenate the pyrolysis bio-oil to generate a stable intermediate that can be transported over long distances. Additionally, ECH employs mild conditions that allows it to be implemented at a local small-scale facility. This offers a key advantage in a bioenergy system, where transporting the low bulk density biomass can incur large transportation costs. The denser ECH-ed bio-oil can hence be transported at lower costs to conventional hydroprocessing facilities to produce a gasoline/diesel range fuel. In this study, a bioenergy system (Py-ECH) was developed that combines fast pyrolysis with ECH at decentralized depots, followed by hydroprocessing at a central refinery. The mass, carbon and energy flux through the system and the fuel yields were estimated. The fuel yields for the Py-ECH system were found to be better than CE in terms of energy, mass and carbon.

To evaluate the economics of Py-ECH, a full techno-economic analysis was conducted using a discounted cash flow rate of return (DCFROR) approach and nth plant assumptions. The minimum fuel selling price (MFSP) of the Py-ECH fuel was found to be \$ 3.62/gge (in 2018 \$) compared to \$ 3.70/gge (in 2018\$) for CE. Through sensitivity analyses, key cost-contributing parameters were identified, and a pathway was charted for MFSP reduction to < \$3/gge (in 2018 \$).

The environmental impacts of Py-ECH were investigated by performing a cradle-to-grave life cycle assessment for environmental impact categories of global warming potential (GWP), eutrophication potential (EUP) and water scarcity footprint (WSF). While the EUP and WSF for the Py-ECH system were lower than that for CE, it was observed that the GWP was dependent on the source of electricity in the Py-ECH system. Major improvements were identified that can result in a carbon negative Py-ECH system.

Finally, a kinetic model was developed to examine the kinetics of the electrochemical, surface and adsorption/desorption reactions for the ECH of phenol (a model bio-oil compound) to cyclohexanol. The experiments were performed in a rotating disk electrode setup with Ru/ACC catalyst as the working electrode and an Ag/AgCl reference electrode to define the effects of mass transport.

This thesis is dedicated to my FAMILY Thank you for your unconditional support

ACKNOWLEDGEMENTS

These last five years of my life at Michigan State University have been a great learning curve to say the least. While the destination seemed steep in the beginning, the journey towards it has been truly enjoyable. This would not have been possible without the contribution of some exceptional people I encountered along the way.

First and foremost, I would like to express my heartfelt thanks and gratitude to my advisor, Dr. Saffron, who has been a constant source of support, guidance and inspiration. I have simply learnt so much from him. I would like to extend my gratitude to Dr. Barton, who has been mentored me in different roles, starting from the ChEMS Graduate Student Association to serving on my Graduate Committee. I am also grateful to him for allowing me to work in his lab. I would also like to thank Dr. Jackson and Dr. Miller for their constructive feedback and encouragement regarding my work.

A special mention to my collaborators at Ford – Dr. James Anderson, Dr. Mike Tamor, Dr. Timothy Wallington and Mr. Robert De Kleine for their guidance and mentoring during our collaboration work.

I would also like to thank all my teachers starting from my high school to Jadavpur University to MSU. They have been my source of inspiration to keep pursuing my quest for knowledge.

A huge thanks to all past and present group members (Mahlet, Peyman, Dr. Redko, Zhongyu, Rachel and Meheryar) for supporting me whenever required and help create a friendly environment for all of us to thrive. I would also like to extend my deep appreciation for Tiffany Owen, Jennifer Keddle, Donna Fernandez, Heather Dainton and Brad Tobin in the Chemical Engineering Department for helping me in navigating through departmental requirements and having me stay

updated on different opportunities. A special thanks to the amazing graduate student community in the Chemical Engineering Department. I have been lucky to have made so many awesome friends here- Alex, Hong-Kang, Christine, David, Natalia, Iman and Neda. I would certainly cherish all those shared memories at the different potluck and game nights.

A special mention to my family away from home here: Kanchan, Saptarshi, Preetam, Aritra, Sayli, Yashesh, Tarang, Vikram, Swati, Abhinav, Kamla, Kokil, Mayank and Yogesh. These guys have been a source of constant and unwavering support and have been like a cure to my homesickness. This journey would be a lot lonelier without their presence.

Lastly, but definitely not the least, I would like to thank my parents (Baba and Ambu), grandparents (Dadu and Amma) and my sister (Bullu) for their unconditional support through the ups and downs of this journey. They have been my source of motivation throughout this journey. Finally, I would like to express my thanks to friends and family in the U.S. and India- Anuj, Dipto, Didibhai, Jammy, Bhuton Mama, Mishta, Pratik, Souradeep, Anshumaan, Piyush, Satyaki, Pritha and so many others, who have also been an integral part of this journey.

As I approach the end of this Spartan journey, I'll probably miss MSU the most. It has become a part of my identity. No matter where I go, I will always carry a bit of "Green and White" with me and all those cherished memories that have become entangled with it over time.

TABLE OF CONTENTS

LIST OF TABLES	ix
LIST OF FIGURES	xii
Chapter 1 : INTRODUCTION	1
Chapter 2 : LITERATURE REVIEW	8
Fast pyrolysis	8
Bio-oil upgrading	9
Decentralized processing of biomass at depots	18
Technoeconomic analysis (TEA) of biomass to fuels	20
Life cycle assessment (LCA) of biomass to fuels	25
Kinetic modeling of ECH	29
Chapter 3: PY-ECH SYSTEMS ANALYSIS: DEVELOPMENT OF MASS, ENER	
CARBON FLUX	
Abstract	
Introduction	
Methods	
Results	
Discussion and Outlook	
Conclusions	
APPENDIX	49
Chapter 4: TECHNOECONOMIC ANALYSIS OF THE PY-ECH SYSTEM	
Abstract	
Introduction	
Materials and Methods	
Results	
Discussion	
APPENDIX	106
Chapter 5 : LIFE CYCLE ASSESSMENT OF THE PY-ECH SYSTEM	115
Abstract	115
Introduction	115
Methodology	118
Results and Discussion	
Conclusion	141
APPENDIX	145
Chapter 6: KINETIC MODELING FOR ECH OF PHENOL	150
Abstract	150

Introduction	
Model Formulation	152
Experimental Setup	158
Results	160
Discussion	163
APPENDIX	165
Chapter 7 : CONCLUSIONS AND FUTURE WORK	171
Conclusions	171
Future Work	173
BIBLIOGRAPHY	175

LIST OF TABLES

Table 2.1 : Causes and undesirable effects of different properties of pyrolysis bio-oil (adapted from Bridgwater et al.,) ¹⁹
Table 2.2 : Technoeconomic analyses of bioenergy systems involving thermochemical conversion of biomass, followed by upgrading. The year mentioned in parenthesis in each entry of the "Cost" column denotes the \$ year; gge stands for gallon of gasoline equivalent
Table 2.3 : LCA studies of biomass pyrolysis 27
Table 3.1 : Label Definitions for the Process Flow Diagram. 50
Table 3.2 : Feedstock Data for Py-ECH. 52
Table 3.3 : Operating conditions for grinding
Table 3.4 : Operating conditions for drying
Table 3.5 : Representative Compounds in PyV 59
Table 3.6 : Fast Pyrolysis Data. 59
Table 3.7 : Condensation Data 61
Table 3.8 : Key Data for ECH63
Table 3.9 : Hydroprocessing Data 66
Table 3.10 : Electrolysis Operating Conditions 67
Table 3.11 : Stream Table for Py-ECH Process
Table 3.12 : Balance on combustor for heat integration in BUD for Py-ECH process
Table 3.13 : Extracted Stream Table for CE Process (adapted from Humbird et al.) ¹¹
Table 3.14 : Energy Balance in CE process 72
Table 3.15 : Mass Balance for CE Process 74
Table 3.16 : Carbon Balance for CE Process 77
Table 3.17: Water Balance for CF Process 78

Table 4.1 : Summary of the economic assumptions in the technoeconomic model	85
Table 4.2 : Depot Capital and Operating Costs.	94
Table 4.3 : Refinery Capital and Operating Costs	96
Table 4.4 : Assumptions for Calculating the Total Capital Investment and Total Operating Cos	
Table 4.5 : Range of values of biochar found in literature (adapted from Campbell et al.,) ²¹⁵ . 1	
Table 4.6 : Summary of factors determining assumed costs for corn stover transport to depots a assumed by Kim et al. ⁷⁴	as 12
Table 4.7 : Summary of supply chain costs for corn stover for CE and Py-ECH systems as used in model. All values in 2018\$/tonne of delivered biomass	
Table 4.8 : Key ECH and Pyrolysis parameters 1	14
Table 4.9 : Installation multipliers for different processing units 1	14
Table 5.1 : Description of energy ratios ²⁷⁹	39
Table 5.2 : Energy ratios for the CE and Py-ECH systems. ER _t stands for Total Energy Ratio; RF stands for Renewability Factor; E _y stands for Energy Yield; EROI stands for Energy Return on Investment; ER _f stands for Fossil Energy Ratio. FE stands for Fossil electricity while RE represents renewable electricity	
Table 5.3 : Parameters in the modified Weidema method and the description of the scores (adapted from Couillard et al.). 248	46
Table 5.4: Life cycle input data for both Py-ECH and CE systems with their source and data quality indicator score. 1	46
Table 5.5: Contribution of each operation in the determination of Global Warming Potential (GWP) for both CE and Py-ECH systems 1	47
Table 5.6 : Contribution of each operation in the determination of Eutrophication Potential (EUP) for both CE and Py-ECH systems. 1	.48
Table 5.7: Contribution of each operation in the determination of Water Scarcity Footprint (WSF) for both CE and Py-ECH systems. 1	.48
Table 5.8 : Life cycle impact summary for the CE process. Allocation scenarios 1 and 2 are reported to observe the effects of avoiding allocation and applying minimal allocation to cultivation	49

Table 5.9 : Life cycle impact summary for the Py-ECH process. Allocation scenarios 1 and are reported to observe the effects of avoiding allocation and applying minimal allocation to	
cultivation.	149
Table 6.1 : Reaction rate expressions	154
Table 6.2 : Expressions for reaction rate constants	156
Table 6.3 : Legend for different variables	158
Table 6.4 : Parameter values used in generating model current vs potential curve	169

LIST OF FIGURES

Figure 1.1 : A schematic of the Py-ECH system. ⁵ Biomass is brought from the fields to a localized depot, where it undergoes C-efficient upgrading (fast pyrolysis, followed by ECH) to generate a stable bio-oil that can be transported to a centralized refinery for further petroleum-like hydroprocessing to produce a sustainable hydrocarbon fuel for transportation. The CO ₂ emissions from combusting this fuel is captured by the plant biomass(the system feedstock) via photosynthesis.
Figure 2.1 : Schematic for ECH of bio-oil in a batch divided cell. BO represents the pyrolysis bio-oil, whereas SBO represents the ECH-ed stable bio-oil. n denotes the number of moles of electrons passed. ⁵
Figure 3.1 : Comparison of the annual energy balance in the U.S. transportation sector and projected harvestable biomass. Projections are made based on the available biomass by 2030 (U.S. Billion Ton Study 2016). The specific energy for petroleum is 48 MJ kg ⁻¹ and for dry biomass is 20.6 MJ kg ⁻¹ . Energy is presented in exajoules (EJ), equivalent to 1018 J. Mass is in units of a "billion tonnes", equivalent to 10^{12} kg
Figure 3.2 : Sankey diagrams for energy flow. (a) Pyrolysis–electrocatalytic hydrogenation (Py–ECH) energy analysis. Yield: 89%; (b) CE energy analysis. Yield: 44%
Figure 3.3 : Sankey diagrams for mass flow. (a) Pyrolysis–electrocatalytic hydrogenation (Py–ECH) mass analysis. Yield: 38%; (b) CE mass analysis. Yield: 26%
Figure 3.4 : Sankey diagrams for carbon flow. a) Pyrolysis–electrocatalytic hydrogenation (Py–ECH) carbon analysis. Yield: 63%; (b) cellulosic ethanol (CE) carbon analysis. Yield: 30% 44
Figure 3.5 : Energy, mass and carbon yield comparison of CE and Py–ECH. The energy yield is significantly higher because of addition of electrical energy
Figure 3.6 : Process Flow Diagram for Py-ECH Process
Figure 3.7 : Process Flow Diagram for Pyrolysis of Biomass
Figure 3.8: General Distribution of Functional Groups in Bio-oil ¹⁸
Figure 3.9: Process flow diagram for pyrolysis
Figure 3.10 : Condenser Flow Diagram
Figure 3.11 : Schematic of ECH Apparatus
Figure 3.12 : ECH Reactions Considered in this Analysis

Figure 3.13 : Process Flow Diagram for ECH 65
Figure 3.14: Hydroprocessor Process Flow Diagram 66
Figure 4.1 : Process flow diagram of the Py-ECH process
Figure 4.2 : Illustration of depot distribution geometry. (a) Illustration of depot distribution relative to central refinery, for a central refinery with 18 depots. (b) Variation of farm-to-depot and depot-to-refinery distance with depot size, for a 2000 tpd central refinery
Figure 4.3 : Variation of MFSP from Py-ECH with depot size. C _R denotes capacity of central refinery
Figure 4.4 : Breakdown of raw material supply chain costs from farm to the depot gate for (a) Py-ECH system and (b) CE system
Figure 4.5 : Distribution of costs at depot (a) Installed capital costs contribution analyses at a depot (b) Variable operating cost contribution analyses at a depot
Figure 4.6 : Distribution of costs at refinery (a) Installed capital cost contribution at the refinery (b) Variable operating cost contribution at the refinery
Figure 4.7: Tornado plot showing single parameter sensitivity analyses on MFSP 100
Figure 4.8: Effect of depot size on MFSP for different refinery sizes. C _d denotes depot capacity 101
Figure 4.9 : Waterfall chart showing potential reduction in MFSP assuming combinations of improvements in selected model parameters. The light green bars indicate the reductions in MFSP owing to the stacking up of system improvements. The dark green bars denote the initial and final MFSP (after all improvements). The yellow bars denote alternate scenarios, not considered in the baseline model
Figure 4.10 : Electricity costs from different sources. Red dashed line indicates the MFSP using MRO-West U.S. grid electricity, assumed as a baseline in the model. ¹⁹⁷
Figure 4.11 : Sensitivity analyses on MFSP for all parameters. Larger the slope, greater the sensitivity to that parameter
Figure 5.1 : System boundaries for Py-ECH system
Figure 5.2 : System boundaries for CE system
Figure 5.3 : System carbon flow for (a) Py-ECH and (b) CE, for GREET assumed value of carbon sequestration

Figure 5.4 : Global Warming Potential (GWP) Contribution Analysis; Subscript 1 refers to Scenario 1 whereas Subscript 2 refers to Scenario 2. 'F' refers to a fossil fuel electrical grid and 'R' refers to renewable power
Figure 5.5 : Eutrophication Potential (EUP) contribution analysis (a) Total EUP contribution analysis; subscript 1 refers to Scenario 1 whereas subscript 2 refers to Scenario 2. (b) EUP contribution analysis excluding cultivation and harvesting; F stands for fossil electricity and R stands for Renewable electricity
Figure 5.6 : Water Scarcity Footprint (WSF) contribution analysis; subscript 1 refers to Scenario 1 whereas subscript 2 refers to Scenario 2
Figure 5.7 : Sensitivity of system GWP with % renewable in MROW Electricity Grid. (For Scenario 2)
Figure 5.8 : Sensitivity of system Global Warming Potential (GWP) with annual C sequestration rate for Scenario 2
Figure 5.9 : Sensitivity of system EROI with (a) % renewable heat at refinery and (b) % renewable electricity
Figure 5.10 : Waterfall chart showing the resultant global warming potential of stacking improvements in the Py-ECH system
Figure 6.1 : Setup for RDE experiments
Figure 6.2: Experimental setup for catalyst preparation
Figure 6.3 : (a) Current vs potential data as obtained from RDE experiments (b) Electrode overpotential vs log(current density)
Figure 6.4 : GC-MS chromatogram of electrolyte solution post ECH of phenol in an RDE 162
Figure 6.5 : Current vs potential curve as predicted by model for different values of R _r 169
Figure 6.6 : Effect of increasing mass transfer coefficient and kinetic rate constant for hydrogen adsorption on model predicted curve. Blue line denotes experimental data

Chapter 1: INTRODUCTION

According to the World Energy Council's 2013 survey report, fossil fuels still account for more than 80% of the world's energy consumption. This trend is expected to continue till 2020, when the consumption would be reduced by a mere 4%. The survey estimates reserve of 890 billion tonnes of coal, 225 billion tonnes of crude oil and 210 trillion cubic meters of natural gas (2011data). In fact, based on the data provided, natural gas is set to last only 55 years, whereas the other two sources have more than 100 years left. Irrespective of the time span, fossil fuel reserves are bound to get depleted, owing to their inherent characteristic of being non-renewable. Moreover, fossil fuel energy is a major cause for pollution. The IPCC, in 2014, reported that carbon dioxide accounts for 76% of the total global greenhouse gas emissions. About 85% of those CO₂ emissions originate from fossil fuel and industrial processes.² This is in addition to other greenhouse gases like methane, and nitrous oxide. Therefore, fossil fuel sources are both non-renewable and severely polluting. The Energy Independence and Security Act (EISA), passed by the U.S. government, in 2007, recognizes this and includes, within its aims, the development and production of clean renewable fuels.³ Among other renewable sources, it provides impetus to reduce baseline greenhouse gas emissions (established in 2005) by 50% by developing and producing advanced biofuels. These biofuels include ethanol, derived from corn starch or stover, ethanol derived from waste material, butanol from renewable biomass, biogas or any other fuel derived from biomassbased resources.

Biomass, as a renewable energy source is unique in its potential to be converted into liquid, solid or gaseous fuels and is the only renewable source of carbon.⁴ This is because plants (biomass) essentially capture CO₂ from the atmosphere at very low costs via photosynthesis. They also store solar energy in chemical form via this process. However, the photosynthetic efficiencies are very

low in the range of 1-2% of incident solar energy being actually stored.⁵⁻⁷ Moreover, biomass has only about one-third of the specific energy content of crude oil. Therefore, biomass-derived fuels, without any energy upgrading, cannot hope to compare to petroleum derived fuels. Additionally, the Billion Ton Report, published in 2016, estimates that the total amount of harvestable biomass (under \$60/dry ton) in the U.S. available by the year 2030, to be about 1.3 billion dry tons. Such a quantity is not sufficient for complete petroleum replacement. In fact, it is not even enough to support the energy and carbon demands of only the U.S. transportation sector.⁵

Traditional and prevalent bioenergy systems such as cellulosic fermentations to ethanol⁸⁻¹² are carbon inefficient. This is owing to the fact that about 1/3rd of the carbon present in the starting biomass is lost as carbon dioxide in such processes. The final energy content of the fuel (ethanol) also does not match up to that of gasoline-like fuels, because the lignin component of biomass, which accounts for 40% of the biomass energy, is not processed. This lignin is instead combusted to provide heat and power at the refinery. Only the holocellulose (cellulose and hemicellulose) is processed to produce the fuel. On the other hand, thermochemical treatment of biomass processes all three components of biomass. These employ high temperatures and pressures for the production of a complex mixture of organic compounds. Products from thermochemical conversions can be obtained in all three physical states. The relative proportion of each state depends on the process conditions employed. Gasification of biomass, as the name suggests, is the process of heating biomass to high temperatures, around 700°C in the presence of controlled amount of oxygen, followed by the water gas shift reaction to generate syngas. 13, 14 Direct combustion of biomass can only be used to produce heat. ^{15, 16} Torrefaction, which includes heating the biomass to temperatures between 200°C and 300°C in an inert environment, produces a solid product that is 70 wt.% of the starting biomass and 90% of the initial biomass energy. 17 However, liquid products are beneficial

in terms of their higher density and ease in transportation.8 In this regard, fast pyrolysis is the thermochemical treatment of biomass, that produces the largest amount of liquid products, about 75%. The gas and liquid yields are approximately 13% and 12% respectively. The process employs a temperature of 500°C and a vapor residence time of 1 second. 18, 19 Heat is provided in the absence of oxygen, at a heating rate of about 10-200K/s.¹⁹ The liquid product obtained from fast pyrolysis, known as bio-oil, is a mixture of many organic compounds and includes functional groups like carboxylic acids, ketones, aldehydes and phenols.²⁰ These compounds are responsible for the undesirable properties of bio-oil like high oxygen content (~35%), low heating value (~19 MJ/kg) and high acidity (~pH of 2-3). Furthermore, the bio-oil has variable viscosity ranges, between 35-1000 cP, at 40°C, due to the high reactivity of these compounds. ²¹ All these factors render the biooil unstable and unfit for storage and transportation. Furthermore, energy content of this bio-oil is not comparable to that of gasoline or diesel and therefore, there is a need for energy upgrading. There are numerous physical and chemical methods for bio-oil stabilization and/or upgrading. Physical methods mainly include emulsification, hot vapor filtration and microfiltration, whereas hydrotreating, esterification and catalytic cracking are the predominant chemical methods. 19, 21 Of these, hydrotreating, which involves hydrogenation and hydrodeoxygenation, is the most popular and commercially available method for bio-oil stabilization and upgrading. The use of such hydroprocessing techniques for stabilizing and upgrading bio-oil also presents the opportunity to take advantage of existing petroleum infrastructure.¹⁹

However, it must be noted here that biomass is a distributed source feedstock as compared to a point source like petroleum. Biomass is a solid of low energy density and hauling it over large distances can incur huge transportation costs. In this regard, a decentralized bioenergy system that employs local densification/processing depots near the source and produces an intermediate fuel

that is denser (than biomass) and fit for transport to larger processing facilities, can be a potential solution.²² While pyrolysis achieves the required densification by converting the solid biomass to a liquid bio-oil, it requires a method of subsequent bio-oil stabilization. Furthermore, such a method should be effective at a small-scale depot, near the biomass source. This is where hydrotreating fails as an option. The costs of producing H₂ gas is very high at the small scale of the depot and also poses safety concerns related to handling of flammable gas. The method also requires extreme conditions in terms of temperature and pressures. A promising solution, in this regard, can be electrocatalytic hydrogenation (ECH). 23-33 ECH employs mild temperatures and pressures to hydrogenate the unsaturation present in the reactive bio-oil compounds and helps stabilize bio-oil. Therefore, the need for H₂ gas storage and use is avoided. ECH employs electrolysis of water to generate in-situ hydrogen ions that can reduce (via the addition of hydrogen) the pyrolysis bio-oil on a catalytic cathode. Through this process, it also helps store electrical energy as chemical energy in the reduced bonds of the ECH-ed bio-oil, thereby, slightly upgrading it in energy content. This electrical energy may be derived from renewable energy sources like wind farms and solar photovoltaics. ECH can, in fact, be an answer to the intermittency problems of such renewable electricity technologies. It can provide a timeinsensitive method of storing this wind/solar renewable electricity, that is inherently dependent on time cycles of wind/light availability.⁵ The stable bio-oil after ECH, is therefore, fit for transportation to a central processing facility, where it can undergo further upgrading and refining to a gasoline/diesel like fuel. It must be noted here that the ECH also reduces H₂ gas consumption at the central refinery since the stable bio-oil after ECH is already upgraded to some degree. ^{32, 34} Therefore, fast pyrolysis, followed by subsequent ECH stabilization can be a potent biomass processing technology at local decentralized depots, that ship the ECH-ed stable bio-oil to a central

petroleum-style hydroprocessing facility to produce a final gasoline/diesel like fuel. In this study, such a system, nicknamed the Py-ECH system, has been proposed with an aim to improve upon popular traditional systems like cellulosic fermentations to ethanol and also, simultaneously chart a pathway for the ultimate replacement of fossil fuel systems. A schematic of the proposed Py-ECH system can be seen in Figure 1.1.



Figure 1.1 : A schematic of the Py-ECH system.⁵ Biomass is brought from the fields to a localized depot, where it undergoes C-efficient upgrading (fast pyrolysis, followed by ECH) to generate a stable bio-oil that can be transported to a centralized refinery for further petroleum-like hydroprocessing to produce a sustainable hydrocarbon fuel for transportation. The CO₂ emissions from combusting this fuel is captured by the plant biomass(the system feedstock) via photosynthesis.

In summary, the goal of this study is to investigate the merits of the Py-ECH system as a viable alternative to prevalent bioenergy systems like cellulosic fermentations to ethanol, and ultimately, as a possible replacement for fossil fuel systems.

The entire study may be divided into four major component studies. Each component study achieves a sub-objective, in an attempt to realize the primary goal of the study, as stated earlier. These component studies include:

- 1. Systems analysis: The objective of this component study was to determine the different process flows and yields of the Py-ECH system and compare them to traditional cellulosic fermentations to ethanol. A model was developed that calculated the process flows if corn stover biomass is processed by the Py-ECH system to produce a gasoline-like fuel. The subsequent fuel yields in terms of mass, energy and carbon of the starting biomass, were also determined. A comparison was made with the cellulosic fermentation to ethanol (CE) system.
- 2. Investigation of Py-ECH economics: The objective of this component study was to investigate the economics of the Py-ECH system and identify key cost contributors. A discounted cash flow rate of return (DCFROR) analysis was performed to determine a minimum fuel selling price (MFSP) of the final fuel assuming nth plant economics.
- 3. Investigation of environmental impacts: The objective of this component study was to investigate the environmental impacts of the Py-ECH system in comparison to cellulosic fermentations to ethanol (CE). A full-scale cradle-to-grave life cycle assessment was conducted to determine the global warming potential, eutrophication potential and water scarcity footprint of the Py-ECH system and compared to that for the CE system.
- **4.** Investigation of ECH kinetics: The objective of this study was to determine the kinetic rate constants associated with the ECH of phenol. A mathematical model was developed for the ECH of phenol (a model bio-oil compound) to cyclohexanol, in a rotating disc electrode

(RDE) with a Ru/ACC working electrode. Preliminary experimental data (current vs voltage) was collected in this regard.

Chapter 2: LITERATURE REVIEW

Fast pyrolysis

The Py-ECH system combines fast pyrolysis and electrocatalytic hydrogenation of biomass at localized depots, followed by petroleum style hydroprocessing at a central refinery. Biomass fast pyrolysis has been studied before. Reed studied pyrolysis as a method of biomass conversion to fuels as early as 1980.35 While exploring different methods of biomass thermochemical conversion, he concluded that pyrolysis is a good pathway for synthesis to liquid fuels such as gasoline. Fast pyrolysis is described as a process that employs high temperatures to provide rapid heat in absence of oxygen. Specifically, the key features of fast pyrolysis have been described as having very high reaction temperatures around 500°C and employing very low residence times of less than 2 s.36 The main products of pyrolysis are a liquid mixture of organics and water, along with some gaseous products and solid char. The yield of each product is a function of the reaction temperature employed. The organic liquid product, which is basically a mixture of carboxylic acids, ketones, aldehydes and phenols²⁰ is maximized at a temperature of around 500°C.³⁶ The solid char, known as biochar is a high energy density solid, compared to the starting biomass and has an energy content of around 18 MJ/kg.³⁷ The biochar product may be combusted to produce heat and power or may be land applied for carbon sequestration. 38-42 The liquid product, known as bio-oil has similar heating value (~16-19 MJ/kg), which is less compared to crude oil (~44 MJ/kg), owing to the high oxygen content (~35%) in bio-oil compared to crude oil (<1%).⁴³ Bio-oil, as a fuel, has other undesirable properties too and these have been presented in Table 2.1, along with the possible reasons. These properties render bio-oil unsuitable for storage, transport or use as a fuel. Therefore, there is a need for upgrading, with the aim of alleviating these properties.

Table 2.1: Causes and undesirable effects of different properties of pyrolysis bio-oil (adapted from Bridgwater et al.,)¹⁹

Property of bio-oil	Cause	Undesirable effect
Acidity	Organic acids from	Corrosion of vessels and
	biopolymer degradation	pipework
Aging	Secondary polymerization	Slow increase in viscosity;
	reactions	potential phase separation
Presence of alkali metals	High ash feed	Catalyst poisoning;
		deposition of solids in
		combustion; erosion and
		corrosion
Presence of char	Incomplete char separation	Sedimentation; filter
		blockage; catalyst blockage
High O_2 content	Biomass composition	Poor stability; non-miscibility
		with hydrocarbons
Water content	Pyrolysis reactions	Lower heating value

This upgrading may be achieved through several chemical and physical methods that stabilize the bio-oil via reduction in the reactivity of bio-oil.

Bio-oil upgrading

Hydrodeoxygenation (HDO)

HDO employs hydrogen gas at high pressures (~20MPa) and temperatures around 400°C, in the presence of a catalyst, to effect removal of oxygen as water.⁴⁴ Venderbosch et al., reports the formation of two liquid phases, when HDO of bio-oil is carried out under these conditions, in the presence of Ru/C catalyst. The organic phase is lean in oxygen content as most of the oxygen is transferred to the aqueous phase. The percentage of oxygen reduced from 52.1% in the feed bio-oil to 14.2% (on a weight basis) for a 2-stage HDO process.⁴⁵ Water percentage also decreased from 29% to 3.5%. Elliott et al., found similar results, when bio-oil derived from pyrolysis of corn stover was subjected to a pressure of 200 bar and temperatures around 340°C, in the presence of Pd/C catalyst. Oxygen content decreased from 55.43% (on a wet basis) to 11.9%. It was further observed that the oxygen content passed through a minimum when temperature of the HDO was increased. The yield of the oil layer, however, decreased with increase in temperature.⁴⁶ Oil yield

and deoxygenation, were therefore found to be inversely related with respect to temperature, implying that higher degree of deoxygenation must be accompanied by lower oil yields. The conventional catalysts employed are sulfided transition metal salts, supported on γ -Al₂O₃.⁴⁷ These catalysts can sometimes lead to the formation of sulfur containing compounds and contaminate the bio-oil being hydrotreated.⁴⁸ Gutierrez et al., investigated the effect of catalyst by using ZrO₂ supported noble metal catalysts⁴⁹ for the hydrotreating of guaiacol, a model biooil compound.⁵⁰ The performance was found to be superior to conventional sulfided catalysts due to less carbon deposition and no sulfur addition.⁴⁹ However, carbon formation and subsequent deactivation of the catalyst is recognized as a major drawback of the HDO process. The carbon forming tendency is found to increase with increasing amount of unsaturation and aromatics in the feed. Increase in temperature and acidity of the catalyst support also enhances carbon deposition.⁴³ Wildschut et al., investigated the effect of varying catalyst and catalyst supports on the yield, extent of deoxygenation and H2 consumption in HDO of fast pyrolysis oil. It was found that Ru/C gave the best performance with yields of ~65%, oxygen contents of approximately 6%, HHV of 43 MJ/kg and least H₂ consumption (400 Nl/kg dry pyrolysis oil).⁵¹ It was also found out that carbon formation is lower for carbon supports (~4 wt%) when compared to alumina supports (26 wt%). Therefore, variation of the parameters and catalyst involved in HDO of bio-oil can significantly affect the overall efficiency of the process. However, the fact remains that HDO requires large amounts of hydrogen gas at high pressures. This is a major barrier for this bio-oil upgrading technique, owing to the distributed nature of biomass feedstock. Often, it is difficult to find an enormous source of required H₂ at local distributed facilities.⁵²

Zeolite Cracking

This upgrading scheme involves the heating of the bio-oil to temperatures around 350°C to 600°C at atmospheric pressures in the presence of zeolite catalysts.⁵³ The predominant reactions are cracking reactions, wherein, the long chain oxygenated hydrocarbons in the pyrolysis bio-oil are reduced to shorter molecules. The products are formed in three phases, namely the organic phase, the aqueous phase and a gaseous phase.⁴³ The process does not require an external source for the hydrogen gas since it is generated in situ due to the water gas shift reaction.⁵³ HZSM-5 is the preferred catalyst due to the presence of a greater number of acidic sites compared to other silicallumina and silicalite catalysts. Therefore, the conversion of the bio-oil to reduced aromatic compounds is greater for HZSM-5 catalyst.^{43, 54} The extent of deoxygenation is found to increase with an increase in temperature. The reduced oxygen content, however, is accompanied by a decreased yield and an increase in coke formation with rise in temperature.⁴³ Moreover, coke formation in zeolite cracking is a major drawback, with amounts to around 26-39 wt%.⁵⁵ Other disadvantages include high total acid number, low H/C ratios and consequently, lesser heating value of the upgraded bio-oil.⁴³

Esterification and Acetalization

A primary reason behind the reactivity and instability of pyrolysis bio-oils is the presence of functional groups like carboxylic acids, aldehydes and ketones. These can be converted into more stable esters and acetals respectively, by the addition of alcohols in the presence of a catalyst.²¹ Wang et al., added methanol to bio-oil, in the presence of two catalysts, namely 732 resin and NKC-9 resin. The resultant upgraded bio-oil was noted to have improved stability. The acid number reduced by about 86-89%, compared to raw bio-oil. The heating values increased by ~32%. Furthermore, there was reduction in moisture content (~27-30%) and decrease in viscosity

by approximately 97%.⁵⁶ Li et.al., investigated the effect of reaction parameters on the extent of conversion of esterification and acetalization reactions in the presence of Amberlyst-70 catalyst, for mallee woody biomass pyrolysis bio-oil. It was found that the conversion for both reactions increased with increase in temperature and catalyst loadings.⁵⁷ However, catalyst coking, and "poor recyclability limit" are some drawbacks associated with this process.²¹

Physical methods

Of the physical methods employed to upgrade bio-oil, emulsification is a promising route. This involves the mixing of the bio-oil with petroleum-based fuels, in the presence of a surfactant. The process reduces the viscosity of the pyrolysis bio-oils.²¹ Ikura et al., performed the emulsification of pyrolytic bio-oil with diesel fuel in the presence of surfactant Hypermer 2234. It was found that the viscosity and corrosion properties of the emulsions were lower than that of the raw bio-oil.⁵⁸ However, the process involves high cost and high energy inputs.⁵⁹ Char particles in bio-oil are associated with trapping alkali metal ions in them, which in turn can act as catalysts for undesirable polymerization reactions.^{21,60} Generally, cyclone separators are used for separation, whereas hot vapor filtration is employed to remove very fine particles (<10 µm). Compared to cyclone separators, hot vapor filtration is shown to have a tenfold reduction in viscosity growth rates.²¹ Other techniques employ ceramic membranes, under a driving force, to affect the separation of very fine char particles (0.02-10 µm). Although efficient, the high costs of the membranes are significant challenges faced by this technique.²¹

Therefore, in summary, all the physical and chemical methods for stabilization and upgrading of pyrolytic bio-oils have significant challenges. HDO is the most promising and popular route as it is a product of the extrapolation of the hydrodesulfurization (HDS) technique for petroleum fuels to bio-oils.⁴³ However, the extreme conditions and challenges associated with availability and

storage of H₂ gas restrict its application in bio-oil upgrading. In this context, electrocatalytic hydrogenation (ECH) offers an alternative route that employs milder conditions and eliminates the requirement of a source for H₂ gas. The lower operating temperatures and pressure also reduce carbon deposition compared to HDO.³²

Electrocatalytic Hydrogenation

Electrocatalytic Hydrogenation (ECH) is an approach for mild hydrogenation of pyrolysis biooil.⁶¹ Pletcher defined electrocatalysis as "the acceleration of a particular electrode reaction by the appropriate choice of electrode material".⁶² Over the years, the most investigated electrode reaction has been the Hydrogen Evolution Reaction (HER), owing to its immense applications in fuel cells and chlor-alkali processes.⁶³ The HER reaction is known to proceed through two steps⁶⁴,

1. Adsorption of hydrogen on the catalyst surface by electroreduction of water molecules.

$$H_3O^+ + e^- + M \rightarrow MH_{ads} + H_2O$$

(1)

(2)

This is also known as the Volmer Reaction.

- 2. Desorption as molecular H₂
 - a. Chemical Desorption

$$2MH_{ads} \rightarrow 2M + H_2$$

This is known as the Tafel reaction.

b. Electrochemical Desorption

$$H_3O^+ + MH_{ads} + e^- \rightarrow M + H_2 + H_2O$$

This is known as the Heyrovsky reaction. (3)

ECH is employed for stabilization of bio-oil because it offers several advantages over the more popular HDO process. The conditions required for upgrading of bio-oil are milder and there is no need for H₂ gas storage or transport.⁶⁴ However, when ECH is employed for stabilization and

upgrading of bio-oil, reactions (2) and (3) are undesirable side reactions. The adsorbed hydrogen in (1) must ideally react with the unsaturated compounds in bio-oil and reduce them. Li et al., describes the desired reactions between the adsorbed hydrogen and adsorbed unsaturated compounds as follows:

$$(Y = Z)_{aq} + A \rightarrow (Y = Z)_{ads}A \tag{4}$$

$$2(H)_{ads}M + (Y = Z)_{ads}A \to (YH - ZH)_{ads}A + 2M$$
 (5)

$$(YH - ZH)_{ads}A \to (YH - ZH)_{aq} + A \tag{6}$$

where, Y=Z represents the unsaturated organic compounds present in bio-oil, (Y=Z)_{ads}A is the adsorbed organic compound and (YH-ZH)_{ads}A is the adsorbed hydrogenated product.²³

Principle of operation

The principle of operation of an ECH setup, is very similar to that of a general electrolytic cell.

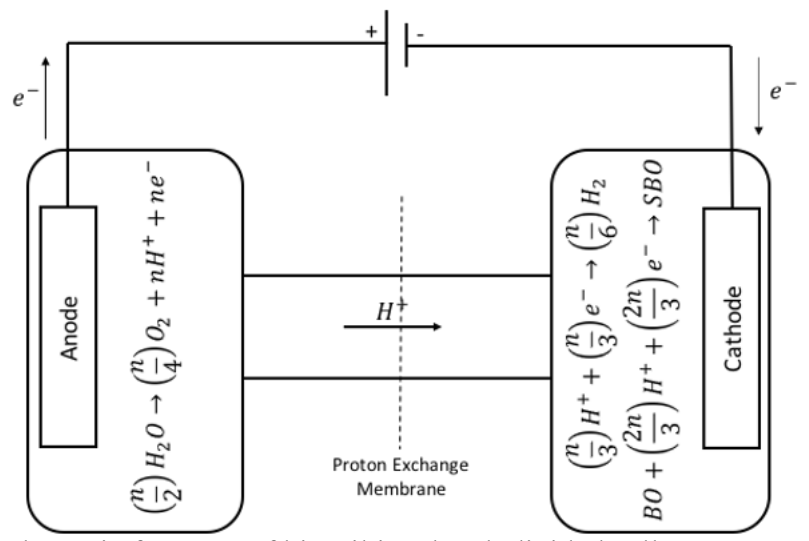


Figure 2.1 : Schematic for ECH of bio-oil in a batch divided cell. BO represents the pyrolysis bio-oil, whereas SBO represents the ECH-ed stable bio-oil. n denotes the number of moles of electrons passed.⁵

As shown in the Figure 2.1, the process involves oxidation of water to yield oxygen gas and hydrogen ions. This is a non-spontaneous reaction, owing to a positive Gibbs free energy. Therefore, an external voltage must be applied. On application, water splits up at the anode to

generate oxygen gas and hydrogen ions, which, under the applied electric field, pass through a proton exchange membrane (for eg., Nafion 117) to be adsorbed as H atoms on the catalytic cathode. The pyrolytic bio-oil is dissolved in a solvent to serve as the catholyte, in a divided cell batch reactor, as shown in Fig. 2.1. It can alternatively, be circulated past the cathode in a continuous solid polymer electrolyte (SPE) reactor²⁴ The adsorbed H atoms on the catalytic cathode, will either hydrogenate the adsorbed organic molecules on the cathode or get desorbed to evolve H₂ gas. As stated above, this is an undesirable side reaction that adversely effects the performance of the ECH process for bio-oil upgrading. The anodic reactions are shown in Fig. 1, and the cathodic reactions are given by reactions (1) to (6). Nafion-117, which may be used as the proton exchange membrane is a commercial product of DuPont. It is "a sulfonated tetrafluorethylene copolymer, consisting of a hydrophobic fluorocarbon backbone (-CF2-CF2-) to which hydrophilic sulfonate groups (SO3-) are attached". It is known for its high proton conductivity and much lower conductivity for other cations.⁶⁵

Performance Parameters

The performance of an ECH process can be evaluated by determination of the following performance parameters:^{24, 32}

1. Electrochemical efficiency (EE)

$$EE = \frac{elctrons \ used \ to \ generate \ hydrogenated \ products}{total \ electrons \ passed}$$

2. Conversion (X)

$$X = \frac{moles\ of\ substrate\ consumed}{initial\ moles\ of\ substrate}$$

3. Selectivity (S)

$$S = \frac{moles \ of \ desired \ product}{total \ moles \ of \ product}$$

4. Yield (Y)

$$Y = \frac{moles\ of\ desired\ product}{initial\ moles\ of\ substrate}$$

5. Production Rate (P_R)

$$P_R = (i * EE)/(charge\ required\ to\ fully\ saturate\ 1\ kg\ of\ substrate)$$

6. Power Consumption (P_W)

$$P_W = (i * V)/(P_R)$$

where *i* is current density

V is applied voltage

High values for EE, X, S, Y, P_R and low values for P_W are desirable for better performance.

Operating Parameters

Operating parameters in an ECH setup play major roles in determining the performance, based on the aforementioned performance parameters. The parameters that have been mostly investigated are temperature, electrode materials, pH, starting reactant concentration and current density.^{32, 33} *Effect of Temperature*

Li et al., studied the effects of temperature on the electrochemical efficiency, product selectivity and conversion of guaiacol, during its ECH, in a two-compartment reactor that was separated by a Nafion-117 membrane. It was found that the electrochemical efficiency passed through a maximum at around 50°C. Below this temperature, electrocatalytic hydrogenation was the predominant reaction, and above this temperature, hydrogen desorption was dominant. Conversion was found to increase with temperature. Selectivity of cyclohexanol, the desired product, also increased with increase in temperature and the change was more pronounced during the temperature rise from 50°C to 80°C. Green et al., observed an increase in rate of conversion of furfural, another model bio-oil compound, with increase in temperature, when ECH of furfural

was carried out in a continuous electrocatalytic membrane reactor. Electrochemical efficiency was found to continuously decrease with rise in temperature, and no maxima was obtained.²⁷ Dabo et al., however, found a direct relationship of electrochemical efficiency and temperature for the ECH of 4-phenoxy phenol.²⁶

Effect of pH

It may be expected that higher values of pH are more suitable for hydrogenation reaction since lower pH values should ideally favor the undesirable H₂ evolution.²³ Investigations, however, point to the contrary. Robin et al., investigated the effect of pH on the ECH of phenanthrene, using Raney Ni electrodes. It was found that an initial pH of 2.6-2.7, with Boric acid as the buffer, gave the best results in terms of electrochemical efficiency, yield and conversion of phenanthrene.²⁹ The best results for the ECH of furfural was reported at pH value of 7. The conversion, furfuryl alcohol yield and selectivity dropped on increasing or decreasing the pH.²³ For the ECH of guaiacol, acidic conditions were preferred as was indicated by the increase in conversion, cyclohexanol selectivity and electrochemical efficiency.³²

Effect of electrodes

The electrodes used in the ECH reaction, especially the cathode, which acts as the catalyst, plays a major role in deciding the performance of the process. For the ECH of furfural in a divided cell, Fe and Ni cathodes were observed to be superior to Cu, Al and stainless steel.²³ Green et al., carried out the ECH of furfural using both Pd/C and Pt/C electrodes and found a much higher current efficiency for the Pd/C cathodes.²⁷ For ECH of glucose to sorbitol, however, the most suitable catalysts were found to be Zn, Cd and other late transition metals, compared to Pt and Pd electrodes.²⁵ Ru/C catalyst has also been identified as a suitable catalyst for the ECH of model bio-oil compounds.^{25, 29} It is important to point out that while non-precious metals have been

demonstrated to have catalytic activity for ECH of certain model compounds, they are incompatible with the acidic Nafion membrane in a continuous SPE reactor.⁶¹ Therefore, these reactors must employ precious metal catalysts like Pt and Pd.

Effect of current density

Electrochemical efficiency was found to increase with an increase in current density for the ECH of phenanthrene.²⁹ However, for the ECH of furfural, it was found to decrease with increasing current density.²³ Santana et al., found that the electrochemical efficiency for the ECH of benzaldehyde passed through a maximum as current density was increased.³¹ These results point to the fact that there exists an optimum current density at which the highest electrochemical efficiency is obtained.²³

Effect of reactant concentration

Green et al., observed a slight increase, followed by continuous decrease in conversion and current efficiency for the ECH of acetone, as the initial concentration of acetone was increased.⁶¹ Similar results were also obtained for the ECH of furfural.²³ This is, however, not expected as increase in starting concentration of substrate should ideally increase the electrochemical efficiency.

It can be inferred that the performance parameters are complex functions of the various operating parameters. The optimization of these operating parameters is, therefore, crucial to the efficient and economical performance of the ECH process. Li et al., performed such an optimization and found that ECH of model bio-oil compounds like guaiacol, syringol and phenol can be performed using Ru/ACC catalyst with best performance at temperatures around 80°C and acidic pH.³²

Decentralized processing of biomass at depots

Biomass is a feedstock source that is distributed in nature and hence renders the need of decentralized chemical processes for handling it.⁶⁶ Being a solid of low energy density, biomass

can incur huge transportation costs if hauled over long distances.²² Therefore, a good strategy would be to reduce transportation costs by establishing local depots that densify the biomass.²² These depots can then supply the densified biomass to a much larger central refinery and take advantage of economies-of-scale to reduce final product cost. Petrou et al., recognizes the importance of local depots while studying biomass supply chains.⁶⁷ Parkhurst et al., studied a system where torrefaction was performed in depots to supply the torrefied biomass to a centralized combustion facility.⁶⁸ Chai et al., performed a study to find the optimum depot capacity for the comparison between the production of conventional and torrefied pellets at the depot. Bals et al., also studied the economic influence of the incorporation of depots with different biomass densification and processing technologies.⁶⁹ These included fast pyrolysis, ammonia fiber expansion (AFEX) pretreatment and leaf protein processing. They concluded that fast pyrolysis at local depots is a slightly profitable venture for corn stover, even without any animal feed sales. Quddus et al., also investigated the application of different densification technologies like conventional and high moisture pellet processing and ammonia fiber expansion in depots.⁷⁰ Roni et al., found out that a distributed supply chain design can greatly increase the supply chain collection area (~57%), without a rise in the delivered feedstock cost.⁷¹ Furthermore, they also concluded that the biomass resource and the depot scale can play an important role in determining the economics of these distributed supply chains. Lamers et al., established the difference between a "standard depot" and a "quality depot". While a standard depot is responsible for only basic biomass supply chain requirements such as increased bulk density and storage, a quality depot improves upon the quality of the biomass feedstock. 72 These quality improvements may be in the form of lower contamination levels or enhanced feedstock intermediates that have higher energy content. Jacobson et al., further elaborates on this idea and shows how incorporation of different

technologies at depots can help reduce overall cost for the process.⁷³ Kim et al., compares a centralized cellulosic ethanol system with a decentralized system and reports that while the centralized system has better economic performance for smaller biorefineries, the depot-based system performs better at larger scale biorefineries.⁷⁴ Crandall et al., investigated the different rural benefits of including biomass depots for woody biomass in Western Oregon and concluded that they can positively contribute to the rural economy.⁷⁵ Several other studies have also investigated the role of decentralized processing/densification depots in biomass supply chain optimization and determined their effect on process economics⁷⁶⁻⁷⁸ and their environmental impacts.^{79, 80} In the present study, the Py-ECH system is a decentralized bioenergy system that combines fast pyrolysis of biomass and subsequent electrocatalytic hydrogenation of the pyrolysis bio-oils to produce a stable denser bio-oil intermediate that can, in turn, be hauled over long distances to a central hydroprocessing facility to produce a gasoline/diesel like fuel.

Technoeconomic analysis (TEA) of biomass to fuels

For the commercial application of any technology, economics can play a vital role. To evaluate the economic performance of any bioenergy system, technoeconomic analyses are performed. These analyses combine the process modeling and engineering design with economic evaluation. While the primary objective is to determine the economic feasibility of the process, these can also help identify the important bottlenecks of the system and help minimize the cost. For bioenergy systems that produce fuel, TEA generally involves determining a minimum selling price for a certain profitability or internal rate of return. Al. 82-86 TEA of any bioenergy system involves estimating the capital (equipment costs) and operating costs. These operating costs may be fixed, (such as insurance, rent, salaries etc.) that do not vary with production rate, or they may be variable, (such as raw material, utilities etc.) that change with production rate. This is subsequently

followed by profitability analyses such as profitability ratio analysis, break-even analysis or discounted cash flow rate of return analysis (DCFROR) to generate a selling price for the fuel. Of the three, DCFROR accounts for the time value of money and equates the net present value of all cash flows during the lifetime of the biorefinery, to a value of zero. The fixed discount rate that achieves this is known as the internal rate of return. 88 For the DCFROR analysis, the annual cash flow in year i (CF_i) may be expressed in terms of the tax rate (r_t), the annual revenue (R), the annual expenditure (E) and the annual depreciation D as:

$$CF_i = (1 - r_t).(R - E) + r_t.D$$

If $V_{p,i}$ is the present value of the cash flow of a future year i and r_d is the discount rate, then,

$$V_{p,i} = CF_i/(1+r_d)^i$$

Assuming I_T is the total capital cost, I_{WC} is the working capital, I_s is the salvage value of the fixed capital cost and n is the total plant life, then the net present value (NPV) of the entire investment in the plant over its entire lifetime may be expressed as:

$$NPV = -I_T + \sum_{i=1}^{n} V_{p,i} + \frac{I_W + I_S}{(1 + r_d)^n}$$

The internal rate of return (IRR) may then be defined as the discount rate that results in an NPV of zero.^{88,89}

In the present study, the TEA of the Py-ECH system was performed using the DCFROR approach. The economic assumptions in this approach were considered to be for a nth plant. A nth plant assumes that the technology being used in the plants have already been developed and operated and therefore, does not account for any additional pioneer plant costs. 90 Although the Py-ECH is a novel approach for processing biomass to fuels, the nth plant assumption still works since the technologies employed in this system are not new. TEAs have previously been performed for the

thermochemical conversion of biomass to fuels. Shahabuddin et al., performed a comprehensive review of production of hydrogen from biomass gasification and pyrolysis. They determined a range of \$ 2.8-3.4/kg of H₂ for the levelized cost of hydrogen, produced from gasification. 91 Patel et al., in 2016, conducted a review for the TEAs of different types of thermochemical conversions for lignocellulosic biomass. 92 These included almost all thermochemical methods like pyrolysis, gasification, liquefaction, co-firing, carbonization and combustion. Table 2.2 lists many such TEAs and highlights the feedstock used, the technology employed and the evaluated cost. Most of the TEAs listed in Table 2.2 have been performed for technologies like gasification, pyrolysis and hydrothermal liquefaction. The feedstock is mostly lignocellulosic biomass like corn stover, poplar and woody biomass. TEAs of biomass gasification generally involved the production of gaseous fuels like H₂ or syngas, as the first step. These were subsequently followed by an upgrading step, that converted this gaseous intermediate to produce a liquid hydrocarbon fuel. 93-95 However, TEAs that involved pyrolysis of biomass proceeded to bio-oil upgrading via a liquid intermediate.^{84, 85,} 95, 96 The upgrading technique, too, was almost always hydrotreating, as can be seen in Table 2.2. This is highlighted even more by Sorunmu et al., in 2019, who lists numerous TEAs that utilize hydrotreating as the designated technique for pyrolysis bio-oil upgrading.⁹⁷ Moreover, the H₂ used for upgrading in these studies, is generated either from natural gas, off gases from the process or purchased.^{84, 85, 96} This is different from the Py-ECH system that considers electrolysis as the source for generation of hydrogen. Wright et al.⁸⁴ does consider a scenario, where the hydrogen used for upgrading is produced via electrolysis. However, they consider the production of hydrogen gas, whereas the Py-ECH system involves the generation of in-situ hydrogen ions for electrocatalytic reduction of the pyrolysis bio-oil. Most of the TEA studies in literature also consider a single integrated refinery, housing both the pyrolysis and upgrading systems. 82, 84, 85, 96,

98 This is again different from the Py-ECH system that considers a decentralized system, where the pyrolysis and electrocatalytic upgrading is occurring in local depots. Lamers et al., does study the economics of biomass processing at depots and investigates different depot scenarios with different processing abilities.⁷² Jacobson et al., also reports the economic benefits of the decentralized system for processing biomass in local depots. 73 Bals and Dale also perform a similar kind of economic analysis for comparing different biomass processing technologies at local depots for the production of biofuel intermediates or high value co-products. ⁶⁹ However, all these studies are only concerned with the economics at the depot and do not consider a full bioenergy system for production of gasoline/diesel range fuels. Moreover, none of these consider the combination of fast pyrolysis and electrocatalytic hydrogenation at the biomass processing depots, as in the Py-ECH system. Previous TEAs have also been performed for electrocatalytic systems in fuel cells. 99-¹⁰¹ These are important for estimation of costs for the electrocatalytic hydrogenation of pyrolysis bio-oil, because the capital cost for such systems should be very similar. This is owing to the fact that the equipment employed for ECH of bio-oil should be very similar to that for fuel cell systems, although the operation is very different. Orella et al., did develop a technoeconomic model for evaluating the economics of the electrocatalytic hydrogenation of pyrolysis model bio-oil compounds. 102 This is however, restricted to only ECH and does not account for the cost of previous pyrolysis or subsequent hydroprocessing.

To summarize, while previous TEAs have focused on fast pyrolysis and upgrading via hydroprocessing, none have evaluated the economics of incorporating the ECH unit as a stabilizing technique. Most of these studies have also been for integrated biorefineries and have not considered decentralized systems like the Py-ECH system. Therefore, a full scale technoeconomic analysis of the Py-ECH system will address this knowledge gap.

Table 2.2: Technoeconomic analyses of bioenergy systems involving thermochemical conversion of biomass, followed by upgrading. The year mentioned in parenthesis in each entry of the "Cost" column denotes the \$ year; gge stands for gallon of gasoline equivalent.

of the "Cost" column denotes the \$ year; gge stands for gallon of gasoline equivalent.				
Biomass	Technology	Cost	Remarks	Source
Corn stover	Fast pyrolysis to bio-oil followed by upgrading	\$ 3.09/gge (2010)	When upgrading H ₂ is	Wright et al., ⁸⁴
	to naphtha and diesel fuel ranges via hydrotreating	(=)	produced by electrolysis	
Corn stover	Fast pyrolysis to bio-oil followed by upgrading to naphtha and diesel fuel ranges via hydrotreating	\$ 2.41/gge (2010)	When upgrading H ₂ is purchased	Wright et al., ⁸⁴
Woody biomass	Gas Technology Institute's integrated hydropyrolysis and hydroconversion to gasoline/diesel	\$ 1.68/gge (2007)	Minimum fuel selling price (MFSP)	Tan et al., ⁸²
Corn stover	Gasification followed by catalytic Fischer Tropsch synthesis and hydroprocessing to liquid hydrocarbon fuels	\$ 4- \$ 5/gge (2010)	Discounted cash flow, rate of return analysis	Swanson et al., ⁹⁴
Woody biomass	Hydrothermal liquefaction and hydrotreating to liquid hydrocarbon fuel	\$ 4.44/gge (2014)	State of technology MFSP	Zhu et al., ¹⁰³
Corn stover	Fast pyrolysis and hydroprocessing to gasoline/diesel	\$ 2.57/gge (2011)	MFSP	Brown et al., ⁸⁵
Woody biomass	Catalytic production of methanol from syngas (from gasification and electrolysis of water)	€ 11.8-25.3/ GJ _{exergy} of fuel energy	Methanol fuel	Clausen et al., 104
Poplar wood	Gasification to syn gas to methanol to gasoline using zeolite catalyst	\$ 1.95/gallon (2007)	Discounted cash flow, rate of return	Philips et al., ⁹³
Woody biomass	Mild catalytic pyrolysis, followed by upgrading to liquid hydrocarbon fuel	\$ 3.69/gallon (2014)	Hydrocarbon fuel composed of aromatics, cycloalkanes, olefins and paraffins	Thilakaratne et al., ⁹⁶

Table 2.2 (cont'd)

Table 2.2 (Cont	u)			
Wood chips	Gasification to syngas converted to methanol	\$ 2.79/gallon (2008)	Carbon monoxide and	Zhu et al., ⁸³
	to acetic acid, followed		hydrogen gas	
	by hydrogenation to ethanol.		were purchased	
Straw	Decentralized pyrolysis	35 €/MWh of	Biosyncrude	Trippe et al., ¹⁰⁵
	to biosyncrude (bio-oil	fuel energy	price	
	and biochar) which can	(2010)		
	be upgraded to			
	synthetic fuels via			
	gasification at central			
	refinery			
Pine wood	Fast pyrolysis, followed	£ 6.25/gge	Electricity co-	Shemfe et al.,98
	by hydroprocessing of	(2015)	produced	
	bio-oil to	,	•	
	gasoline/diesel			
Corn stover	Pyrolysis, gasification	\$ 2-5.50/gge	Fuel price is	Anex et al.,95
	and biochemical	(2010)	lowest for	
	scenarios to liquid fuels		pyrolysis	

Life cycle assessment (LCA) of biomass to fuels

The advantage of bioenergy systems can be best realized in regard to their environmental performance. Therefore, any evaluation of a bioenergy system is incomplete without quantification of the environmental impacts. Presently, the best tool for such quantification is life cycle assessment (LCA). A LCA can be used to determine the overall environmental impacts of any process, subject to the system boundaries selected. In regard to bioenergy systems, a cradle-to-grave LCA estimates its environmental impacts, starting from acquiring raw material for the system to the product end use. Any LCA study has four phases, namely 109, 110:

1. Goal and Scope Definition: During this phase, the goal and scope of the LCA is used to set the system boundaries and the purpose of the study. The functional unit, which is a quantitative measure of the function/use of the product is also decided in this phase

- 2. Life Cycle Inventory Analysis: The technical database is created in this phase. In other words, the process inputs and outputs, as defined by the system boundaries, are determined here.
- 3. Life Cycle Impact Assessment: This phase is aimed at evaluating the potential environmental impacts of the system via the calculation of several midpoint/endpoint indicators. While endpoint indicators indicate the environmental impact on specific areas of protection, the midpoint indicators represent the impact between the emission point and the endpoint. The specific impact categories to be investigated are also decided in this phase, depending on the LCA goal.
- 4. Interpretation: In this phase of the LCA, the results are from the impact assessment phase are interpreted in view of the goal and scope. Decisions or recommendations can be made here about the system being studied.

Previous LCAs have been performed for the fast pyrolysis of biomass and their subsequent hydroprocessing to gasoline/diesel range fuel. Some LCAs have also studied the generation of biochar via slow pyrolysis. These studies have been listed in Table 2.3, highlighting the biomass feedstock used in the study and the employed processing technology. In all these studies, the biomass is first subjected to pyrolysis (fast or slow), followed by the presence/absence of a subsequent upgrading technique. However, none of these studies combined fast pyrolysis with electrocatalytic hydrogenation as a stabilizing method, as in the Py-ECH system. Decentralized biomass processing has also not been considered in any of these studies barring Peters et al., who compared the environmental performance of localized fast pyrolysis and centralized hydrotreating to integrated fast pyrolysis and hydrotreating at single refinery. They concluded that the relative environmental impacts, in regards to the global warming potential and eutrophication potential of

the two scenarios were heavily dependent on the utilization of the by-product biochar generated from pyrolysis. Other studies that investigated the environmental impacts of establishing local biomass processing depots did not consider biomass pyrolysis itself at the depots.^{79, 80, 112} In fact, in the system studied by Lan et al., pyrolysis occurred at the central biorefinery, whereas the depot was concerned with biomass preprocessing units such as drying, grinding and pelleting.¹¹²

Table 2.3: LCA studies of biomass pyrolysis

Table 2.5: LCA studies of blomass pyrolysis				
Biomass feedstock	Technology	Source		
Short rotation poplar biomass	Fast pyrolysis, followed by hydrotreating and hydrocracking to gasoline/diesel	Iribarren et al., ¹¹³		
Lignocellulosic energy crops	Slow pyrolysis to biochar	Peters et al., ¹¹⁴		
Corn stover	Fast pyrolysis, coupled with anaerobic digestion	Righi et al., ¹¹⁵		
Corn stover, yard waste, switchgrass	Slow pyrolysis to biochar	Roberts et al., ¹¹⁶		
Poplar, willow, logging residues	Pyrolysis to bio-oil to electricity through co- combustion in conventional power plants	Fan et al., ¹¹⁷		
Forest residues	Fast pyrolysis and hydroprocessing to produce gasoline/diesel	Hsu ¹¹⁸		
Municipal solid waste	Pyrolysis or gasification, coupled with gas turbine and combined cycle to generate electricity	Dong et al., ¹¹⁹		
Corn stover	Fast pyrolysis, followed by hydroprocessing to gasoline/diesel	Dang et al., ¹²⁰		
Corn stover	Fast pyrolysis and hydrotreating (using H ₂ gas produced by catalytic reforming of a portion of produced bio-oil) to produce gasoline/diesel	Zhang et al., ¹²¹		
Hybrid poplar	Fast pyrolysis at local plant, followed by hydrotreating, hydrocracking, distillation and steam reforming at biorefinery	Peters et al., ¹²²		
Hybrid poplar	Fast pyrolysis, followed by hydrotreating in biorefinery (1)when pyrolysis is integrated with biorefinery and (2) when pyrolysis occurs in decentralized plants	Peters et al., ¹¹¹		
Rice straw	Integrated biomass pyrolysis, gasification and methanol synthesis	Im-orb et al., ¹²³		
Pine trees	Fast pyrolysis to bio-oil	Steele et al., 124		
Wood waste	Flash pyrolysis for power generation	Zhong et al., 125		

Table 2.3 (cont'd)		
Corn stover	Pyrolysis followed by bio-oil upgrading via	Vienescu 126 et al.,
	different combinations of esterification,	
	ketonisation, hydrotreating and hydrocracking	
Palm empty fruit	Fast pyrolysis compared with hydrothermal	Chan et al., 127
bunch	liquefaction	
Corn stover and corn	Corn to ethanol; stover subjected to fast	Kauffman et al., 128
	pyrolysis, followed by refining to naphtha and	
	diesel range fuel	

Moreover, in most of the LCAs listed in Table 2.3, emissions associated with cultivation of the biomass are not considered. Only a few include cultivation in their system boundaries. 114, 117, 122 Some LCAs that handle corn stover biomass only include the emissions associated with the collection and harvesting of stover. 115, 120, 121, 126, 128 These studies omit the emissions/benefits associating with cultivation of corn, such as soil carbon sequestration and fertilizer emissions. Such an omission is only justified by assuming that corn stover is a waste product of corn cultivation and only affects it via the withdrawal of nutrients in the corn stover removed from the fields. It is only these nutrients that must be replenished through excess fertilizer application. However, since cultivation is an integral part of any bioenergy system, such assumptions need to be investigated further, especially for biomass feedstocks like corn stover, whose cultivation boundaries intersect with other systems like corn grain to ethanol or corn grain as food. Additionally, some LCAs also do not include end use emissions in the analysis, thereby making it a cradle-to-plant gate LCA or a farm gate-to-plant gate LCA.

Therefore, a full scale cradle-to-grave LCA of the Py-ECH system needs to be performed in order to address these knowledge gaps and get a full understanding of the environmental impacts of the Py-ECH system.

Kinetic modeling of ECH

As discussed before, the novelty of the Py-ECH systems lies in combining electrocatalytic hydrogenation with fast pyrolysis, as a mild stabilization method for pyrolysis bio-oils. ECH is therefore, integral to the Py-ECH system. However, while pyrolysis of biomass is a sufficiently mature technology, 18, 19, 84, 85, 129 ECH of bio-oil is still in nascent form. It is mostly studied via labscale batch experiments of ECH of model bio-oil compounds.^{23, 130-132} Although ECH of edible oils^{24, 133} and ECH of furfural to furfuryl alcohol²⁷ in solid polymer membrane reactors have been reported, most ECH experiments involve 2-compartment divided batch cells. Also, most of ECH literature is focused on finding better catalysts for ECH of different model compounds based on product yield and electrochemical efficiency. 32, 34, 134 In this regard, Laplante et al., found that for the ECH of phenol to cyclohexanol, 5%Pd/Al₂O₃ catalyst performed better in terms of reactant conversion and current efficiency than other Pd catalysts with different supports. ¹³⁵ Greater current efficiencies and conversion were observed by Lam et al., for the ECH of guaiacol to cyclohexanol using Raney Ni electrodes.³⁴ Li et al., discovered even better efficiencies and rates of conversion for the ECH of phenol to cyclohexanol using ruthenium catalyst on activated carbon cloth (Ru/ACC).³² From these studies, it may be concluded that Ru/ACC electrode is a better catalyst for the ECH of phenol to cyclohexanol. Also, slightly acidic conditions were more favorable for the ECH of guaiacol than basic or neutral conditions and the optimum ECH temperature was found to be 80°C.³² Very recently, the ECH of phenolic compounds and dimers, in presence of ruthenium catalyst (supported on carbon cloth) was performed by Garedew et al. 136, 137 Sanyal et al., in 2020, investigated the simultaneous ECH of aldehydes and phenol in presence of catalysts like Ru, Rh, Pd and Cu, supported on carbon. While such studies provide great insight into the thermodynamics of the process, there is work to be done on the kinetic aspect of ECH, which is key for any

successful scale-up operation. 138 Few kinetic studies have been performed previously. Kinetics for the ECH of ethylene over Pd black catalyst was studied by Langer et al. 139 Anantharaman and Pintauro performed the kinetics for the ECH of glucose to sorbitol in a batch slurry reactor and a flow through reactor with Raney Ni powder as catalyst.³⁰ Sedighi et al., carried out kinetic studies for ECH of ethylene in a polymer electrolyte membrane (PEM) reactor using Ni catalyst. 140 A mathematical model for the ECH kinetics of phenol was developed by Bannari et al., employing Pd/Al₂O₃ catalyst. 141 Song et al. performed preliminary kinetics for ECH of phenol in a divided batch cell with Pd/C, Pt/C and Rh/C catalysts¹³⁰ and also studied the kinetics for the ECH of benzaldehyde to benzyl alcohol over the same catalysts. 142 Singh et al., also investigated the effect of temperature on the ECH rates of phenol on Pt and Rh catalysts. 143 Sherbo et al., studied the kinetics of electrocatalytically reducing phenylacetylene to ethyl benzene in a Pd membrane reactor. 144 However, the kinetics of ECH of model bio-oil compounds using Ru/ACC have not been performed. This presents a knowledge gap that needs to be addressed. A good starting point would be to investigate the kinetics of ECH of phenol. This is because phenol is one of the simplest bio-oil model compounds, whose ECH in presence of Ru/ACC has already been studied. 136 This kinetic modeling study for the ECH of phenol over Ru/ACC may be aimed at estimating the kinetic rate constants of all related electrochemical, adsorption/desorption and surface reactions, while also accounting for mass transfer effects.

Chapter 3: PY-ECH SYSTEMS ANALYSIS: DEVELOPMENT OF MASS, ENERGY AND CARBON FLUX

(Reproduced directly from Lam, **Das**, Erickson, Hyzer, Garedew, Anderson, Wallington, Tamor, Jackson, Saffron, *Sustainable Energy & Fuels*, **2017**); https://doi.org/10.1039/C6SE00080K

<u>Abstract</u>

The carbon efficiency of bioenergy systems is of critical importance in discussions pertaining to biomass availability for the displacement of petroleum. Classical carbohydrate fermentations to make simple alcohols are carbon inefficient as they discard 1/3 of biomass holocellulose as CO₂. Biomass' lignin is typically burned for heat and power instead of liquid fuel, discarding another sizeable fraction of the biomass carbon. Carbon is the backbone element in hydrocarbon fuels and these losses limit full utilization of the carbon captured by photosynthesis. The DOE Billion-ton Study Update optimistically projects enough biomass carbon to cover 2/3 of the estimated fuel usage in the transportation sector by 2030. Fast pyrolysis combined with electrocatalytic energy upgrading using renewable electricity offers a more carbon-retentive pathway for biomass to renewable fuels. This fast pyrolysis-based sequence offers the added benefit fixing atmospheric carbon in the form of biochar, which provides a mechanism for long-term carbon storage. An associated challenge is that the liquid "bio-oil" from biomass fast pyrolysis contains functional groups like carboxylic acids, carbonyls, and oxygenated aromatics. Their presence hinders the storage and transportation of bio-oil. We propose a potential solution with localized electrocatalytic hydrogenation as an immediate measure to stabilize bio-oil via oxygen removal and carbonyl saturation. Electrocatalytically stabilized bio-oil can be stored and/or transported to centralized refineries for further upgrading. Compared to microbial bioconversion, the strategy proposed here enables significantly higher yields of renewable hydrocarbon fuels and

offers a large-scale mechanism for chemical storage of renewable but intermittently generated electrical energy as transportation fuel.

Introduction

It is now widely recognized that drastic reductions in CO₂ and other greenhouse gas (GHG) emissions from human activities will be necessary to avert serious environmental, economic and social dislocations due to climate change. Reduction in CO₂ emissions from transportation is significantly more challenging than from stationary applications simply because mobile vehicles must carry their energy supplies with them. This places a large premium on specific and volumetric energy density, where liquid hydrocarbons reign. For example, gasoline carries almost 47 times more energy per unit mass (44.4 vs. 0.95 MJ kg⁻¹ on a higher heating value (HHV) basis) than the most advanced commercially available lithium battery, 145 and approximately five times that of liquid hydrogen when containers and insulation are included. 146 These characteristics, along with compatibility with existing infrastructure and vehicles, make a renewable liquid hydrocarbon fuel highly desirable. U.S. annual energy consumption for transportation is estimated to be approximately 29 EJ for the year 2015. 147 With a transportation energy consumption growth rate of <0.1% per year for the years 2012–2040,¹⁴⁸ this value is unlikely to change much until 2030. Considering a specific energy of 48 MJ kg⁻¹ (HHV), this amounts to about 0.6 billion tonnes of petroleum. The projected U.S. annual harvestable biomass by 2030 is estimated optimistically to be 1.04 billion dry tonnes, ¹⁴⁹ carrying only 21 EJ of energy, which would still not satisfy the energy demand for transportation (Fig. 3.1). Assuming simple empirical formulae for hydrocarbon fuel (CH₂; carbon ½ 86% of mass 14) and biomass (CH₂O; carbon ½ 40% of mass 30), it can be seen that the carbon content in the biomass feedstock falls short of that needed to meet the hydrocarbon fuel needs of U.S. transportation (Fig. 3.1).

In this regard, it must be noted that typical processes for biofuel production can only utilize a fraction of the biomass carbon. This carbon loss is illustrated by considering cellulosic ethanol production. Though biological and thermochemical processes to convert biomass to ethanol have seen impressive advances in recent years, 12 their intrinsic stoichiometry loses at least 1/3 of the starch/sugar carbon as CO₂, while concentrating the feedstock's energy content into a smaller fraction of the starting mass. Most of these biofuel strategies are also powered via combustion of part of the biomass itself, discarding additional CO₂.

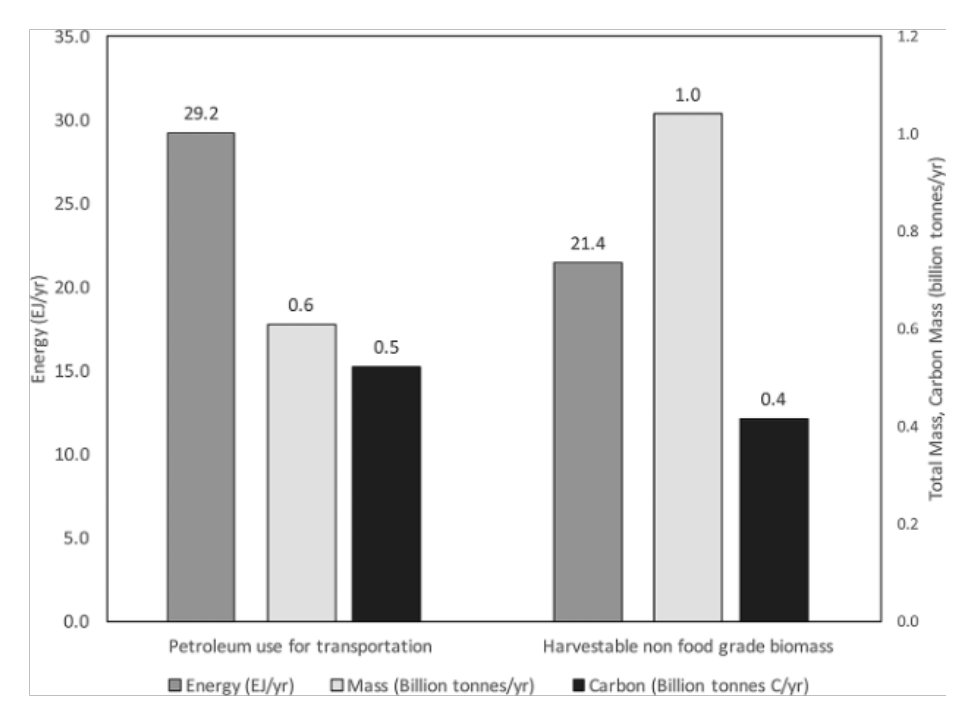


Figure 3.1: Comparison of the annual energy balance in the U.S. transportation sector and projected harvestable biomass. Projections are made based on the available biomass by 2030 (U.S. Billion Ton Study 2016). The specific energy for petroleum is 48 MJ kg⁻¹ and for dry biomass is 20.6 MJ kg⁻¹. Energy is presented in exajoules (EJ), equivalent to 1018 J. Mass is in units of a "billion tonnes", equivalent to 10^{12} kg.

However, the carbon quantity supplied annually from biomass is already below that consumed in fuels. The key limiting factor must then be recognized as carbon, rather than the energy content of the feedstock. Biomass to fuel conversion should thus aim to maximize carbon retention. This makes a fuel process that combines biomass and renewable electricity particularly attractive.

Considering biomass carbon as a limited resource, biomass-to-biofuel conversion strategies that augment energy content and minimize carbon loss are imperative. One example consistent with this approach is fast pyrolysis followed by electrocatalytic hydrogenation (ECH). Biomass can be liquefied through fast pyrolysis, a thermal process characterized by rapid heating in the absence of oxygen, to produce bio-oil. 19, 36 The bio-oil composition is complex and varies with feedstock. It typically contains a great variety of lower carbon number organic compounds such as aldehydes, ketones, carboxylic acids, aromatics, and about 20 wt% water. As a result of these reactive oxygenated moieties, bio-oil has a low energy content (comparable to the starting biomass), and is vulnerable to polymerization, increasing viscosity, even under ambient temperature storage conditions. Hydrodeoxygenation (HDO) of bio-oil, as used for petroleum upgrading, is of great interest as a strategy to achieve deoxygenation and stabilization of bio-oil. Such a practice could potentially take advantage of the existing petroleum infrastructure. 19, 51, 150-160 However, transportation of biomass to a distant centralized location for pyrolysis and upgrading would be costly and energy inefficient on a large scale. Further, the aforementioned instability of untreated bio-oil makes such transport problematic. So far, two common strategies, organic solvent dilution and low temperature storage, have been proposed to improve the bio-oil storage life. 161 Neither of these approaches is economically applicable on a large scale. Bio-oil pipelines would require acidresistant coatings to prevent corrosion of metal surfaces, but these would not address bio-oil stability and thus would only be viable for on-site or short distance transport. 162 Ground transportation of untreated bio-oil would require costly stainless steel containers and refrigeration systems. One alternative is to build a small-scale hydrogenation reactor at the pyrolysis site that would stabilize bio-oil for transportation. However, the costs of small-scale H₂ production are undesirably high and the need for flammable/explosive gas handling poses safety concerns. With

a simpler and safer alternative, electrocatalytic hydrogenation (ECH) is proposed as a mild upgrading approach that could be implemented practically as an immediate stabilization strategy local to the biomass pyrolysis sites. These regional biomass processing depots,²² with facilities for pyrolyzing biomass and stabilizing the resultant bio-oil via ECH will henceforth be referred to as Biomass Upgrading Depots (BUDs).

Any strategy for direct biomass-to-fuels conversion is fundamentally a solar energy and carbon capture scheme. Plants are naturally evolved as atmospheric CO₂ collectors and do so with very low fixed and operating cost. However, while excellent at fixing carbon, plants are relatively inefficient at capturing the sun's energy and storing it in chemical form, with no evolutionary driving force to store more energy than needed for growth and reproduction. Most plants in nature have photosynthetic efficiencies of approximately 1–2%; with 98–99% of the incident solar energy lost to optimal wavelength mismatch, respiration, reflection and transmission.^{6, 7} Furthermore, biomass has only about one third of the specific energy of liquid hydrocarbon fuels; therefore, unmodified plant matter is energetically unsuitable as transportation fuel. Human technologies can capture solar energy much more efficiently than plants, but they do so in the form of electricity which is difficult to store. Commercially available lower-end photovoltaic cells, mostly made of single crystalline silicon, have an energy efficiency of 12–15%. ¹⁶³ In other words, even the oldest form of photovoltaic device on the market still captures solar energy at least ten times more efficiently than plants. Wind electricity is also increasingly cost effective. 164 It is a national goal to replace fossil fuels (petroleum oil) with renewable fuels, ideally liquid fuels. Using renewable electricity to raise the energy content of biomass increases carbon utilization, maximizing yields of biomass-derived fuels. In fact, Clausen has demonstrated that fuel yields per unit biomass fed in a thermochemical biorefinery do indeed increase when energy is added via

electrolysis. 165 However, that strategy uses H2 gas from water electrolysis in conventional hydrodeoxygenation at relatively high temperatures and pressures. In contrast, the direct electrocatalytic reduction scheme (at the BUD) outlined in this study avoids the use of high pressures or H₂ gas and operates at near-ambient conditions. It can be argued that for renewable fuel production purposes, ECH is a promising strategy to achieve bio-oil stabilization because (a) it operates at mild conditions; (b) it avoids the storage and use of H₂ gas; (c) the chemisorbed hydrogen density and reactivity on the cathode surface can be controlled by current density; and (d) most important of all, ECH reduces H₂ consumption during on-site petroleum-style hydroupgrading.^{32, 34} Furthermore, due to a mismatch between the times of human power demand and the cycles of light and wind availability, renewable electric power generating capacity may go unused at some times; energy upgrading of biomass-derived fragments via ECH thus represents a much needed time-insensitive method of using and storing alternative energy. Recently, it was demonstrated that the aqueous fraction of bio-oil can be stabilized via ECH.²³ The resulting stabilized bio-oil contained significantly greater alcohol content and was resistant to polymerization and aging. 132

Methods

The ECH scheme discussed in the preceding sections is a mild technique to stabilize bio-oil resulting from fast pyrolysis of biomass feedstocks. The stabilized bio-oil can then be transported to more centralized petroleum refinery complexes for further upgrading. ECH reduction is therefore only one part of the entire biomass conversion process. In this context, it is important to adopt a holistic approach that studies the results of implementing ECH in the overall biomass conversion process. This study models a complete biomass conversion that incorporates ECH for mild upgrading. Henceforth referred to as the Py–ECH process, it starts from the grinding and

drying of the raw feedstock and ends with the production of a gasoline-like fuel. The major processes employed are biomass fast pyrolysis (BFP), followed by ECH and hydroprocessing. Detailed descriptions of each of these processes, along with model assumptions, can be found in the Appendix at the end of this chapter. The values obtained from the developed spreadsheet model along with all necessary sources have also been listed in the Appendix. The Py–ECH approach is then compared to a cellulosic ethanol (CE) process for the biochemical conversion of lignocellulosic feedstock to ethanol in terms of mass, energy and carbon fluxes through each system. The values for these fluxes were extracted from a NREL report published in 2011. 11 All necessary values were extracted and then scaled for a fair comparison. Both sets of extracted and scaled values can be found in Tables 3.13–3.17 in the Appendix. For comparing Py–ECH to CE, corn stover was chosen as the biomass feedstock for each process, starting with the same higher heating value (HHV, 16.498 MJ kg⁻¹ wet weight) and moisture content (20 wt%). The biomass feed rate was fixed at 1.0 billion dry tonnes per year for both systems, which approximates the predicted available biomass in the United States, by the year 2030, that could be produced at approximately \$60 per ton. All the energy calculations for the Py–ECH process were performed on a higher heating value (HHV) basis. The reported energy values are a summation of the HHVs at the reference state and the sensible and latent heats required to attain the stream conditions, starting from the reference state. The reference state used for the calculations was 25°C and 1 bar pressure.

Renewable hydrocarbons by fast pyrolysis, electrocatalysis and hydroprocessing (Py–ECH)

The Py–ECH approach is a thermochemical and electrochemical biomass conversion technique that creates stabilized bio-oil, biochar and hydrogen gas from corn stover. The primary processes involved are fast pyrolysis, electrocatalytic hydrogenation (ECH) in BUDs and a subsequent

hydroprocessing step in petroleum refinery complexes. Fast pyrolysis produces the unstable liquid bio-oil product that is subsequently stabilized by the ECH process in the BUD. This stable bio-oil is then transported to the petroleum refinery complexes to be further hydrogenated at high temperature and pressure to yield the upgraded fuel. Both the ECH and the hydroprocessing steps use renewable electricity to generate the H₂ for hydrogenation. A detailed description of the entire process, along with all necessary assumptions and calculations can be found in the Appendix.

Cellulosic ethanol (CE) by fermentation

The CE approach considered in this study follows the process described in detail in NREL's 2011 report. According to a classification approach adopted by Cherubini et al., the CE process can be best described as a three-platform (hydrolysate, lignin, and bio-gas) biorefinery for ethanol and electricity from corn stover. He major processes involved in the CE approach are pretreatment, hydrolysis, fermentation, distillation, aerobic digestion and anaerobic digestion. The major product is ethanol; electricity, which comes from incinerating the non-fermentable components, is generated as a by-product. In fact, the energy requirement of the entire process is more than satisfied by this generated electricity. The entire design for the CE process has been performed by NREL using Aspen software. Therefore, for our study, all data required for the analyses were extracted from this report. For equal comparison, all the energy, mass and carbon data for the CE process were scaled to accommodate 1 billion tonnes of biomass as is processed by the Py–ECH system.

Results

The energy analyses for the two renewable fuel production systems are summarized in the Sankey diagrams presented in Figure 3.2. Balances for each system component were performed for the Py–ECH system, while overall balances were performed for the CE system. The analysis shows

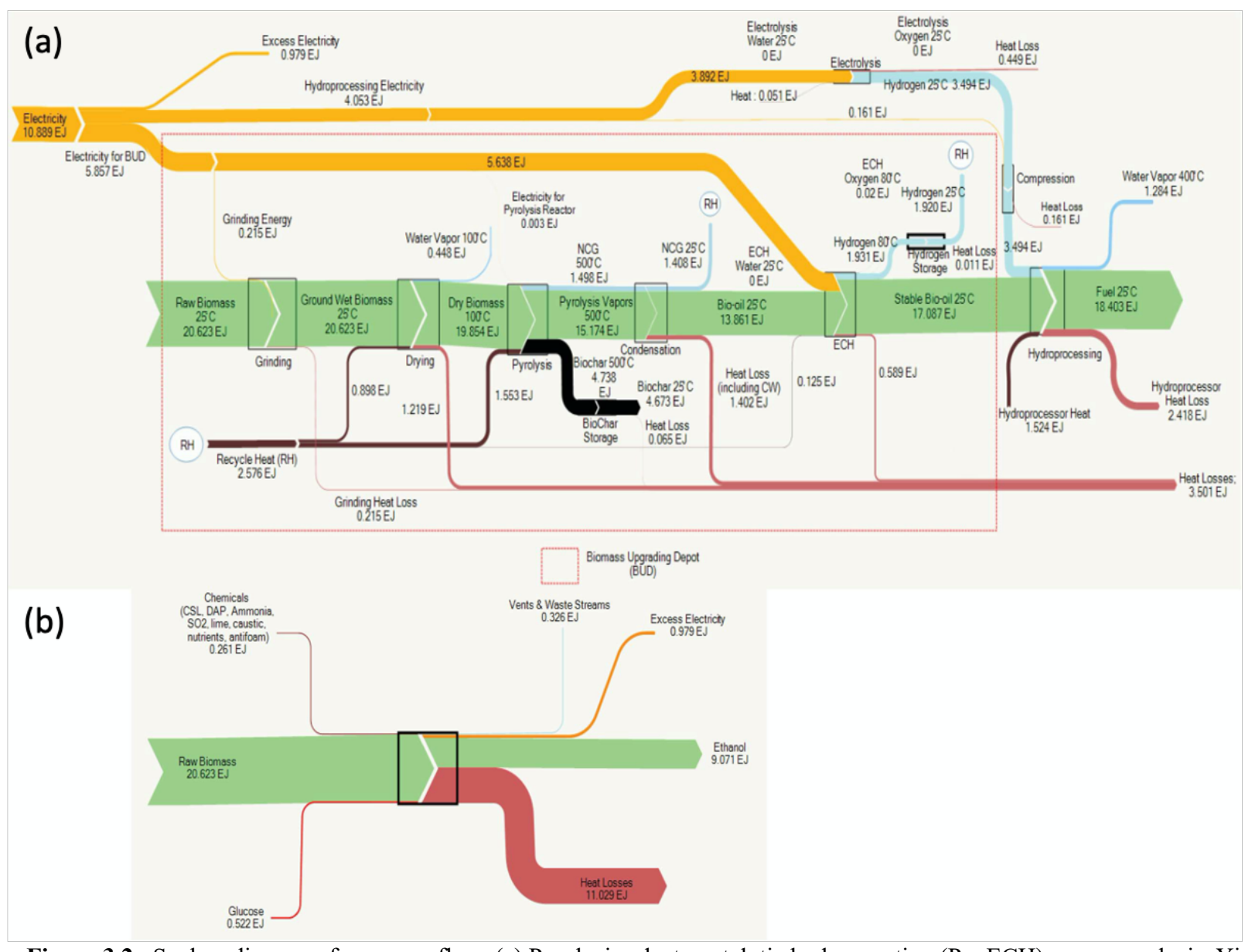


Figure 3.2: Sankey diagrams for energy flow. (a) Pyrolysis–electrocatalytic hydrogenation (Py–ECH) energy analysis. Yield: 89%; (b) CE energy analysis. Yield: 44%.

that the fuel energy produced by the two systems is markedly different, as almost twice as much liquid fuel energy is produced by Py–ECH than by CE using the same biomass input. During CE production, the energy content in the primary fuel stream decreases in every stage, especially during fermentation. In the end, the amount of energy (HHV) available in the product ethanol is 44% of that in the starting biomass. In contrast, the Py–ECH system involves a more modest energy loss through bio-oil production but then regains much of that energy during ECH and hydroprocessing, ultimately yielding hydrocarbon fuel products with approximately 89% of the biomass energy.

These differences in fuel energy yield are explained by differences in electrical power utilization, heat losses, and excess electricity output. The Py–ECH process is a net consumer of electricity, while the CE process generates electricity. In order to neutralize the advantage of excess electricity produced in the CE process, a similar electrical power output of 0.979 EJ was added to the Py-ECH process (as seen in Figure 3.2a). This was done by raising the electrical power input requirement of the Py-ECH process by an equivalent amount. The most noticeable difference between the two systems is the 10.9 EJ of electricity required by the Py-ECH system, while no electrical energy is needed by the CE system. As discussed earlier, this electrical energy input actually benefits the Py-ECH system, as renewable electricity is converted into chemical energy that is stored in the resultant fuel. Net heat losses explain most of the difference, with losses from the Py-ECH process being approximately half of the heat loss from the CE process. No overall heat input is required for the CE process (due to heat integration) or at the BUD for the Py–ECH process as sufficient heat can be provided internally by combustion of the co-product biochar, noncondensable gases (NCG), and H₂ gas. At the central refinery, the stable bio-oil can be preheated using the heat from the outgoing hot water vapor stream. This approach reduces the heat input

required, and subsequently minimizes external fuel combustion required at the central refinery. Additional process modifications to improve fuel energy yield are possible. As seen in Figure 3.2a, the combustion energy of the NCG and the H₂ streams (together indicated by RH in Figure 3.2a) is more than sufficient to support the entire heat requirement of the BUD. In fact, the excess energy, after compensating for the heat requirement, can also be employed to reduce the electricity requirement of the process. When not combusted, the co- product biochar can be used in a number of ways,³⁸ including land application for carbon sequestration. Use of the molecular hydrogen coproduct, generated during ECH, to further hydrogenate bio-oil in depots should also be considered, though the current analysis only utilizes some of its combustion energy for heat.

The CE approach is also expected to be more sensitive to the biomass type, specifically as this relates to lignin content. Fuel energy yield for woody biomass, which typically contains greater lignin content, would be less than for corn stover because energy from the lignin does not become liquid fuel in the CE approach but does in the Py–ECH approach.

The mass balance analyses reveal that the expected Py–ECH fuel mass yield of 38% (Figure 3.3a) is greater than the CE fuel mass yield of only 26% (Figure 3.3b). Biochar and NCG formation account for a mass loss of about 30% as this is not converted into liquid fuel. The overall mass yield for Py–ECH is limited by the high oxygen content of biomass, much of which is converted to water during hydroprocessing. In the CE process shown in Figure 3.3b, a smaller fraction of the feedstock is converted into ethanol as lignin is burned for heat and power and 1/3 of the carbohydrate carbon is converted into carbon dioxide. A striking characteristic of Figure 3.3b, is the significant water requirement in the process. Much of the incoming water can be attributed to process water consumption, mostly lost during cooling water evaporation. The exiting water stream is larger than the incoming stream as water is generated in the combustor, where the lignin

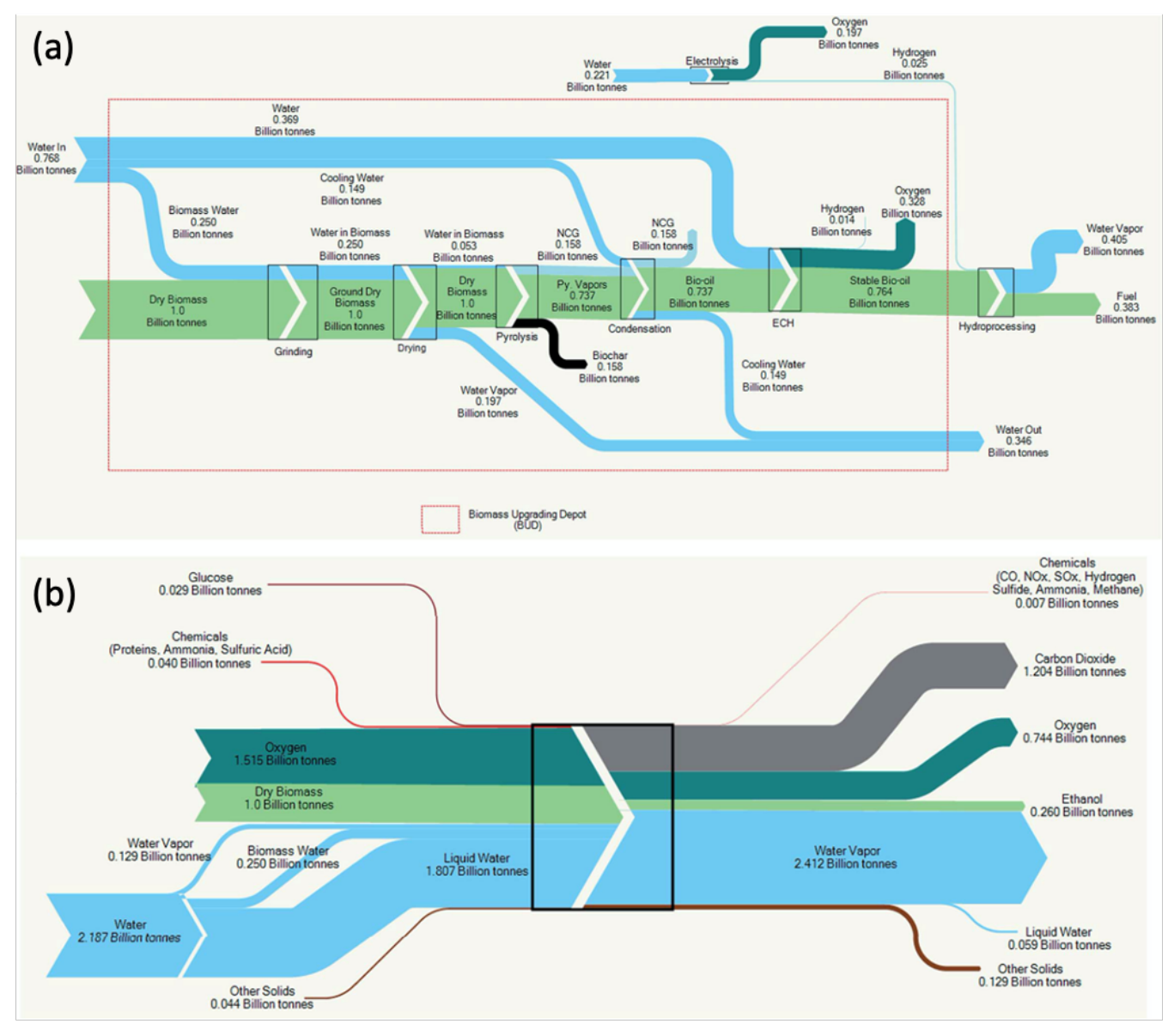


Figure 3.3: Sankey diagrams for mass flow. (a) Pyrolysis–electrocatalytic hydrogenation (Py–ECH) mass analysis. Yield: 38%; (b) CE mass analysis. Yield: 26%.

is combusted. A more detailed analysis can be found in the Appendix. For Py–ECH, much less water is likely to be used in the process. Water consumption in the BUD can be attributed to the ECH unit, which splits water to create hydronium ions that are then recombined with electrons and incorporated into the bio-oil and generated H₂. However, the total water consumption is reduced after combining the hydroprocessing step, as the water vapor generated during hydroprocessing may be condensed for heat integration. The air required in the Py–ECH process for combusting the NCG and H₂ for heat integration, along with the subsequent products of combustion have been excluded from the analysis shown in the Sankey diagram. However, including them does not dramatically change the results as shown in Table 3.12 in the Appendix, which depicts the mass balance that includes air and stack gases. Generally, the mass balance analyses show that the two systems manage matter in greatly different ways. Py–ECH loses mass as biochar, which can be used to mitigate climate change, while CE loses carbon as CO₂, itself a climate gas.

The carbon balance analysis provides additional insight into the fuel product yields discussed previously. In Py–ECH, 63% of the feedstock carbon is retained in the liquid fuel product, while only 30% of feedstock carbon is converted to ethanol by CE as shown in Figure 3.4. In fact, for the CE process, most of the carbon is lost as CO₂ from the combustion flue gas stack. The retention of carbon in the final fuel is important as the carbon–carbon and carbon–hydrogen bonds are the energy carriers in hydrocarbon fuels. ¹⁶⁷ In the case of CE, corn stover is considered an optimistic case for high ethanol yield when compared to other likely feedstocks. Though not the composition used in this study, dried corn stover can contain as much as 81.9% of fermentable holocellulose (comprised of cellulose and hemicellulose) and 14.4% of non-fermentable lignin. ¹⁶⁸ Further, the highest sugar recovery, by acid hydrolysis, has been reported to be 98.4%. ¹⁶⁹ Regardless,

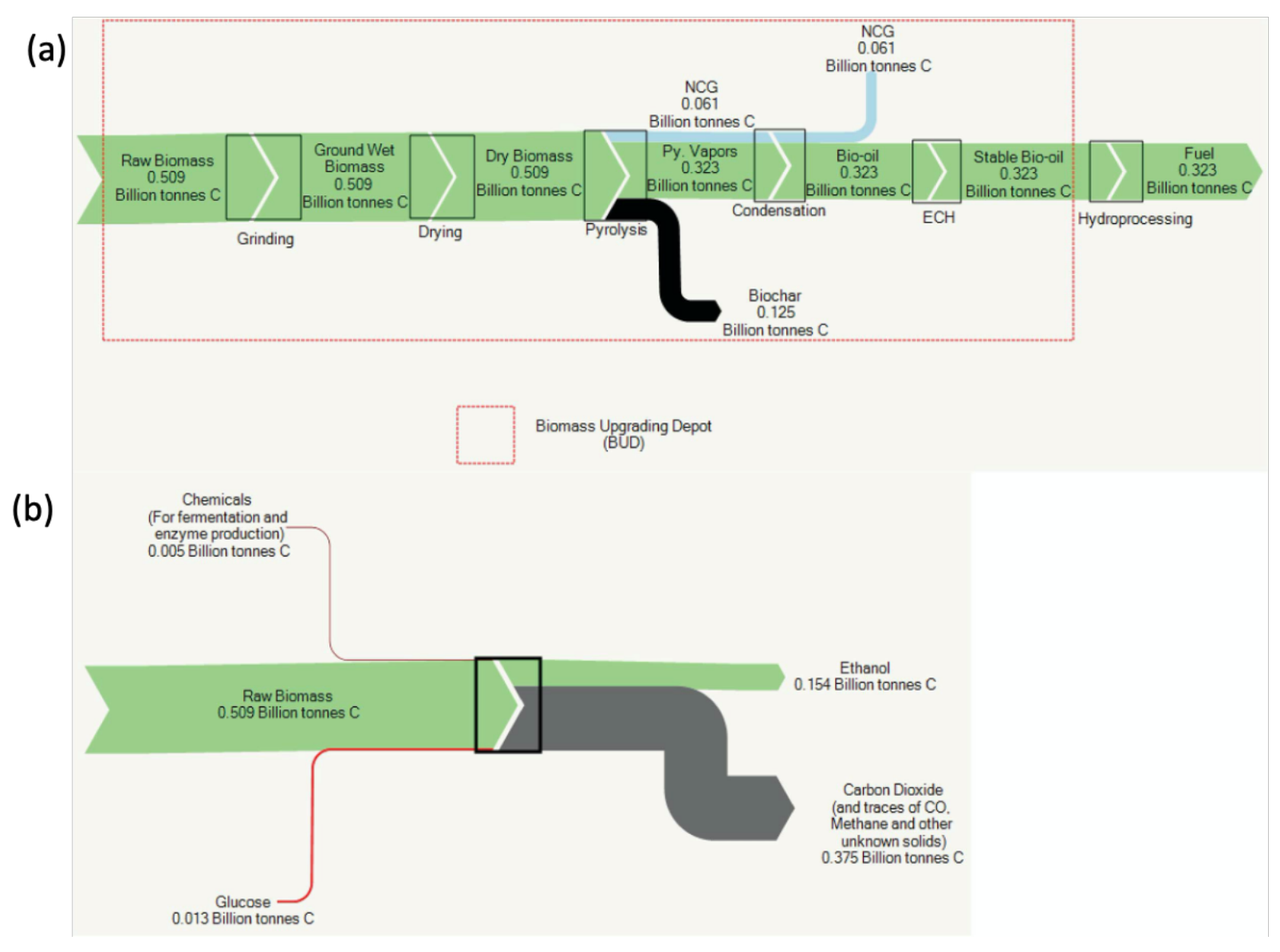


Figure 3.4: Sankey diagrams for carbon flow. a) Pyrolysis–electrocatalytic hydrogenation (Py–ECH) carbon analysis. Yield: 63%; (b) cellulosic ethanol (CE) carbon analysis. Yield: 30%.

fermentation converts glucose to ethanol at the expense of liberating 1/3 of the carbon as CO₂, which constrains the final ethanol yield accordingly. Py–ECH also loses a portion of carbon as non-condensable gases (NCG) and char. However, the NCG (about 12%) released can be utilized for heating. The char, on the other hand, which accounts for about 25% of the biomass carbon, is a useful by-product that may be densified to form a renewable solid fuel or land applied as a soil amendment.¹⁷⁰ The liquid bio-oil, with the majority (about 63%) of the carbon, can be stabilized via a localized ECH system. Through ECH, electrical energy is stored in the newly formed chemical bonds in the upgraded bio-oil, increasing its energy density and bridging renewable electricity with liquid fuel. The partial removal of bio-oil's oxygen improves its storage stability and increases its energy density, which enables and improves the efficiency of transporting bio-oil to distant refineries.¹³² Once there, conventional H₂ upgrading of stabilized bio-oil to fuel becomes more economically feasible as a result of the locally available hydrogen and improved stability.

Comparison of Yields

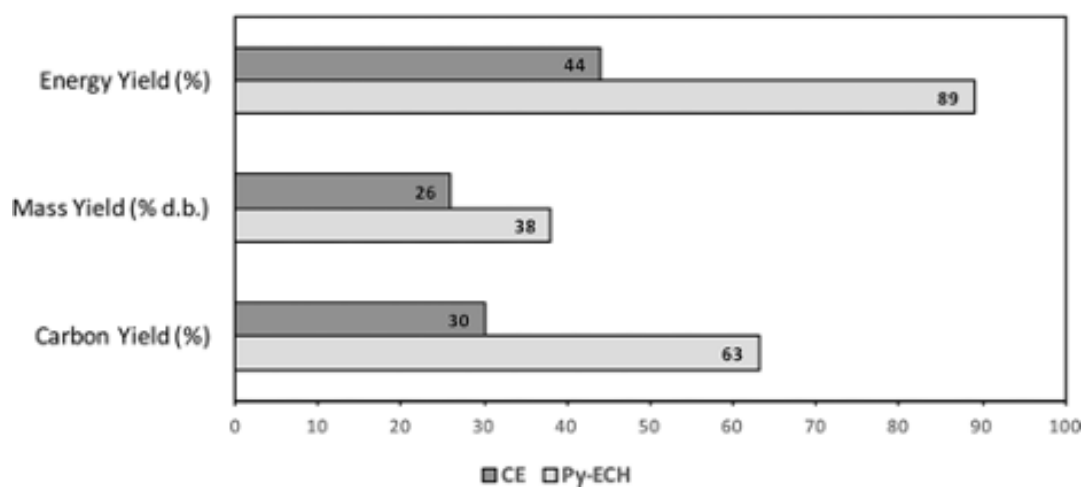


Figure 3.5: Energy, mass and carbon yield comparison of CE and Py–ECH. The energy yield is significantly higher because of addition of electrical energy.

In summary, Py–ECH is superior to CE in terms of energy yield, carbon yield and mass yield of the final liquid fuel product, as shown in Figure 3.5. The difference in energy yield is primarily a result of upgrading bio-oil using renewable electricity and hydrogen that is derived from renewable

electricity. Although fast pyrolysis initially discards almost 31% of the biomass energy and 37% of the biomass carbon as biogas and char, the lost energy is mostly replaced as hydrogen incorporated during electrocatalysis and hydroprocessing – a key step of energy upgrading that is not present in the CE scheme. About 75% of the biomass energy, lost during pyrolysis, is recovered after the ECH and hydroprocessing steps. This is because both these processes add electrolytic hydrogen to the pyrolysis bio-oil and the low molecular weight and high specific energy of hydrogen serves as an ideal upgrading ingredient. Further details of the quantitative analysis of hydrogen formation and its incorporation into bio-oil can be found in the Appendix. Stabilized bio-oil gains little mass while dramatically increasing in energy content and stability relative to raw bio-oil. Fuel production from stabilized bio-oil using hydrodeoxygenation requires less hydrogen than raw bio-oil as significant hydrogenation has already occurred through electrocatalysis. In other words, the stabilized bio-oil, leaving the BUD, is upgraded in energy content, relative to the raw bio-oil. In fact, as seen in Fig. 3.2a, about 71% of the total upgrading is already achieved by ECH before leaving the depot. Further, if the electricity is derived from renewable sources, then the entire energy content of the fuel would have been derived from renewable sources. Although electrocatalysis has limited ability to deoxygenate bio-oil when compared to traditional hydroprocessing, the energetic and economic value of bio-oil can be augmented substantially under mild conditions by electrocatalysis after pyrolysis in regional biomass upgrading depots.

Discussion and Outlook

Py–ECH systems appear to be advantaged in terms of energy, mass and carbon balances, though further work is certainly needed to assess the economics and environmental impacts associated with this hydrocarbon fuel strategy. Although the Py– ECH process produces less carbon dioxide

than the CE process, a full life-cycle assessment is needed to ascertain its environmental benefits with and without biochar land application. It is noteworthy that climate change potential is significantly reduced when co-product biochar is land applied.⁴¹ In addition to reversing the greenhouse effect, biochar has a range of potential applications, 38, 171 including pollutant remediation⁴⁰ or stationary power production, although its optimum usage depends on many factors that are location specific. Biomass upgrading depots are integral features of the Py- ECH concept. For commercial adoption, the number, size, and design of these depots should be optimized to balance the logistical advantage of depots with the economies of scale of a large refinery complex. Real geographical landscapes must be considered when deciding where depots should be located in relation to feedstocks and centralized facilities. Therefore, technoeconomic and life-cycle analyses, with system-wide optimization, should be conducted.⁶⁹ Until direct aircapture of CO₂ and subsequent reduction processes are proven economically viable at very large scale, carbon efficient bioenergy systems may prove essential to meeting future demand for lowfossil carbon transportation fuel. As ECH of bio-oils is a nascent technology, its technology readiness level will need to elevate before it is ready for commercial application. In this regard, bench and pilot-scale studies of ECH reactor conditions, such as optimization of temperature, catalyst activity, catalyst reusability, current density, residence time, and proton exchange membrane properties must be performed to maximize economic viability.^{23, 132} A similar progression of experimentation is needed to convert post ECH bio-oil into finished hydrocarbons, presumably by catalytic hydroprocessing. Finally, the finished fuel should possess comparable energy content and fuel properties to commercial hydrocarbon fuels (e.g. gasoline, diesel, and jet fuel) and a robust analytical characterization will be needed to determine the quality of such fuels.

Conclusions

The incorporation of hydrogen and electricity from renewable sources, such as wind and solar energy, significantly improves bio-oil's potential as a sustainable alternative fuel. In this analysis, carbon retention in the Py–ECH scheme is twice that of producing cellulosic ethanol. The process also consumes significantly less water and thus the distributed Py–ECH process offers many system-level benefits. At the scale of this analysis, synthesis of fuel would use very roughly as much electrical energy as all existing electricity consumers, while the inventory of precursors and fuel products equates to an energy storage system several orders of magnitude larger and cheaper than any that could be assembled from electrochemical batteries. The controllable electrical load of these distributed conversion plants may play an essential role in managing the electric grid with its growing fraction of variable renewable generators. The synergies between carbon efficient use of biomass, familiar liquid hydrocarbon fuel and renewable electricity may be the foundation of a future fossil-carbon-free energy economy.

APPENDIX

This section details the calculation methods used to determine the values depicted in the Sankey diagrams for both the Py-ECH and the CE processes.

Py-ECH Process

Table 3.1: Label Definitions for the Process Flow Diagram

Label	Process
A	Grinding
В	Drying
C	Fast Pyrolysis
D	Condensation
E	Electrocatalytic Hydrogenation
F	Fuel Storage
G	Fuel Transportation
Н	Electrolysis
I	Hydrogen Compression
J	Hydroprocessing
K	Biochar Storage
L	Hydrogen Storage

Overview of the Process:

For the Py-ECH process, as shown in Figure 3.6, harvested biomass feedstock is first milled in a series of grinders (A) and then dried in a rotary dryer (B) to a moisture of 5%. The ground dry biomass (BM) is then fast pyrolyzed in a screw reactor. The biochar (BC) is collected, while the pyrolysis vapors (PyV) are condensed in a condenser (D) to produce the primary product bio-oil. The non-condensable gases (NCG) may be used for heating purposes. The bio-oil (BO) is subsequently fed into the electrocatalytic hydrogenation (ECH) unit, wherein it is chemically reduced to produce the stable bio-oil (SBO). The ECH unit (E) is considered to be a 2-compartment electrolytic cell, separated by a proton-exchange membrane. The mildly hydrogenated product from E is then transported to a petroleum refinery, where it is upgraded to a gasoline-like fuel. This upgrading occurs in a hydroprocessor unit (J) under more severe operating conditions. The compressed hydrogen gas required for the process is provided by the electrolysis

of water in a local electrolyser unit (H). The product from the hydroprocessor unit is referred in the following sections as upgraded biooil (UBO).

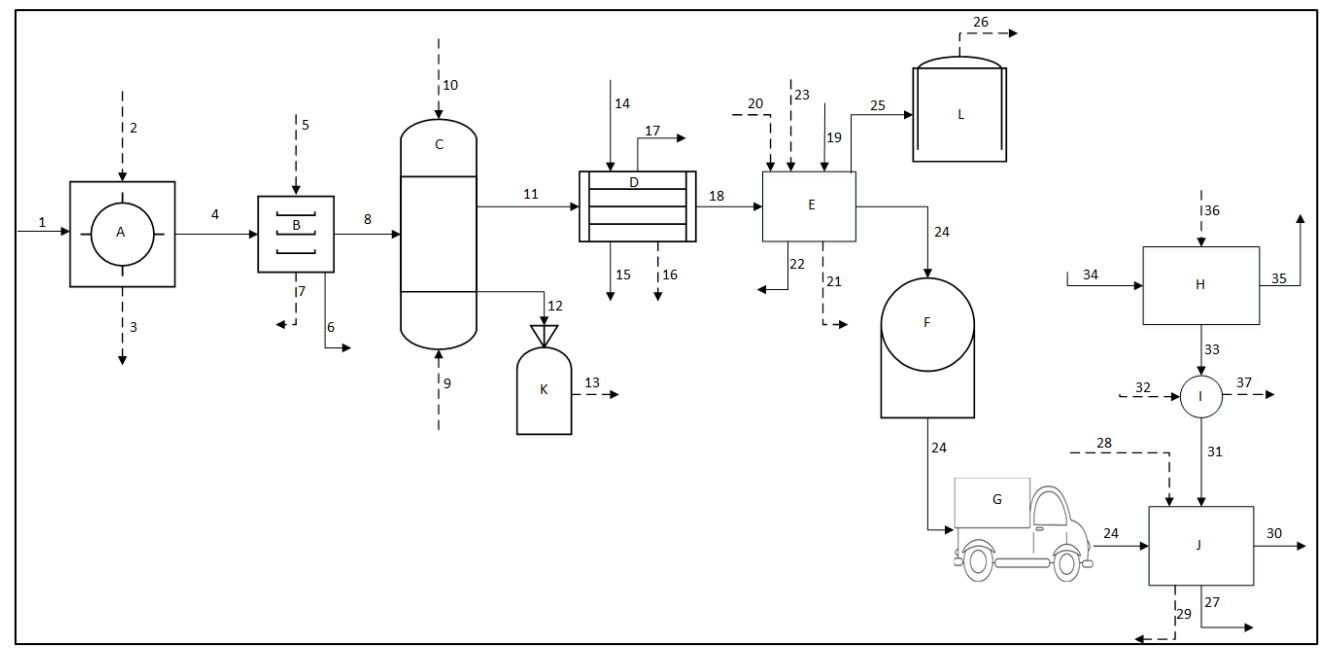


Figure 3.6: Process Flow Diagram for Py-ECH Process

Feedstock:

To compare the Py-ECH process to NREL's CE process, the biomass feedstock selected was corn stover. The empirical formula was determined from the ultimate analysis data for corn stover.⁸⁴ The extracted mass percentages were normalized to exclude all elements but carbon, hydrogen and oxygen. Feedstock moisture content was reduced from 20% for the raw biomass to 5% for the ground, dried biomass.

The feed rate of biomass was assumed to be 1.0 billion dry tonnes/year, which is approximately the entire biomass potential of the United States, in 2030, that can be produced at \$60/dry ton or less.¹⁷² The higher heating value of corn stover was evaluated from ultimate analysis data.⁸⁴ The feedstock data have been summarized in Table 3.2.

Table 3.2: Feedstock Data for Py-ECH

Tuble Cole : T country I was fell I just I j		
Feedstock	Corn Stover	
Empirical Formula	$CH_{1.412}O_{0.714}$	
Raw biomass moisture %	20%	
Dried biomass moisture %	5%	
Dried biomass HHV	18.860 MJ/kg	
Dried biomass feed rate	1.050 Billion tonnes/year	

The mass and energy balances for all primary unit operations involved in the Py-ECH process were performed as described in the next section.

Major Processes:

1. Calculation Methods

- A. Mass Balances: The mass values for each stream were reported in units of Billion tonnes/yr.
- B. Carbon Balances: The carbon values were reported in units of Billion tonnes C/yr.
- C. Energy Balances: The energy values were reported in units of EJ/yr. The energy balances were performed on a higher heating value basis. This implies that the energy value of each stream had three components:
 - a. The higher heating value of the stream at the reference state.
 - b. A sensible heat component to raise the temperature of the stream from the reference state temperature.
 - c. A latent heat component for any change of phase of all or part of the stream.
- D. Reference State: The reference state was selected to be 25°C and 1 bar pressure.

E. Higher Heating Values: The higher heating values (HHV) required for making the energy balances, were calculated using the Gaur and Reed formula:¹⁷³

$$HHV = (0.3491X_C) + (1.1783X_H) + (0.1005X_S) - (0.0151X_N)$$
$$- (0.1034X_O) - (0.0211X_{ash})$$

where Xi's = mass percentage and HHV is in MJ/kg.

The mass percentages were determined from ultimate analysis data provided in the literature. On certain occasions however, the HHV values were directly extracted from literature.

- a) Thermophysical Properties: The thermophysical properties like specific heat and latent heat of vaporization were extracted from the NIST database in Aspen or were estimated using Group Contribution Theory. 174-178
- b) Sample Calculation: A sample calculation is shown below for the energy balance around the pyrolysis reactor. The fast pyrolysis reaction can be modelled by the following equation:

Biomass $\rightarrow N_1$ Pyrolysis Vapors + N_2 Biochar + N_3 CO + N_4 H₂ + N_5 CO₂ where N_i refer to the stoichiometric coefficients.

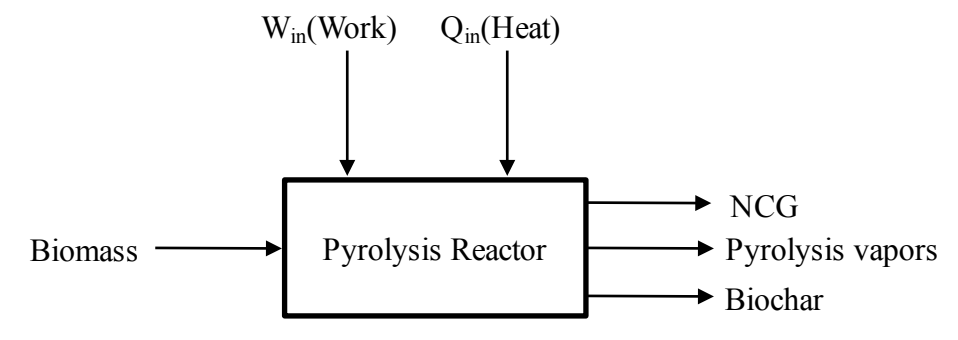


Figure 3.7: Process Flow Diagram for Pyrolysis of Biomass

For the reactor shown in Figure 3.7, the energy balance is given by:

$$m_{BM}h_{f,BM}^{0} + Q_{in} + W_{in}$$

$$= m_{PyV} \left(h_{f,PyV}^{0} + (h_{PyV} - h_{PyV,r}) \right) + m_{BC} \left(h_{f,BC}^{0} + (h_{BC} - h_{BC,r}) \right)$$

$$+ m_{CO} \left(h_{f,CO}^{0} + (h_{CO} - h_{CO,r}) \right) + m_{H_{2}} \left(h_{f,H_{2}}^{0} + (h_{H_{2}} - h_{H_{2},r}) \right)$$

$$+ m_{CO_{2}} \left(h_{f,CO_{2}}^{0} + (h_{H_{2}O} - h_{CO_{2},r}) \right)$$
.....(1)

which can be rearranged to:

$$m_{BM}h_{f,BM}^{0} + Q_{in} + W_{in} - \sum_{i} m_{i}(h_{i} - h_{R,i})$$

$$= m_{BO}(h_{f,PyV}^{0}) + m_{BC}(h_{f,BC}^{0}) + m_{CO}(h_{f,CO}^{0}) + m_{H_{2}}(h_{f,H_{2}}^{0})$$

$$+ m_{CO_{2}}(h_{f,CO_{2}}^{0})$$
......(2)

where m_i refers to mass of the i^{th} stream and $h_{f,i}^o$ refers to enthalpy of formation of the the i^{th} stream.

The heat of combustion for Biomass (BM), Pyrolysis Vapors (PyV), CO, H₂ and Biochar (BC) are given by:

$$-m_{CO_2}h_{f,CO_2}^0 - m_{H_2O}h_{f,H_2O}^0 = H_{C,BM} - m_{BM}h_{BM}^0 ...$$
(3)

$$-m_{CO_2}h_{f,CO_2}^0 - m_{H_2O}h_{f,H_2O}^0 = H_{C,PyV} - m_{PyV}h_{PyV}^0 ...$$
(4)

$$-m_{CO_2}h_{f,CO_2}^0 - m_{H_2O}h_{f,H_2O}^0 = H_{C,BC} - m_{BC}h_{BC}^0 ...$$
(5)

$$-m_{CO_2}h_{f,CO_2}^0 = H_{C,CO} - m_{CO}h_{f,CO}^0 ...$$
(6)

$$-m_{H_2O}h_{f,H_2O}^0 = H_{C,H_2} - m_{H_2}h_{f,H_2}^0 ...$$
(7)

where H_{C,i} refers to the heat of combustion of the ith component.

(3) to (7) are derived by considering the complete combustion of each component to CO_2 and H_2O . The heat of combustion of any compound is the negative of the enthalpy change for the combustion reaction. The standard enthalpy of formation of O_2 is zero, and therefore does not appear in (3) to (7). Subtracting equations (4) to (7) from (3):

$$\left(-m_{CO_2}h_{f,CO_2}^0 - m_{H_2O}h_{f,H_{2O}}^0\right)_{BM} - \left(-m_{CO_2}h_{f,CO_2}^0 - m_{H_2O}h_{f,H_{2O}}^0\right)_{PyV}$$

$$- \left(-m_{CO_2}h_{f,CO_2}^0 - m_{H_2O}h_{f,H_{2O}}^0\right)_{BC} + m_{CO_2}h_{f,CO_2}^0 + m_{H_2O}h_{f,H_{2O}}^0$$

$$= -H_R - m_{BM}h_{BM}^0 + m_{PyV}h_{PyV}^0 + m_{BC}h_{BC}^0 + m_{CO}h_{f,CO}^0 + m_{H_2}h_{f,H_2}^0$$

$$\dots \dots (8)$$

where $H_R = -H_{C,BM} + H_{C,PyV} + H_{C,BC} + H_{C,CO} + H_{C,H_2}$ is the heat of reaction of the pyrolysis process. The heat of combustion of carbon dioxide is zero and therefore is not included.

As $H_R = -m_{BM}h_{BM}^0 + m_{PyV}h_{PyV}^0 + m_{BC}h_{BC}^0 + m_{CO}h_{f,CO}^0 + m_{H_2}h_{f,H_2}^0 + m_{CO_2}h_{f,CO_2}^0$ also, the left hand side of (8) equals $-m_{CO_2}(h_{f,CO_2}^0)$.

Adding (8) to (2):

$$m_{BM}h_{f,BM}^{0} + \left(-m_{CO_{2}}h_{f,CO_{2}}^{0} - m_{H_{2}O}h_{f,H_{2}O}^{0}\right)_{BM} + Q_{in} + W_{in} - \sum_{i} m_{i} \left(h_{i} - h_{R,i}\right)$$

$$= \left(m_{PyV}\left(h_{f,PyV}^{0}\right) + \left(-m_{CO_{2}}h_{f,CO_{2}}^{0} - m_{H_{2}O}h_{f,H_{2}O}^{0}\right)_{PyV}\right) + \left(m_{BC}\left(h_{f,BC}^{0}\right) + \left(-m_{CO_{2}}h_{f,CO_{2}}^{0} - m_{H_{2}O}h_{f,H_{2}O}^{0}\right)_{BC}\right) + \left(m_{CO}\left(h_{f,CO}^{0}\right) + m_{H_{2}}\left(h_{f,H_{2}}^{0}\right) - m_{CO_{2}}\left(h_{f,CO_{2}}^{0}\right) - m_{H_{2}O}\left(h_{f,H_{2}O}^{0}\right)\right)$$

$$\dots (9)$$

Where $m_i HHV_i = \sum_{reactants} m_i h_{f,i}^0 - \sum_{products} m_i h_{f,i}^0$ for the complete combustion reaction of the corresponding component with product water in the liquid state. Note that NCG refers to the combined stream of CO, CO₂ and H₂.

Therefore, for the pyrolysis reactor:

- i. Energy associated with incoming biomass (E_{BM}): $m_{BM}HHV_{biomass}$
- ii. Energy associated with Pyrolysis Vapors (E_{PyV}) :

$$\left(m_{PyV}HHV_{PyV}+m_{PyV}\left(h_{PyV}-h_{PyV,R}\right)\right)$$

iii. Energy associated with Biochar (E_{BC}):

$$\left(m_{BC}HHV_{BC}+m_{BC}\left(h_{BC}-H_{BC,R}\right)\right)$$

iv. Energy associated with non-condensable gases (E_{NCG}):

$$\left(m_{NCG}HHV_{NCG}+m_{NCG}(h_{NCG}-h_{NCG,R})\right)$$

- v. Work input required (W_{in}): Electrical energy required by the pyrolysis reactor.
- vi. Heat required by pyrolysis (Qin):

$$Q_{in} = E_{BM} - E_{PyV} - E_{BC} - E_{NCG} - W_{in}$$

Finally, both the sensible and the latent heat components are included in the $(h_i - h_{i,R})$ term.

2. Grinding

The raw biomass feedstock is ground from a size of 50 to 200 mm to about 2 mm using hammer mills. The grinding energy requirement was evaluated from literature.¹⁷⁹ The

entire energy supplied was assumed to be lost as heat and there was no change in energy of the biomass.

Table 3.3: Operating conditions for grinding

110010 010 1 0	bername communers for Simoning
Temperature	25°C
Pressure	1 bar
Grinding Energy	0.215 MJ/kg of dry biomass

3. Drying

The ground biomass feedstock is dried in a rotary dryer from an initial moisture content of 20% to a final moisture content of 5%. The minimum drying energy requirement was calculated by determining the amount of heat required to evaporate moisture in the feedstock from 20% to 5%. This heat was doubled to approximate the actual energy required for the process. 180

Table 3.4: Operating conditions for drying

Temperature	100°C
1	100 6
Pressure	1 bar
Feed Moisture Content	20%
\mathbf{p} 1 \mathbf{M} \mathbf{r}	50 /
Product Moisture Content	5%

4. Fast Pyrolysis

In the pyrolysis screw reactor, the dried biomass is heated to a temperature of 500°C at atmospheric pressure in the absence of air. The vapor residence time is assumed to be 30 seconds. The pyrolysis products were considered to be pyrolysis vapors (forms bio-oil when condensed), biochar, and NCG, with the yields assumed as 70%, 15%, and 15% by weight respectively. The NCG was composed of only CO, CO₂ and H₂. To arrive at a stoichiometric balanced reaction for the fast pyrolysis reaction, the empirical formulae of biochar and pyrolysis vapors were determined.

- a) Biochar: The empirical formula for the biochar was determined from literature.⁸⁴ The HHV was also calculated using the Gaur and Reed formula by utilizing the ultimate analysis data provided.⁸⁴
- b) Pyrolysis Vapors: In order to determine an empirical formula for the pyrolysis vapors, which is an extremely complex mixture of organic compounds, certain representative compounds were selected. The mass fractions of these representative compounds, corresponding to different functional groups were estimated from Figure 3.8. The mass fraction of water was assumed to be 18% and the mass fractions of the other representative compounds were normalized accordingly. The pyrolysis vapors were subsequently condensed, and the condensed liquid was referred to as bio-oil. The model representative compounds and the assumed mass percentages are presented in Table 3.5. Subsequently, the empirical formula was determined. The HHV was once again calculated using the Gaur and Reed formula.
- c) NCG: The NCG were assumed to be composed of CO, CO₂ and H₂ only.

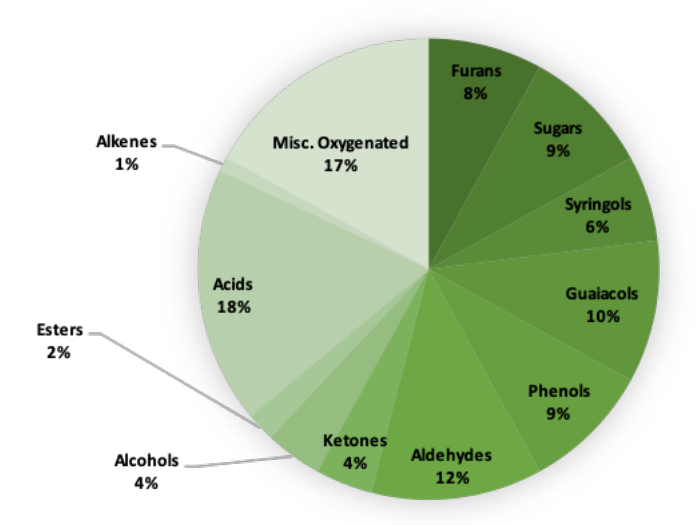


Figure 3.8: General Distribution of Functional Groups in Bio-oil¹⁸

Table 3.5: Representative Compounds in PyV

Compound	Mass percentage
Water	18.00
Acetic Acid	19.17
Glycolaldehyde	9.05
Phenol	9.58
Furfural	8.52
Guaiacol	10.65
Levoglucosan	9.58
Acetol	9.05

After evaluation of the empirical formulae of biochar and pyrolysis vapors, the balanced stoichiometric equation was determined as follows:

$$CH_{1.42}O_{0.71} \rightarrow 0.63CH_{1.99}O_{0.84} + 0.25CH_{0.50}O_{0.17} + 0.02CO_2 + 0.02H_2 + 0.10CO$$

Table 3.6: Fast Pyrolysis Data

1 abic 3.0 . 1 ast 1 yrorysis	Data
Temperature	500°C
Pressure	1 bar
Pyrolysis Vapor Empirical Formula	$CH_{1.99}O_{0.84}$
Biochar Empirical Formula	$CH_{0.50}O_{0.17}$
HHV of pyrolysis vapors	18.811 MJ/kg
HHV of biochar	29.594 MJ/kg

The biomass enters the reactor at 25°C and heat is provided to raise the temperature to 500°C. The products are evolved at the latter temperature. Assuming no heat loss from the reactor and calculating the electrical input required (as shown below), the heat required for pyrolysis can be calculated from the difference in enthalpy streams of the reactants and the products. While the biochar is sent to storage, the NCG and the pyrolysis gases are fed to the condenser. The electrical energy required for rotating the auger in the pyrolysis reactor was calculated as follows:

The auger was assumed to have: 181

- Shaft Diameter $(d_s) = 0.064m$
- Flight Diameter $(d_f) = 0.25m$
- Pitch length $(l_p) = 0.229$ m

As the density of corn stover (ρ) is 90 kg/m³,¹⁸² a 100 dry ton/day facility corresponds to a volumetric flow rate of about 0.7 m³/min. Using the relation,

$$Q_a = A * l_p * n * \eta$$

where Q_a is the actual volumetric flow rate in m^3 /min; A is the cross-sectional area occupied by the reacting material in m^2 ; n is the rotations per minute, and η is the volumetric efficiency (the ratio of actual and theoretical volumetric flow rates).¹⁸³ Therefore,

$$Q_a = \left(\frac{\Pi}{4}\right) * \left(d_f^2 - d_s^2\right) * l_p * n * \eta$$

Assuming a volumetric efficiency of 35%, n can be evaluated to be approximately 200 rpm, which corresponds to about 3 kW of power.¹⁸² This scales up to about 0.003 EJ/yr for processing 1 Billion tonnes/year of dry corn stover.

It must also be noted that the reactor length required for a residence time of 30s and a pitch of 0.229m for the 100 ton/day reactor was found to be less than 75 ft, which is a feasible reactor length.¹⁸⁴

Figure 3.9 shows the streams entering and leaving the pyrolysis reactor, information on the energy content, mass content, and carbon content is given in the tables at the end of this appendix.

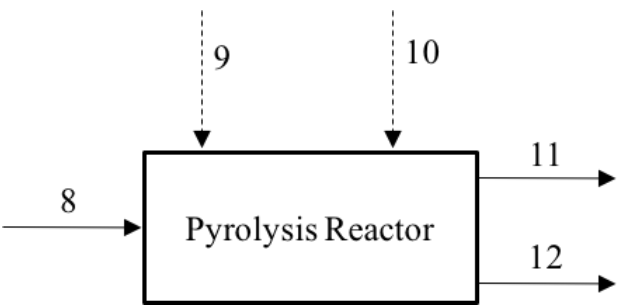


Figure 3.9: Process flow diagram for pyrolysis

5. Condensation

Well water entering at 13.33°C and leaving at 20°C was assumed in order to cool the entering gases from 500°C to 25°C. The condensed pyrolysis vapors formed the bio-oil, whereas the NCG gases were separated. The NCG gases contain energy and may be burned to heat the pyrolysis reactor. Heat losses are considered in the condenser.

Table 3.7: Condensation Data

Empirical formula of condensed Bio-oil	$CH_{1.99}O_{0.84}$
HHV of formed bio-oil	$18.811 \mathrm{MJ/kg}$
Inlet temperature of cooling water	13.33°C
Outlet Temperature of Cooling water	20°C

The streams entering and leaving the condenser are shown in Figure 3.10.

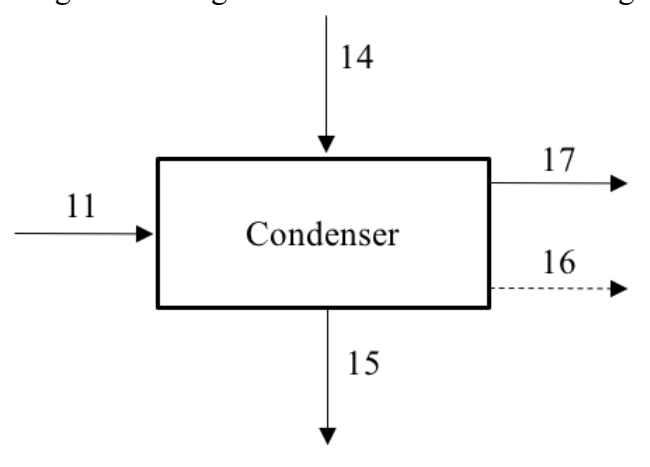


Figure 3.10: Condenser Flow Diagram

6. Electrocatalytic Hydrogenation

The pyrolysis vapors were fed to the ECH unit, where they were electrocatalytically hydrogenated to stable bio-oil (SBO). As this is only a thermodynamic model, the ECH unit was assumed to be a 2-compartment electrolytic cell, separated by a Nafion-117 membrane. Oxidation was performed at the Pt anode and reduction at the Ru cathode, which is supported on Activated Carbon Cloth (ACC).³² The apparatus considered is shown in Figure 3.11.

The ECH unit uses external electrical power to split water into oxygen and H⁺ ions at the anode. These H⁺ ions then migrate through the Nafion membrane (a proton exchange membrane) and hydrogenate the bio-oil at the catalytic cathode. An undesirable side reaction involving the evolution of H₂ was also considered at the cathode. In summary, the reactions involved at the cathode and anode are as follows:

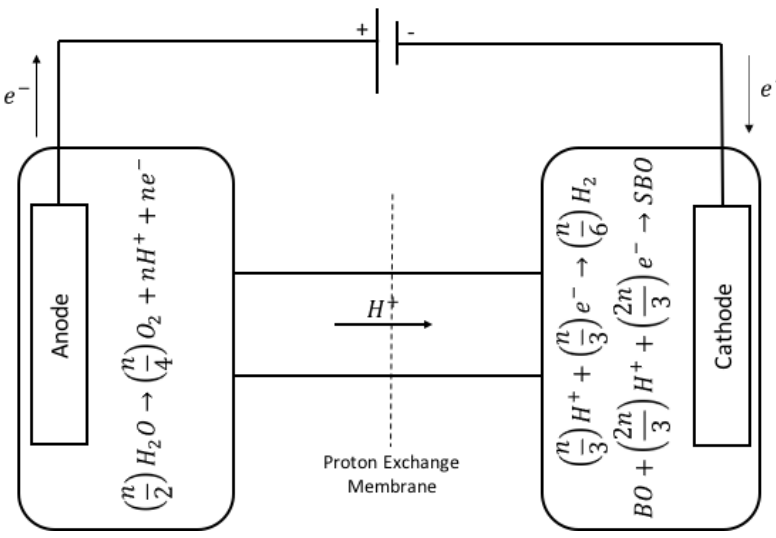


Figure 3.11: Schematic of ECH Apparatus

Cathode Reactions:

1) Bio-oil+
$$\frac{2n}{3}$$
 H⁺+ $\frac{2n}{3}$ e⁻ \rightarrow Stable bio-oil
2) $\frac{n}{3}$ H⁺ + $\frac{n}{3}$ e⁻ $\rightarrow \frac{n}{6}$ H₂

Anode Reaction:

$$\frac{n}{2}H_2O \rightarrow nH^+ + ne^- + \frac{n}{4}O_2$$

Where n is the number of moles of hydrogen ions required to reduce 1 mole of bio-oil to stable bio-oil.

To find the value of n, the empirical formula of SBO was determined. Here too, certain representative compounds were selected. These compounds were selected such that they result from the hydrogen addition to one or more compounds selected as part of the bio-oil mixture. The mass fractions for SBO were evaluated from the stoichiometry of these

hydrogen addition reactions by knowing the mass fractions of the representative compounds in the bio-oil. During this reaction, only the number of H atoms changed in the empirical formula of bio-oil to make SBO, as only hydrogen addition takes place. The value of n was then determined by balancing the cathode reaction (1).

Assuming a current efficiency (electrons in desired products divided by total electrons passed) equal to 67%, the needed water splitting and the amount of H₂ liberated were calculated. Using Group Contribution Theory to estimate the Gibbs free energies for the reduction reaction for each species, the minimum external voltage required for the ECH of bio-oil was found to be 1.07V. To account for the resistance associated with the electrolyte, the electrode overpotentials, and the required activation energies, this voltage value was increased to a value of 1.43V, by assuming a voltage efficiency of 75%. The power consumption was then determined by the following formula:²⁴

$$P_W = (i*V)$$

where i is current, V is applied voltage, and P_{W} is the power consumption.

The assumed operating conditions and the empirical formulae determined for the BO and the SBO are presented in Table 3.8. The reactions considered for the hydrogenation of bio-oil to stable bio-oil are presented in Figure 3.12.

Table 3.8: Key Data for ECH

	Butta for Bell
Temperature	80°C
Pressure	1 bar
Bio-oil Empirical Formula	$CH_{1.99}O_{0.84}$
Stable Bio-oil Empirical Formula	$CH_{3.01}O_{0.84}$
Stable Bio-oil Model Compounds	Water, methanol, ethanol, levoglucosan,
	propylene glycol, ethylene glycol,
	furfuryl alcohol and cyclohexanol

Figure 3.12: ECH Reactions Considered in this Analysis

The balanced overall chemical reaction for the ECH reaction is given as:

$$CH_{1.99}O_{0.84} + 0.51H_2 \rightarrow CH_{3.01}O_{0.84}$$

A heat input was considered for the ECH reactor to raise the temperature of the reactant streams to the required temperature. Heat losses were considered in the ECH reactor. A schematic showing the input and output streams to the ECH reactor is shown in Figure 3.13.

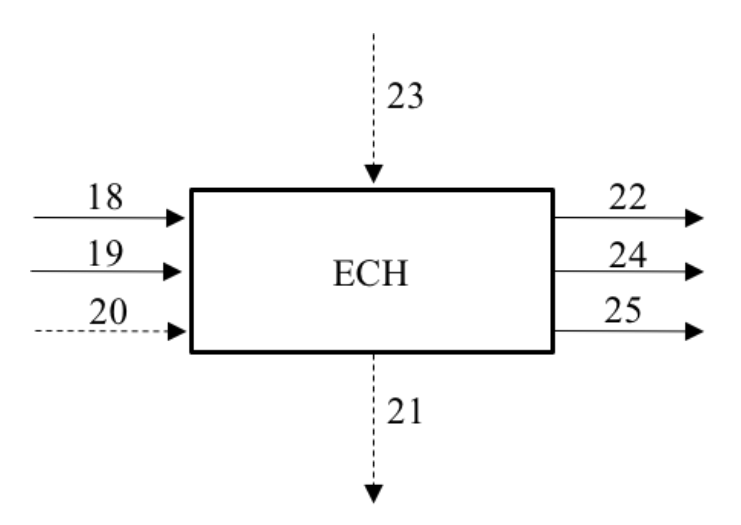


Figure 3.13: Process Flow Diagram for ECH

7. Hydroprocessing

SBO is transported from the depot to a centralized refinery for hydroprocessing. In the hydroprocessor, the SBO is reacted with H₂ at elevated temperatures and pressures. For simplicity, hydroprocessing was assumed to only produce octane and water at these extreme conditions.

The overall balanced reaction for hydroprocessing was determined as:

$$CH_{3,01}O_{0.84} + 0.46H_2 \rightarrow 0.13C_8H_{18} + 0.84H_2O$$

Heat was provided to the reactants balanced reaction for hydroprocessing was determined to achieve the desired temperature. The hydrogen gas required for the process was supplied by performing local electrolysis of water.

The operating conditions for the hydroprocessor are provided in the Table 3.9.

Table 3.9 : Hydroprocessing Data				
Temperature	400°C			
Pressure	20 bar			
Empirical Formula of SBO	$CH_{3.01}O_{0.84}$			
Empirical Formula of UBO	C_8H_{18}			

A schematic for the hydroprocessing unit is shown in Figure 3.14.

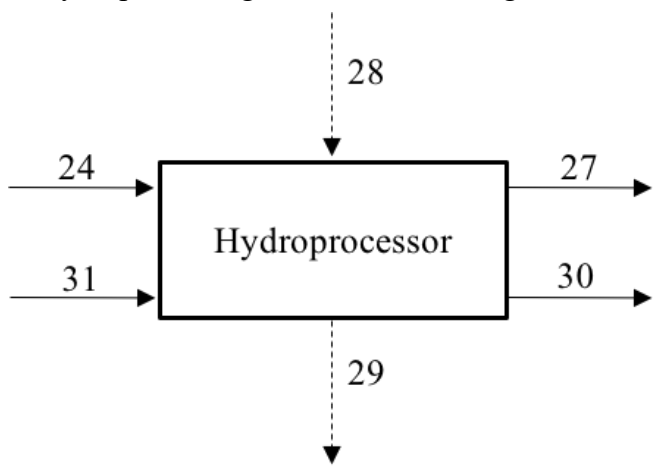


Figure 3.14: Hydroprocessor Process Flow Diagram

8. Electrolysis

Electrolysis was used to provide the hydrogen needed by hydroprocessing at the petroleum refinery. The minimum external voltage required was assumed to be 1.23 V, corresponding to electrolysis of water. Here too, the voltage efficiency was assumed to be 75%. The current efficiency is not applicable here since hydrogen evolution is the only reaction occurring at the cathode. The electrical energy required for the process and the required heat input to raise the reactant temperatures to the reactor temperature were calculated in

the same way as for ECH. The operating conditions for the electrolysis unit are given in the Table 3.10.

Table 3.10: Electrolysis Operating Conditions

	<u> </u>	1 8
Temperature		80°C
Pressure		1 bar

The electrolysis unit is followed by a compressor, which isothermally compresses the produced H₂ to a pressure of 200 bar, which is then fed to the hydroprocessing reactor.

9. Storage

Storage heat losses have been considered for the biochar storage and hydrogen gas storage. These have been determined by estimating the amount of heat liberated when the stored substance thermally equilibrates with the surroundings. The surrounding temperature was assumed to be 25°C at atmospheric pressure.

10. Heat Integration

No external heat source is required for the Biomass Upgrading Depot (BUD), as the evolved NCG and H₂ gases have sufficient combustion energy to provide heat to the BUD. Biochar that is not needed for combustion energy can be land applied to sequester carbon. Finally, the air requirement and the composition of the stack gas for the required combustor at the BUD is detailed in Table 3.12.

The heat needed to preheat the stable bio-oil feed may, in part, be provided by recycling thermal energy present in the water vapor product that exits the hydroprocessor. Heat can also be transferred from the hydroprocessor itself during its operation.

The most important values to construct the Sankey diagrams for the Py-ECH process are listed in Table 3.11. The stream numbers mentioned in Table 3.11, correspond to the stream numbers used through Figures 3.4, 3.5, 3.8 and 3.9.

CE Process

For the CE (cellulosic ethanol) process, all values were extracted from the 2011 NREL report detailing the cellulosic ethanol biorefinery. The extracted values are listed in Table 3.13. These values were then normalized to the scale assumed for the Py-ECH process, to enable a fair comparison. The Sankey diagrams for the CE process were drawn for the entire system upon formulating overall mass, energy and carbon balances, as shown in Tables 3.14-3.16. The water balance for the CE process is included in Table 3.17.

Stream Tables

This section lists the carbon, energy and mass values of all streams involved in the different bioenergy systems, i.e. Py-ECH and CE. Tables 3.11 and 3.12 are for the Py-ECH process, whereas Tables 3.13-3.17 cover the CE process.

Table 3.11: Stream Table for Py-ECH Process

Stream	Content	Mass	Carbon	Energy	Temperature	Pressure
		Billion	Billion	EJ	°C	bar
		tonnes	tonnes C	LJ		Uai
1	Grinder Biomass In	1.250	0.509	20.623	25.000	1.000
2	Grinding Work In			0.215		
3	Grinding Heat Loss			0.215		
4	Dryer Biomass In	1.250	0.509	20.623	25.000	1.000
5	Drying Heat In			0.898		
6	Dryer Water Vapor Out	0.197		0.448	100.000	1.000
7	Drying Heat Loss			1.219		
8	Dryer Biomass Out	1.053	0.509	19.854	100.000	1.000
9	Pyrolysis Heat In			1.553		
10	Pyrolysis Work In			0.003		
11	Pyrolysis (Py Vapors + NCG) Out	0.895	0.384	16.671	500.000	1.000
12	Pyrolysis Biochar Out	0.158	0.125	4.738	500.000	1.000
13	Storage Pyrolysis Biochar Heat Loss			0.065		

Table 3.11 (cont'd)

Table 3.	ll (cont'd)					
14	Condenser Cooling Water In	0.149		-0.134	13.333	1.000
15	Condenser Cooling Water Out	0.149		-0.056	20.000	1.000
16	Condenser Heat Loss			1.324		
17	Condenser NCG Out	0.158	0.061	1.408	25.000	1.000
18	ECH Bio-Oil In	0.737	0.323	13.861	25.000	1.000
19	ECH Water In	0.369		0.000	25.000	1.000
20	ECH Work In			5.639		
21	ECH Heat Loss			0.590		
22	ECH Oxygen Out	0.328		0.017	80.000	1.000
23	ECH Heat In			0.125		
24	ECH Stable Bio-oil Out	0.764	0.323	17.087	25.000	1.000
25	ECH Hydrogen Out	0.014		1.931	80.000	1.000
26	Storage ECH Hydrogen Heat Loss			0.011		
27	Hydroprocessor Water Out	0.405		1.284	25.000	1.000
28	Hydroprocessor Heat In			1.524		
29	Hydroprocessor Heat Loss			2.418		
30	Hydroprocessor Fuel Out	0.383	0.323	18.403	25.000	1.000
31	Hydroprocessor H ₂ In	0.025		3.494	25.000	200.000
32	Compressor Work In			0.161		
33	Electrolysis Hydrogen Out	0.025		3.494	25.000	1.000
34	Electrolysis Water In	0.221		0.000	25.000	1.000
35	Electrolysis Oxygen Out	0.197		0.000	25.000	1.000
36	Electrolysis Work In			3.892		
37	Compressor Heat Loss			0.161		

Table 3.12: Balance on combustor for heat integration in BUD for Py-ECH process

		IN		
COMPONENT	SOURCE	Description	Qty. Billion tonnes/yr	Total Billion tonnes/yr
Air	External	Nitrogen	0.661	tomics, yi
		Oxygen Water	0.199	
		Vapor	0.017	
			0.877	0.877
NCG	Pyrolysis	CO	0.118	
		CO2	0.039	
		H2	0.001	
			0.158	0.158
H_2	ECH		0.007	0.007
				1.041
		OUT		
COMPONENT	SOURCE	Description	Qty. Billion tonnes/yr	Total Billion tonnes/yr
Stack Gas	Combustor	N_2	0.661	
		O_2	0.066	
		CO_2	0.224	
		H_2O	0.091	
			1.041	1.041
BALANCE				0.000

Table 3.13: Extracted Stream Table for CE Process (adapted from Humbird et al.)¹¹

Component	Stream		Mass (calc)	Carbon	Energy	Temp.	Press.
			kg/hr	kmol C/hr	Gcal/hr	°C	atm
			IN				
Hydrolysis & Fermentation Chemicals	309.00	CSL	211.00			20.00	1.00
	311.00	CSL	948.00			20.00	1.00

Table 3.13 (cont'd)

1 able 5.15 (coll u)							
	310.00	DAP	26.00			20.00	1.00
	312.00	DAP	116.00			20.00	1.00
		Total	1,301.00	22.00	-2.00		
Pre-Treatment Chemicals	273.00	NH3	1,051.00			20.00	9.00
	710.00	CSL	1,981.00			21.00	5.40
		Total	3,032.00	0.00	-3.00		
Biomass Feedstock	105.00		104,167.00	3,117.00	-316.00	25.00	1.00
Air for Recovery	-		12,105.00			-	-
Glucose for Enzyme Production	401.00		2,845.00	81.00	-8.00	28.00	1.00
Enzyme Production Chemicals	404.00	CSL	8.00			20.00	1.00
	443.00	CSL	157.00			20.00	1.00
	406.00	NH_3	6.00			28.00	9.00
	441.00	NH_3	109.00			28.00	9.00
	440.00	Nutri ents	67.00			20.00	1.00
	442.00	SO_2	16.00			28.00	3.00
	446.00	Antif oam	13.00			20.00	3.20
		Total	376.00	6.00	-1.00		
Air for Enzyme Production	-		32,853.00				
Air for WWT	-		223,602.00				
WWT Chemicals	632.00	Caust ic	4,504.00	0.00	2.00	20.00	2.00
Air for Boiler/ Turbogenerator	-		284,495.00				

Table 3.13 (cont'd)

851.00	Lime	895.00	0.00	0.00	25.00	1.00
904.00		147,140.00	0.00	87.00	33.00	5.00
		OUT				
550.00		21,398.00	471.00	0.00	34.00	0.90
515.00		21,808.00	941.00	-139.00	35.00	2.50
				-24.00		
435.00		1,586.00			25.00	1.00
423.00		31,801.00			28.00	1.00
	Total	33,387.00	54.00	0.00		
622.00		221,417.00	88.00	-1.00	25.00	1.00
627.00		9,929.00	4.00	8.00	100.00	1.00
				-26.00		
				-12.00		
				-11.00		
				-4.00		
809.00	Ash	5,725.00			0.00	1.00
810.00	Stack	363,445.00			145.00	1.00
821V	Stack -2	2,580.00			100.00	1.00
	Total	371,750.00	1,680.00	-12.00		
-		137,362.00	0.00	-20.00	37.00	1.00
	904.00 550.00 515.00 435.00 423.00 622.00 627.00 809.00 810.00	904.00 550.00 515.00 435.00 423.00 Total 622.00 627.00 809.00 Ash 810.00 Stack 821V Stack -2	904.00 OUT 550.00 515.00 21,398.00 21,808.00 435.00 423.00 Total 33,387.00 622.00 627.00 809.00 Ash 5,725.00 810.00 Stack -2 Total 371,750.00	904.00	904.00	904.00 87.00 33.00 550.00 21,398.00 471.00 0.00 34.00 515.00 21,808.00 941.00 -139.00 35.00 435.00 1,586.00 -24.00 25.00 423.00 31,801.00 28.00 28.00 622.00 221,417.00 88.00 -1.00 25.00 627.00 9,929.00 4.00 8.00 100.00 627.00 9,929.00 4.00 8.00 100.00 809.00 Ash 5,725.00 -11.00 -4.00 809.00 Stack 363,445.00 - 145.00 821V 2580.00 -2580.00 -12.00 -12.00

Table 3.14: Energy Balance in CE process

		IN			_
COMPONENT	SOURCE	Description	Qty.	Norm.	Total
			(Gcal/hr)	(EJ/yr)	(EJ/yr)
Biomass		Raw Feedstock	-316.000	20.623	20.623
Chemicals	Fermentation	CSL, DAP	-2.000	0.131	

Table 3.14 (cont'd)

Table 3.14 (contro	1)				
	Pre-treatment	Ammonia, dil.			
	_	Sulfuric Acid	-3.000	0.196	
	Enzyme	CSL, Ammonia,	1 000	0.065	
	Production WWT	SO ₂ , Corn Oil Caustic	-1.000	0.065	
	Boiler/ Generator	Lime in FGD,	2.000	-0.131	
	Bollet/ Gelierator	Ammonia,			
		Phosphate	0.000	0.000	0.261
Glucose		Glucose for			
		Enzyme Production	-8.000	0.522	0.522
Air	Recovery		0.000	0.000	
	Enzyme		0.000	0.000	
	WWT		0.000	0.000	
	Boiler/Generator		0.000	0.000	0.000
					21 406
					21.406
		OUT			
COMPONENT	SOURCE		Qty.	Norm.	Total
			(Gcal/hr)	(EJ/yr)	(EJ/yr)
Ethanol			-139.000	9.071	9.071
Electricity	Out		-11.000	0.718	
	Reserve		-4.000	0.261	0.979
Losses	Dagayany Haat	Heat Loss			
LUSSES	Recovery Heat Loss	Heat Loss	-24.000	1.566	
	WWT Heat Loss	Heat Loss	-26.000	1.697	
	Boiler/Generator	Heat Loss		-10,	
	Heat Loss		-12.000	0.783	
	CW Heat Loss	Heat Loss	-107.000	6.983	11.029
Vents &Waste	Recovery Vent				
Streams	•		0.000	0.000	
	Enzyme		0.000	0.000	
	Production Vent Boiler Stack &	CO ₂ ,CO,SOX,	0.000	0.000	
	Ash	O_2 , O_3 , O_3 , O_2 , O_3 , O_3 , O_4 , O_2 , O_3 , O_4 , O_4 , O_5 , O_5 , O_5 , O_7 , O_8 , O_8 , O_9 ,			
		N ₂ ,NH ₃	-12.000	0.783	

Table 3.14 (cont'd)

10010 211 : (10111 0)					
	WWT	CO ₂ ,CO,SOX,			
	Evaporation	NOX , H_2S , O_2 , N_2 ,			
		$\mathrm{CH_4}$	-1.000	0.065	
	WWT Brine	Predominantly			
		$NaNO_3$	8.000	-0.522	0.326
					21.406
BALANCE					0.000

 Table 3.15 : Mass Balance for CE Process

IN						
COMPONENT	SOURCE	Stream No.	Qty.	Norm.	Total	
			(kg/hr)	Billion tonnes/yr	Billion tonnes/yr	
Oxygen	Air for Enzyme Production Air for	450	7440.00	0.09		
	Recovery Section	559	2764.00	0.03		
	Air for WWT	630	51061.00	0.61		
	Air for Boiler	804	64966.00	0.78		
				1.51	1.51	
Nitrogen	Air for Enzyme Production Air for	450	24504.00	0.29		
	Recovery Section	559	9104.00	0.11		
	Air for WWT	630	168162.0 0	2.02		
	Air for Boiler	804	213957.0 0	2.57		
				4.99	4.99	
Water	Air for Enzyme Production Air for	450	638.00	0.01		
	Recovery Section	559	237.00	0.00		
	Air for WWT	630	4379.00	0.05		

Table 3.15 (cont'd)

Table 5.15 (cont d)					
		Air for Boiler	804	5572.00	0.07	
		Feedstock	105	20833.00	0.25	
		Fermentation Chemicals	309,310, 311,312	582.00	0.01	
		Pre-Treatment Chemicals	273,710	139.00	0.00	
		Glucose Solution	401	427.00	0.01	
		Enzyme Production Chemicals	404,443, 406,441, 440	83.00	0.00	
		Wastewater Chemicals	632	2252.00	0.03	
		Well Water	904	147140.0 0	1.77	
					2.19	2.19
Glucose		Glucose Soln.	401	2418.00	0.03	0.03
Chemicals	Protein	Fermentation Chemicals	309,310, 311,312	290.00	0.00	
		Enzyme Chemicals	404,443, 406,441, 440	41.00	0.00	
	Ammonia	Pre-Treatment Chemicals	273,710	1051.00	0.01	
		Enzyme Chemicals	404,443, 406,441, 440	115.00	0.00	
	Sulfuric Acid	Pre-Treatment Chemicals	273, 710	1842.00	0.02	
	12010				0.04	0.04
Dry Biomass		Feedstock	105	83334.00	1.00	1.00
Other Solids		Fermentation Chemicals	309,310, 311,312	429.00	0.01	
		Enzyme Production Chemicals	404,443, 406,441, 440	108.00	0.00	
		Wastewater Chemicals	632	2252.00	0.03	
		Boiler Chemicals	851	895.00	0.01	

Table 3.15 (cont'd)

				0.04	0.04
					9.80
	JO				
COMPONENT	SOURCE	Stream No.	Qty.	Norm.	Total
		1100	(kg/hr)	Billion tonnes/yr	Billion tonnes/yr
Oxygen	WWT Evaporation	622	44765.00	0.54	
	Stack & Ash	809,810, 821V	11324.00	0.14	
	Enzyme Production Vent	435,423	5727.00	0.07	
	Recovery Vent	550	172.00	0.00	
				0.74	0.74
Nitrogen	WWT Evaporation	622	168157.0 0	2.02	
	Stack & Ash	809,810, 821V	223985.0 0	2.69	
	Enzyme Production Vent	435,423	24504.00	0.29	
				5.00	5.00
Water	WWT Evaporation	622	4350.00	0.05	
	Stack & Ash	809,810, 821V	57031.00	0.68	
	Brine Enzyme	627	4967.00	0.06	
	Production Vent	435,423	774.00	0.01	
	Recovery Vent	550	522.00	0.01	
	Cooling Tower Evaporation	948 - 949	138293	1.66	
	Product	519	108.00	0.00 2.47	2.47

Tab	le 3.1	15	(cont	'd)
-----	--------	----	-------	-----

Chemicals	CO/NOx/ SOx/H2S	WWT	622	284.00	0.00	
	SUX/112S	Evaporation Stack & Ash	809,810, 821V	178.00	0.00	
		Brine	627	44.00	0.00	
	Ammonia	WWT Evaporation	622	1.00	0.00	
		Stack & Ash	809,810, 821V	30.00	0.00	
		Brine	627	3.00	0.00	
	Methane	WWT Evaporation	622	3.00	0.00	
					0.01	0.01
CO2		WWT Evaporation	622	3857.00	0.05	
		Stack & Ash	809,810, 821V	73396.00	0.88	
		Enzyme Production Vent	435,423	2382.00	0.03	
		Recovery Vent	550	20669.00	0.25	
		Vent			1.20	1.20
Ethanol		Product	519	21673.00	0.26	0.26
Other Solids		Stack & Ash	809,810, 821V	5805.00	0.07	
		Brine	627	4907.00	0.06	
					0.13	0.13
						9.81
BALANCE						-0.01

 Table 3.16 : Carbon Balance for CE Process

		IN		
COMPONENT	SOURCE	Qty.	Norm.	Total
		(kmol/hr)	Biilion tonnes/yr	Billion tonnes/yr
Biomass		3117.000	0.509	0.509

Tabl	le 3.1	6 (cont	'd)

14010 5.10 (00111)	-)			
Chemicals	Fermentation	22.000	0.004	
	Pre-treatment	0.000	0.000	
	Enzyme Production	6.000	0.001	
	WWT	0.000	0.000	
	Boiler/ Generator	0.000	0.000	0.005
Glucose		81.000	0.013	0.013
				0.526
		OUT		
COMPONENT	SOURCE	Qty.	Norm.	Total
		(kmol/hr)	Biilion tonnes/yr	Billion tonnes/yr
Ethanol		941.000	0.154	0.154
CO2 and traces	Recovery Vent Enzyme Production	471.000	0.077	
	Vent	54.000	0.009	
	WWT Evaporation	88.000	0.014	
	Brine	4.000	0.001	
	Stack & Ash	1680.000	0.274	0.375
				0.528
BALANCE				-0.002

 Table 3.17 : Water Balance for CE Process

		Water Balance			
	Component	Stream No.	Qty.	Norm.	Total
			kmol/hr	Biilion tonnes/yr	Billion tonnes/yr
In	Air for Enzyme Production Air for Recovery	450	638.00	0.01	•
	Section Air for WWT	559 630	237.00 4379.00	0.00 0.05	
	Air for Boiler	804	5572.00	0.07	
	Feedstock Fermentation	105	20833.00	0.25	
	Chemicals Pre-Treatment	309,310,311,312	582.00	0.01	
	Chemicals Glucose Solution	273,710 401	139.00 427.00	0.00 0.01	

Table 3.17 (cont'd)

	Enzyme Production				
	Chemicals	404,443,406,441,440	83.00	0.00	
	Wastewater				
	Chemicals	632	2252.00	0.03	
	Well Water	904	147140.00	1.77	
				2.19	2.19
Out	WWT Evaporation	622	4350.00	0.05	
	Stack & Ash	809,810,821V	57031.00	0.68	
	Brine	627	4967.00	0.06	
	Enzyme Production				
	Vent	435,423	774.00	0.01	
	Recovery Vent	550	522.00	0.01	
	Cooling Water				
	Evaporation	948 - 949	138293.00	1.66	
	Product	519	108.00	0.00	
				2.47	2.47
Generated	Enzyme Production		1291	0.02	
	Fermentation	T. 1.1. 2.5	121	0.00	
	WWT	Table 37	2680	0.03	
	Combustor		23869	0.29	
			25007	0.34	0.34
Consumed	Pretreatment		2473	0.03	
	Enzymatic	Table 37	2.,0	0.02	
	Hydrolysis		2631	0.03	
	, ,			0.06	0.06
Balance					-0.01

Chapter 4: TECHNOECONOMIC ANALYSIS OF THE PY-ECH SYSTEM

Abstract

Maximizing fossil fuel displacement and reducing atmospheric carbon dioxide levels requires that bioenergy systems exhibit high efficiency of carbon incorporation. The availability of biomass carbon is a constraint globally, and strategies to increase the efficiency of bioenergy production and biogenic carbon use are needed. Previous studies have shown that "energy upgrading" of biomass by coupling with fossil carbon-free electricity through electrocatalytic hydrogenation offers a potential pathway to near full petroleum fuel displacement even when annual U.S. biomass production is limited to 1.3 billion dry tons. Given that commercial application of such technology requires economic feasibility, the present work formulates and describes a technoeconomic model of a process that combines decentralized pyrolysis and electrocatalytic hydrogenation with centralized hydroprocessing (Py-ECH) to produce a liquid hydrocarbon fuel and provides a comparison to a cellulosic ethanol pathway using consistent assumptions. Using a discounted cash flow approach, a minimum fuel selling price (MFSP) of \$ 3.62/gallon-gasoline equivalent (gge) is estimated for the Py-ECH fuel derived from corn stover, considering nth plant economics and a fixed internal rate of return of 10%. This is comparable to the MFSP for cellulosic ethanol from fermentation with the same feedstock (\$ 3.71/gge) and also in the range of gasoline prices over the last 20 years that have varied from as low as \$ 1/gge to \$ 4.44/gge (in 2018\$). Sensitivity analyses were performed to find key parameters that affect the Py-ECH MFSP, with electricity cost, raw material costs, bio-oil yields, and cell efficiencies identified as the most influential parameters. With system improvements, a pathway to fuel at a cost of less than \$ 3/gge is articulated for this Py-ECH route.

Introduction

The U.S. Department of Energy's "2016 Billion-Ton Report" projected the total harvestable biomass available in the U.S. to be 1.3 billion dry tons by the year 2030 for biomass obtained at a cost of less than \$60/dry ton. While this is a large quantity, the carbon and energy content of this biomass is insufficient to meet the energy demands of the U.S. transportation sector. This has been demonstrated in the work by Lam et al., 5 which also highlights the importance of establishing bioenergy systems that utilize renewable energy and carbon efficiently. Prevalent systems such as cellulosic ethanol fermentations are inherently carbon inefficient, as one-third of the holocellulosic carbon is lost as carbon dioxide. Moreover, combusting lignin for internal heat and power, also diverts carbon away from incorporation into higher-value liquid fuels. These considerations further stress the need to devise bioenergy systems that are more carbon and energy efficient.

All liquid biofuel strategies require biomass deconstruction as an early step in processing. The literature on deconstruction is immense and growing, as new techniques involving acids, bases, solvents, enzymes, heat, and combinations thereof continue to emerge. Of the many existing deconstruction techniques, biomass fast pyrolysis is well-studied and can be done with low capital cost and high yield because of short residence times. Further, it converts a portion of the biomass lignin along with the holocellulose into the primary product, bio-oil. 18, 19, 129 Regional biomass processing depots to produce bio-oil are capable of lowering overall hauling costs because bulk density is increased, 22 however the reactivity of bio-oil limits its ability to be transported. Functional groups such as carbonyls, carboxylates, and alcohols, react to form polymers which increase viscosity and form sludges. Further, bio-oil from pyrolysis is corrosive to metals as it contains weak acids and has high total acid number (TAN).

Being highly unsuitable for transport and storage, bio-oil needs to be stabilized immediately after pyrolysis. Thermal hydrogenation and hydrodeoxygenation has been used for hydrogenating and stabilizing bio-oil, ^{19, 51, 150-160} however, these techniques operate under high temperature and pressure and are not suited for widespread deployment in small-scale plants (depots). A milder alternative is electrocatalytic hydrogenation (ECH), which involves the electrolysis of water to produce *in-situ* hydrogen ions on the anode that electrocatalytically react with bio-oil on the cathode. This technique has been found to successfully hydrogenate and deoxygenate the variety of compounds found in raw biomass-derived bio-oil as well as lignin-derived bio-oil. ^{32, 34, 132, 136, 137, 187} ECH is a promising strategy because it operates at mild conditions, avoids storage or use of hydrogen gas, and also reduces hydrogen consumption at the centralized refinery where hydroprocessing can be safely utilized to create finished fuels. ^{32, 188} As previously investigated, ⁵ sequential fast pyrolysis and electrocatalysis (Py-ECH) co-deployed in a biomass upgrading depot, followed by petroleum-style hydroprocessing in central refineries, potentially offers a carbon and energy efficient strategy for making liquid hydrocarbon biofuels.

While such a decentralized biorefinery system shows promise in terms of carbon and energy efficiency, its economic metrics must also be investigated. Previously, technoeconomic analyses have been completed for centralized pyrolysis followed by hydroprocessing. Wright et al. estimated a minimum fuel selling price (MFSP) of \$2.41/gge in 2018\$ when the merchant H₂ is purchased at \$1.47/kg H₂ for hydroprocessing.⁸⁴ However, when a portion of the bio-oil is steam reformed to make the H₂ gas required for upgrading the remaining bio-oil, the MFSP of the fuel increased to \$3.55/gge in 2018\$. Brown et al. estimated a MFSP of \$2.64/gge in 2018\$ for a pyrolysis and hydroprocessing facility that processed 2,000 tonnes/day of corn stover.⁸⁵ Neither of these systems considered decentralized upgrading or the use of ECH.

Orella et al. investigated the technoeconomics of the ECH process alone and developed a model to estimate the minimum fuel selling price of reducing guaiacol, a pyrolysis bio-oil representative compound to phenol. It was reported that with enhanced current density, decreased selectivity for hydrogen evolution and increased faradaic efficiencies for the desired product, the selling price for phenol can drop to \$0.42/kg. This is equivalent to a rough approximation of the cost of electrocatalytic hydrogenation of pyrolysis bio-oil in the Py-ECH process being studied here.

In the present work, a full-scale technoeconomic analysis has been performed for the combined Py-ECH process that 1) upgrades biomass (corn stover) to a stable fuel intermediate in decentralized depots which is then delivered to a 2) centralized refinery that uses traditional hydroprocessing to create finished hydrocarbon liquid fuels. The final fuel in this present analysis has been assumed to be octane, to represent a gasoline-like fuel. Sensitivity analyses have also been carried out to identify key parameters that influence the MFSP, with the objective of guiding researchers towards economically relevant process improvements.

Materials and Methods

Process Description

The Py-ECH process under investigation combines fast pyrolysis of corn stover in depots and subsequent electrocatalytic hydrogenation with hydroprocessing in a central refinery to produce liquid fuels from biomass. This system has been described in detail in the supplementary information file of the work by Lam et al.⁵ In brief, the Py-ECH system involves hauling biomass from the cultivation fields to regional depots where it is ground and dried prior to feeding to a fast pyrolysis reactor at 500°C and atmospheric pressures. The mass percentages of the pyrolysis products are 70%, 15% and 15% for liquid bio-oil, biochar and non-condensable gases respectively. The resultant bio-oil is then fed into an ECH unit where it is electrocatalytically reduced at 80°C and atmospheric pressure. Ruthenium metal serves as the electrocatalyst. ECH

stabilized bio-oil is then transported to a central hydroprocessing facility where it is further upgraded to the finished fuel using hydrogen gas at 400°C and 200 bar pressure in the presence of zeolite catalyst. The hydrogen gas is assumed to be renewably generated by the electrolysis of water at the central refinery. A process flow diagram of the Py-ECH process has been provided in Figure 4.1.

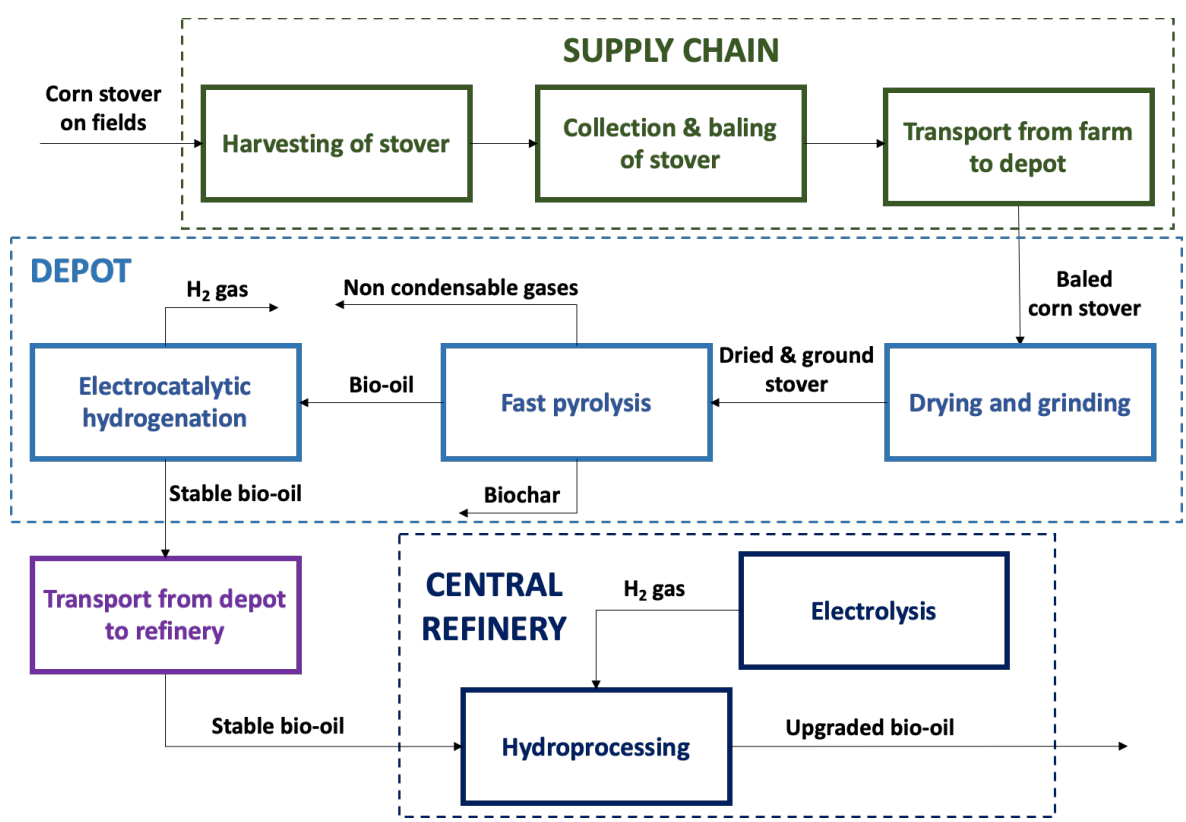


Figure 4.1: Process flow diagram of the Py-ECH process

Economics for cellulosic ethanol produced via fermentation from corn stover feedstock was evaluated for comparison, using the prior analysis by Humbird et al., at National Renewable Energy Laboratory (NREL).¹¹ The analysis was used as a framework for the Py-ECH analysis, using the same assumptions where possible and appropriate. To remain consistent with the Humbird et al., report, a 2,000 metric tonnes/day biomass processing scale was assumed as the combined input to all depots. Multiple depots, equally sized, supplied a single centralized refinery

to make finished fuel. Depot sizes in previous literature have varied from Eranki et al., reporting values of 100 tonnes/day²² and Lamers et al. assuming a maximum of about 215 tonnes/day.⁷² The depot size in the present analysis was fixed after an optimization study that minimized the total transportation cost. This has been described in later sections of this analysis. The composition and moisture content of the delivered corn stover at the depot gate was assumed in accordance with the Humbird et al., report.¹¹ All material and energy balances required for the Py-ECH and CE economics respectively were extracted from Lam et al.,⁵ and the Humbird et al., report respectively.

Economic Model

All economic assumptions for the Py-ECH system were similar to those made for an nth plant in the Humbird et al., report for ethanol production via fermentation of cellulose.¹¹ The minimum fuel selling price (MFSP) of the fuel produced from the Py-ECH system was determined using a discounted cash flow analysis (DCFA) with a fixed internal rate of return. This was performed by iterating the MFSP until the net present value of all cash flows for the entire plant life equaled zero. It must be noted here that the DCFA was done twice, first at the depot and then at the central refinery. For the depot, the raw material was the corn stover biomass and the finished product was the ECH stable bio-oil. For the central refinery, the raw material was this ECH stable bio-oil and the product was the final gasoline-like fuel. The assumed values for the parameters have been summarized in Table 1.

Table 4.1: Summary of the economic assumptions in the technoeconomic model

Parameter	Value		
Plant life	30 years		
Plant location	Midwest USA		
Cost basis year	2018		
Internal rate of return	10%		
Depreciation method	200% double declining balance		
Federal tax rate	35%		

Table 4.1 (cont'd)

ruote 1.1 (cont u)			
Working capital	5% of fixed capital investment		
Salvage value	0 \$		
Construction period	1 year		
Startup period	3 months		
Revenues during startup	50%		
Variable costs during startup	75%		
Fixed costs during startup	100%		
Loan Terms	8% APR; 10 years		
Financing	40% equity		

The total capital investment was calculated as the sum of fixed capital investment (FCI), land, and working capital (assumed 5% of FCI). The FCI, in turn, was determined as the sum of direct and indirect costs, which are functions of the total installed equipment costs. Installed equipment costs were calculated by multiplying the estimated equipment cost with an installation multiplier. The assumptions and methods behind estimating these equipment costs have been described in sufficient detail in the Appendix at the end of this chapter. Operating costs were determined by summing the fixed costs (e.g., employee salaries, insurance, and maintenance costs) and variable costs (e.g., raw materials and utilities). While the fixed operating costs were determined as percentages of the total capital investment, the variable operating costs were either estimated from literature data or calculated. For instance, the raw material cost for the Py-ECH system was estimated from a supply chain analysis, described in the next section. Table 4.4 in the Appendix lists all assumptions for determining the total capital investment and the total operating cost.

By-products

The Py-ECH system generates two by-products at the depot, along with ECH bio-oil, which is the primary product. These two by-products are biochar and H₂ gas generated from the ECH unit. While the biochar is not utilized in the process; some amount of the ECH H₂ gas is utilized, in combination with the non-condensable gases from the pyrolyser to meet the heat requirements at the depot. Therefore, this excess H₂ gas and the total amount of biochar may be sold for additional

revenue to bring down the cost of the final Py-ECH fuel. This is similar to the approach adopted by Humbird et al., where they incorporate the revenue from selling excess electricity in the cash flows that determine the final MFSP of the fuel. In the present analysis, the cost of H₂ gas was fixed at \$ 2/kg of H₂, which is the 2020 delivery cost target of the U.S. Department of Energy for H₂ gas generated from electrolysis.¹⁸⁹ This also falls within the range for the cost of H₂ gas generated from steam reforming, which varies from \$ 1.25/kg for large systems to \$ 3.50/kg for smaller systems.¹⁹⁰ Meanwhile, biochar selling prices vary over a large range in the literature. Campbell et al. performed a review of different biochar production scenarios and found that costs varied from \$80/tonne to about \$13,000/tonne in 2013\$¹⁹¹ The selling price of biochar depends heavily on its quality as determined by its carbon and ash contents among other factors, the biomass source and whether it is a wholesale or retail price.¹⁹¹ Table 4.5 in the Appendix provides a range of biochar prices from the literature. Due to the immense variability in the selling prices of biochar and limited information of the quality of biochar being generated, it is assumed that biochar is not being sold in the present study.

Supply Chain

The price of corn stover delivered, for the CE system was taken from the Humbird et al., report and scaled to 2018\$ using Chemical Engineering Plant Cost Indices. The costs in that report were originally estimated from the Department of Energy's Multi-Year Program Plan (MYPP), published in 2011. While the 2016 MYPP has since been published, the present analysis still employed the 2011 values, as the 2016 MYPP mostly explores blended feedstock with less focus on corn stover as the sole feedstock. The major components of the feedstock price are harvesting and collection, feedstock storage, preprocessing, transportation and handling, and the grower payment. To maintain consistency, the same assumptions were used for the Py-ECH system with

a few exceptions. The preprocessing costs involved drying and grinding operations, aimed at making the raw material being delivered, fit for processing at the location being delivered. These costs had been handled as separate unit operations at the depot for the Py-ECH system. Therefore, these were excluded from the raw material cost for the Py-ECH system. Another key difference between the two systems is logistics. While all the corn stover is directly brought to a single cellulosic ethanol biorefinery in the CE system, the transportation in the Py-ECH system occurs in two stages. In the first leg, corn stover is transported over short distances from the farm to the depot, whereas in the second leg, the stable bio-oil is transported from the depots to the central refinery. This is bound to have an impact on the transportation component of the raw material cost. To estimate the transportation cost associated with delivering raw corn stover to the depots in a Py-ECH system, an optimization study was performed to determine the least minimum fuel selling price (MFSP) of the fuel. Previous studies to determine depot sizes had been performed by Kim and Dale, who calculated a farm-to-depot transportation distance from the equation provided in Table 4.6 of the Appendix.⁷⁴ Fundamentally, these studies assumed a solar system like model, where the refinery is located at the center, with all the depots located in a circular orbit around the refinery. Each depot, in turn, have their own collection radius. The depot-to-refinery distance is subsequently calculated from the difference in the collection radii of the refinery and the depot, as determined from the equation in Table 4.6 of the Appendix.

In the present analysis however, a square geometry has been assumed as land is commonly parceled in rectangular fashion. Figure 4.2 (a) shows the assumed depot distribution system. The central refinery, represented by the red square is located in the center, while the depots, represented by black stars are scattered all around the refinery. The green squares represent the biomass collection area for the depot located at its center. It must be noted here that the depot arrangement

shown in Figure 4.2 (a) is one of many arrangements, each of which can result in a different average depot-to-refinery distance and consequently, different transportation costs. Therefore, an optimization was performed for determining the optimal placement of the depots around the central refinery. A depot size was assumed, and the average farm-to-depot distance calculated from the geometry. The total number of depots were determined from the central refinery capacity and the assumed depot size. The depots and their collection squares were then randomly placed around the refinery such that there is no overlap between the collection squares of any two depots. It was also assumed that all the depots are located in a square region around the refinery, only 25% of which is dedicated for crop cultivation. The white spaces in Figure 4.2 (a) denote the 75% not dedicated to crop cultivation. Care was also taken to ensure that no depots were located in a region adjacent to the refinery, denoted by the blue boundary, to avoid a situation where the biomass is closer to the refinery instead of the depot. Any biomass in this region can directly be transported to the refinery (because of refinery proximity), where it can be combusted for required heat and power, offsetting natural gas used in the refinery. However, this offset was not considered in the present analysis; all heat requirement at the refinery is derived from burning natural gas. Based on the placement of the depots around the refinery, an average depot-to-refinery distance was evaluated. This distance was then minimized over successive iterations, each of which considered a different random arrangement of depots. The arrangement that resulted in the minimum depot-to refinery distance was chosen as the optimal arrangement of depots for that particular depot size. It must also be noted that a road winding factor of 1.23 was assumed for transportation by trucks, as suggested from literature for truck transportation over distances less than 400 km. ^{74, 192-194} Figure 4.2 (b) shows how the depot-to refinery distance and the farm-to-depot distance varies with depot size for a 2,000 tonne/day central refinery.

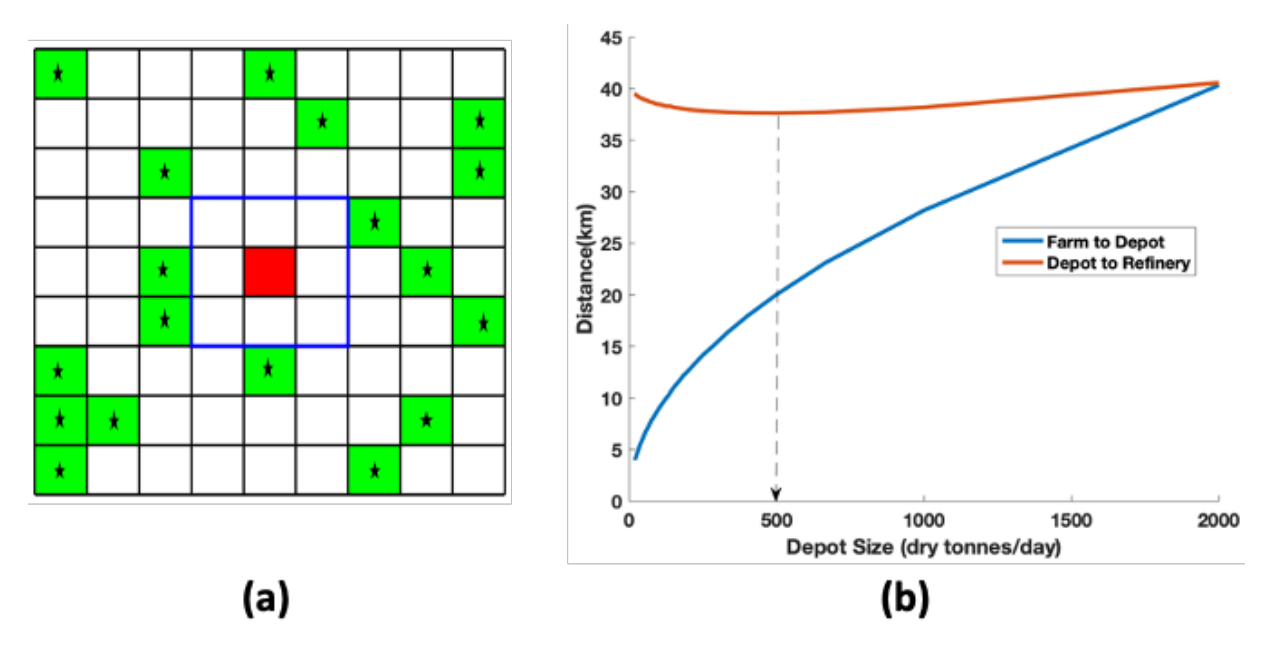


Figure 4.2: Illustration of depot distribution geometry. (a) Illustration of depot distribution relative to central refinery, for a central refinery with 18 depots. (b) Variation of farm-to-depot and depot-to-refinery distance with depot size, for a 2000 tpd central refinery

It can be seen that the farm-to-depot distance varies as the square root of the depot size as the land has been parceled as squares. The depot-to-refinery distance goes through a slight minimum at a depot size of 500 tonnes/day but does not vary significantly because the depots are fairly close together when the central refinery size is 2,000 tpd.

Results

Supply Chain Costs

Using the optimization strategy and the economic model outlined in the previous sections, the minimum fuel selling price (MFSP) of the final fuel was calculated for different depot and refinery sizes. Figure 4.3 shows the variation in MFSP of the final fuel with depot sizes for different refinery capacities. It can be seen that for all refinery sizes (except for a 1000 tpd central refinery), the MFSP passes through a minimum as depot sizes are increased. This is owing to two opposing forces at play. As depot sizes increase, the MFSP initially goes down owing to economies-of-scale effects.

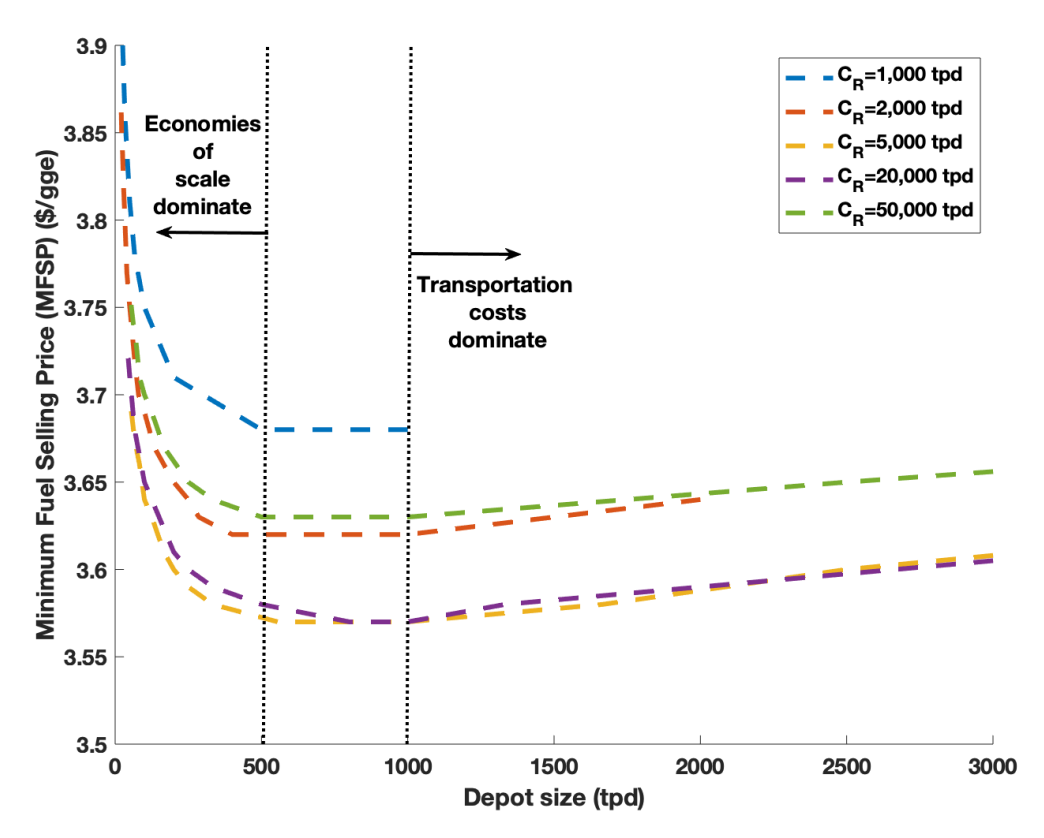


Figure 4.3: Variation of MFSP from Py-ECH with depot size. C_R denotes capacity of central refinery

However, after a certain depot size, transportation distances and consequently transportation costs are large enough that they overpower the benefit of economies-of-scale. Therefore, at lower depot sizes, economies-of-scale dominate whereas at higher depot sizes, transportation costs dominate. There is, however, a middle zone where these two contrasting effects balance each other. While this zone of depot sizes is different for different refinery capacities, it is always contained within the depot sizes of 500-1000 tpd. This has been highlighted in Figure 4.3 by dotted lines. For a 1000 tpd central refinery, a minimum was not observed since transportation distances at this refinery scale never become large enough to overpower the economies-of-scale effects. For the present analysis, however, which assumes a refinery capacity of 2000 tonnes/day, the minimum was observed around a depot size of 500 tpd. This is also consistent with Figure 4.2 (b), where the depot to refinery distance goes through a minimum at around a depot size of 500 tpd. Assuming

equal sized depots, this corresponds to 4 depots (each having a 500 tpd capacity) supplying one central refinery.

Having established an optimized capacity and arrangement of depots that together supply the single 2,000 tonne/day central refinery, the cost of transporting biomass from the farm to depot and transporting the ECH bio-oil from depot to refinery was determined. In this regard, the average farm-to-depot and depot-to-refinery distances for the optimized depot arrangement were calculated and a trucking cost of \$ 1.82/mile (in 2018\$) was assumed. 195 It must be noted that this cost of trucking includes both fixed costs like lease payments, driver wages, benefits, insurance premiums, permits, etc. and variable costs like fuel, repairs, tolls, etc.. For a depot capacity of 500 tpd and a refinery capacity of 2000 tpd; this corresponded to a cost of \$ 2.97/tonne of biomass being delivered from the farm to a depot and a cost of \$7.71/ tonne of ECH bio-oil delivered from a depot to refinery. This makes up a total of \$7.82/ tonne of biomass in transportation costs for the Py-ECH system. This is lower than the \$10/tonne of biomass, assumed by Humbird et al., for the CE system. This only highlights the advantages of the decentralized system in relation to reducing overall transport costs. It must be reiterated here that this is the only difference in supply chain costs of the two systems. All other costs related to harvesting, collecting and storing the biomass and the grower payment costs are same for both systems. In this regard, the total cost of raw biomass delivered from the farm to the refinery gate for the CE system was determined to be \$ 68.33/tonne of dry biomass. The equivalent total cost of raw biomass delivered from the farm to a depot for the Py-ECH system was evaluated to be \$ 61.30/tonne of dry biomass. The relative contributions of the different components of the supply chain in both systems have been shown in Figure 4.4 (a) and 4.4 (b). The absolute values have been reported in Table 4.7 of the Appendix. It can be seen that the grower payment costs, which include the cost of production of corn stover and

the profit margin of the grower are the largest for both systems. This is followed by the costs associated with harvesting, baling and collecting stover. The major difference between the cost contribution of the two systems is in transportation, which is expected from the preceding discussion. While transport accounts for 15% of the supply chain costs in the CE system, it merely accounts for 5% in the Py-ECH system. It must be noted, however, that the transportation costs for the Py-ECH system shown here only account for the farm-to-depot leg. The depot-to-refinery transportation costs were included in the cost of the ECH stable bio-oil being delivered as the raw material to the central refinery.

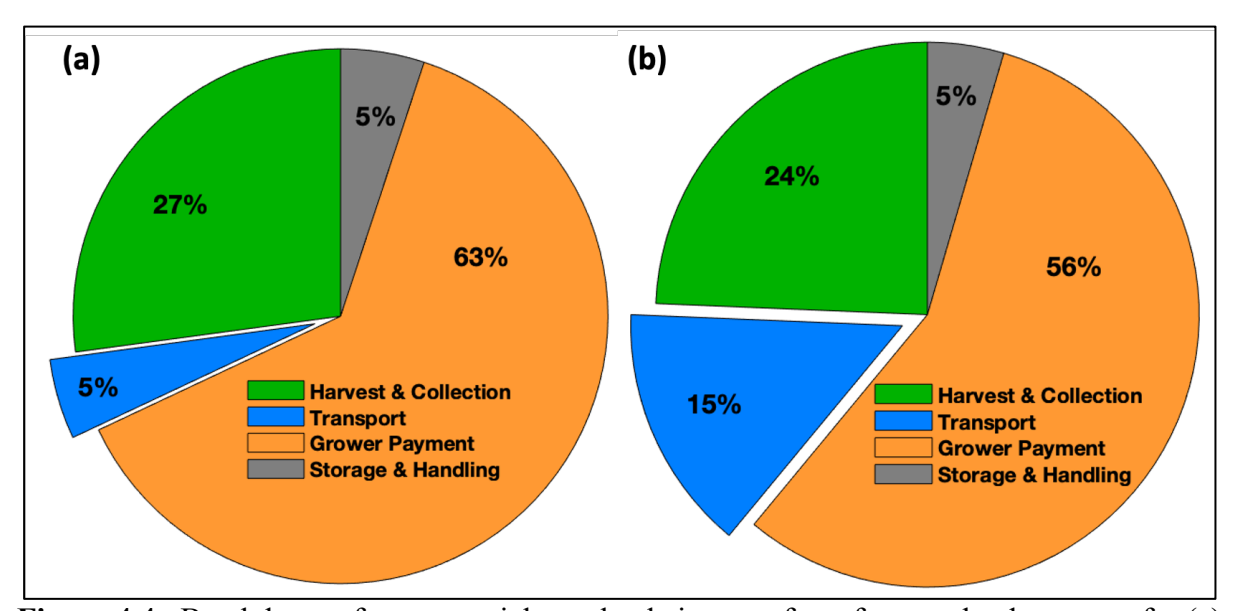


Figure 4.4: Breakdown of raw material supply chain costs from farm to the depot gate for (a) Py-ECH system and (b) CE system

Depot Costs

Table 4.2 shows the capital and operating costs at the depot. The total capital investment for a single 500 tpd depot is \$ 29M, while the annual operating costs are about \$ 25M. Capital costs at the depot are dominated by the ECH unit followed by the pyrolysis, combustion and drying units. Grid electricity and raw materials comprise most of the variable cost.

Table 4.2	: Depo	t Capital	and O	perating	Costs
------------------	--------	-----------	-------	----------	-------

	ital and Operating Costs				
Total Capital Cost (2018\$)					
Unit	Installed Cost				
Drying	1.24E+06				
Grinding	1.67E+05				
Pyrolysis	1.30E+06				
Condensation	1.45E+04				
ECH	9.92E+06				
Combustion	1.49E+06				
Storage	7.58E+05				
Total Installed Capital Cost	1.49E+07				
Inside Battery Limits Capital Cost	1.26E+07				
v					
Direct Costs					
Warehouse	5.05E+05				
Site Development	1.14E+06				
Additional Piping	5.69E+05				
Total Direct Costs	1.71E+07				
Total Direct Costs	1.712.07				
Indirect Costs					
Proratable Costs	1.71E+06				
Field Expenses	1.71E+06 1.71E+06				
Home Office and Construction	3.42E+06				
	1.71E+06				
Project Contingency Other costs	1.71E+06 1.71E+06				
Total Indirect Costs	1.03E+07				
Eived Conital Investment (ECI)	2.74E+07				
Fixed Capital Investment (FCI) Land	2.74E+07 2.38E+05				
Working Capital	1.37E+06				
Total Capital Investment (TCI)	2.90E+07				
Total Operating Costs (2018\$/yr)					
Variable Operating Costs					
Raw Material	8.84E+06				
Grid Electricity	1.56E+07				
Fresh Water	1.97E+04				
ECH Stack Replacement	2.12E+05				
Total Variable Operating Costs	2.47E+07				
Total variable Operating Costs 2.4/E+U/					
Fixed Operating Costs					
Salaries	1.45E+05				
Labor Burden	1.43E+05				
Maintenance	3.79E+05				
iviamitemance	3./9E±U3				

1 55-10 1.12 (0 5110 55)		
Property Insurance	1.92E+05	
Total Fixed Operating Costs	8.46E+05	
Total Operating Costs	2.55E+07	

Figure 4.5 (a) show that the largest contributor to the installed equipment costs at the depot is the ECH reactor, which accounts for 67% of the total installed costs. This is owing to the high cost of the membrane electrode assembly stacks that comprise expensive noble metals, that serve as anode (Pt) and cathode (Ru). Combustion, pyrolysis and drying are the next highest costs, as high-temperature reaction vessels are needed for these units.

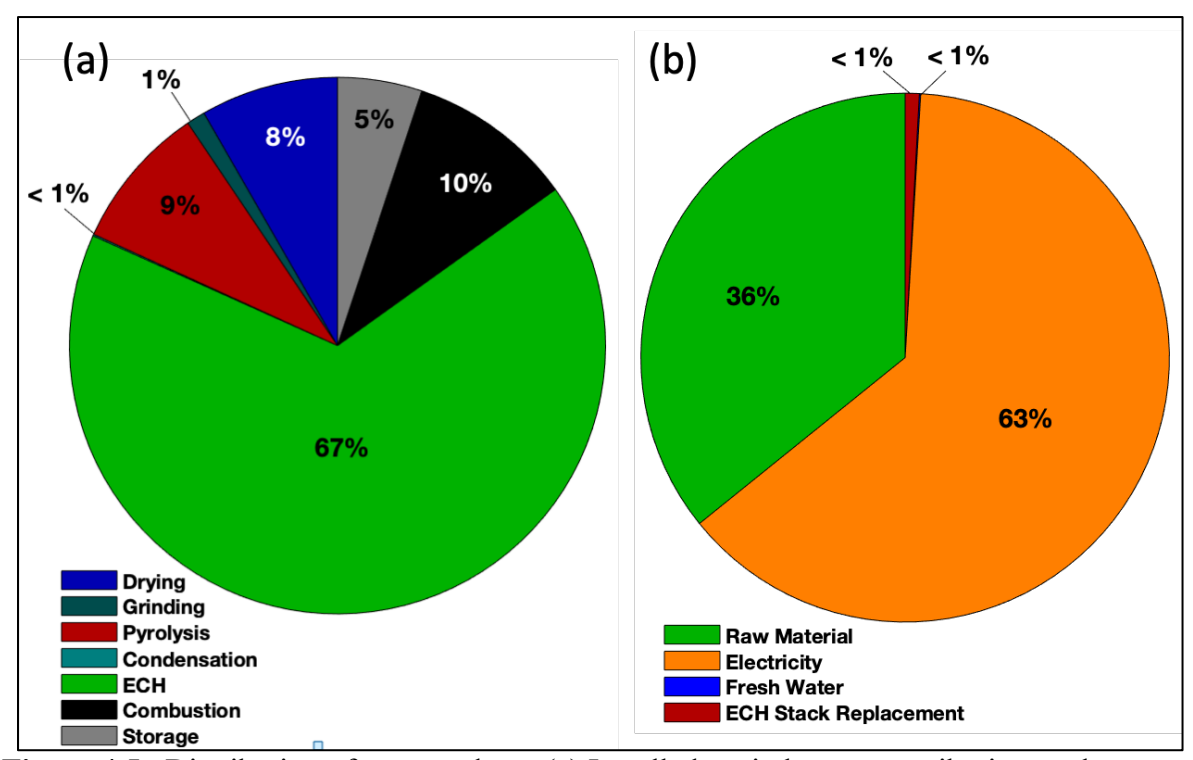


Figure 4.5: Distribution of costs at depot (a) Installed capital costs contribution analyses at a depot (b) Variable operating cost contribution analyses at a depot

The variable operating costs at the depot include the costs of raw materials, electricity, fresh water for ECH, and ECH stack replacement. Grid electricity (assumed as \$0.0656/kWh)¹¹ accounts for about 63% of operating costs, due to the immense electric energy requirement of ECH. Raw

material costs (36%) are also significant because of the various supply chain costs already described. ECH stack replacement costs, assumed at 15% of the installed capital costs with a replacement schedule of 7 years are comparatively negligible (<1%), as seen in Figure 4.5(b).

Refinery Costs

Table 4.3 shows the estimated capital and operating costs at the refinery. The total capital investment for the central refinery is \$227M for processing the amount of bio-oil generated from pyrolysing a total of 2000 tonnes/day of raw biomass from all the depots combined. The annual operating costs are around \$161M.

Table 4.3 : Refinery	/ Capita	l and O	perating	Costs
-----------------------------	----------	---------	----------	-------

Total Capital Cost (2018\$)		
Unit Installed Cost	t	
Hydroprocessing	4.79E+07	
Electrolysis	6.60E+07	
Storage	2.10E+05	
Total Installed Capital Cost	1.14E+08	
Inside Battery Limits Capital Cost	1.14E+08	
Direct Costs	4.5.CD + 0.6	
Warehouse	4.56E+06	
Site Development	1.03E+07	
Additional Piping	5.13E+06	
Total Direct Costs	1.34E+08	
Indirect Costs		
Proratable Costs	1.34E+07	
Field Expenses	1.34E+07	
Home Office and Construction	2.68E+07	
Project Contingency	1.34E+07	
Other Costs	1.34E+07	
Total Indirect Costs	8.04E+07	
Fixed Capital Investment (FCI)	2.15E+08	
Land	1.83E+06	
Working Capital	1.07E+07	
Total Capital Investment (TCI)	2.27E+08	

Table 4.3 (cont'd)

Total Operating Costs (2018\$/yr)		
Variable Operating Costs		
Raw Material	1.00E+08	
Grid Electricity	4.27E+07	
Natural Gas	7.23E+06	
Electrolyser Stack Replacement	1.41E+06	
Hydroprocessor Catalyst Replacement	2.64E+06	
Total Variable Operating Costs	1.54E+08	
Fixed Operating Costs		
Salaries	1.14E+06	
Labor Burden	1.02E+06	
Maintenance	3.42E+06	
Property Insurance	1.50E+06	
Total Fixed Operating Costs	7.08E+06	
Total Operating Costs	1.61E+08	

At the refinery, the electrolysis and the hydroprocessing capital costs are comparable, with the electrolyzer costs accounting for 58% and the hydroprocessing costs at about 42% of the total. The high costs for the electrolyser are again attributed to the high cost of the membrane electrode assembly stacks in the electrolyser. The capital cost distribution has been shown in Figure 4.6(a). The variable operating costs at the refinery include the raw material (stable bio-oil procured from the depots), electricity for the electrolyzer to produce H₂ gas, natural gas for process heating, electrolyser stack replacement costs and hydroprocessing catalyst replacement costs. The chief contributor to the operating costs (65% of total) is the raw material purchased from the depots. This is essentially the MFSP (considering an internal rate of return of 10%) of the ECH bio-oil at the depot exit and the cost of transporting the stable bio-oil from the depot to the refinery. Electricity accounts for 28% of the operating costs at the refinery; while the cost for natural gas (5%) is small in comparison. All other costs are negligible. This has been represented in Figure 4.6(b).

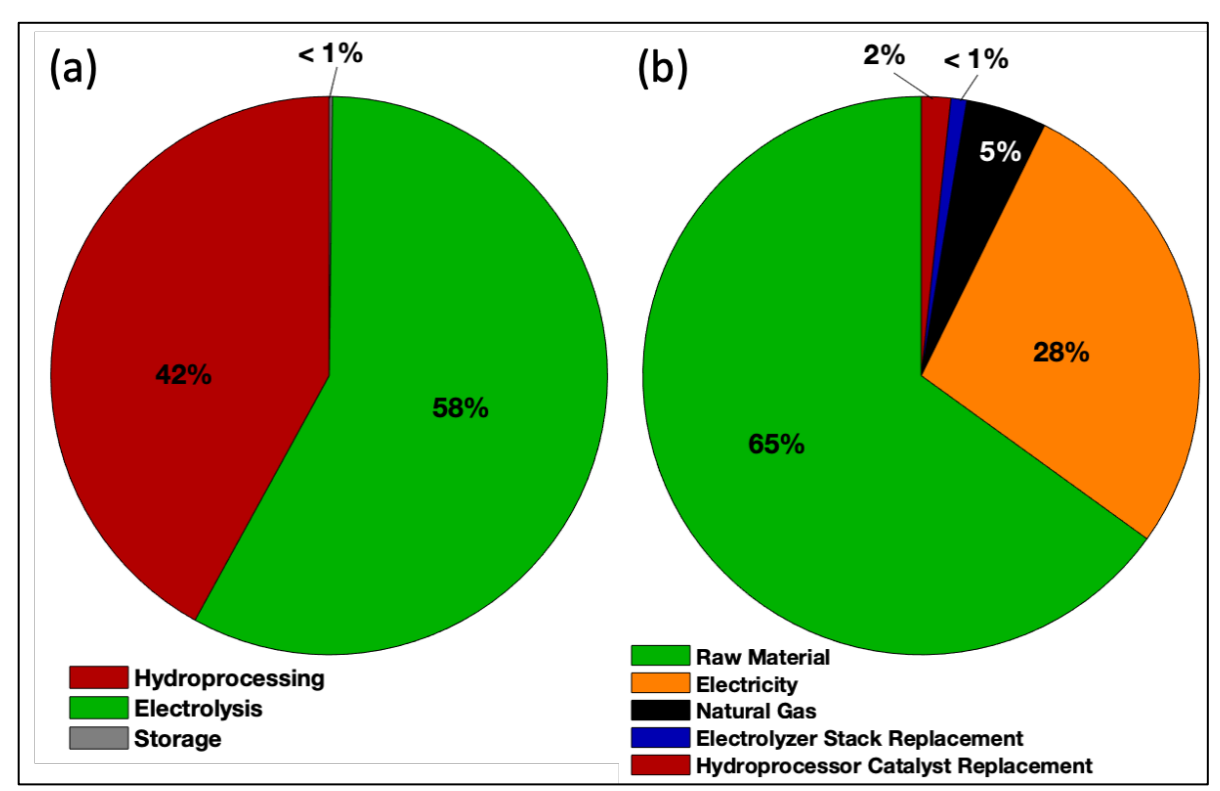


Figure 4.6: Distribution of costs at refinery (a) Installed capital cost contribution at the refinery (b) Variable operating cost contribution at the refinery

Minimum Fuel Selling Price

Technoeconomic analysis of the Py-ECH system, using a DCFA approach with an internal rate of return of 10% yields a MFSP of \$1.17/gge for the stable bio-oil produced by the depot and a MFSP of \$3.62/gge for fuel produced by the refinery, both in 2018\$.

In comparison, MFSP for ethanol in the cellulosic ethanol system was calculated to be \$2.47/gallon in 2018\$ (\$2.15/gallon in 2007\$). This corresponds to \$3.71/gge in 2018\$. Therefore, under the current assumptions, Py-ECH fuel is slightly cheaper than the ethanol produced from cellulosic fermentations. Moreover, the Py-ECH fuel may be functionally more attractive than ethanol, since it has greater energy density than ethanol and, as a hydrocarbon, it has greater potential for blending at higher levels into existing gasoline or diesel fuel-based transportation systems (distribution system and vehicles).

Sensitivity Analyses

Effect of model parameters

Sensitivity analyses were performed to determine the key parameters affecting the MFSP of the product fuel at the refinery outlet (Figure 4.7). Electricity cost, raw material cost, bio-oil yield, internal rate of return (IRR), electrocatalytic cell efficiencies, catalyst price and thickness, costs associated with catalyst replacement, capital costs at both depot and refinery and the selling price of by-product hydrogen were the parameters that were investigated. The values of these parameters were increased and decreased by either 50% or 25% and the results have been shown in the form of a tornado chart in Figure 4.7. A change of 25% for a parameter was only employed when a change of 50% from the value used in the model was impractical, e.g., a 50% increase from a biooil yield of 70% is not possible. Since the percentage change is not the same for all parameters, the tornado chart may not be the most reliable tool in ranking their sensitivity accurately. Therefore, another plot has been provided in Figure 4.10 of the Appendix, where the slopes of the plotted lines can provide a more accurate description of the relative ranking of the sensitivities. Higher the slope, more sensitive the parameter. A tornado plot is however easier to read. As evident from Figure 4.7, electricity cost and raw material costs are the most sensitive parameters in determining MFSP. This is intuitive since the Py-ECH system is a major consumer of electricity and any change in the price of electricity will benefit the system greatly. Similarly, the other major input is the biomass raw material and reduction in its cost would certainly decrease the MFSP. Bio-oil yield, current and voltage efficiencies, the assumed internal rate of return, and catalyst price and thickness are also important parameters; followed by the selling price of the by-product excess H₂ gas. This is also understandable as increase in bio-oil yield and the cell efficiencies essentially means reduction of losses in the system and an increase in the overall yield of the final

fuel and therefore, a reduction in MFSP. Catalyst price and thickness are also sensitive owing to the high cost of the noble metal catalyst, Ru, being used in the system. The catalyst replacement costs, whether in the ECH unit at the depot or the hydroprocessor unit at the central refinery are not sensitive parameters.

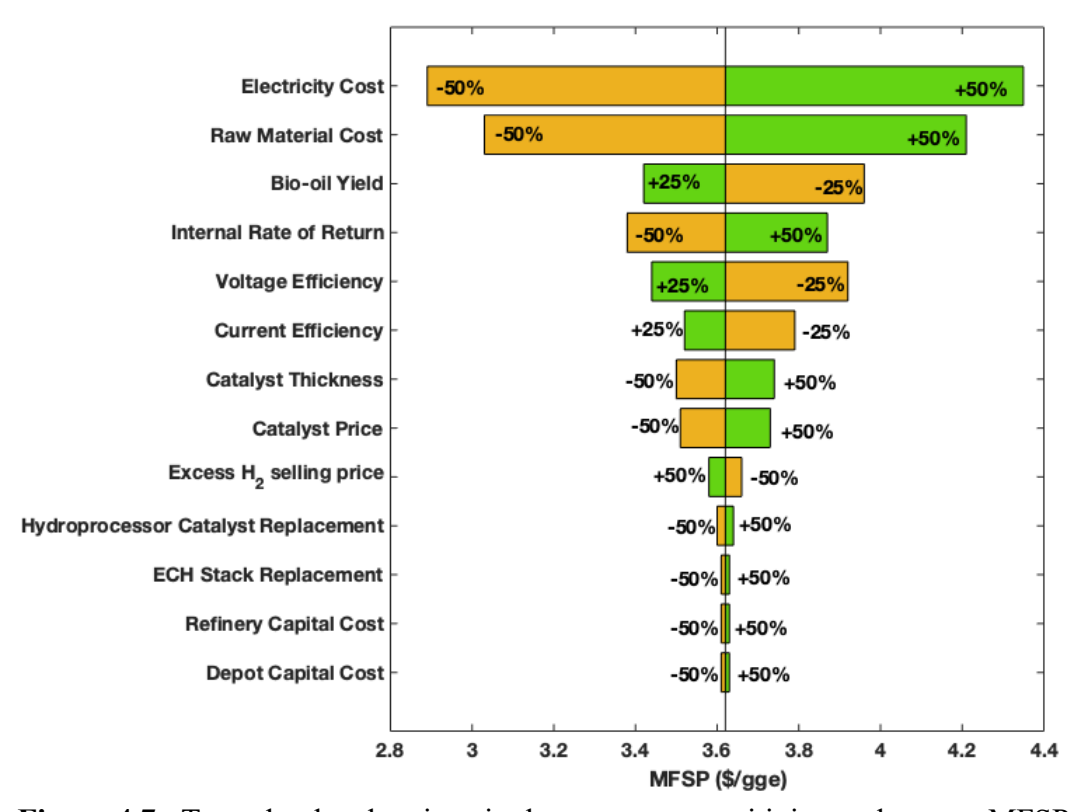


Figure 4.7: Tornado plot showing single parameter sensitivity analyses on MFSP

Similarly, the MFSP is hardly sensitive to the capital costs at the depot and refinery. From the observed list of eight most sensitive parameters, it can be seen that at least five are directly linked to the ECH unit. This highlights the significance of ECH in the Py-ECH bioenergy system. Of the remaining three, two are related to the pyrolysis unit and the last one, namely the IRR is an economic parameter. As both the pyrolysis and ECH units are at the depot, the sensitivity analysis essentially points towards opportunities at the depot for further optimizing the economics of the Py-ECH system. Furthermore, it is evident from the analysis that attention must be focused on

optimizing the ECH catalyst, process conditions and efficiencies in comparison to equipment costing.

Effect of Refinery Size

In order to be consistent with the NREL cellulosic ethanol process analysis, the refinery size was assumed to be 2,000 tonnes/day. However, it must be recognized that this might not be the optimum refinery size that generates the minimum MFSP. Therefore, variation of MFSP with refinery size for different depot sizes was investigated, as shown in Figure 4.8. Similar to the optimization of depot sizes in Figure 4.2, the MFSP goes through a minimum as refinery sizes are increased, for different depot sizes.

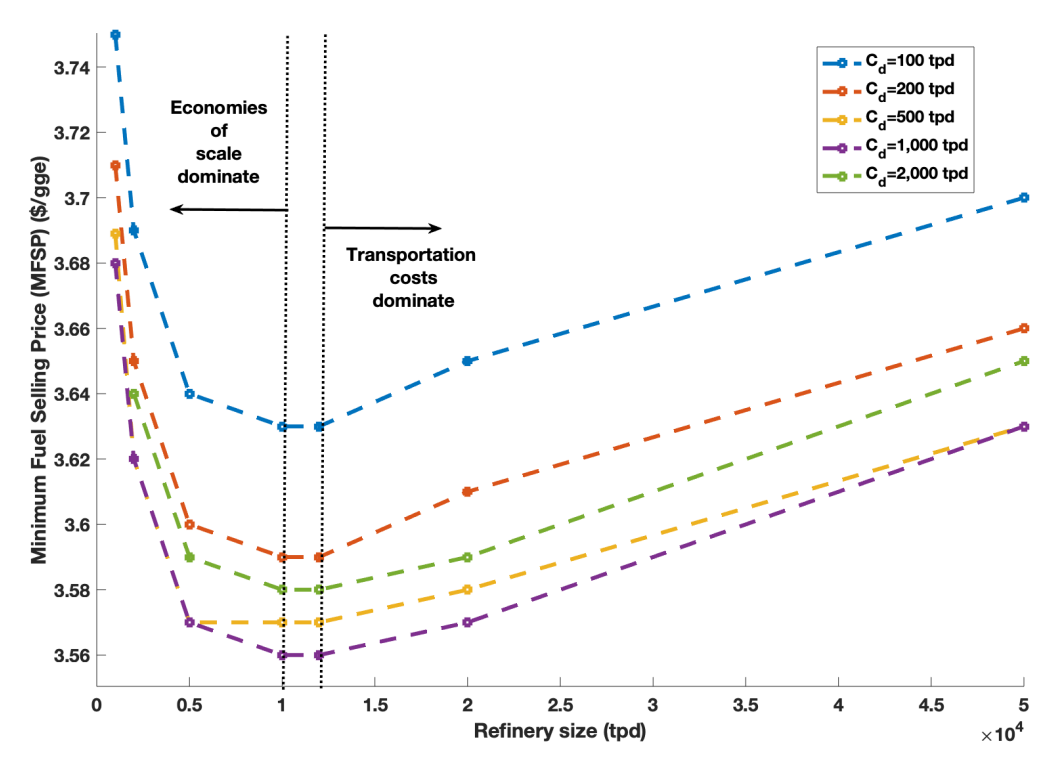


Figure 4.8: Effect of depot size on MFSP for different refinery sizes. C_d denotes depot capacity

This is again because there are the opposing forces of economies-of-scale and transportation costs at work here. At lower refinery sizes, economies-of-scale dominate and at higher refinery sizes,

transportation costs dominate. There is also the middle zone where these two forces counterbalance. This happens at refinery sizes of 10,000-12,000 tpd.

This shows that the Py-ECH system can achieve even lower MFSPs at higher refinery capacities. From Figure 4.8, a MFSP of \$ 3.56/gge can be achieved for a refinery size of 10,000 tpd, employing 10 depots, each having a capacity of 1000 tpd. This is crucial, when viewing the Py-ECH system, independent of the comparison to the CE system.

Discussion

While a MFSP of \$3.62/gge for the Py-ECH fuel is better than the \$3.71 for ethanol in the CE system, the long-term goal, of course, is to try and compete with gasoline and diesel prices. In this regard, the sensitivity analysis points to areas, where there is further scope of improvement in this value. In this regard, Figure 4.7 shows the effect of individual improvements in the parameters, on the final MFSP. It would, therefore, be interesting to investigate the effect of stacking up these major improvements on the MFSP. The reductions in MFSP, gained by stacking up these improvements have been plotted in a waterfall chart in Figure 4.9. From the sensitivity analysis in Figure 4.8, it is clear that the electricity cost, bio-oil yield, raw material cost, cell efficiencies, catalyst price and thickness and the internal rate of return are the key parameters. However, it is difficult to improve upon the value assumed in the present model for some of these parameters. For example, the pyrolysis bio-oil yield has been assumed at 70%, which is among the highest values observed in literature. Raw material costs on the other hand, have already been fairly optimized by optimizing the transport costs via the decentralized approach in the present model. There is little scope of improvement there. Also, internal rates of return less than 10%, as assumed in the model are unlikely. However, there is great potential in optimizing the cost of electricity. While electricity has been assumed to cost at 6.56 ¢/kWh in the model, future costs as low as \$0.03

/kWh are projected for wind and solar photovoltaics with advances in materials and manufacturing improvements. 196 The U.S. EIA 197 also reports the levelized cost of electricity from different sources, with and without tax credit. It ranges from 3.91 ¢/kWh (for hydroelectric sources) to 15.70 ¢/kWh (for solar thermal sources), without any tax credit. The effect on MFSP of using these different electricity sources have been explored in Figure 4.11 of the Appendix. Furthermore, the Wind Energy Technologies Office at the U.S. Department of Energy estimates a price of 1-2 ¢/kWh for electricity produced from wind sources, after applying the production tax credit. Therefore, a reduction of the price in electricity to 3 ¢/kWh is very much feasible. Such an improvement would result in a 65¢ drop in the MFSP. Similarly, a current efficiency of 67% has been assumed in the current model, but An et al., have reported current efficiencies of 70% for hydrogenation of soybean oil in a solid polymer electrolyte reactor when hydrogen is generated from electrolysis of water.²⁴ Pintauro et al., also observed current efficiencies as high as 97% when hydrogen gas was used for electrochemical hydrogenation of soybean oil.¹⁹⁸ Therefore an improvement in current efficiency from 67% to 95% may be achievable. This can cause a further 15 ¢ reduction in MFSP. The catalyst (Ru) price, assumed at \$263/troy oz, the average 2019 price, has ranged from \$40-270/troy oz over the last 10 years with an average of approximately \$121/troy oz. 199 While prices were as high as \$ 180/troy oz in 2011, they dipped to around \$ 40/troy oz in 2016 while again climbing as high as \$270/troy oz in 2019. Therefore, it is very much plausible that there would again be a future dip in prices. Therefore, a future drop to a 10-year average value of \$ 121/troy oz is a reasonable improvement. Such a reduction in price of catalyst would result in a further 8 ¢ decrease in the MFSP. Future improvements in voltage efficiencies and the thickness of catalyst layer that would give similar yields and current efficiencies are difficult to estimate due to lack of sufficient relevant information and hence, were not considered in this stack up analysis.

It was discussed in the previous section that a change in the refinery size can lead to a lesser MFSP. Since the optimum refinery size was evaluated at 10,000 tpd; the change in refinery size from the assumed 2,000 tpd to the optimum 10,000 tpd was another improvement that was stacked. This resulted in a further drop in the MFSP by 6 ¢/kWh. Finally, although ECH stack replacement cost is not a sensitive parameter, it was still investigated to see if there is much change in the MFSP, when such an improvement is stacked with the other improvements. The ECH stack replacement was changed from 15% of installed capital costs with a replacement schedule of 7 years to 12% of installed capital costs with a replacement schedule of 10 years.²⁰⁰ The final MFSP after stacking up all the improvements is \$2.67/gge. This is shown in the green bar at the extreme right. A further reduction in MFSP may be achieved by selling the by-product biochar being generated at the depot. This was not considered in the basic analysis due to lack of information on the quality of biochar that would be generated and inability to fix a price for the vast range of values in literature without compromising the integrity of the comparative analysis. Therefore, it is handled as an alternate scenario, represented by the yellow bar on the right. If biochar is sold at \$ 78.26/tonne (most conservative value observed in literature)¹⁹¹, the final MFSP of the Py-ECH fuel can drop to as low as \$ 2.57/gge. Finally, Figure 4.9 also highlights the benefit from the optimization of the transportation costs in the decentralized Py-ECH system. This is shown by the yellow bar on the extreme left. If the transportation cost contribution to the raw material cost wasn't optimized and the feedstock cost of \$68.33/dry tonne (as assumed in the CE system in the Humbird et al., report) was used in the Py-ECH system, the MFSP would increase to \$ 3.76/gge. In other words, the optimization of the transportation costs helped reduce the MFSP by 14 ϕ /gge.

In summary, the present technoeconomic analysis for the Py-ECH system (where four 500

tonne/day depots process corn stover and supply ECH-stabilized bio-oil to a central refinery for further hydroprocessing) yields a projected MFSP of \$3.62/gge for the final hydrocarbon fuel. This MFSP is slightly lesser than that for ethanol from cellulosic ethanol refineries (\$3.71/gge) using consistent assumptions. Pathways for further reductions in MFSP were determined in a sensitivity analysis by identifying key sensitive parameters. These were electricity cost, raw material costs, pyrolysis bio-oil yield, ECH current efficiencies and the price and thickness of ECH catalyst. Finally, it was observed that stacking up some of the feasible major improvements can reduce the MFSP to as low as \$2.67/gge and \$2.57/gge when the by-product biochar is sold at approximately \$80/tonne.

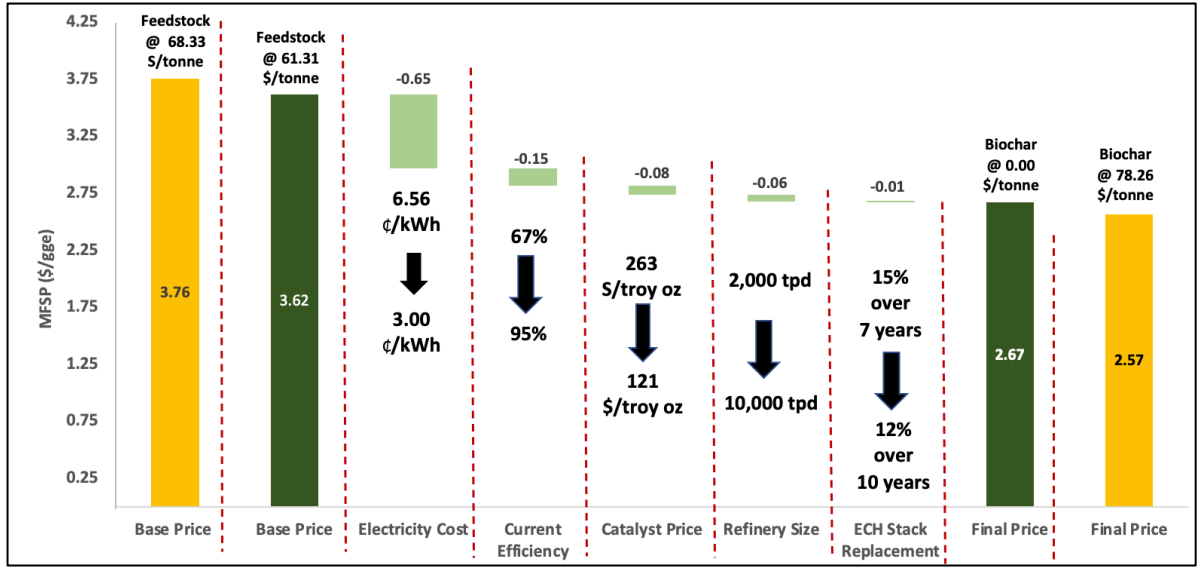


Figure 4.9: Waterfall chart showing potential reduction in MFSP assuming combinations of improvements in selected model parameters. The light green bars indicate the reductions in MFSP owing to the stacking up of system improvements. The dark green bars denote the initial and final MFSP (after all improvements). The yellow bars denote alternate scenarios, not considered in the baseline model.

APPENDIX

Equipment Costing & Operating Costs

This section provides the assumptions for calculating the equipment costs for the different unit operations at the depot stage and the refinery stage.

Depot Equipment Costs:

The depot was subdivided into six distinct areas, namely: Drying and Grinding, Pyrolysis, Condensation, Electrocatalytic Hydrogenation, Storage, and Combustion. Most of the purchased equipment costs at the depot were estimated using the online calculator for "Equipment Costs-Plant Design and Economics for Chemical Engineers" by Peters and Timmerhaus.^{201, 202}

Drying and Grinding:

Drying equipment cost was calculated for a rotary dryer using the rate of water evaporation needed to reduce biomass moisture content from 20% to 5% by mass.^{201, 202} A ball mill was selected to reduce the feedstock from >50 mm to 2 mm particles.^{201, 202}

Pyrolysis:

The purchased equipment costs for pyrolysis were estimated based on the calculated heat duty of the pyrolysis furnace.^{201, 202}

Condensation:

For condensation of the bio-oil after pyrolysis, the heat transfer area was calculated from the heat transfer rate, the log mean temperature difference of the two fluids, and the heat transfer rate coefficient of a shell and tube heat exchanger.²⁰³ Using the required heat transfer area, the cost of a shell and tube heat exchanger was estimated.^{201, 202}

Electrocatalytic Hydrogenation (ECH):

The ECH reactor system have been described in detail in the work by Lam et al.,²⁰⁴ and previous literature.^{23, 32, 34, 136, 137, 196, 198, 205} The ECH reactor for this analysis have been considered to be a

collection of polymer electrolyte membrane (PEM) stacks.^{30, 198, 205, 206} In these PEM stacks the catalytic Ru cathode and the Pt anode are pasted on two sides of a Nafion proton exchange membrane. Capital costs for the ECH reactor system are dominated by the costs of the Pt anode, Ru cathode, and the Nafion membrane. The amounts of Pt and Ru required for the ECH reactor were estimated from the current densities, bulk densities, catalyst thickness, and the electricity requirements to chemically reduce the pyrolysis bio-oil. The surface area and costs for the Nafion membrane were determined using the Nafion bulk density, acid capacity, and the electricity requirements. It has been estimated that the membrane and electrode costs are only 60% of the total stack cost; the stack, in turn accounts for only about 40% of the total electrolyser capital cost.²⁰⁷ Therefore, the total electrolyser capital costs were estimated from the membrane and electrode costs using these percentages. The replacement costs were estimated to be about 15% of the installed capital costs, with a replacement schedule of 7 years. 200, 207 This cost was incorporated in the analysis as an annual variable cost. The installation costs were assumed to be 15% of the total uninstalled capital costs.²⁰⁰ Electricity costs were assumed, in accordance with the Humbird et al., report at 6.56 ¢/kWh. Similarly, fresh water costs were also assumed from the same report at \$ 0.22/tonne in 2007\$.11

Storage:

Storage costs for H₂ generated from ECH at the depot were calculated by assuming underground storage.²⁰⁸ Stable bio-oil storage at the depot was assumed in shop-fabricated stainless steel tanks with walls of thickness 6.35 cm.²⁰¹ Stainless steel was chosen as the storage material, as only 304L and 316L stainless steel satisfy the criterion for corrosion rates of <0.25 mm/year when in contact with ECH-treated bio-oil.²⁰⁹ Lu et al., also observed that stainless steel was the most resistant to

corrosion from bio-oil when compared to mild steel, aluminum and brass.²¹⁰ This, in spite the fact that ECH renders bio-oil much less corrosive than pyrolysis bio-oil.

Combustion:

A gas-fired furnace was sized to combust the non-condensable gases (NCG) and a fraction of the H₂ gas to provide heat for all processes at the depot such as pyrolysis.²¹¹

Refinery Equipment Costs:

The central refinery was sub-divided into three units, namely, the electrolysis unit (used to make hydrogen for hydroprocessing), the storage unit, and the hydroprocessing unit. The raw material for the refinery is the stable bio-oil product delivered from the depots.

Storage:

Storage costs for the final hydroprocessed bio-oil were estimated from fabricated stainless steel tanks with wall thickness equal to 6.35 cm.^{201, 202}

Electrolysis:

Electrolyzer capital costs for making H_2 gas for hydroprocessing the stable bio-oil at the refinery can vary over a large range. Saba et al., in 2018, conducted a comprehensive review of the cost of electrolyzers over the past 30 years and found them to range between ϵ 306 (per kW of HHV of H_2 gas produced in 2017 ϵ) and ϵ 37521(per kW of HHV of H_2 gas produced in 2017 ϵ), depending on type of electrolyzer, assumed efficiency, scale of production and year of estimation. Based on the values reported by Saba et al., to be an estimation by PEM experts, projected electrolyser costs in 2030 will be ranging from ϵ 397 to ϵ 955 (per kW of HHV of H_2 gas produced in 2017 ϵ). Therefore, for the purposes of this analysis, an average value of ϵ 676 (per kW of HHV of H_2 gas produced in 2017 ϵ) was chosen. This translates to assuming a cost of \$ 1420/(kg/day) of H_2 gas produced in 2018 ϵ). Stack replacement costs were considered to be 15% of installed capital costs

over 7 years as assumed for ECH at the depot. Electricity costs were again, assumed at $6.56 \, \text{¢/kWh}$, in line with the Humbird et al., report.

Hydroprocessing:

Hydroprocessing costs were estimated by scaling-up the costs associated with a hydroprocessing facility that subjects pyrolysis bio-oil to H₂ gas at elevated temperatures and pressures in the presence of zeolite catalyst, as determined by Dutta et al., in a joint report by NREL and PNNL in 2015.²¹³Although the biomass feedstock for the Dutta et al. report, is a blended woody biomass; however, the hydroprocessing area houses equipment that is very similar to what would be expected in the hydroprocessing section of the Py-ECH plant, namely, a hydrotreater, hydrocracker, compressors, product separation columns and heat integration facilities. Therefore, when scaled by the amount of hydroprocessor feed, the estimated capital costs should be a good approximation for the Py-ECH process. A scaling factor of 0.6 was used to account for the change in the amount of feed being handled. The amount of catalyst required was estimated by assuming a weight hourly space velocity (WHSV) of 0.5 hr⁻¹, in accordance with the Dutta et al., report, purchased at \$ 20/lb (in 2011 \$), with replacement of the initial fill every 2 years.²¹³ Natural gas required for heating purposes at the refinery were estimated at \$ 7.86/1000 cubic feet (in 2007\$).²¹⁴

Table 4.4: Assumptions for Calculating the Total Capital Investment and Total Operating Cost

Total Installed Capital Cost is the sum of installed equipment costs

Inside Battery Limits (ISBL) is the total installed capital cost excluding storage

Direct Costs

Warehouse 4% of ISBL
Site Development 9% of ISBL
Additional Piping 4.5% of ISBL **Total Direct Cost (TDC)** is the sum of all direct costs

Indirect Costs

Pro-ratable Costs 10% of TDC Field Expenses 10% of TDC Home Office and Construction 10% of TDC Table 4.4 (cont'd)

Project Contingency	10% of TDC	
Other costs	10% of TDC	
Total Indirect Cost (TIC) is the sum of all indirect costs		
E' LC '/ LL / / (ECD ' / CTDC 1TIC		

Fixed Capital Investment (FCI) is the sum of TDC and TIC

Land 1.6% of total installed capital cost

Working Capital 5% of FCI

Total Capital Investment (TCI) is the sum of FCI, land, and working capital

Fixed Operating Cost

Salaries 0.5% of TCI
Labor Burden 90% of salaries
Maintenance 3% of ISBL
Property Insurance 0.7% of FCI

Total fixed operating cost is the sum of all fixed operating costs

Total variable operating cost is the sum of variable costs, e.g. utilities and raw materials

Total Operating Cost is the sum of total fixed and variable operating costs

Table 4.5: Range of values of biochar found in literature (adapted from Campbell et al.,)²¹⁵

Biochar Price (in 2018\$)	Price Based on	Technology	Description	Citation
(\$/tonne) 230.31	Breakeven price	Pyrolysis	When biochar quantity is maximized @ 300°C Produced alongside methanol	216
293.12	Breakeven price	Pyrolysis	When biochar quality is maximized @450°C Produced alongside methanol	216
117.44	Energy value	Pyrolysis	Relative to cost of Central Appalachian coal	217
68.34	Soil enhancement ability	Pyrolysis	Includes fertilizer application cost of \$40/tonne Includes hauling cost of \$8/tonne	218
78.26	Energy value	Fast pyrolysis	Price for optimal temp of 525°C Yield: bio-oil: 55% and biochar: 20% Max revenue: \$118.48/tonne Assumption: Price/unit energy of bio-oil is equal to that of fossil oil Price/unit energy of biochar is equal to that of coal \$75/tonne for pyrolysis at 500°C	219
142.98	Technoeconomic analysis	Pyrolysis	For Sub-Saharan Africa region (Range 99-165) Discount Rate of 10%	220
224.21	Technoeconomic analysis	Pyrolysis	For Northwestern Europe (Range 155-259) Discount Rate of 10%	220
2,868.42	Survey of biochar sellers		US average from survey of 23 companies Based on the survey of 43 companies worldwide, 23 in the US Does not include shipping or handling costs Mix of retail and wholesale prices Mix of pure biochar and blends	39 215

111

Table 4.5 (cont'd)

1,834.00	Communication with industry		Wholesale price	
88.98	Energy value	Slow pyrolysis	Bio-oil produced (38%) sold at \$ 192/tonne Biochar produced (26%) Revenue of \$ 93/tonne of forest-based feedstock	221
2,382.94	Market value		Market value for soil amendment @\$2.2/kg; possibly retail price	
414.97	Technoeconomic analysis	Pyrolysis	This is average price in UK Min: \$222/tonne; Max: \$584/tonne Includes shipping and handling	223
1,763.81	Market survey		Most often cited price Dependent on volume and packaging	

Table 4.6 : Summary of factors determining assumed costs for corn stover transport to depots as assumed by $\underline{\text{Kim}}$ et al. 74

	$d_f = w $	$f_s.h_r/24$ $Y_{stover}.r\%.f_{corn}.\pi.f_a.(1-f_l)$
Symbol	Unit	Meaning
d_{f}	$10^2 \mathrm{m}$	Farm to Depot Distance
f_s	tonnes/day	Facility Size
$h_{\rm r}$	hours	Annual operating hours
f_a		Percentage of participating farms
W		Road winding factor
f_l		Transportation and Storage loss factor
f_{corn}		Ratio of harvested corn area to total land
		area
Y_{stover}	tonnes/ha	Dry corn stover yield
r%	%	Fraction of corn stover collected

Table 4.7 : Summary of supply chain costs for corn stover for CE and Py-ECH systems as used in model. 225 All values in 2018\$/tonne of delivered biomass

	Supply Chain Operation	CE system	Py-ECH system
		(\$/tonne)	(\$/tonne)
	Harvest and Collection	16.64	16.64
	Storage and Handling	3.10	3.10
	Grower Payment	38.59	38.59
7	Transportation and Handling	10.00	2.97
	TOTAL	68.33	61.30

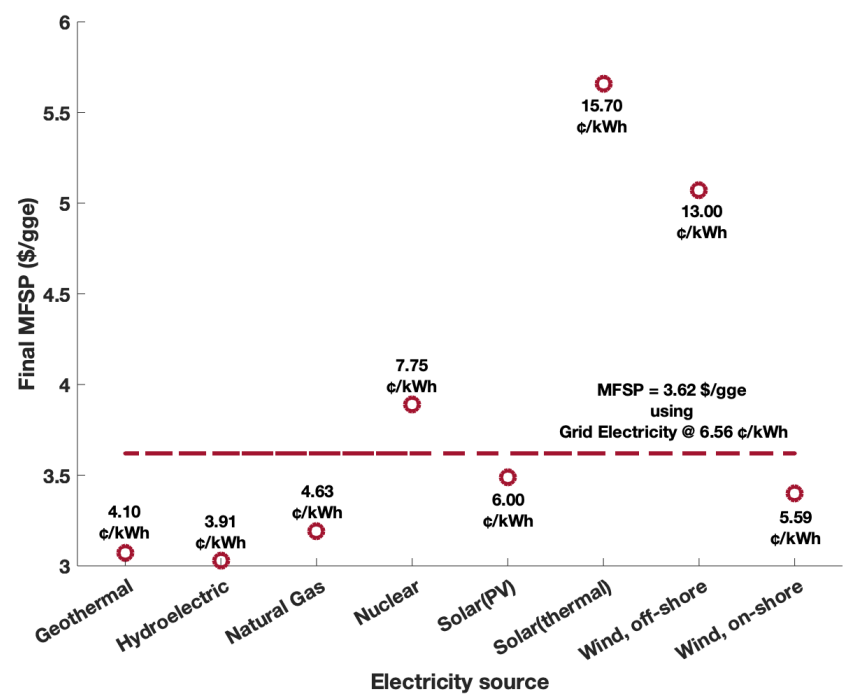


Figure 4.10 : Electricity costs from different sources. Red dashed line indicates the MFSP using MRO-West U.S. grid electricity, assumed as a baseline in the model. ¹⁹⁷

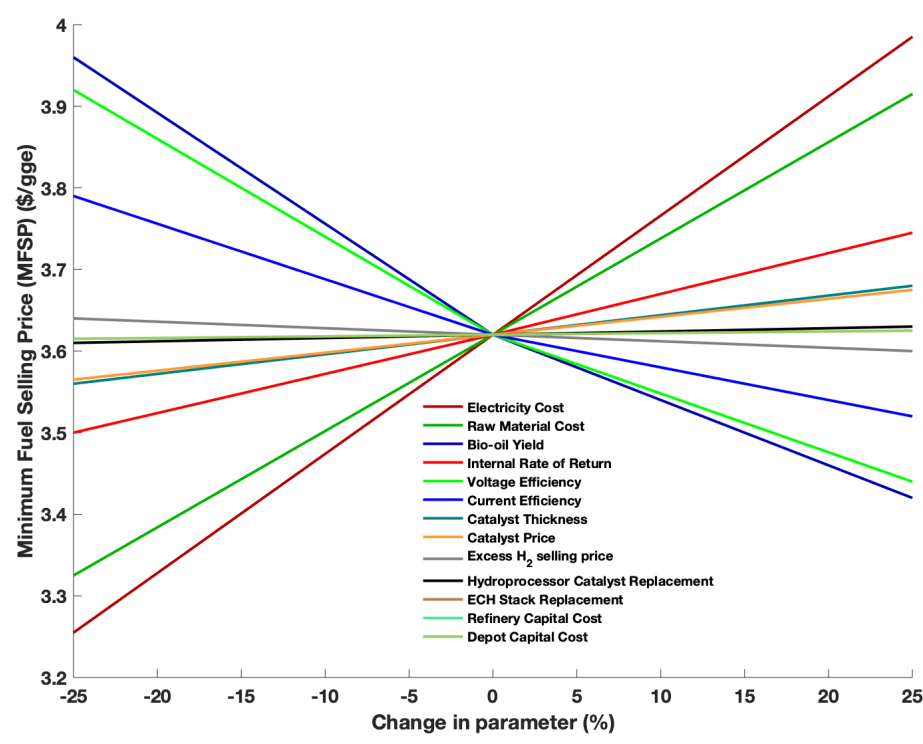


Figure 4.11: Sensitivity analyses on MFSP for all parameters. Larger the slope, greater the sensitivity to that parameter.

Data Inventory

Table 4.8: Key ECH and Pyrolysis parameters

Table 4.6. Rey Echi and Fylorysis parameters			
Parameter	Value	Source	
ECH			
Platinum current density	1000 mA/cm^2	Kreuter et al., ²²⁶	
Platinum thickness	100 nm		
Platinum density	21.45 g/cm^3		
Platinum price	29.33 \$/gram		
Nafion 117 conductivity	10 S/m	Liu et al., ²²⁷	
Nafion 117 price	$2222.22 \ \text{m}^2$		
Nafion acid capacity	0.9 meq cations/g dry Nafion		
Nafion thickness	0.1778 mm		
Ruthenium current density	10 mA/cm^2		
Ruthenium thickness	100 nm		
Ruthenium density	12.2 g/cm^3		
Ruthenium price	263 \$/troy oz		
ECH Current Efficiency	67%		
ECH Voltage Efficiency	75%		
ECH Temperature	80°C		
ECH Pressure	1 atm		
Pyrolysis			
Pyrolysis Bio-oil Yield	70%		
Pyrolysis Biochar Yield	15%		
Pyrolysis NCG yield	15%		
Pyrolysis Temperature	500°C		
Pyrolysis Pressure	1 atm		

Table 4.9: Installation multipliers for different processing units

Processing Unit	Installation Multiplier
At Depot	
Drying	1.70
Grinding	1.70
Pyrolysis	1.80
Condensation	2.20
ECH	1.15
Combustion	1.80
Storage	
At Central Refinery	
Hydroprocessing	1.70
Electrolysis	1.15
Storage	1.80

Chapter 5: LIFE CYCLE ASSESSMENT OF THE PY-ECH SYSTEM

<u>Abstract</u>

Quantification of the environmental impacts of bioenergy systems is essential when deciding how to replace fossil-based systems. Life cycle assessments are the most reliable and established means of estimating the environmental impacts of any such system. Bioenergy systems employing localized fast pyrolysis combined with electrocatalytic hydrogenation, followed by centralized hydroprocessing (Py-ECH) potentially have higher carbon and energy efficiencies vs. traditional cellulosic biorefineries. In this study, a cradle-to-grave LCA was performed to calculate the environmental performance of this Py-ECH system in three impact categories, namely, global warming potential, eutrophication potential, and the water scarcity footprint. Results were compared to those for traditional cellulosic ethanol fermentations using both NREL and GREET models. Analyses reveal that the Py-ECH system has much lower eutrophication potential and water scarcity footprint compared to cellulosic ethanol biorefineries. It also highlighted the importance of finding sources of renewable electricity in ascertaining favorable global warming potentials. A sensitivity analysis shows that the annual carbon sequestration rate can play a significant role in determining system-wide global warming potential.

Introduction

Fossil fuel energy, such as the range of liquid fuels derived from crude oil or natural gas, have often been shown to be significant contributors to air and water pollution. Such fuels are non-renewable as the rate of replenishment is much slower than the rate of use. There is a need to look for alternative energy production systems that are less polluting and renewable. In fact, the Energy Independence and Security Act (EISA),³ passed in 2007, aims to increase the production of cleaner renewable fuels, as part of the overall mission of improving U.S. energy independence and

security. The EISA promotes an increase in the production of biofuels as a cleaner and renewable alternative to fossil fuels by producing at least 21 billion gallons of advanced biofuels (with 16 billion gallons of cellulosic biofuels) by the year 2022. In accordance with EISA, these advanced biofuels should reduce 50% of the greenhouse gas emissions compared to the baseline established in 2005.

Fermentation of lignocellulose-derived sugars into ethanol has been arguably the most studied advanced biofuel system since the enactment of the EISA. However, traditional cellulosic ethanol systems are inherently carbon and energy inefficient as one-third of the carbon in biomass is lost as carbon dioxide and the process does not typically use biomass' lignin (accounting for 40% of biomass energy) for making liquid fuel. These are significant shortfalls, especially vis-à-vis the Billion Ton Report of 2016, 172 which highlights the importance of carbon and energy efficiencies of biofuel production systems. The report suggests that there is not enough energy in biomass (that can be procured at \$60/dry ton or less) in the entire United states to satisfy the demands of even the transportation sector in 2019. This was the motivation for developing the concept of a decentralized pyrolysis and electrocatalysis (Py-ECH) bioenergy system that is advantageous in carbon and energy efficiency when compared to traditional cellulosic fermentations to ethanol.⁵ The Py-ECH system combines localized fast pyrolysis and subsequent ECH, with centralized petroleum-style hydroprocessing to produce "drop-in" liquid hydrocarbon fuels. While fast pyrolysis deconstructs the biomass to liquid bio-oil, solid biochar and non-condensable gases, the ECH employs mild conditions to sufficiently hydrogenate and upgrade the energy content of the bio-oil, so that it is stable for storage and transport to a central refinery. At the refinery, the stable bio-oil is subjected to high temperatures and pressures to produce liquid fuel-range hydrocarbons that is similar to gasoline in terms of energy content. Corn stover was selected for the analysis to

fairly compare with the cellulosic ethanol (CE) process as established by Humbird et al., in 2011,⁵ which also used corn stover. In parallel work as this LCA, technoeconomic analyses of the Py-ECH system revealed a minimum fuel selling price (MFSP) of \$3.62/gge (for a fixed internal rate of return of 10%) in comparison to \$3.70/gge for the CE system, in 2018\$. However, with sufficient improvements in technology, the MFSP for the Py-ECH system could drop under \$3/gge.

With a pathway for thermodynamic and economic favorability of the Py-ECH system already established, in comparison to the CE system, the present work takes the next step by comparing the environmental impacts through LCA. Though many CE LCAs have already been conducted using different biomass feedstocks, 228-235 this exercise was repeated to maintain consistent assumptions for the two systems under consideration. While conducting a full cradle-to-grave analysis, including corn cultivation through end-use fuel combustion in vehicles, this work's primary goal is to compare the two technologies under study, namely, Py-ECH and CE. Previous LCA studies have proven the environmental advantages of CE systems over fossil fuel systems. The present comparative environmental analysis of the Py-ECH and CE systems, serves as an integral step in the commercial application of the Py-ECH system, as a viable alternative to fossil fuel systems. It must be noted that life cycle analyses have also been performed for biomass pyrolysis (followed by upgrading using hydrogen gas from different sources), which have highlighted the advantage of pyrolysis upgrading systems over fossil fuel systems.²³⁶ Similarly, a recent life cycle analysis on a depot based bioenergy system have also shown a pathway to carbon negative cellulosic biofuels.²³⁷ The Py-ECH system, however combines biomass pyrolysis upgrading (using mild electrocatalytic hydrogenation) with a decentralized system approach.

<u>Methodology</u>

A full-scale comparative "cradle-to-grave" life cycle assessment (LCA) was conducted for the Py-ECH and the CE processes for three environmental impact categories: global warming potential, eutrophication potential, and water scarcity footprint. Additionally, the energy return on investment for the two systems was also determined to compare their fossil energy footprint. The life cycle inventory was built in spreadsheets, combining appropriate values from well-established models like GREET, ²³⁸ CCLUB, ²³⁹ and process flow data as provided in the work by Lam et al...⁵

Functional Unit

Since the primary functionality of the two bioenergy systems is to produce fuel energy, the functional unit chosen for the LCAs was 1 MJ of produced fuel energy. Therefore, all emission values calculated in the present analysis are for the production of 1 MJ of fuel energy.

<u>Life Cycle Impact Categories</u>

Global Warming Potential (GWP)

Climate change or global warming potential is a worldwide grand challenge to human existence that is primarily caused by carbon dioxide, methane, and nitrous oxide emissions. Traditionally, climate change has been measured by the GWP (Global Warming Potential) from the TRACI model developed by the U.S. EPA (Environmental Protection Agency).^{240, 241} Although the GWP values in this model are for a 100 year time horizon and are not exactly accurate for a 20 year time horizon, they are sufficient for a fair comparison between the two processes.

Water Scarcity Footprint (WSF)

Bioenergy systems are inherently water intensive and therefore, water depletion/use is an important parameter that needs to be investigated. Bayart et al., defines Freshwater Depletion as the "Net reduction in the amount/availability of freshwater in a watershed or/and fossil

groundwater stock. Depletion occurs when freshwater consumptive use exceeds the renewability rate of the resource over a significant time period."242 In 2018, Boulay et al., developed characterization factors for water use in LCA, based on the amount of water remaining in a given watershed per unit area relative to the global average after all human and ecosystem demands have been met.²⁴³ These characterization factors are known as "AWARE" (available water remaining) factors. Multiplication of the inventory data with these characterization factors gives the potential for depriving another user of water, which is proportional to the water use and inversely proportional to the water availability. The characterization factors range from 0.1 to 100, with 1 being equivalent to the world average, 0.1 being areas where 10 times more water is available and 100 being areas with most water scarcity. The average AWARE characterization factor in the United States for agricultural use and non-agricultural use is 36.49 and 9.51 respectively. 150 However, in this analysis, the AWARE characterization factors used were the average for the major corn producing states in the Midwest, which are also part of the Midwest Reliability Organization (MRO)-West e-GRID subregion, namely, Minnesota, Wisconsin, North Dakota, South Dakota, Nebraska, and Iowa. The average AWARE factors for these states for agricultural use and non-agricultural uses are 10.20 and 9.59 respectively. The expressions used in evaluating the Water Scarcity Footprint (WSF) are provided below:

$$WSF = w_i. CF_{AWARE}$$

$$CF_{AWARE} = \frac{1/AMD_i}{1/AMD_{world\ avg}} = \frac{AMD_{world\ avg}}{AMD_i}$$

$$AMD_i = \frac{(Availabilty - HWC - EWR)}{Area}$$

AMD is Availability minus Demand

HWC is *Human Water Consumption*;

EWR is Environmental Water Requirement

 w_i is total inventory of substance i (in m^3)

Eutrophication Potential (EUP)

Biomass production, which is an integral part of all bioenergy systems, is associated with the use of NPK fertilizers. These fertilizers are a major source for eutrophication in aquatic systems, which is defined as excess nutrient availability leading to exponential algal and cyanobacteria growth that harms marine sytems.²⁴⁴ The eutrophication potentials for the two systems were estimated using the TRACI Model,²⁴⁰ assuming little variation in the characterization factors for the Eutrophication Potential for 20 year and 100 year time horizons. The TRACI characterization factor for estimating Eutrophication Potential is a combination of a nutrient potency factor and a transport factor.²⁴⁵ While the potency factor is a measure of the effect of a particular nutrient, the transport factor accounts for the release of emissions into different media (e.g., air, water), ultimately reaching aquatic systems. The expression used in evaluating the Eutrophication Potential (EUP) is provided below:

$$EUP_i = e_i. CF_{air/water}$$

 $CF_{air/water}$ is the TRACI characterisation factor for substance i in air or water medium e_i is inventory data of substance i (in kg)

System Definition

The results of an LCA analysis can vary greatly depending on the placement of system boundaries. For this analysis, the Py-ECH system boundaries are defined by the cultivation of the corn plant (for the generation of stover) at the front end and by the combustion of the produced hydrocarbon

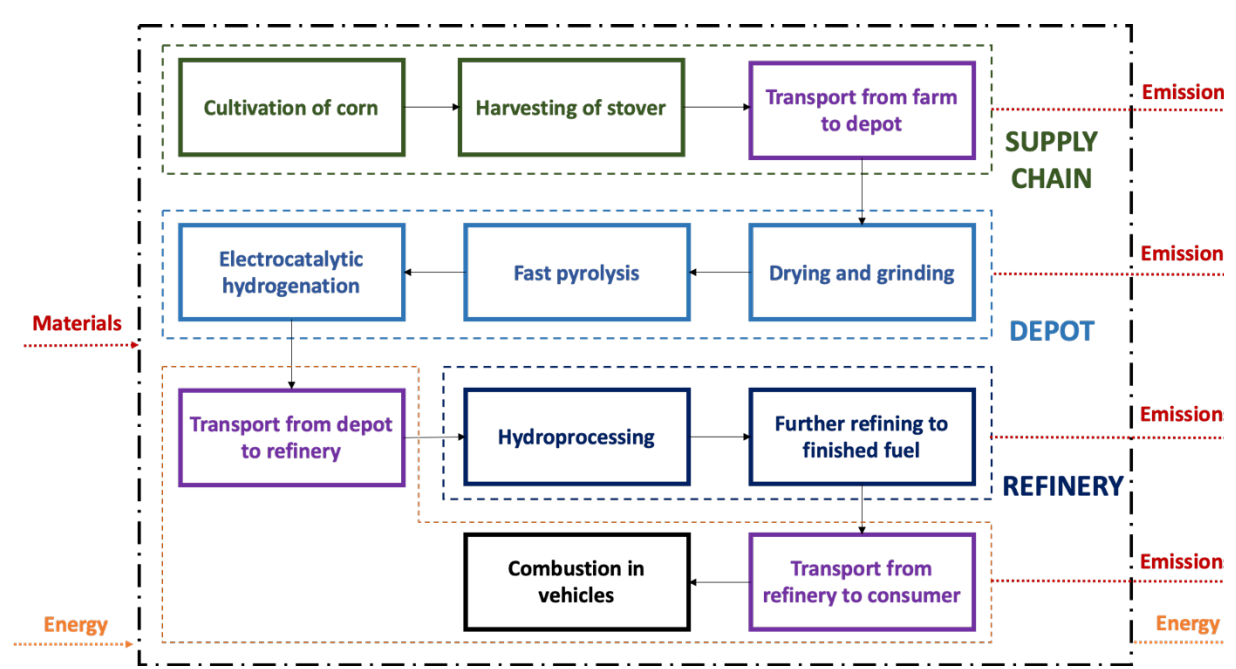


Figure 5.1: System boundaries for Py-ECH system

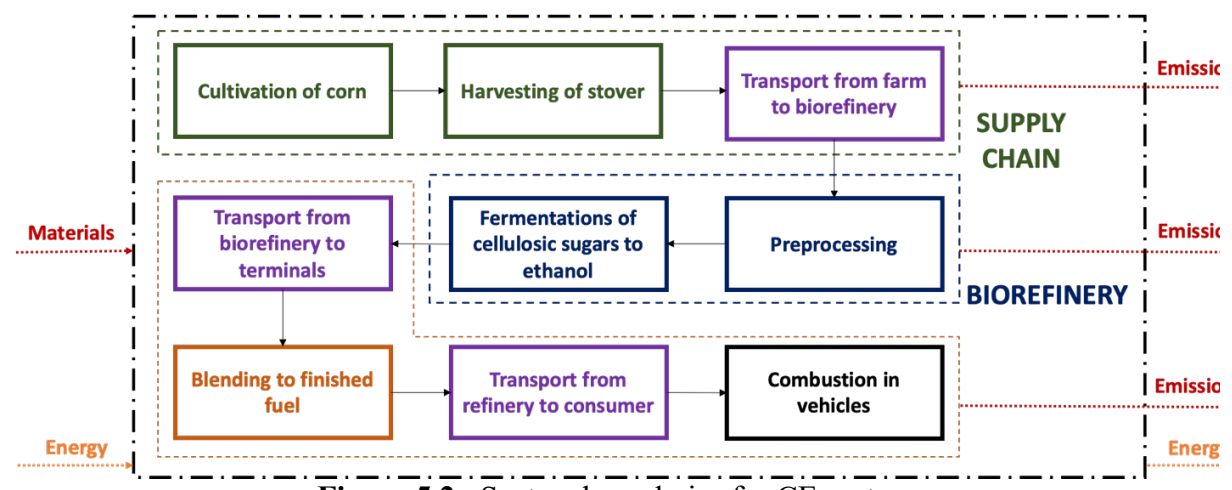


Figure 5.2: System boundaries for CE system

fuel at the back end. The CE system boundaries are similarly defined. This has been pictorially represented in Figures 5.1 and 5.2, where the two boundaries of the two bioenergy systems are shown. The major components of the whole system are depicted in different colors: the supply chain (green), processing at refineries (dark blue) or depots (light blue), transport (purple) and fuel combustion (black). For the CE system, similar flow diagrams may be found in the Humbird et al., report.¹¹

Time Horizon

A time horizon of 20 years was selected for the LCA to accommodate the transient response of the soil organic matter deposition.

Life Cycle Inventory (LCI)

The process flow data for the Py-ECH system were adopted from the work by Lam et al..⁵ For the CE system, the process flow data were extracted from NREL's report published in 2011. 11 All key LCI data were determined from established and well-known models like Argonne National Laboratories' GREET and CCLUB models. Other relevant data, that were absent from these models were extracted from reliable data sources like reports published by IPCC, EPA, and NREL. To qualify the collected inventory, data quality indicators (DQI) were assigned using the modified Weidema method.²⁴⁶ Originally Weidema et al. suggested five parameters to evaluate data quality: reliability, completeness, temporal correlation, geographical correlation, and technological correlation. However, Toffel et al. in 2004, renamed the completeness parameter with 'representativeness' and the temporal correlation parameter with 'data age'. They also split the reliability parameter into the acquisition method and independence of data supplier parameters to better characterize the data reliability.²⁴⁷ This modified Weidema method has been applied in the current study. Table 5.3 of the Appendix, at the end of this chapter, summarizes these parameters and describes the meaning of the scores assigned to the data on a scale of 1 to 5.248 All life cycle data used in this study have been listed, with their data quality indicators, in Table 5.4 of the Appendix.

Key LCI data and assumptions

As discussed before, the two bioenergy systems can be broadly classified into 4 major areas.

These are (a) the Supply Chain, (b) Processing, (c) Transport, and (d) Combustion.

Supply Chain

The supply chain consists of mainly two sub-processes, namely, the cultivation of the corn and the collection of the generated stover.

Cultivation of corn

Almost all data pertaining to the cultivation of corn were obtained from the GREET and CCLUB models. ^{238, 239} For the present analysis, it was assumed that corn is being cultivated in a continuous corn cropping system with no tillage. The cropland for corn cultivation is considered to be previously used for cropland or pastures. It was assumed that only 60 wt.% of the generated corn stover was removed from the fields, an important value because the percentage stover removal can impact the final GWP and EUP values.²⁴⁹ GREET provides only two options for stover removal, namely 60% and 30% by weight. To increase harvest yield, the 60 wt.% stover removal option was selected while also recognizing that retaining a minimum of 30% corn stover on the field decreases wind erosion by 70% compared to bare soil.²⁵⁰ GREET was again used for fertilizer input values, which includes the associated emissions for production and soil application. The carbon sequestration data were obtained from the CCLUB model and found to be 0.273 Mg C/ha/yr for 30% stover removal, which translates to 0.174 Mg C/ha/yr for a 60% stover removal, assuming a linear dependence on stover removal. It must be noted that soil carbon sequestration data are a function of soil texture, rainfall, tillage, stover removal, soil depth measured, crop rotation system, and geographical location. A comprehensive review on the range of values and their dependence on the aforementioned factors has been performed by Alvarez.²⁵¹ The sequestration values for no till corn cultivation varies greatly in literature, from 0.1 Mg C/ha/yr to about 5 Mg C/ha/yr, depending on these factors. 204, 252-258 To account for this range of data, a sensitivity analysis was performed to determine the effect of annual carbon sequestration rate on the total GWP. This

carbon sequestration rate is the net accumulation of carbon in the soil over the selected time horizon and it accounts for the translocation of carbon, fixed by photosynthesis, the carbon in root exudates, the carbon deposited in soil organic matter pools, and the carbon liberated as carbon dioxide due to soil respiration and microbial decomposition. Figure 5.3 diagrammatically shows the carbon flow for the CE and Py-ECH systems using GREET assumption for the annual carbon sequestration rate.

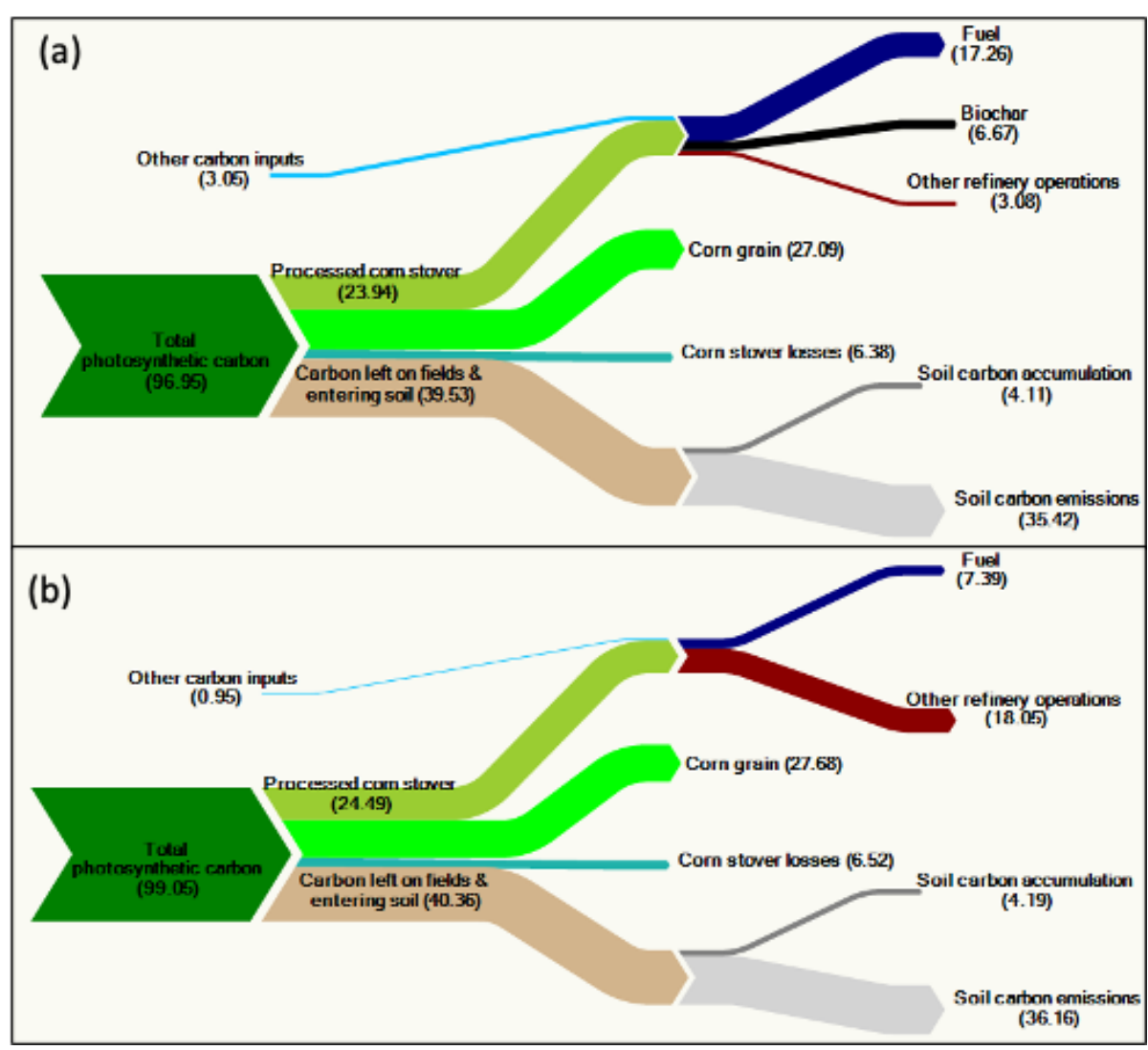


Figure 5.3: System carbon flow for (a) Py-ECH and (b) CE, for GREET assumed value of carbon sequestration.

The amount of water required for cultivation was extracted again from the GREET model. Water

can be separated into three categories: blue water (surface water and ground water), green water (water associated with precipitation) and grey water (water required to incorporate pollutants being discharged into freshwater bodies).²⁵⁹ For cultivation of crops, GREET only includes blue water consumption, where consumption is defined as the amount of freshwater used by the process for anthropogenic purposes and not returned due to evapotranspiration or degradation in quality.²⁶⁰ Green water consumption in cultivation may be neglected because it does not affect blue water use. 261-264 The underlying assumption is that green water consumption by the land area did not change due to crop cultivation. In fact, it is also argued in literature that the effects of green water consumption is better handled as a contributing parameter when estimating emissions due to change in land use. 262, 264 Grey water has also not been considered because its environmental consequences overlap with other impact categories, such as eutrophication in this study. Atmospheric emissions of nitrogen oxides (NOx), contributing to eutrophication potential in the cultivation stage due to fertilizer application and production, were extracted from GREET. Ammonia emissions, due to volatilization of a fraction of the applied fertilizers, were estimated from IPCC data. 265, 266 All three fertilizer nutrients (N, P, K) were considered; emissions due to N and P fertilizer runoff to water resources were obtained from a report published by NREL in 2005.²⁶⁶ N runoff to surface water was considered in the analysis, as runoff to groundwater was found negligible owing to geographic assumptions. The value for N surface runoff (as nitrates) was fixed at 24% of total fertilizer N added, as assumed in GREET. 266 Phosphorus only contributes to pollution in surface water due to runoff. There is only negligible quantities of P in the atmosphere²⁶⁷ and no contribution to ground water pollution owing to the strong sorption of P to soil minerals. The P runoff (as phosphates) to surface water bodies was estimated at an average of 7% of the total phosphorus added as fertilizer, which was found to vary between 1-14%. 266 Based

on the report, it is also assumed that potassium does not partition to air or water and has minimal impact on air and water eutrophication.

Collection of stover

The three basic operations associated with stover harvesting are windrowing, baling, and collection.²⁶⁸ A stalk chopper/windrower was selected to avoid collecting foreign material with the stover feedstock. For baling, square balers are assumed, as square bales are transported more easily. Moreover, square bales have the advantage of higher bulk density, thereby reducing transportation costs. ^{269, 270} For collection, tractors with bale forks are used, which handles a single bale at a time.²⁶⁸ All collection equipment were assumed to run on diesel and the total diesel required for the full harvest of stover, excluding grain, were estimated from GREET at 3.58 gallons of diesel per acre. The emissions associated with burning diesel were also determined from GREET. It must be noted that stover collection emissions are calculated after accounting for storage, transportation, and farm handling losses of 8.4%, 2%, and 2% of dry stover respectively.²³⁸ The emissions from the decomposition of this lost biomass are dependent on temperature and moisture content of the feedstock²⁷¹ and were estimated to vary between 2.3 to $8.4~{\rm g~CO_2}$ e/MJ for the cellulosic ethanol processes. ²⁷² Therefore, for the CE process, an average of 5.35 g CO₂ e/MJ was assumed. For Py-ECH, a value of 2.3 g CO₂ e/MJ was calculated based on the ratio of carbon present in the feedstock biomass for the two processes.

Processing

LCI data for the Py-ECH process components were extracted from the work by Lam et al..⁵ Similarly, all data for the CE system were obtained from the Humbird et al. report on cellulosic sugar fermentations to ethanol by NREL.¹¹ The emissions from electricity and biochar application (for the Py-ECH process only) were estimated using the MRO-West electrical grid data, which

comprises the states of Minnesota, Iowa, West Wisconsin, North Dakota, South Dakota, and Nebraska. To estimate the carbon credit from biochar application, the resident carbon percentage in biochar that is sequestered in the soil was estimated from literature to vary from 65-100 wt.%.²⁷³, Therefore an average value of 82.5% was assumed for this analysis. Biochar application has additional soil benefits, ranging from decreasing fertilizer requirement, reducing NO_x emissions, and decreasing leaching of soil nutrients,^{42,275} which offset emissions. However, these reductions are difficult to estimate and were not considered in this analysis.

At the central refinery, heat is required for the Py-ECH system. This heat was assumed to be provided by burning natural gas with a heating value of 52.2 MJ/kg. While carbon dioxide emissions from natural gas combustion at the PY-ECH refinery were measured stoichiometrically from methane combustion, associated NOx emissions were estimated from GREET. No external heat and power are required by the CE system as it burns the biomass lignin and the wastewater treatment sludge to provide sufficient heat and electricity for all plant utilities. In fact, there is an associated credit from selling excess electricity to the grid. Similarly, the Py-ECH depots are self-sufficient in heat and power requirements owing to the heating value of the non-condensable gases (NCG) generated during pyrolysis. The NOx emissions due to the burning of the lignin and the sludge at the CE biorefinery and the NCG at the Py-ECH depots were estimated using a value of 0.31 kg/MWhr of heating value of combusted fuel.¹¹

Water use in both systems was assessed and compared. Most of the water in the CE system is recycled by treating the wastewater and the only water consumption is the make-up well water to compensate for the water lost in cooling tower evaporation. The Py-ECH system utilizes water predominantly in the ECH and electrolysis units. While most emissions from the processing stages of CE and the Py-ECH are atmospheric in nature, there is one liquid stream (the treated 50% brine

solution from the wastewater treatment plant) in the CE system¹¹ that is considered a waste. However, with recent advances in membrane-based and thermal-based technologies for brine treatment, the concept of zero-liquid-discharge systems is fast emerging.²⁷⁶ Therefore, no liquid discharge stream was assumed in the present analysis. Consequently, no grey water consumption or water eutrophication was considered for the processing stage of the two systems.

Transport

For transportation of corn stover, 53 ft trailer trucks, 8.5 ft wide, and 13.5 ft high have been selected. 268, 277 The transportation weight limit of 80,000 lbs for roadways in Iowa was adopted in this analysis. Assuming the average dry weight of a 3 ft x 5 ft x 8 ft bale to be 950 lbs, the average wet weight for a similarly sized bale with 20% moisture is approximately 1,200 lb.²⁷⁷ If the weight of the trailer is assumed to be 30,000 lbs, then a maximum of 48 bales, amounting to about 50,000 lb can be transported on a single trip. Because the volume constraints limit the maximum number of bales to 63, the weight limitations restrict the number of bales per truck to less than 48. Additionally, the average corn stover collection radius from the fields to the biorefinery in the CE system is assumed to be 50 miles or 80.5 km.²⁴⁹ For the Py-ECH process, the distance between the corn fields and upgrading depots have been optimized for the lowest cost of finished fuel to be 7 miles or about 11.5 km. This is consistent with literature data that predict the distance to be between 9 and 55 km. 10 Similarly, the mean distance from a depot to the central refinery was also estimated to be approximately 51 km, by minimizing the final fuel price. The mean distance for the finished fuels from the refinery to the distribution terminals and then to the pumps is assumed to be 110 miles,²⁷⁸ which is the same for the Py-ECH and the CE systems. Truck mileage was assumed to be 5 miles/gallon for field-to-depot, depot-to-refinery, and refinery-to-terminal

transportation segments. Fossil diesel is assumed to be the fuel for all transportation and the emissions associated with burning diesel were assigned using GREET.

Combustion

The emissions for finished fuel combustion were calculated for the complete combustion of ethanol and all hydrocarbons to CO₂ for the CE and Py-ECH processes respectively. The NOx emissions, contributing to eutrophication potential were estimated from GREET.

Allocation

Corn stover, the crop residue from corn cultivation after grain harvest, is the selected feedstock for this analysis. Corn grain is a major food crop and has its own separate environmental impacts, depending on the method for processing corn grain. However, corn grain and stover are connected at the cultivation stage of the corn plant. The burdens and benefits due to cultivation emissions and below-ground carbon sequestration must be appropriately allocated between the grain and stover. Allocation is a controversial topic in LCA as it can lead to drastically differing results depending on how it is performed. LCA methodologies in the literature describes different ways to avoid allocation in multifunctional processes, first by process subdivision or by system expansion. 279, 280 If allocation cannot be avoided then burdens must be allocated based on some biological, physical, or chemical relationships that link the system functions to process inputs or outputs. If such a physical relationship cannot be established, then the allocation can be based on other factors like economic value.

In the present analysis, allocation is an issue only in the cultivation stage of the two systems and therefore, it was decided to consider two scenarios, (a) Scenario 1: with no allocation (b) Scenario 2: with minimal allocation. In Scenario 1, allocation was avoided by making the assumption that the feedstock, corn stover is a waste product of the corn grain generation

process.²⁸¹ This assumption makes it possible to neglect any cultivation emissions or benefits that were shared with the corn grain, like soil carbon sequestration. The only emissions from the cultivation stage in this scenario are from the production and application of the excess fertilizers to be added to the soil for removing the nutrients in the harvested corn stover that otherwise would be returned to the soil. In Scenario 2, mass-based allocation was performed when subdivision was not possible. The grain-to-stover mass ratio in a corn plant is approximately 1:1.²⁸² However, since only 60% of the corn stover is harvested and 40% is left on the fields, the mass-based allocation percentage were evaluated from GREET to be 34% being allocated to stover. This means that only 34% of the fertilizer emissions and the net carbon sequestration were allocated to stover in this scenario. As with Scenario 1, the second pass harvest emissions for stover "only" were similarly accounted for in Scenario 2. Apart from cultivation, emissions from all other stages were the same for both scenarios. These two scenarios were examined to reveal which allocation procedure has a more pronounced effect on the LCA results.

Results and Discussion

Life Cycle Impact Assessment (LCIA)

The LCIA phase of the LCA quantifies the environmental impacts of the various emissions that were compiled in the life cycle inventory phase. In this study, the LCIA was completed for three impact categories: GWP, EUP, and WSF.

The total GWP, EUP, and WSF for the Py-ECH and CE processes, employing both allocation procedures, is summarized in Tables 5.8 and 5.9 (in the Appendix), respectively where the contribution of the four primary areas in each impact category has been shown for both scenarios.

Contribution Analyses

Global Warming Potential (GWP)

As global climate change is accelerating, the GWP was calculated and compared for each system and allocation scenario. Figure 5.4 shows the contributions of different system components by highlighting 13 GWP contributors (as listed in the plot legend) for the two systems for both scenarios. On this figure, the Py-ECH system is shown for the case when fossil electricity is used for upgrading during ECH and hyroprocessing, while a second case shows Py-ECH when renewable electricity is instead utilized. When renewable electricity is used to power the Py-ECH system, it outperforms the CE system in terms of GWP. However, if instead grid electricity is used for Py-ECH, the CE system is less impactful to GWP.

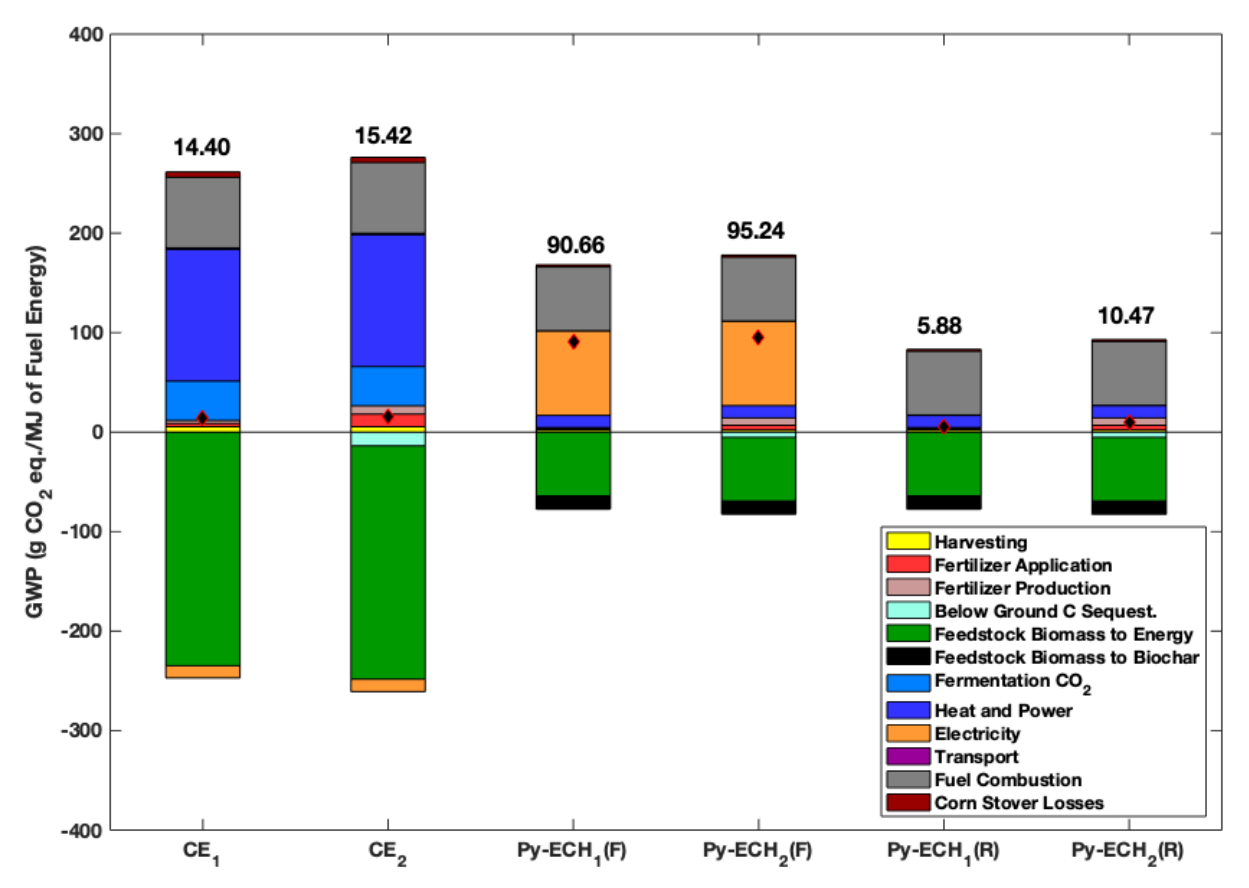


Figure 5.4: Global Warming Potential (GWP) Contribution Analysis; Subscript 1 refers to Scenario 1 whereas Subscript 2 refers to Scenario 2. 'F' refers to a fossil fuel electrical grid and 'R' refers to renewable power.

This highlights the importance of clean electrical power in the Py-ECH system, which is expected,

owing to the large amount of electricity utilized for fuel upgrading. Another major feature of this plot is the difference in the amount of biomass feedstock (green bars) used for both systems. This difference in needed feedstock results as the CE system has a lower energy yield than Py-ECH and therefore requires greater biomass feedstock to make the same amount of fuel energy (in this analysis the functional unit is 1 MJ). Though somewhat counterintuitive, the CE system exhibits greater benefits from biogenic carbon fixation by the feedstock. Though there are increased emissions from harvesting, fertilizer application and fertilizer production, with handling a larger biomass feed in the CE system, these emissions are counterbalanced by a greater amount of feedstock carbon being fixed. Additionally, there is more carbon sequestration (cyan bar) from generating larger quantities of corn stover. The GWP contribution of the processing components for the two systems has been further subdivided here into four sub-components. The first subcomponent (dark blue bars) is the contribution for heat and power generation, which is much greater for the CE system because of lignin and wastewater sludge combustion. For the Py-ECH system, these emissions are from heat production needed for performing pyrolysis. The power requirement for the Py-ECH system is met by grid electricity (orange bar), which also happens to be the second processing sub-component. In fact, the CE system gets a benefit from selling the excess electricity to the grid, thereby displacing fossil fuel usage. The third processing subcomponent is the carbon dioxide generated by fermentation of holocellulose sugars, a characteristic of the CE system that is not present in the Py-ECH system (light blue bar) The fourth sub-component is associated with co-products, which is excess electricity sold to the grid for the CE system and land applied biochar for the Py-ECH system. As biochar sequesters carbon when land applied, it has a negative value on Figure 5.4 (black bar). The biochar carbon reported is the net carbon sequestered after subtracting the non-resident carbon fraction (liberated as CO₂) from

the resident carbon. The transport stage for both processes is negligible in comparison to the other stages and is not visible in Figure 5.4. The emissions from fuel combustion, although not negligible, does not distinguish between the two systems as it is nearly equal for both. The emissions associated with corn stover losses during harvesting, transport, and storage, are also minimal. Finally, there is not much difference between allocation scenarios within a single system as only a slight increase in all values results when using mass allocation vs. avoiding allocation.

Eutrophication Potential (EUP)

Similar to the GWP, the EUP contribution analyses are shown in Figure 5.5 for both systems, both scenarios, and the renewable electricity Py-ECH scenario. From Figure 5.5a, the cultivation component in the two systems dominates EUP in Figure 5.5a. The major cultivation contributors are the P and N runoff values and the same result is achieved for both systems. Fertilizer atmospheric emissions like NOx and NH₃ have lesser contributions. The contribution from processing (denoted by blue and orange bars) for both systems is minimal, and not observable for the Py-ECH system. Transport and fuel combustion EUP are also negligible. To investigate the relative contribution of processing, transport, and fuel combustion, Figure 5.5b was constructed without the EUP contributions from cultivation. In comparison to Py-ECH, the CE processing component has a much higher EUP in part because of greater NOx emissions from the boilercombustor of the CE system, which combusts a larger amount of fuel (lignin and wastewater sludge) than the combustors in the Py-ECH system (NCG in depots and natural gas in refineries). Although the Py-ECH has additional emissions from utilization of grid electricity, the rate of NOx emissions is not nearly as high. The CE system also has atmospheric NH₃ emissions from its wastewater treatment plant. From Figure 5.5b, the fuel combustion EUP values are similar for both systems and scenarios. Finally, the transport emissions are negligible and do not appear on Figure

5.5b. In contrast with GWP on Figure 5.4, there is a larger impact of allocation assumptions on EUP values. The difference across scenarios disappears when the cultivation stage is excluded, as is expected. In summary, it is important to recognize that although cultivation dominates in EUP contribution analyses, Py-ECH performs better than CE, both at the technological level and overall.

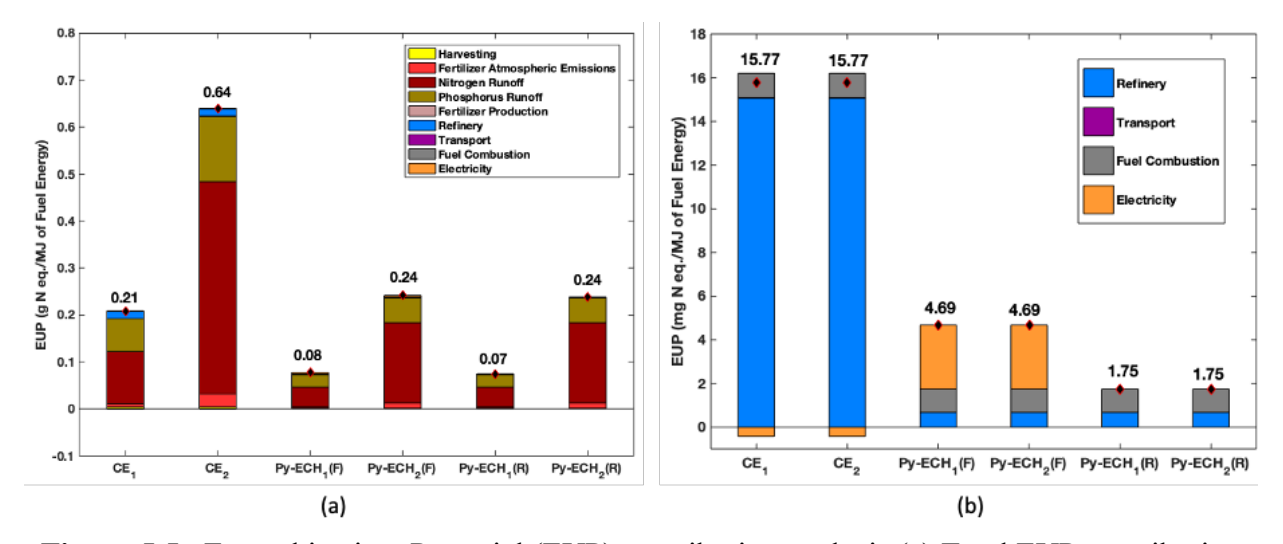


Figure 5.5: Eutrophication Potential (EUP) contribution analysis (a) Total EUP contribution analysis; subscript 1 refers to Scenario 1 whereas subscript 2 refers to Scenario 2. (b) EUP contribution analysis excluding cultivation and harvesting; F stands for fossil electricity and R stands for Renewable electricity.

Water Scarcity Footprint (WSF)

The WSF contribution analyses are shown in Figure 5.6 for both systems and scenarios, including the renewable electricity scenario for Py-ECH. WSF is only relevant in two components of the two systems, the supply chain and processing. There is no contribution in WSF from the transportation and fuel combustion areas. The biggest contributor to WSF for both processes is the cultivation component (green bar), which includes freshwater (blue water) consumption for agriculture but not precipitation, as discussed before. The water demand for cultivation for the CE system is much more than for the Py-ECH system, owing to the larger amount of biomass required to produce the same amount of fuel energy and therefore, larger land area to be cultivated. Py-ECH does require

water for the ECH and electrolysis units, however, the fresh make-up water for the CE system to compensate for cooling tower evaporation is much larger (blue bars). When powered by fossil electricity, the Py-ECH system consumes water because of water use at thermal power plants that generate electricity.

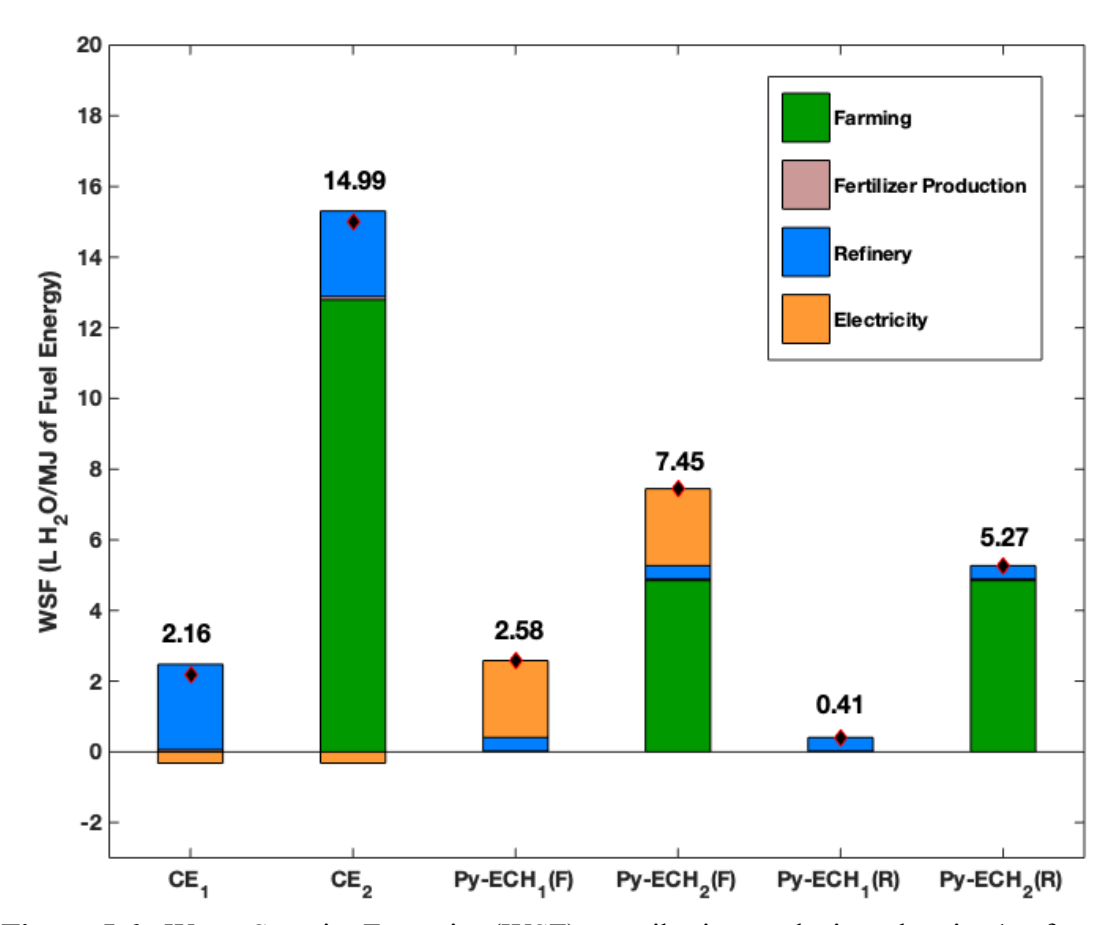


Figure 5.6: Water Scarcity Footprint (WSF) contribution analysis; subscript 1 refers to Scenario 1 whereas subscript 2 refers to Scenario 2.

The CE system again benefits by selling the excess electricity it generates back to the grid. When Py-ECH is powered by fossil electricity, its WSF is slightly higher than CE for Scenario 1 allocation assumptions. This is because, while Py-ECH suffers from indirect water usage due to grid electricity use, the system benefits from selling its excess electricity to the grid. This result changes when the Py-ECH system uses renewable electricity sources as the water consumption for electricity use is greatly reduced when using solar farms and is zero when using wind farms, as

plotted in Figure 5.6 (Py-ECH₁—renewable electricity). Finally, the farming water consumption, which is the largest contributor, does not appear in the analysis of Scenario 1, which allocates all water consumption to corn grain, as stover is considered a waste product. As more water is required when growing more biomass over a larger area, CE₂ has the largest WSF. Again, processing yields are very important for reducing environmental impacts.

Sensitivity Analyses

Sensitivity analyses are an important tool to investigate "what if" scenarios. These are especially relevant for studying dependence of output variables on sensitive input parameters, or when there is great variability in a certain input parameter. One result that is featured by the contribution analyses is the importance of the electricity source, particularly for the Py-ECH system. If the source is grid electricity, which is 29.2% renewable, then the GWP for the Py-ECH system is greater in comparison to the CE system. However, if the source is 100% renewable, then the Py-ECH system performs better. Therefore, the GWP was plotted as a function of the percentage renewability of the MRO-West electrical grid and the result is shown in Figure 5.7. The GWP for the CE system increases with percentage renewability because greater renewability on the MROgrid means a lower amount of fossil electricity to displace, and hence a lower benefit. On the contrary, GWP decreases for the Py-ECH system, because greater percentage renewability leads to lower emissions from utilizing the same amount of grid electricity. A key observation from Figure 5.7 is that the negative slope of the Py-ECH line is more than the positive slope of the CE line because the amount of electricity required by the Py-ECH electricity is greater than the excess electricity sold by the CE system to the grid. A key result is that the CE system performs better than the Py-ECH system until the percentage renewability in the electrical grid is about 87.4%. Greater percentages make the Py-ECH system perform better in terms of GWP.

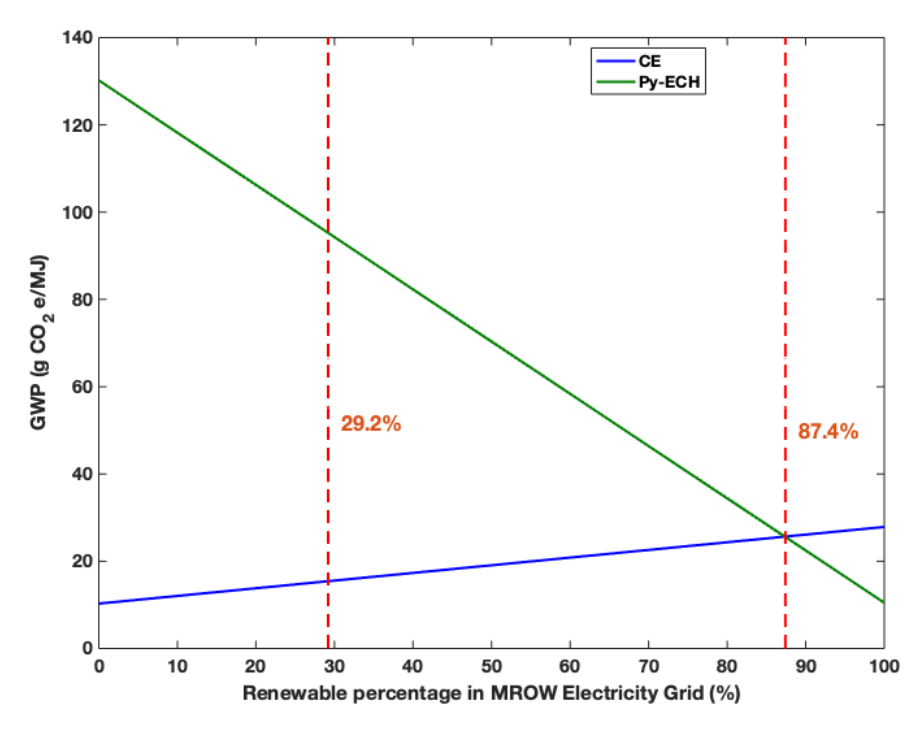


Figure 5.7: Sensitivity of system GWP with % renewable in MROW Electricity Grid. (For Scenario 2)

As stated before, there is great variability in literature in the value of annual carbon sequestration data. Carbon sequestration varies based on soil texture, rainfall, tillage, stover removal, soil depth measured, crop rotation system and geographical location. To investigate the effect of variation of this assumption on the total GWP, the annual carbon sequestration was varied from 0 to 2.5 Mg C/ha/yr for a continuous corn system, with no tillage, and 60% stover harvest. The two limits were chosen as most data fell within this range. Figure 5.8, which was a result of this exercise, shows that for low sequestration values, the Py-ECH, with renewable electricity performs better than the CE system. This is owing to the fact that there is less biomass involved in the Py-ECH system for producing the same amount of fuel energy and therefore, lesser benefit from C sequestration. This also explains the difference in the slopes of the two lines, with the CE system, depicted by the blue line, having a larger slope. However, the Py-ECH system, when using fossil or grid electricity is never better than the CE system, no matter what the annual C sequestration

rate assumption. Two sequestration values from literature, indicated by red dashed lines, have been plotted in Figure 5.8.

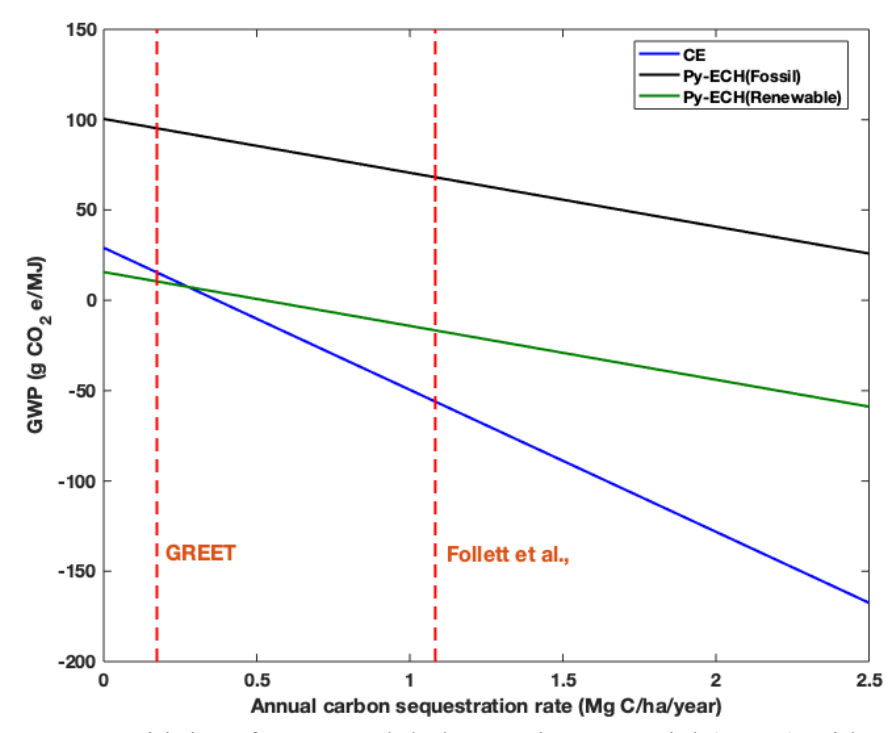


Figure 5.8: Sensitivity of system Global Warming Potential (GWP) with annual C sequestration rate for Scenario 2.

The first value is from GREET and has been used in the present analysis. The second value is from Follett et al., ²⁸³who determined a value of 1.3 Mg C/ha/yr for no till corn stover, with a 50% removal, when soil depth up to 150 cm is considered. This amounts to 1.08 Mg C/ha/yr for 60% removal, assuming a linear dependence. It is evident that the Follett assumption will benefit the CE system more and in fact, make it a more carbon negative system than the Py-ECH system. It is important to note that this result is restricted by the choice of functional unit, in this case 1 MJ of fuel produced. Because Py-ECH requires substantially less biomass and land area, opportunities for sequestering carbon by cultivating land not planted with corn for bioenergy production should be explored. For example, if this unplanted land were allowed to become natural forest and was

included in the Py-ECH system boundary to equalize land area with the CE system, then Py-ECH GWP would be far lower than CE for all values of carbon sequestration.

Energy Ratio

To evaluate the energy efficiency in terms of renewable energy produced vs. fossil energy consumed, there are several different energy ratios that may be calculated to measure the efficacy and renewability of the system (Table 5.1).²⁷⁹ Five such energy ratios have been calculated and presented in Table 5.2 for the two different processes and for the Py-ECH scenario when renewable electricity is used.

Table 5.1: Description of energy ratios²⁷⁹

Energy Ratio	Abbreviation	Description
Total Energy Ratio	ER_t	Total usable energy output/ Total energy
		input
Renewability Factor	RF	Fuel energy output/ Fossil energy input
Energy Yield	E_{y}	Fuel energy/Feedstock energy
Energy Return on Investment	EROI	Total energy of fuel and co-products/Energy
		invested in the process
Fossil Energy Ratio	ER_{f}	Fuel energy + co-product energy output/
		Fossil energy input

While ER_t is a measure of the total efficiency of the system and accounts for both product and coproduct energy, the E_y only calculates what fraction of the feedstock energy resides in the primary
product, which is the fuel. Therefore, the ER_t considers the energy associated with excess hydrogen
gas in the Py-ECH system and the excess electricity in the CE system. Biochar in the Py-ECH
system is not considered an energy co-product since it is land applied to sequester carbon. EROI
is similarly defined as ER_t, with the exception that it does not include the energy associated with
the biomass feedstock input. It is more concerned with the additional energy inputs to the process
that are essential for manufacturing the fuel and the co-products. However, ER_t, E_y, and EROI do
not distinguish between energy sources for the inputs and do not measure renewability of the
system. Although there are other ways to determine the renewability of a system, such as Energy

Renewability Efficiency,²⁷⁹ RF is the most simple and transparent method. It is the ratio of the energy of the primary product (the fuel in this case) and all non-renewable energy inputs. The higher the RF, the greater is the renewability of the system. ER_f on the other hand is the ratio of all energy products (fuel and co-products) and all fossil energy inputs. It can be seen from Table 5.2 that the RF, ER_f, and EROI of the CE system is greater than for the Py-ECH system. This is because the CE system manufactures its own heat and power by combusting some of its biomass feed, thereby greatly reducing non-renewable inputs resulting in a larger RF and ER_f. Similarly, for the EROI, which excludes the feedstock energy as an input, the CE system gains over the Py-ECH system, as it is using a part of the biomass feed as heat and power. The Py-ECH on the other hand, relies on grid electricity, reducing its RF, ER_f and EROI. However, whenever the energy ratios include biomass feed as an energy input, the Py-ECH performs better, since it is overall more energy efficient than the CE system, and the biomass feed energy is the greatest contributor to all energy inputs. Therefore, the Py-ECH has a higher ERt and Ey. When using renewable electricity, the RF and ER_f of the Py-ECH system increases substantially due to the much lower fossil energy inputs. There is, however, no change in the ER_t, E_v and EROI of the system.

Table 5.2: Energy ratios for the CE and Py-ECH systems. ER_t stands for Total Energy Ratio; RF stands for Renewability Factor; E_y stands for Energy Yield; EROI stands for Energy Return on Investment; ER_f stands for Fossil Energy Ratio. FE stands for Fossil electricity while RE represents renewable electricity

Energy Ratio	CE	Py-ECH (FE)	Py-ECH(RE)				
ER_t	0.44	0.70	0.70				
RF	9.66	1.98	8.22				
E_{y}	0.42	0.91	0.91				
EROI	10.43	1.85	1.85				
ER_{f}	10.40	2.42	10.03				

The reasons behind the Py-ECH system's lower RF and ER_f is the utilization of fossil grid electricity and the combustion of natural gas for heat at the central refinery. If the grid electricity is more renewable and the source of heat at the central refinery is made renewable, then the RF

and ER_f of the Py-ECH system markedly increases, as seen in Figure 5.9. It is clear that the CE system would have a high RF of about 10, owing to very little fossil energy input, since the biomass lignin itself is burnt for heat and power. While Figure 5.9 (a) shows the variation of RF and ER_f with % renewable heat at the refinery, Figure 5.9 (b) shows the variation of RF and ER_f with % renewable electricity. If either the electricity or heat source is 100% fossil based, then the Py-ECH system can never match the RF and ER_f of the CE system. However, if the heat source at refinery is 100% renewable, then the Py-ECH system has a better RF and ER_f at about 80-90% renewable electricity. Similarly, if the electricity source is 100% renewable, the heat source at refinery would have to be at least 25% renewable and 5% renewable for the Py-ECH system RF and ER_f, respectively, to overtake that of the CE system.

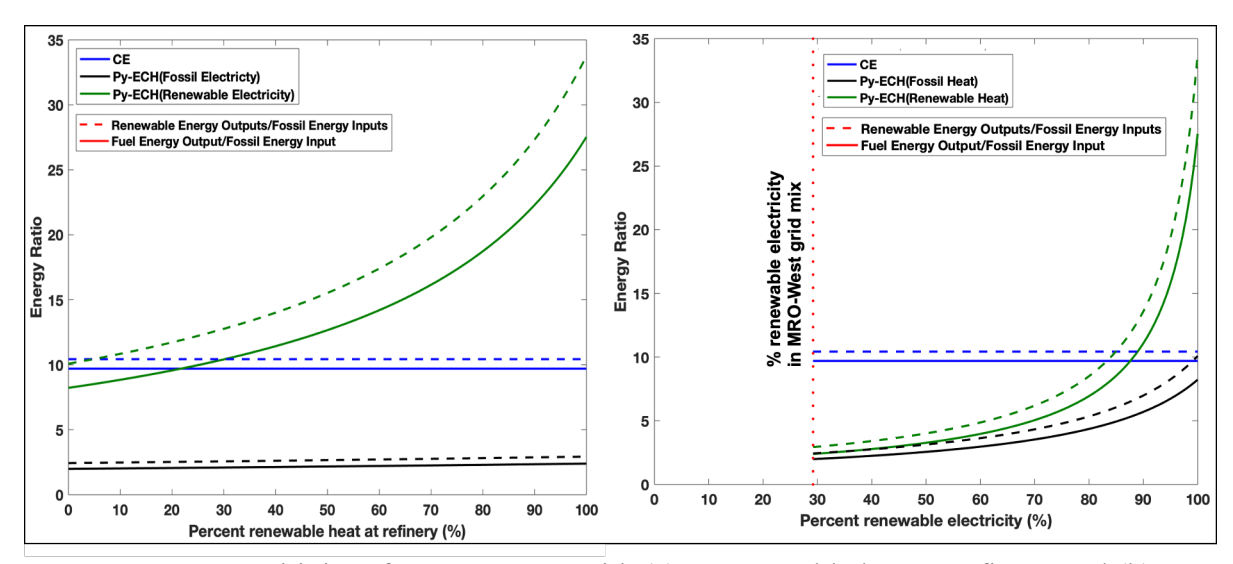


Figure 5.9 : Sensitivity of system EROI with (a) % renewable heat at refinery and (b) % renewable electricity

Conclusion

From the present analysis, it is clear that that the environmental performance of the Py-ECH system is better than that of the CE system, when the source of electricity is renewable, such as wind or solar photovoltaics. The sensitivity analysis in Figure 5.7 shows that this source only has to be

about 87% renewable for Py-ECH to perform better than CE. The eutrophication potential and the water scarcity potential for the Py-ECH system is always lower than that for the CE system. Even the renewability factor, which measures the amount of renewable energy generated based on the amount of fossil energy inputs, also surpasses that of the CE system when the source of electricity is about 85% renewable. This is remarkable since the CE system uses the lignin of the feedstock biomass to generate its own heat and power and therefore, has a very high renewability factor. To summarize, an electricity source that is more than 87% renewable, makes the Py-ECH system more environmentally favorable than the CE system in all the aspects that have been studied in this analysis. This is significant since the GHG emissions of the CE system, as presented here, are itself 10-15% of that for gasoline from crude oil for a 20 year time horizon.²⁸⁴Therefore, the Py-ECH system, with 87% renewable electricity improves upon the environmental performance of the CE system while maintaining a produced fuel with same energy content as that of gasoline. The Py-ECH system has lesser GHG emissions than that for gasoline, even without the improvement in renewability of electricity sources. It must be recognized that the Py-ECH technology is not yet at the same technology readiness level as the CE process or the production of gasoline from crude oil. However, this analysis excludes certain benefits of the Py-ECH system, such as the effect of biochar on the reduction of nitrous oxide emissions. Furthermore, the rate of biochar degradation, in literature, has been determined to be very slow.²⁸⁵ Kuzyakov et al., in fact measured a degradation rate of 0.5% every year under optimal conditions. This amounts to 90% biochar carbon retained in 20 years, significantly higher than the assumed 82.5% in this analysis. Furthermore, they estimate a mean residence time of 2,000 years under natural conditions and a half-life of 1,400 years, which is significantly larger than the time horizon considered in this analysis for there to be any biochar carbon decomposition.²⁸⁶ Another key parameter that

disadvantages Py-ECH climate change potential compared to CE, is the requirement of greater biomass feedstock for the CE system, owing to its lesser energy yield. The extra land area that is saved in the Py-ECH system can be dedicated to forestland to sequester more carbon and reduce the GWP of the Py-ECH system. In fact, the annual rate of carbon accumulation in forests can vary from 0.8 tonnes/ha/yr to 5.1 tonnes/ha/yr, depending on the type of forest.²⁸⁷ The CCLUB model from GREET estimates an annual carbon sequestration rates from forests in the United States at 2.4 tonnes C/ha/yr, which is well within this range. Although this would make the eutrophication potential and water scarcity footprints of the two systems almost equal, it would be interesting to find out the resultant impact of stacking these improvements on the GWP of the Py-ECH system. This has been shown in Figure 5.10 for both allocation scenarios considered in the analysis. The annual carbon sequestration rate for forests have been assumed conservatively to be 0.8 tonnes/ha/yr, the lower limit of the range of values found in literature. Higher values will only lower the global warming potential further.

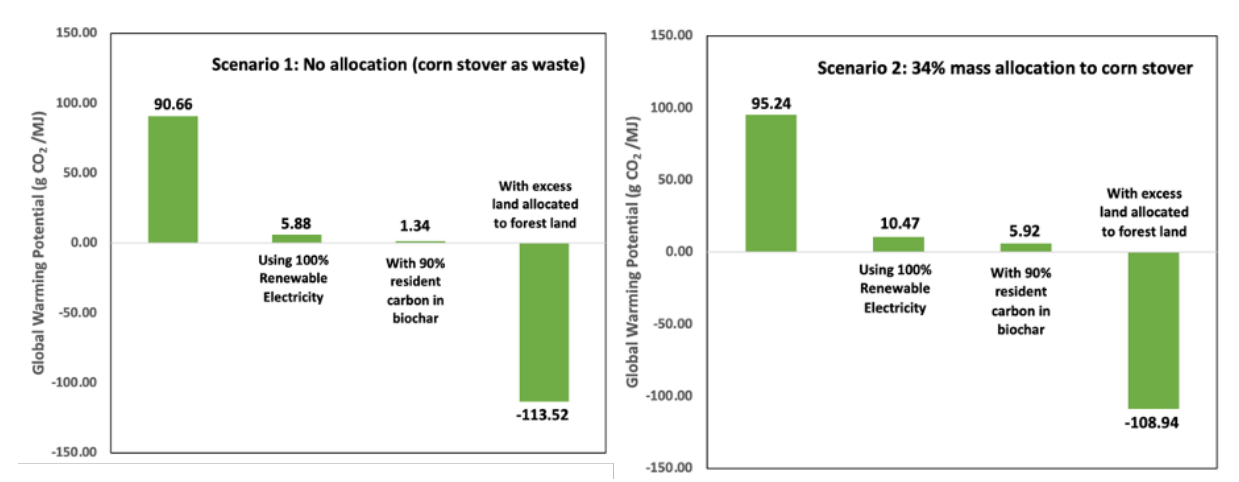


Figure 5.10: Waterfall chart showing the resultant global warming potential of stacking improvements in the Py-ECH system.

From Figure 5.10, it is clear that stacking improvements in the source of electricity and the quality of biochar produced can lower the GWP of the Py-ECH system to values that are almost carbon

neutral for Scenario 1. Furthermore, the Py-ECH system can become carbon negative if the excess land area that is saved, owing to its better energy yield, can be assigned to forests. Given the apparent advantages of a Py-ECH system operated with renewable electricity vs. a CE system for the three environmental impacts examined in this analysis, there remains ample opportunity for improvements that can lead to carbon negative values for the Py-ECH system.

APPENDIX

Life Cycle Inventory

Life cycle data was collected from different sources in literature and qualified using data quality indicators, as described by the modified Weidema method in Table 5.3.²⁴⁷ The scoring range is from 1-5, with 1 indicating that the data is most reliable while 5 is least reliable. Each data was qualified using a 6-digit score, with each digit ranging from 1 to 5. Each digit represents the reliability of the data in each of the 6 categories, with the first digit representing parameter A and the last digit representing parameter F respectively.

Table 5.3: Parameters in the modified Weidema method and the description of the scores (adapted from Couillard et al.).²⁴⁸

	Parameter	Description	Scoring range
A	Acquisition method	Method of acquiring the data,	1: measured data
		whether measured directly or estimated based on assumptions	5: non-qualified estimate
В	Independence of	Source of information and its	1: independent verified source
	data supplier	bias towards the concerned study	5: unverified source with bias
C	Representativeness	Degree of application of data to even out fluctuations	 representative data from sufficient large samples incomplete data from relatively small samples
D	Data age	Temporal relevance of data	1: less than 3 years 5: unknown or greater than 20 years
E	Geographical correlation	Spatial relevance of data	1: data from area under study 5: data from area unknown or different conditions
F	Technological correlation	Technological relevance of data with processes in study	 data from processes under study data from related processes but different technology

Table 5.4: Life cycle input data for both Py-ECH and CE systems with their source and data quality indicator score.

Parameter	Value	Source	Data quality indicator (ABCDEF)
Technical Data for Py-ECH system		Lam et al., ⁵	211111
Technical Data for CE system		Humbird et al.,	211321
Annual C sequestration rate	0.174 Mg C/ha/yr	GREET ²³⁸	211321

Table 5.4 (cont'd)			
Corn stover storage losses	8.40%	GREET ²³⁸	211321
Corn stover transport losses	2.00%	GREET ²³⁸	211321
Corn stover farm handling losses	2.00%	GREET ²³⁸	211321
Diesel for harvesting corn stover	3.58 gallons/acre	GREET ²³⁸	211321
Fraction of N leached to surface	24% of total	GREET ²³⁸	211321
waters	applied N		
Fraction of P leached to surface	7% of total applied	Powers et	311421
waters	P	al., ²⁶⁶	
Fraction of fertilizer N emitted as NO	0.8% of total	GREET ²³⁸	211321
	applied N		
Fraction of fertilizer N emitted as	10% of total	$IPCC^{265}$	211421
NH_3	applied N		
Fraction of fertilizer N emitted as	1.5% of total	GREET ²³⁸	211321
N_2O	applied N		
Corn stover yield	2.39 dry ton/acre	GREET ²³⁸	211321
Distance from field to refinery for CE	50 miles	Kim et al., ²⁴⁹	212122
system			
Weight limitation on trucks	80,000 lbs	Edwards et	221311
		al., ²⁶⁸	
Distance from refinery to pumps for	110 miles	Kumar et al., ²⁷⁸	212322
both Py-ECH and CE systems			

Tables 5.5, 5.6 and 5.7 show the values of contribution of each unit operation to the total GWP, EUP and WSF of both systems for both scenarios while Tables 5.8 and 5.9 depict the life cycle impact summary of the Py-ECH and CE systems respectively.

Table 5.5: Contribution of each operation in the determination of Global Warming Potential (GWP) for both CE and Py-ECH systems

Operations	Scena	irio 1	Sce	nario 2
	CE	Py- $ECH(F)$	CE	Py- $ECH(F)$
	(g CO	2/MJ)	(g C	O_2/MJ)
Supply Chain:				
Harvesting	5.51	2.09	5.51	2.09
Fertilizer Application	3.09	1.17	1.26	4.78
Fertilizer Production	3.15	1.19	8.33	7.36
Below ground C sequestration	0.00	0.00	-13.70	-5.19
Feedstock Biomass to Energy	-235.00	-64.20	-235.00	-64.20
Corn Stover Losses	5.35	2.03	5.35	2.03
Processing				
Heat and Power	132.00	12.40	132.00	12.40
Fermentation CO ₂	39.50	0.00	39.50	0.00

Table 5.5 (cont'd)

Feedstock Biomass to Biochar	0.00	-13.30	0.00	-13.30
Electricity Transport	-12.40	84.80	-12.40	84.80
Transportation	1.46	0.37	1.46	0.37
Combustion				
Fuel combustion	71.00	64.10	71.00	64.10

Table 5.6: Contribution of each operation in the determination of Eutrophication Potential (EUP) for both CE and Py-ECH systems.

Operations	Scen	ario 1	Sce	nario 2
	CE	Py- $ECH(F)$	CE	Py-ECH(F)
	(mg C	$O_2/MJ)$	(mg	C O ₂/MJ)
Supply Chain:				
Harvesting	4.18	1.58	4.18	1.58
Fertilizer Application	6.86	2.60	28.00	10.60
Nitrogen runoff	111.00	42.00	452.00	171.00
Phosphorus runoff	70.20	26.60	139.00	52.70
Fertilizer Production	0.35	0.13	0.80	0.66
Processing				
Refinery operations	15.10	0.66	15.10	0.66
Electricity	-0.43	2.94	-0.43	2.94
Transport				
Transportation	1.46	0.37	1.46	0.37
Combustion				
Fuel combustion	71.00	64.10	71.00	64.10

Table 5.7: Contribution of each operation in the determination of Water Scarcity Footprint (WSF) for both CE and Py-ECH systems.

Operations	Scen	ario 1	Scenario 2	
	CE	Py- $ECH(F)$	CE	Py- $ECH(F)$
	(L H)	2O/MJ)	(L H	I_2O/MJ)
Supply Chain:				
Farming	0.00	0.00	12.80	4.85
Fertilizer Production	0.006	0.002	0.009	0.004
Processing				
Refinery operations	2.42	0.38	2.42	0.38
Electricity	-0.32	2.18	-0.32	2.18

Table 5.7 (cont'd)

Transport				
Transportation	0.00	0.00	0.00	0.00
Combustion				
Fuel combustion	0.00	0.00	0.00	0.00

Table 5.8: Life cycle impact summary for the CE process. Allocation scenarios 1 and 2 are reported to observe the effects of avoiding allocation and applying minimal allocation to cultivation

	GWP		EU	IP	WSF		
Allocation	1	2	1	2	1	2	
	kg CO2 eq /MJ		kg N e	kg N eq/MJ		$L H_2O/MJ$	
Supply							
Chain	-2.18E+02	-2.17E+02	1.92E-01	6.24E-01	5.98E-02	1.29E+01	
Processing	1.60E+02	1.60E+02	1.46E-02	1.46E-02	2.10E+00	2.10E+00	
Transport	1.46E+00	1.46E+00	3.02E-05	3.02E-05	0	0	
Combustion	7.10E+01	7.10E+01	1.11E-03	1.11E-03	0	0	
TOTAL	1.44E+01	1.54E+01	2.08E-01	6.39E-01	2.16E+00	1.50E+01	

Table 5.9: Life cycle impact summary for the Py-ECH process. Allocation scenarios 1 and 2 are reported to observe the effects of avoiding allocation and applying minimal allocation to cultivation.

	G'	WP	EU	UP	W	SF	
Allocation	1	2	1	2	1	2	
	kg CO2 eq /MJ		kg N	kg N eq/MJ		$L H_2O/MJ$	
Supply Chain	-5.77E+01	-5.31E+01	7.29E-02	2.37E-01	2.27E-02	4.89E+00	
Processing	8.39E+01	8.39E+01	3.60E-03	3.60E-03	2.56E+00	2.56E+00	
Transport	3.68E-01	3.68E-01	7.61E-06	7.61E-06	0	0	
Combustion	6.41E+01	6.41E+01	1.07E-03	1.07E-03	0	0	
TOTAL	9.07E+01	9.52E+01	7.76E-02	2.41E-01	2.58E+00	7.45E+00	

Chapter 6: KINETIC MODELING FOR ECH OF PHENOL

<u>Abstract</u>

Electrocatalytic hydrogenation (ECH) can play a key and integral role in carbon and energy efficient bioenergy systems that focus on conversion of biomass to liquid transportation fuels. One such bioenergy system is the Py-ECH system that utilizes ECH as a stabilizing step for the reduction of highly reactive functional groups like aldehydes, ketones and other aromatics present in bio-oil (derived from biomass fast pyrolysis) to more stable alcohols and cycloalkanes. This stabilization is essential for the storage and transportation of pyrolysis bio-oils, a key factor in decentralized bioenergy systems like the Py-ECH system. In this study, a kinetic model was developed that studies the ECH of phenol to cyclohexanol using a rotating disk electrode (RDE), with activated carbon cloth supported ruthenium acting as the catalytic working electrode. The goal of the study was to evaluate the kinetic rate constants associated with the electrochemical, surface, adsorption, and desorption reactions involved in the ECH of phenol to cyclohexanol. This may be achieved by extracting current-voltage data from linear sweep RDE experiments and then fitting the developed kinetic model to these data by solving the inverse problem. The development of this kinetic model is a crucial step in the eventual goal of scaling up the electrocatalytic hydrogenation process for the commercial application of specific bioenergy systems like the Py-ECH system.

Introduction

Bioenergy systems that employ fast pyrolysis to convert biomass to transportation fuels often employ a subsequent upgrading step that converts the intermediate pyrolysis bio-oil to the final hydrocarbon transportation fuel. 19, 36, 45, 46, 60, 84, 85, 97, 288 Most often, it is a hydroprocessing step that subjects the bio-oil to high temperatures and pressures, converting it to a gasoline/diesel range

product. However, the concept of incorporating local biomass processing depots^{22, 68, 72, 76} into bioenergy systems¹⁰² requires that new technologies be developed that can stabilize the pyrolysis bio-oil at these local processing depots, to create an intermediate fit for long-distance transportation. Hydroprocessing is difficult to be implemented at these small-scale local depots due to the extreme conditions employed and the need for storage of flammable H₂ gas. In this regard, electrocatalytic hydrogenation (ECH) presents an opportunity to be utilized as a key technology for pyrolysis bio-oil stabilization, owing to its much milder requirements of temperature and pressure. Bioenergy systems, like the Py-ECH system, have explored the incorporation of ECH in the overall conversion of biomass to liquid transportation fuels.⁵ In this system, biomass is first converted to a stable bio-oil via fast pyrolysis and subsequent ECH at a local depot facility, which is then transported to a central hydroprocessing facility for final conversion to a gasoline/diesel range fuel.

The kinetics of the ECH of pyrolysis bio-oil is key to its scale-up and subsequent commercial application of the Py-ECH bioenergy system. Previous kinetic studies have investigated the ECH of different model bio-oil compounds in the presence of different catalysts. Such studies usually also involve the kinetics of the hydrogen evolution reaction (HER), which is an accompanying side reaction that is undesirable in context of bio-oil ECH. The kinetics of HER have also been studied separately by Oshchepkov et al., ^{289, 290} who investigated the effect of nickel oxide species and temperature on HER kinetics. Moreover, some of these have studies have only considered the surface and adsorption reactions and not mass transfer effects. ^{130, 139, 140, 142, 144} To minimize the effect of slow mass transfer, Singh et al. created a reaction controlled regime by rotating the entire electrochemical cell at 500 rpm. ¹⁴³ Tourwe et al., provided a theoretical model for evaluating kinetics from electrochemical experiments by using a rotating disc electrode setup, ²⁹¹ but studied

metal deposition instead of electrocatalytic hydrogenation. However, such a model may be adopted and modified for the Py-ECH system to study the ECH of a model bio-oil compound. Therefore, in the present study, the kinetics for the ECH of phenol (as model bio-oil compound), in the presence of Ru/ACC (ruthenium supported on activated carbon cloth) catalyst was studied. Such a selection of catalyst in the Py-ECH system is owing to previous studies that investigated different catalysts to determine the conversion and current efficiency for the ECH of model bio-oil compounds. Phenol is selected because of its simplicity owing to the absence of any other functional groups or side alkyl chains that can lead to different ECH products, depending on the alkyl group length and position. ECH of phenol, on the other hand, is known to produce cyclohexanol in the presence of Ru/ACC catalyst. However, its kinetics in the presence of Ru/ACC catalyst have not been investigated. In this regard, the goal of this study was to estimate the kinetic rate constants associated with the electrochemical, adsorption, desorption, and surface reactions involved in the ECH of phenol.

Model Formulation

Reaction Mechanism

According to Li et al.³² and Dabo et al.,²⁶ ECH of a model bio-oil compound proceeds via the following steps: (1) adsorption of atomic hydrogen on the catalyst surface, (2) adsorption of the substrate (the model bio-oil compound), (3) reaction of adsorbed substrate and adsorbed hydrogen, (4) additional hydrogenation reactions of substrate depending on its complexity, and (5) desorption of the formed products.

Along with the hydrogenation reaction, there is also the competing H_2 evolution reaction that may occur via two reaction pathways, namely the Tafel and the Heyrovsky reactions. The Tafel reaction is given by:

$$M(H) + M(H) \rightarrow H_2 + 2M$$

The Heyrovsky reaction is given by:

$$M(H) + H^{+} + e^{-} \rightarrow H_{2} + M$$

where M(H) represents chemisorbed H and M is the active metal site.

A similar reaction mechanism was assumed for the ECH of phenol on Ru/ACC.

Model Development

The objective of the model was to develop an expression of the form:²⁹¹

$$Current = f(E(t), K_i, K'_i, known parameters)$$

Where E(t) is the voltage as a function of time, K_i , K'_i are the forward and backward rate constants.

The model assumptions were as follows:

- The reactions are at steady state.
- Physical properties like diffusion coefficients and kinematic viscosities are constant.
- Solutions are dilute
- All cathode reactions are reversible.

Based on the reaction mechanism described in the last section, the different reactions happening at the cathode for the ECH of phenol on Ru/ACC are provided below:

$$H_3O^+ + M + e^- \leftrightarrow MH + H_2O$$
 (1)

$$Ph + M \leftrightarrow (Ph)M$$
 (2)

$$(Ph)M + 6MH \leftrightarrow (CyH)M + 6M \tag{3}$$

$$(CyH)M \leftrightarrow CyH + M \tag{4}$$

$$MH + H_3O^+ + e^- \leftrightarrow H_2 + M + H_2O$$
 (5)

$$MH + MH \leftrightarrow H_2 + 2M$$
 (6)

The forward and backward kinetic rate constants for each of the above cathode reactions are represented by K_j , K'_j , where the 'j' is the reaction number; M is an active metal site, Ph is Phenol and CyH is cyclohexanol. If there are P partial heterogeneous electrochemical or chemical reactions, N_v electroactive species in electrolyte and N_s electroactive species present in an adsorbed phase on electrode surface, then:

$$N = N_v + N_s$$

Also,

$$\Sigma_{i=1}^{N}(r_{ij}X_i) \leftrightarrow \Sigma_{i=1}^{N}(p_{ij}X_i) \pm n_j e$$

where i is the index for the considered species and j is the index for the partial reactions.

Under steady state, the rate is given by, $v_j = K_j \prod_{i=1}^N (X_i^{r_{ij}}) - K_j' \prod_{i=1}^N (X_i^{p_{ij}})$

where,
$$K_j = k_{rj} \exp\left(-\frac{\alpha_{rj}n_jn_FE(t)}{RT}\right)$$
; $K_j' = k_{oj} \exp\left(\frac{\alpha_{oj}n_jn_FE(t)}{RT}\right)$

$$\alpha_{oj} + \alpha_{rj} = 1$$
; $i_f = F\Sigma_{j=1}^p s_{ej}v_j$, where $s_{ej} = \pm n_j$

At steady state, the rate of transformation of each species at the interface must equal the mass transport flux from the bulk to the surface given by:

$$v_{X_i} = J_{X_i} = -m_{X_i}[X_i^* - X_i] = \sum_{j=1}^p (s_{ij}v_j)$$
 for i=1,2,....,N_v

$$v_{X_i} = J_{X_i} = 0$$
 for i=N_v+1,...,N

where $m_{X_i} = 0.62 D_{X_i}^{2/3} v^{-1/6} \Omega^{1/2}$

Table 6.1: Reaction rate expressions

Table 0.1. Reaction rate expressions		
Reaction	Expression	
1	$\nu_1 = K_1 X_{H_3 O} + \gamma_M - K_1' \gamma_{MH}$	
2	$\nu_2 = K_2 X_{Ph} \gamma_M - K_2' \gamma_{(Ph)M}$	
3	$\nu_3 = K_3 \gamma_{(Ph)M} \gamma_{MH}^6 - K_3' \gamma_{(CyH)M}$	
4	$\nu_4 = K_4 \gamma_{(CyH)M} - K_4' X_{CyH} \gamma_M$	
5	$\nu_5 = K_5 X_{H_3 O} + \gamma_{MH} - K_5' \gamma_M P_{H_2}$	
6	$\nu_6 = K_6 \gamma_{MH}^2 - K_6' \gamma_M^2 P_{H_2}$	

The mass transport rate constant m_{X_i} can be calculated from values of the diffusion coefficient of each species, the kinematic viscosity of the solution, and the rotation speed of the RDE, which can be obtained from the literature or experiment. The rate expressions for the reversible cathodic reactions may be expressed as in Table 6.1, considering the concentration of water is constant due to the assumption of a dilute solution. Now, the rate of transformation of each electroactive species at the electrode surface is given by:

$$u_{H_3O^+} = -\nu_1 - \nu_5$$
 $\nu_{MH} = \nu_1 - \nu_3 - \nu_5 - \nu_6$
 $\nu_{Ph} = -\nu_2$
 $\nu_{(Ph)M} = \nu_2 - \nu_3$
 $\nu_{CyH} = \nu_4$
 $\nu_{(CyH)M} = \nu_3 - \nu_4$

Therefore, we have:

$$v_{H_3O^+} = -v_1 - v_5 = -m_{H_3O^+} \left[X_{H_3O^+}^* - X_{H_3O^+} \right]$$

$$v_{MH} = v_1 - v_3 - v_5 - v_6 = 0$$

$$v_{Ph} = -v_2 = -m_{Ph} [X_{Ph}^* - X_{Ph}]$$

$$v_{(Ph)M} = v_2 - v_3 = 0$$

$$v_{CyH} = v_4 = -m_{CyH} [X_{CyH}^* - X_{CyH}]$$

$$v_{(CyH)M} = v_3 - v_4 = 0$$

From Table 6.1 and the above six equations, it can be concluded, that at steady state:

$$K_2 X_{Ph} \gamma_M - K_2' \gamma_{(Ph)M} - K_3 \gamma_{(Ph)M} \gamma_{MH}^6 + K_3' \gamma_{(CyH)M} \gamma_M^6 = 0$$
$$K_3 \gamma_{(Ph)M} \gamma_{MH}^6 - K_3' \gamma_{(CvH)M} - K_4 \gamma_{(CvH)M} + K_4' X_{CvH} \gamma_M = 0$$

$$\begin{split} K_{1}X_{H_{3}O} + \gamma_{M} - K_{1}'\gamma_{MH} - K_{3}\gamma_{(Ph)M}\gamma_{MH}^{6} + K_{3}'\gamma_{(CyH)M}\gamma_{M}^{6} - K_{5}X_{H_{3}O} + \gamma_{MH} + K_{5}'\gamma_{M}P_{H_{2}} - K_{6}\gamma_{MH}^{2} \\ + K_{6}'\gamma_{M}^{2}P_{H_{2}} &= 0 \\ K_{1}X_{H_{3}O} + \gamma_{M} - K_{1}'\gamma_{MH} + K_{5}X_{H_{3}O} + \gamma_{MH} - K_{5}'\gamma_{M}P_{H_{2}} - m_{H_{3}O} + \left[X_{H_{3}O}^{*} - X_{H_{3}O}^{*}\right] &= 0 \\ K_{2}X_{Ph}\gamma_{M} - K_{2}'\gamma_{(Ph)M} - m_{Ph}[X_{Ph}^{*} - X_{Ph}] &= 0 \\ K_{4}\gamma_{(CyH)M} - K_{4}'X_{CyH}\gamma_{M} + m_{CyH}[X_{CyH}^{*} - X_{CyH}] &= 0 \\ \gamma_{M} + \gamma_{MH} + \gamma_{(Ph)M} + \gamma_{(CyH)M} - 1 &= 0 \end{split}$$

Table 6.2: Expressions for reaction rate constants

Reaction	Forward rate constant	Backward rate constant
1	$K_{1} = k_{1} exp\left(-\frac{\alpha_{1} n_{1} FE(t)}{RT}\right)$	$K_1' = k_1' exp\left(-\frac{\alpha_1' n_1' FE(t)}{RT}\right)$
2	$K_2 = k_2$	$K_2' = k_2'$
3	$K_3 = k_3$	$K_{3}^{''} = k_{3}^{''}$
4	$K_4 = k_4$	$K_4' = k_4'$
5	$K_5 = k_5 exp\left(-\frac{\alpha_5 n_5 FE(t)}{RT}\right)$	$K_5' = k_5' exp\left(-\frac{\alpha_5' n_5' FE(t)}{RT}\right)$
6	$K_6 = k_6$	$K_6' = k_6'$

The expression for each of the forward and backward reaction rate constants are provided in Table 6. The bulk concentrations may be experimentally measured, which hardly change during the length of a typical RDE experiment. The mass transfer coefficients, m_i are constants that can be estimated from literature. Therefore, a system of equations where the number of variables equals the number of equations can be solved to determine the unknown variables in terms of known variables and system parameters K_i .

The model may be simplified by assuming that only adsorption/desorption reactions are reversible. All other surface and electrochemical reactions are irreversible. This is in accordance with a previous study of ECH of phenol over Pd, Ni and Rh based catalysts.²⁹² Therefore:

$$K_1' = 0$$
; $K_3' = 0$; $K_5' = 0$

Furthermore, we can assume that the adsorption/desorption reactions are always at equilibrium.

$$K_2' = K_2 X_{Ph} \gamma_M / \gamma_{(Ph)M}$$

$$K_4' = K_4 \gamma_{(CyH)M} / X_{CyH} \gamma_M$$

$$K_6' = K_6 \gamma_{MH}^2 / \gamma_M^2 P_{H_2}$$

Now, only 6 parameters (six K_i) are to be estimated.

Thus, the above system of equations can now be represented as:

$$(X_{Ph}\gamma_{M} - \frac{X_{Ph}\gamma_{M}}{\gamma_{(Ph)M}})(K_{2}) - K_{3}\gamma_{(Ph)M}\gamma_{MH}^{6} = 0$$

$$K_{3}\gamma_{(Ph)M}\gamma_{MH}^{6} - (K_{4})(\gamma_{(CyH)M} - \gamma_{(CyH)M}/(X_{CyH}\gamma_{M})) = 0$$

$$K_{1}X_{H_{3}O} + \gamma_{M} - K_{3}\gamma_{(Ph)M}\gamma_{MH}^{6} - K_{5}X_{H_{3}O} + \gamma_{MH} - (K_{6})(\gamma_{MH}^{2} - \gamma_{MH}^{2}/(\gamma_{M}^{2}P_{H_{2}})) = 0$$

$$K_{1}X_{H_{3}O} + \gamma_{M} + K_{5}X_{H_{3}O} + \gamma_{MH} - m_{H_{3}O} + \left[X_{H_{3}O}^{*} - X_{H_{3}O}^{*}\right] = 0$$

$$(K_{2})(X_{Ph}\gamma_{M} - \frac{X_{Ph}\gamma_{M}}{\gamma_{(Ph)M}}) - m_{Ph}[X_{Ph}^{*} - X_{Ph}] = 0$$

$$(K_{4})(\gamma_{(CyH)M} - \gamma_{(CyH)M}/(X_{CyH}\gamma_{M})) + m_{CyH}[X_{CyH}^{*} - X_{CyH}] = 0$$

$$\gamma_{M} + \gamma_{MH} + \gamma_{(Ph)M} + \gamma_{(CyH)M} - 1 = 0$$

The Faradaic current is determined from the rates of partial electrochemical reactions as:

$$i_f = F(-\nu_1 - \nu_5) = -F(\nu_1 + \nu_5) = -F(\nu_3 + 2\nu_5 + \nu_6)$$

Therefore:
$$i_f = -F(K_1 X_{H_3O} + \gamma_M - K_1' \gamma_{MH} + K_5 X_{H_3O} + \gamma_{MH} - K_5' \gamma_M P_{H_2})$$

Where $X_{H_3O^+}$, γ_{MH} , and γ_{M} may be expressed in terms of K_i from the system of equations and substituted in this expression. P_{H_2} , on the other hand, may be assumed a constant for the time span of the RDE experiment.

An expression results of the form:

$$Current = f(E(t), K_i, known parameters)$$

This expression may be fit with obtained current vs. potential experimental data from the RDE experiments to estimate the K_j by solving the inverse problem. Table 6.3 provides the description of variables that have not been described in the study before.

Table 6.3: Legend for different variables

Variables	Description
$X_{H_3O^+}$	Hydronium ion concentration at interface
γ_M	Fraction of empty metal sites
X_{Ph}	Phenol concentration at interface
γ_{MH}	Fraction of sites occupied by atomic H
$\gamma_{(Ph)M}$	Fraction of sites occupied by phenol
$\gamma_{(CyH)M}$	Fraction of sites occupied by cyclohexanol
X_{CyH}	Cyclohexanol concentration at interface
P_{H_2}	Hydrogen partial pressure
α	Transfer coefficient

Experimental Setup

The experimental setup used for the ECH experiments was a rotating disk electrode (RDE) with a 3-electrode system setup. The Ru/ACC catalyst was prepared and pasted on a glassy carbon working electrode using carbon conductive paint. These paints usually contain micro-graphite particles dispersed in isopropanol that are air-dried rapidly at room temperature and a small amount of special polymer to lend extra adhesive properties. A graphite carbon counter electrode was employed with an Ag/AgCl electrode as the reference electrode. 30 mL of 0.2 M HCl was selected as the electrolyte.³² Pre-electrolysis was performed through a linear scan from 0V to a reduction volage of 10V at a scan rate of 20 mV/s using a potentiostat to activate the catalyst for ECH. Once the pre-electrolysis was completed, phenol was added such that the final concentration in the electrolyte solution was 20 mM. The ECH was performed at a temperature of 80°C, a rotation speed of 2500 rpm, and a voltage scan rate of 5 mV/s, varied from 0V to a reduction voltage of 5V.

The experimental setup is shown in Figure 6.1.

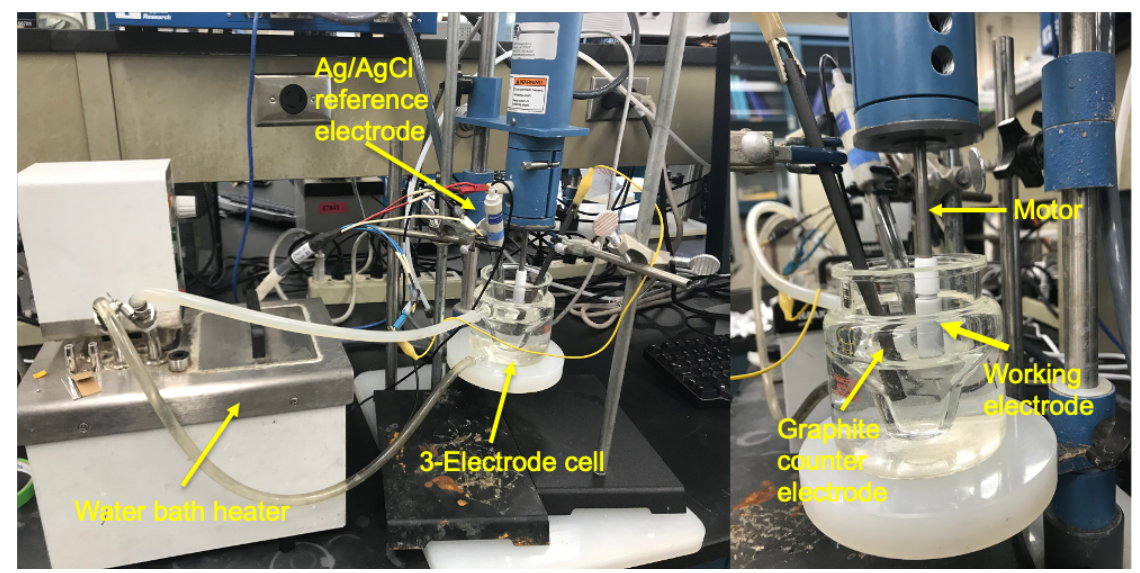


Figure 6.1 : Setup for RDE experiments

Catalyst Preparation

The catalyst was prepared in accordance with the method described by Li et al.³² However, the activated carbon cloth (ACC) was cut into smaller sizes to paste them on the glassy carbon working electrode of the RDE. ACC was cut into 0.6 X 0.6 cm pieces and stirred overnight in deionized water and then dried in an oven at 150°C. 32 such cloths were then soaked in a ruthenium salt solution of 0.102 g Ru(NH)₃Cl₆, 0.196 mL of NH₄OH and 1.302 mL of DI water until the solution was absorbed completely in 12 minutes to saturate the pores of the ACC. Next, overnight drying was performed at room temperature, followed by further vacuum drying for 24 hours. These vacuum dried cloths, 3 at a time, were then electrocatalytically reduced in a divided cell, separated by a proton exchange Nafion membrane, where these functioned as the cathode. Pt wire was used as anode. 0.2 M HCl was used as both catholyte and anolyte. The experiment was run galvanostatically at 150 mA and 60°C. The experimental setup has been shown in Figure 6.2. The catholyte solution initially turned pink until it faded to a yellowish color, before transitioning to a dark blue color. The reduction was stopped when the blue color disappeared. The whole reduction

took about 75 minutes. The reduced cloth was then kept overnight in a drying chamber before being used in the RDE.

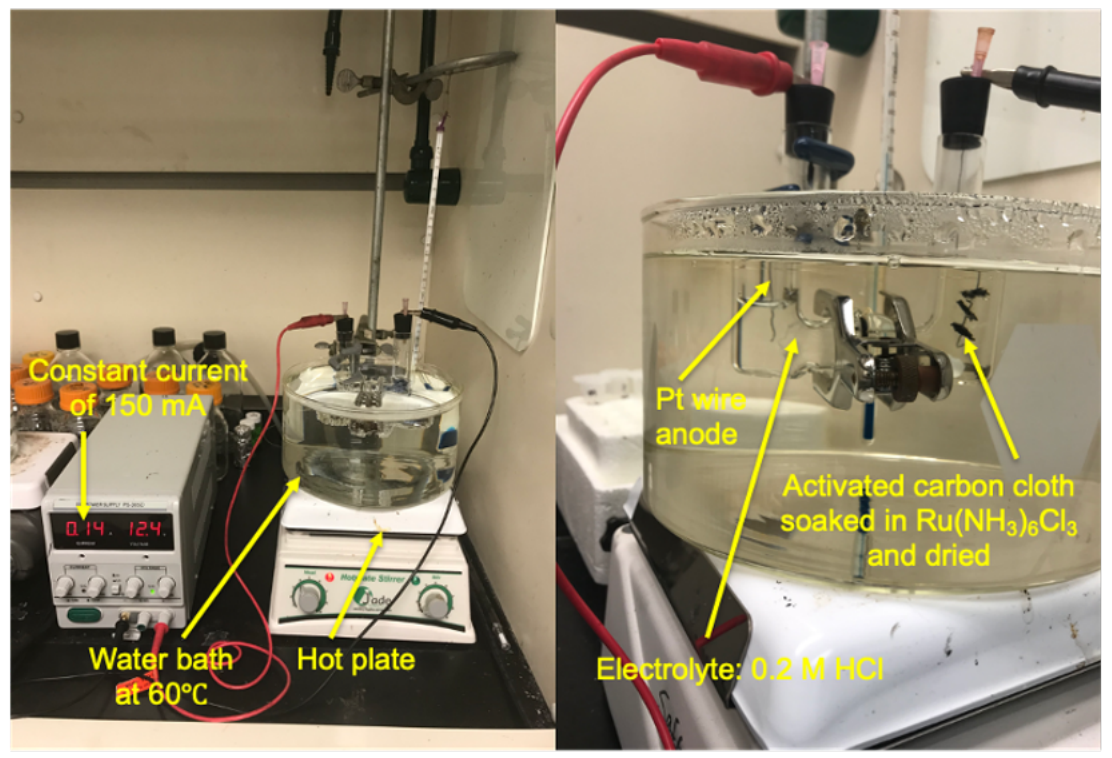


Figure 6.2: Experimental setup for catalyst preparation

Results

Current vs Potential Data from RDE

Current vs potential data were obtained from the RDE experiment and plotted as shown in Figure 6.3 (a). The red line denotes the current vs potential data when the substrate phenol was not added to the electrolyte solution. Therefore, it only indicates the current obtained for the hydrogen evolution reaction (HER). When phenol was added, an increase in the current was observed (denoted by the blue line), which is indicative of the occurrence of additional reactions such as the ECH of phenol to cyclohexanol. As the voltage was varied from 0 V to a reduction voltage of -5V, the HER current (denoted by the red line) increased to about -80 mA whereas the total current (denoted by the blue line) increased to about -90 mA. It may be concluded from Figure 6.3 (a)

that the experiments occur in the kinetically controlled regime as no plateau forms in the current vs potential plot. This means that enough reactant is reaching the catalyst surface on the working electrode and mass transfer does not control the overall kinetics. Furthermore, the small difference in current is indicative of the fact that the HER is the dominant reaction. In Figure 6.3 (b), the electrode overpotential was plotted against the logarithmic current density. The overpotential was determined by subtracting the equilibrium potential from the potentials in Figure 6.3 (a). The equilibrium potential, in turn was estimated from the standard potential of H⁺/H₂, (since the electrolyte is an aqueous solution) for the experimental conditions of 80°C and pH of 0.69, using the Nernst equation. It was determined to be -0.053 V. The current density, on the other hand was estimated by dividing the obtained current by the catalyst surface area of 0.36 cm². It must be noted here that the negative potentials in Figure 6.3 (a) have been plotted as positive reduction overpotentials in Figure 6.3 (b). From the plot in Figure 6.3 (b), the Tafel slope at higher electrode reduction potentials may be estimated. Also, the exchange current density for the overall reaction scheme may be estimating by extrapolating the linear part of the curve to an overpotential of zero, as shown by the red dotted line in Figure 6.3 (b). The exchange current density for any electrochemical reaction is similar to a rate constant for a chemical reaction.²⁹³ It is a function of concentration, temperature, and catalyst surface area. The exchange current density for the overall reaction was determined to be 7.5 mA/cm². The charge transfer coefficient (α), which is defined as the "fraction of electrostatic potential energy affecting the reduction rate in an electrode reaction, with the remaining fraction, affecting the corresponding oxidation rate"²⁹⁴ may also be estimated from the Tafel slope. This was evaluated to be about 0.08; a value different from 0.5 denotes lack of symmetry in the anodic and cathodic reactions.

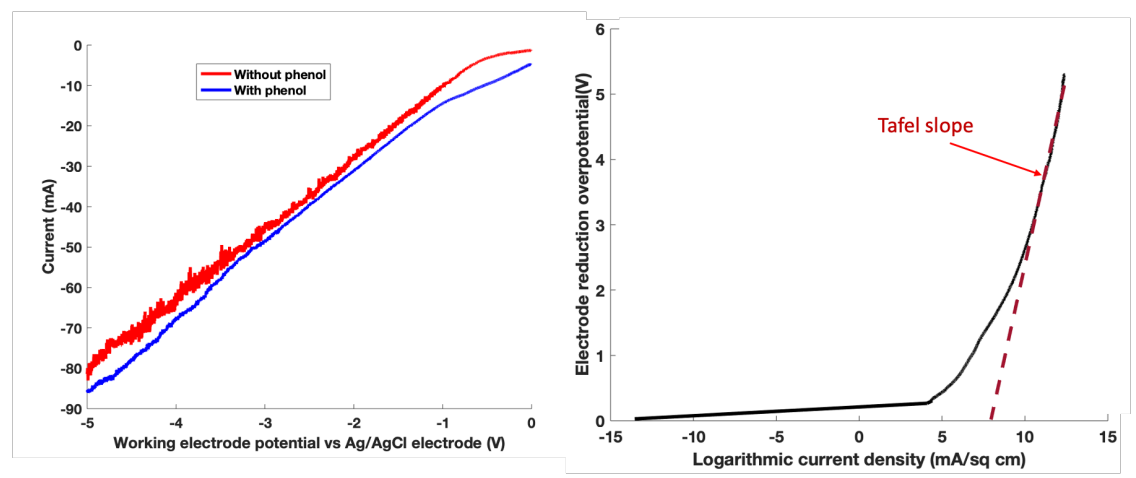


Figure 6.3: (a) Current vs potential data as obtained from RDE experiments (b) Electrode overpotential vs log(current density)

GC/MS of the reaction solution

Gas chromatography-mass spectrometry measurements were made for the electrolyte solution after the RDE experiments were performed. 2 mL of the electrolyte solution was first saturated with 0.8g of NaCl, followed by addition of an equal volume of dichloromethane. The organic layer was then extracted and subjected to GC/MS. The resulting chromatogram showed a distinct phenol peak, as depicted in Figure 6.4.

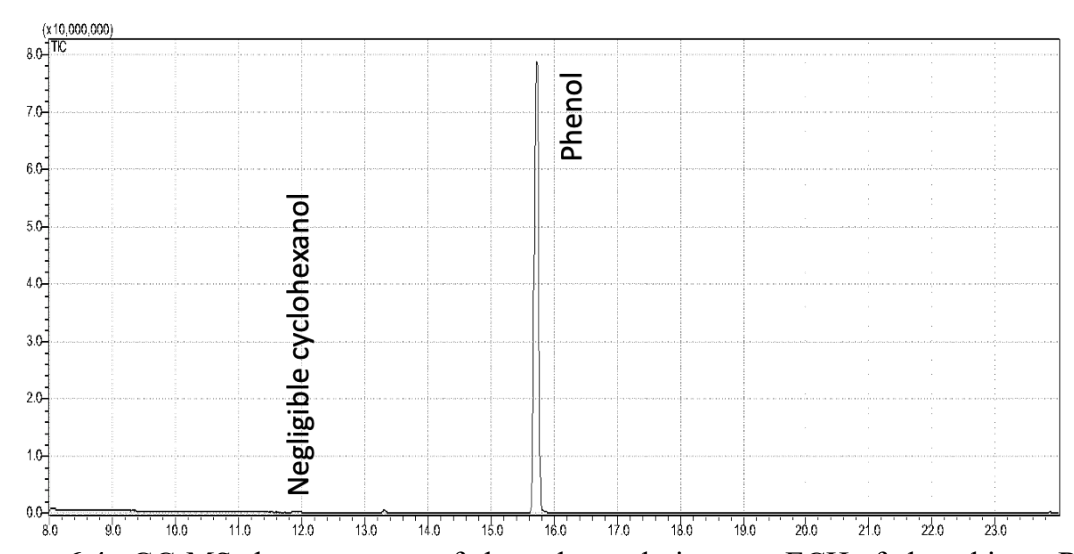


Figure 6.4: GC-MS chromatogram of electrolyte solution post ECH of phenol in an RDE

However, a very small peak was observed for cyclohexanol. Therefore, although an increase in current was observed from the RDE experiment, on adding phenol to the electrolyte solution, the GC/MS of the solution could not confirm the conversion of phenol to cyclohexanol. This indicates that the time span of a linear sweep scan in an RDE experiment may not be long enough to detect any appreciable amount of cyclohexanol.

Discussion

ECH of phenol has been known to produce cyclohexanol in the presence of Ru/ACC catalyst. 136 The present kinetic model was based on this assumption. However, preliminary fitting of currentvoltage data from the RDE experiment to a simplified model, as described in the Appendix at the end of this chapter, did not provide a good fit. This may have been caused by low cyclohexanol production in the RDE setup, as shown in Figure 6.2, and therefore, the predicted values of the model, which accounts for cyclohexanol formation and desorption do not agree with the observed values. Moreover, the model assumes elementary reactions whereas the actual reaction orders may not be dictated by stoichiometry. Another factor may be the noise in the RDE experiments, which may arise from weak electrical connections. In addition, there is the H₂ evolution reaction that can result in bubbles, which can lead to fluctuations in current. Furthermore, the use of carbon conductive paint may have introduced impurities in the solution that may have interfered with the expected reactions. The carbon paint had to be used to attach the Ru/ACC to the surface of the working electrode. This method of attaching the catalyst may have been another source of noise in the experiment. A solution is to use a working electrode with a Ru disk inserted into the Teflon covering, discontinuing the use of carbon cloth and carbon paint altogether. Therefore, more experiments must be performed in the RDE to identify a set of parameters that result in the least on the RDE²⁹⁵ instead of linear sweep voltammetry or cyclic voltammetry. Such a method would probably provide sufficient time for the production of detectable amounts of cyclohexanol as it would hold a constant voltage for a fixed amount of time before stepping up to a higher voltage. This could lead to the collection of better experimental data, and in turn, better parameter fitting for the ECH of phenol using the described model.

APPENDIX

This section describes a preliminary fitting exercise of a simplified version of the model described previously in Chapter 6.

Model Assumptions:

- The reactions are at steady state
- Physical properties like diffusion coefficients and kinematic viscosities are constant
- The adsorption reaction is at equilibrium
- Fast desorption reaction for cyclohexanol
- H₂ evolution occurs via the Tafel reaction

Therefore, the cathode reactions may be described as:

1.
$$H^+ + M + e^- \rightarrow MH$$

2.
$$Ph + M \leftrightarrow (Ph)M$$

3.
$$(Ph)M + 6MH \rightarrow CyH + 7M$$

4.
$$MH + MH \rightarrow H_2 + 2M$$

Where H⁺ are the in-situ generated hydrogen ions from water, Ph denotes phenol, (Ph)M denotes adsorbed phenol, CyH denotes cyclohexanol, M denotes empty metal sites, MH denotes adsorbed hydrogen and H₂ denotes evolved hydrogen gas.

If θ_i are the fractional sites on catalyst surface, occupied by species i, k_i are the rate constants for reaction i, K_i^{eq} are the equilibrium rate constant for reaction i and E(t) is the applied voltage, then the elementary reaction rates (r_i) may be expressed as:

$$r_1=K_1C_H+ heta_M$$
; where $K_1=k_1\exp(-rac{lpha_1n_1FE(t)}{RT})$
$$K_2^{eq}=rac{ heta_{(Ph)M}}{C_{Ph} heta_M}$$

$$r_3=k_3 heta_{(Ph)M} heta_{MH}^6$$

$$r_4 = k_4 \theta_{MH}^2$$

The ratio $R_r = \frac{r_3}{r_4} = \frac{k_3 \theta_{(Ph)M} \theta_{MH}^4}{k_4} = K_r \theta_{(Ph)M} \theta_{MH}^4$ then represents the ratio of rate of cyclohexanol being formed to the rate of hydrogen being evolved.

Now, at steady state, the rate of transformation of species at interface must equal the mass transport flux from bulk to surface. Therefore,

$$r_{H^+} = -r_1 = -m_{H^+} [C_{H^+}^* - C_{H^+}]$$

 $\Rightarrow C_{H^+} = \frac{m_{H^+} C_{H^+}^*}{(m_{H^+} + K_1 \theta_M)}$

where $C_{H^{+}}^{*}$ is the bulk concentration of hydrogen ions and $C_{H^{+}}$ is the interface concentration of hydrogen ions and $m_{H^{+}}$ is the mass transport coefficient.

Similarly, for phenol,

$$r_{Ph} = -r_2 = -m_{Ph}[C_{Ph}^* - C_{Ph}]$$

$$\Rightarrow r_{Ph} = -K_2 C_{Ph} \theta_M + K_2' \theta_{(Ph)M} = -m_{Ph}[C_{Ph}^* - C_{Ph}] = 0$$

$$\Rightarrow C_{Ph} = C_{Ph}^*$$

where C_{Ph}^* is the bulk concentration of phenol and C_{Ph} is the interface concentration of phenol.

For a rotating disk electrode, the mass transport coefficient for species i is given by,

$$m_i = 0.62AD_{c_i}^{2/3} \nu^{-1/6} \Omega^{1/2}$$

where D_i is the diffusion coefficient of species i, ν is the kinematic viscosity of solution, Ω is the rotation speed and A is the catalyst surface area.

Also, from site balance,

$$\theta_M + \theta_{(Ph)M} + \theta_{MH} = 1$$

The faradaic current (i_f) for the set of reactions represented here may be expressed by,

$$i_f = -nFr_1$$

$$\Rightarrow i_f = -nFk_1exp(-\frac{\alpha_1n_1FE(t)}{RT})\frac{m_{H^+}C_{H^+}^*}{(m_{H^+}+K_1\theta_M)}\theta_M$$

Methodology:

The goal was to estimate rate constants and equilibrium constants that can fit the obtained experimental data. For this, an iterative approach was adopted.

- A set of values for k_1 , K_2^{eq} , k_3 , k_4 were assumed and the values for a set of values for K_1 , K_2^{eq} , K_r were then determined
- A value was assumed for R_r
- The θ_i were then evaluated from the set of equations:

$$K_2^{eq} = \frac{\theta_{(Ph)M}}{C_{Ph}^* \theta_M}$$

$$R_r = K_r (\theta_{(Ph)M} \theta_{MH}^4)$$

$$\theta_M + \theta_{(Ph)M} + \theta_{MH} = 1$$

• The current vs potential curve, as obtained by the model, could then be obtained for the set of assumed rate constants and then compared to the experimental data.

The goal was to iterate the steps outlined above, until a good fit was obtained.

Preliminary results:

For the set of values outlined is Table 6.4, the current vs potential curve as predicted by the model, for different values of R_r are shown in Figure 6.5. It can be seen that distinct regimes of kinetic control and mass transfer control are predicted. As the reduction voltage is increased, the current rises in the kinetically controlled regime, until it gets constant for larger reduction voltages in the mass transfer controlled regime. Furthermore, for larger R_r values, greater current is observed, which is indicative of the fact that greater current is required to reduce phenol to cyclohexanol and for the hydrogen evolution reaction.

Table 6.4: Parameter values used in generating model current vs potential curve

Para	meter	Assumed Value	
k		E-07 s ⁻¹ (cm ⁻² of catalyst surface area)	
K	ēq 2	8E-02 mole ⁻¹ L	
	r	9E-02	
	\mathfrak{l}_1	0.08	
C_1	* H ⁺	0.53 M	
m	H ⁺ 5.44E	E-4 cm ³ s ⁻¹ (cm ⁻² of catalyst surface area)	
	Γ	353 K	
0	_		
-5	-	Reaction controlled regime	
-10 (Y m	_	R_=0.1	
Current (mA)	Mass transfer	R _r =10	
-20	controlled regime		
-25	-		
-30			
-5 -4.5 -4 -3.5 -3 -2.5 -2 -1.5 -1 -0.5 0 Working electrode potential vs Ag/AgCl electrode (V)			

Working electrode potential vs Ag/AgCl electrode (V)

Figure 6.5 : Current vs potential curve as predicted by model for different values of R_r

The curves obtained in Figure 6.5 are very different from those obtained experimentally in Figure 6.3 (a). In Figure 6.3 (a) the current increases to values around -90 mA, while it only increases to around -27 mA in Figure 6.5. Furthermore, there is no mass transfer controlled regime observed in Figure 6.3 (a). The lack of a good fit may be due to the numerous reasons outlined in the Discussion section of Chapter 6.

However, the effect of increasing the mass transport coefficient and the kinetic rate constant of the hydrogen adsorption reaction (since it is the only reduction reaction in the model that involves electron transfer) was investigated to see if there was better fit between observed and predicted data. This can be seen in Figure 6.6. As the mass transport coefficient is increased, the constant

current value obtained in the mass transfer controlled regime increases. On the other hand, increasing the kinetic rate constant for hydrogen adsorption reduces the reduction potential required for the onset of the mass controlled regime. However, change in either do not provide a good fit to the experimental data that only shows a kinetically controlled regime. The possible causes behind this lack of fit have been discussed previously in Chapter 6.

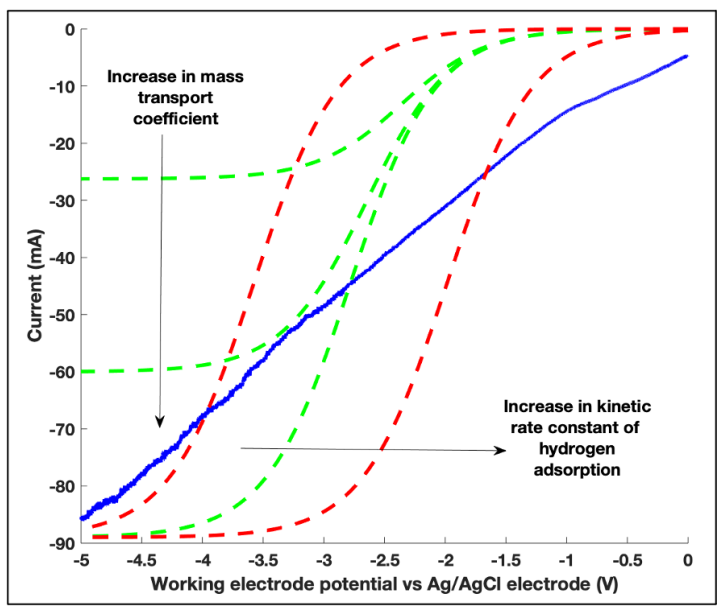


Figure 6.6: Effect of increasing mass transfer coefficient and kinetic rate constant for hydrogen adsorption on model predicted curve. Blue line denotes experimental data.

Chapter 7 : CONCLUSIONS AND FUTURE WORK

Conclusions

The Py-ECH system, which is a bioenergy system that combines depot-based fast pyrolysis and electrocatalytic hydrogenation with centralized hydroprocessing to produce a gasoline range fuel was modeled using thermodynamic assumptions from Aspen's NIST database. The energy, mass and carbon flux through the entire system was determined and plotted in Sankey diagrams. The calculated fuel yields (in terms of mass, energy and carbon) for the Py-ECH system were found to be greater than those for cellulosic fermentations to ethanol. This indicates that incorporation of electricity from renewable energy sources into bioenergy systems that thermochemically process biomass, can lead to systems that are more carbon and energy efficient than traditional cellulosic fermentations to ethanol. It can also be concluded that the Py-ECH system utilizes much less water than the cellulosic fermentations to ethanol. Furthermore, biochar is a valuable by-product that is an added benefit of the Py-ECH system.

The technoeconomic analysis of the Py-ECH system revealed that the fuel had a minimum fuel selling price (MFSP) of \$ 3.62/gge (in 2018 \$) using a discounted cash flow rate of return (DCFROR) analysis and nth plant economics. The evaluated MFSP was for a gasoline range fuel using the Py-ECH system, starting from corn stover biomass. This is less than that for ethanol produced from cellulosic fermentations at \$ 3.70/gge (in 2018 \$), using consistent economic assumptions. The parameters that the MFSP was most sensitive to were determined to be the cost of electricity, the cost of raw material, the pyrolysis bio-oil yield, the ECH cell efficiencies and the catalyst price and thickness. Optimization studies showed that the optimum depot capacity and refinery capacity that resulted in the least MFSP were a depot size of 500 tonnes/day and a refinery size of 10,000 tonnes/day. The analysis showed that by stacking successive realistic improvements

in the Py-ECH system, a MFSP of \$ 2.67/gge (in 2018 \$) may attained. If the biochar by-product may be sold at a price of about \$80/tonnne, the MFSP can drop to as low as \$ 2.57/gge (in 2018 \$).

The life cycle assessment revealed that the eutrophication potential (EUP) and water scarcity footprint (WSF) is always lower for the Py-ECH system than that for cellulosic fermentations to ethanol, making it an environmentally more favorable system in regard to these impact categories. The climate change potential or the global warming potential (GWP) is however dependent on the source of electricity being used in the Py-ECH system. If the electricity source is 87% or more renewable, then the environmental performance of Py-ECH system starts getting better than cellulosic fermentations to ethanol. The energy analysis revealed that the ratio of total renewable energy output to the total fossil energy input of the Py-ECH system, surpasses that of the cellulosic ethanol system under two scenarios (a) when there is 100% renewable heat at the central refinery and ~85% renewable electricity or (b) when there is 100% renewable electricity and ~5% renewable heat at central refinery. Furthermore, a sensitivity analysis of the annual carbon sequestration rate on GWP, revealed that at lower carbon sequestration values the Py-ECH performs better than cellulosic ethanol processes, in terms of climate change. The trend however changes, for larger sequestration values.

Preliminary kinetic studies for the ECH of phenol to cyclohexanol in an RDE cell, yielded the exchange current density and charge transfer coefficient for the overall kinetics. GC/MS of electrolyte solution post RDE experiments yielded negligible amounts of cyclohexanol, indicating that the time in a linear sweep voltammetry in a RDE setup may not be sufficient enough for conversion of phenol to cyclohexanol that can be quantitatively determined. However, increase in

current on adding phenol in the electrolyte solution indicated the occurrence of other reduction reactions than only hydrogen evolution.

Future Work

The Py-ECH system, essentially integrates three technologies, namely, fast pyrolysis, electrocatalytic hydrogenation (ECH) and hydroprocessing. Of these, fast pyrolysis of biomass is a sufficiently mature technology. Hydroprocessing, in regard to fossil fuels is also very popular, and the challenge here is in the successful translation to the handling of different bio-oil compositions, resulting from different biomass feedstocks; as opposed to relatively similar crude oil, in case of petroleum. A major challenge associated with ECH is the continuous operation of a reactor that processes bio-oil. In this regard, research into the solid polymer electrolyte reactor as a potential solution can be the direction to move forward. There is also scope for other future efforts in the successful implementation of the ECH of bio-oil, such as improvement in cell efficiencies and finding cheaper catalysts. Furthermore, there is future work associated with each component study in this analysis:

- 1. The technoeconomic analysis indicates that the key parameters guiding the economics are the raw material cost and the electricity cost. Research must, therefore, be focused on optimizing biomass supply chains with local geographical data that can further reduce the feedstock cost. Research must also be performed to make cost improvements in the generation of electricity from different sources of electrical power.
- 2. The major recommendation from the life cycle assessment is to incorporate renewable sources to meet electricity requirement in bioenergy systems. In this context, as future work, it may be interesting to investigate the holistic effects of incorporating renewable electricity from solar/wind farms in regard to the land usage for setting up these farms.

3. Preliminary kinetic modeling studies indicate that further RDE experiments for ECH of phenol to cyclohexanol need to be performed, possibly using chronoamperometric techniques to generate data that can estimate the kinetic rate constants associated with the electrochemical, adsorption/desorption and surface reactions. Also, it may be better to use a Ru disk embedded inside the Teflon covering as the working electrode instead of Ru/ACC attached to the glassy carbon electrode, using carbon paint, as this might be a source of noise in the experiment. Once the kinetic rate constants are predicted with reasonable accuracy for phenol, the process needs to be repeated for other model bio-oil compounds. Once sufficient number of model compounds are studied, the rates for ECH of pyrolysis bio-oil may be derived out. Such an analysis is key to the scale up of the ECH reactor and subsequent commercial application of the Py-ECH system.

BIBLIOGRAPHY

BIBLIOGRAPHY

- 1. Gadonneix, P.; Nadeau, M.-J.; Kim, Y. D.; Birnbaum, L.; Cho, H.; Choudhury, A. R.; Neto, J. d. C. C.; Dauger, J.-M.; Meyers, K.; Sambo, A.; Statham, B. A.; Lieras, J. A. V.; Ward, G.; Wu, X.; Zatari, T. M.; Frei, C. World Energy Resources-2013 Survey; 2013.
- 2. Victor, D. G.; Zhou, D.; Ahmed, E. H. M.; Dadhich, P. K.; Olivier, J. G. J.; Rogner, H.-H.; Sheikho, K.; Yamaguchi, M. Introductory Chapter. In: Climate Change 2014: Mitigation of Climate Change. Contribution of Working Group III to the Fifth Assessment Report of the Intergovernmental Panel on Climate Change [Edenhofer, O., R. Pichs-Madruga, Y. Sokona, E. Sarahani, S. Kadner, K. Seyboth, A. Adler, I. Baum, S. Brunner, P. Eickemeier, B. Kriemann, J. Savolainen, S. Schlömer, C. von Stechow, T. Zwickel and J.C. Minx (eds.)]; Cambridge, UK and New York, USA, 2014.
- 3. Congress, U. S., Energy Independence and Security Act (EISA). United States, 2007.
- 4. Demirbaş, A., Biomass resource facilities and biomass conversion processing for fuels and chemicals. *Energy Conversion and Management* 2001, *42* (11), 1357-1378.
- 5. Lam, C. H.; Das, S.; Erickson, N. C.; Hyzer, C. D.; Garedew, M.; Anderson, J. E.; Wallington, T. J.; Tamor, M. A.; Jackson, J. E.; Saffron, C. M., Towards sustainable hydrocarbon fuels with biomass fast pyrolysis oil and electrocatalytic upgrading. *Sustainable Energy & Fuels* 2017, *1* (2), 258-266.
- 6. Zhu, X.-G.; Long, S. P.; Ort, D. R., What is the maximum efficiency with which photosynthesis can convert solar energy into biomass? *Current opinion in biotechnology* 2008, *19* (2), 153-159.
- 7. Govindjee; Govindjee, R. What is Photosyntheis? http://www.life.illinois.edu/govindjee/whatisit.htm.
- 8. Luo, L.; Voet, E.; Huppes, G.; Udo de Haes, H. A., Allocation issues in LCA methodology: a case study of corn stover-based fuel ethanol. *The international journal of life cycle assessment 14* (6), 529-539.
- 9. Kim, S.; Dale, B. E., A distributed cellulosic biorefinery system in the US Midwest based on corn stover. *Biofuels, Bioproducts and Biorefining* 2016, *10* (6), 819-832.
- 10. Kim, S.; Zhang, X.; Dale, B. E.; Reddy, A. D.; Jones, C. D.; Izaurralde, R. C., EISA (Energy Independence and Security Act)-Compliant Ethanol Fuel from Corn Stover in a Depot-Based Decentralized System. *Biofuels, Bioproducts and Biorefining* 2018.
- 11. Humbird, D.; Davis, R.; Tao, L.; Kinchin, C.; Hsu, D.; Aden, A.; Schoen, P.; Lukas, J.; Olthof, B.; Worley, M. *Process design and economics for biochemical conversion of*

- lignocellulosic biomass to ethanol: dilute-acid pretreatment and enzymatic hydrolysis of corn stover; NREL/TP-5100-47764; National Renewable Energy Laboratory (NREL), Golden, CO.: 2011.
- 12. Balat, M.; Balat, H.; Öz, C., Progress in bioethanol processing. *Progress in energy and combustion science* 2008, *34* (5), 551-573.
- 13. *Hydrogen Production: Biomass Gasification*; Hydrogen and Fuel Cell Technologies Office.
- 14. Kirubakaran, V.; Sivaramakrishnan, V.; Nalini, R.; Sekar, T.; Premalatha, M.; Subramanian, P., A review on gasification of biomass. *Renewable and Sustainable Energy Reviews* 2009, *13* (1), 179-186.
- 15. Nussbaumer, T., Combustion and Co-combustion of Biomass: Fundamentals, Technologies, and Primary Measures for Emission Reduction. *Energy & Fuels* 2003, *17* (6), 1510-1521.
- 16. Demirbas, A., Combustion of Biomass. *Energy Sources, Part A: Recovery, Utilization, and Environmental Effects* 2007, *29* (6), 549-561.
- 17. Tumuluru, J. S.; Sokhansanj, S. J.; Hess, R.; Wright, C. T.; Boardman, R. D., A review on biomass torrefaction process and product properties for energy applications. *Industrial Biotechnology* 2011, 7 (5), 384-401.
- 18. Bridgwater, A. V., Fast Pyrolysis of Biomass: A Handbook Volume 2. CPL Press: 2008.
- 19. Bridgwater, A. V., Review of fast pyrolysis of biomass and product upgrading. *Biomass and Bioenergy* 2012, *38*, 68-94.
- 20. Moens, L.; Black, S. K.; Myers, M. D.; Czernik, S., Study of the Neutralization and Stabilization of a Mixed Hardwood Bio-Oil. *Energy & Fuels* 2009, *23* (5), 2695-2699.
- 21. Yang, Z.; Kumar, A.; Huhnke, R. L., Review of recent developments to improve storage and transportation stability of bio-oil. *Renewable and Sustainable Energy Reviews* 2015, *50*, 859-870.
- 22. Eranki, P. L.; Bals, B. D.; Dale, B. E., Advanced Regional Biomass Processing Depots: a key to the logistical challenges of the cellulosic biofuel industry. *Biofuels, Bioproducts and Biorefining* 2011, 5 (6), 621-630.
- 23. Li, Z.; Kelkar, S.; Lam, C. H.; Luczek, K.; Jackson, J. E.; Miller, D. J.; Saffron, C. M., Aqueous electrocatalytic hydrogenation of furfural using a sacrificial anode. *Electrochimica Acta* 2012, *64*, 87-93.

- 24. An, W.; Hong, J.; Pintauro, P., Current efficiency for soybean oil hydrogenation in a solid polymer electrolyte reactor. *Journal of applied electrochemistry* 1998, 28 (9), 947-954.
- 25. Kwon, Y.; Koper, M. T., Electrocatalytic hydrogenation and deoxygenation of glucose on solid metal electrodes. *ChemSusChem* 2013, *6* (3), 455-62.
- 26. Dabo, P.; Cyr, A.; Lessard, J.; Brossard, L.; Menard, H., Electrocatalytic hydrogenation of 4-phenoxyphenol on active powders highly dispersed in a reticulated vitreous carbon electrode. *Canadian Journal of Chemistry* 1999, 77 (7), 1225-1229.
- 27. Green, S. K.; Lee, J.; Kim, H. J.; Tompsett, G. A.; Kim, W. B.; Huber, G. W., The electrocatalytic hydrogenation of furanic compounds in a continuous electrocatalytic membrane reactor. *Green Chemistry* 2013, *15* (7), 1869-1879.
- 28. zhao, B.; Chen, M.; Guo, Q.; Fu, Y., Electrocatalytic hydrogenation of furfural to furfuryl alcohol using platinum supported on activated carbon fibers. *Electrochimica Acta* 2014, *135*, 139-146.
- 29. Robin, D.; Comtois, M.; Martel, A.; Lemieux, R.; Cheong, A. K.; Belot, G.; Lessard, J., The electrocatalytic hydrogenation of fused poly cyclic aromatic compounds at Raney nickel electrodes: the influence of catalyst activation and electrolysis conditions. *Canadian Journal of Chemistry* 1990, 68 (7), 1218-1227.
- 30. Anantharaman, V.; Pintauro, P. N., The Electrocatalytic Hydrogenation of Glucose I. Kinetics of Hydrogen Evolution and Glucose Hydrogenation on Raney Nickel Powder. *Journal of the Electrochemical Society* 1994, *141* (10), 2729-2741.
- 31. Santana, D. S.; Melo, G. O.; Lima, M. V. F.; Daniel, J. R. R.; Areias, M. C. C.; Navarro, M., Electrocatalytic hydrogenation of organic compounds using a nickel sacrificial anode. *Journal of Electroanalytical Chemistry* 2004, *569* (1), 71-78.
- 32. Li, Z.; Garedew, M.; Lam, C. H.; Jackson, J. E.; Miller, D. J.; Saffron, C. M., Mild electrocatalytic hydrogenation and hydrodeoxygenation of bio-oil derived phenolic compounds using ruthenium supported on activated carbon cloth. *Green Chemistry* 2012, *14* (9), 2540.
- 33. Dalavoy, T.; Jackson, J.; Swain, G.; Miller, D.; Li, J.; Lipkowski, J., Mild electrocatalytic hydrogenation of lactic acid to lactaldehyde and propylene glycol. *Journal of Catalysis* 2007, *246* (1), 15-28.
- 34. Lam, C. H.; Lowe, C. B.; Li, Z.; Longe, K. N.; Rayburn, J. T.; Caldwell, M. A.; Houdek, C. E.; Maguire, J. B.; Saffron, C. M.; Miller, D. J.; Jackson, J. E., Electrocatalytic upgrading of model lignin monomers with earth abundant metal electrodes. *Green Chem.* 2015, 17 (1), 601-609.
- 35. Reed, T. B. *Combustion, Pyrolysis, Gasification, and Liquefaction of Biomass*; National Renewable Energy Lab. (NREL), Golden, CO (United States): 1980.

- 36. Bridgwater, A. V.; Meier, D.; Radlein, D., An overview of fast pyrolysis of biomass. *Organic Geochemistry* 1999, *30* (12), 1479-1493.
- 37. Laird, D. A.; Brown, R. C.; Amonette, J. E.; Lehmann, J., Review of the pyrolysis platform for coproducing bio-oil and biochar. *Biofuels, Bioproducts and Biorefining* 2009, *3* (5), 547-562.
- 38. Schmidt, H.-P., 55 uses of biochar. *Journal for ecology, winegrowing and climate farming, posted on December* 2012, 29.
- 39. Jirka, S.; Tomlinson, T. 2013 State of the Biochar Industry: A Survey of Commercial Activity in the Biochar Field; 2014.
- 40. Tan, X.; Liu, Y.; Zeng, G.; Wang, X.; Hu, X.; Gu, Y.; Yang, Z., Application of biochar for the removal of pollutants from aqueous solutions. *Chemosphere* 2015, *125*, 70-85.
- 41. Bruun, E.; Müller-Stöver, D.; Ambus, P.; Hauggaard-Nielsen, H., Application of biochar to soil and N2O emissions: potential effects of blending fast-pyrolysis biochar with anaerobically digested slurry. *European Journal of Soil Science* 2011, 62 (4), 581-589.
- 42. Oni, B. A.; Oziegbe, O.; Olawole, O. O., Significance of biochar application to the environment and economy. *Annals of Agricultural Sciences* 2019, *64* (2), 222-236.
- 43. Mortensen, P. M.; Grunwaldt, J. D.; Jensen, P. A.; Knudsen, K. G.; Jensen, A. D., A review of catalytic upgrading of bio-oil to engine fuels. *Applied Catalysis A: General* 2011, 407 (1-2), 1-19.
- 44. Prins, W., and Wagenaar, B. M., Review of rotating cone technology for flash pyrolysis of biomass. In *Proc. Int. Conf. Gasification and Pyrolysis of Biomass*, CPL Press: Stuttgart, Germany, 1997.
- 45. Venderbosch, R. H.; Ardiyanti, A. R.; Wildschut, J.; Oasmaa, A.; Heeres, H. J., Stabilization of biomass-derived pyrolysis oils. *Journal of Chemical Technology & Biotechnology* 2010, 85 (5), 674-686.
- 46. Elliott, D. C.; Hart, T. R.; Neuenschwander, G. G.; Rotness, L. J.; Zacher, A. H., Catalytic hydroprocessing of biomass fast pyrolysis bio-oil to produce hydrocarbon products. *Environmental Progress & Sustainable Energy* 2009, *28* (3), 441-449.
- 47. Sundaramurthy, V.; Dalai, A. K.; Adjaye, J., Tetraalkylthiomolybdates-derived Co(Ni)Mo/γ-Al2O3 sulfide catalysts for gas oil hydrotreating. *Journal of Molecular Catalysis A: Chemical* 2008, *294* (1-2), 20-26.

- 48. Şenol, O. İ.; Ryymin, E. M.; Viljava, T. R.; Krause, A. O. I., Reactions of methyl heptanoate hydrodeoxygenation on sulphided catalysts. *Journal of Molecular Catalysis A: Chemical* 2007, *268* (1-2), 1-8.
- 49. Gutierrez, A.; Kaila, R. K.; Honkela, M. L.; Slioor, R.; Krause, A. O. I., Hydrodeoxygenation of guaiacol on noble metal catalysts. *Catalysis Today* 2009, *147* (3-4), 239-246.
- 50. Kim, K. H.; Eom, I. Y.; Lee, S. M.; Choi, D.; Yeo, H.; Choi, I.-G.; Choi, J. W., Investigation of physicochemical properties of biooils produced from yellow poplar wood (Liriodendron tulipifera) at various temperatures and residence times. *Journal of Analytical and Applied Pyrolysis* 2011, 92 (1), 2-9.
- 51. Wildschut, J.; Mahfud, F. H.; Venderbosch, R. H.; Heeres, H. J., Hydrotreatment of fast pyrolysis oil using heterogeneous noble-metal catalysts. *Industrial & Engineering Chemistry Research* 2009, 48 (23), 10324-10334.
- 52. Lister, T., Lilga, M., and Lin, Y. 2015 Project Peer Review: Electrochemical Methods of Upgrading Pyrolysis Oils.; 2015.
- 53. Bridgwater, A. V., Catalysis in thermal biomass conversion. *Applied Catalysis A: General* 1994, *116* (1), 5-47.
- 54. Adjaye, J. D.; Bakhshi, N. N., Production of hydrocarbons by catalytic upgrading of a fast pyrolysis bio-oil. Part I: Conversion over various catalysts. *Fuel Processing Technology* 1995, 45 (3), 161-183.
- 55. Balat, M.; Balat, M.; Kırtay, E.; Balat, H., Main routes for the thermo-conversion of biomass into fuels and chemicals. Part 1: Pyrolysis systems. *Energy Conversion and Management* 2009, *50* (12), 3147-3157.
- 56. Wang, J.-J.; Chang, J.; Fan, J., Upgrading of Bio-oil by Catalytic Esterification and Determination of Acid Number for Evaluating Esterification Degree. *Energy & Fuels* 2010, *24* (5), 3251-3255.
- 57. Li, X.; Gunawan, R.; Lievens, C.; Wang, Y.; Mourant, D.; Wang, S.; Wu, H.; Garcia-Perez, M.; Li, C.-Z., Simultaneous catalytic esterification of carboxylic acids and acetalisation of aldehydes in a fast pyrolysis bio-oil from mallee biomass. *Fuel* 2011, *90* (7), 2530-2537.
- 58. Ikura, M.; Stanciulescu, M.; Hogan, E., Emulsification of pyrolysis derived bio-oil in diesel fuel. *Biomass and Bioenergy* 2003, *24* (3), 221-232.
- 59. Zhang, Q.; Chang, J.; Wang, T.; Xu, Y., Review of biomass pyrolysis oil properties and upgrading research. *Energy Conversion and Management* 2007, *48* (1), 87-92.

- 60. Kang, B.-S.; Lee, K. H.; Park, H. J.; Park, Y.-K.; Kim, J.-S., Fast pyrolysis of radiata pine in a bench scale plant with a fluidized bed: Influence of a char separation system and reaction conditions on the production of bio-oil. *Journal of Analytical and Applied Pyrolysis* 2006, 76 (1-2), 32-37.
- 61. Green, S. K.; Tompsett, G. A.; Kim, H. J.; Kim, W. B.; Huber, G. W., Electrocatalytic Reduction of Acetone in a Proton-Exchange-Membrane Reactor: A Model Reaction for the Electrocatalytic Reduction of Biomass. *ChemSusChem* 2012, *5* (12), 2410-2420.
- 62. Pletcher, D., Electrocatalysis: present and future. *Journal of applied electrochemistry 14* (4), 403-415.
- 63. Safizadeh, F.; Ghali, E.; Houlachi, G., Electrocatalysis developments for hydrogen evolution reaction in alkaline solutions A Review. *International Journal of Hydrogen Energy* 2015, 40 (1), 256-274.
- 64. Vilar, M.; Oliveira, J. L.; Navarro, M., Investigation of the hydrogenation reactivity of some organic substrates using an electrocatalytic method. *Applied Catalysis A: General* 2010, 372 (1), 1-7.
- 65. Chae, K. J.; Choi, M.; Ajayi, F. F.; Park, W.; Chang, I. S.; Kim, I. S., Mass Transport through a Proton Exchange Membrane (Nafion) in Microbial Fuel Cells. *Energy & Fuels* 2008, 22 (1), 169-176.
- 66. Resasco, D. E.; Wang, B.; Sabatini, D., Distributed processes for biomass conversion could aid UN Sustainable Development Goals. *Nature Catalysis* 2018, *1* (10), 731-735.
- 67. Petrou, E.; Mihiotis, A., Design of a Factories' Supply System with Biomass in Order to Be Used as an Alternative Fuel—A Case Study. *Energy & Fuels* 2007, *21* (6), 3718-3722.
- 68. Parkhurst, K. M.; Saffron, C. M.; Miller, R. O., An energy analysis comparing biomass torrefaction in depots to wind with natural gas combustion for electricity generation. *Applied Energy* 2016, *179*, 171-181.
- 69. Bals, B. D.; Dale, B. E., Developing a model for assessing biomass processing technologies within a local biomass processing depot. *Bioresource technology* 2012, *106*, 161-169.
- 70. Quddus, M. A.; Ibne Hossain, N. U.; Mohammad, M.; Jaradat, R. M.; Roni, M. S., Sustainable network design for multi-purpose pellet processing depots under biomass supply uncertainty. *Computers & Industrial Engineering* 2017, *110*, 462-483.
- 71. Roni, M. S.; Thompson, D. N.; Hartley, D. S., Distributed biomass supply chain cost optimization to evaluate multiple feedstocks for a biorefinery. *Applied Energy* 2019, *254*, 113660.

- 72. Lamers, P.; Roni, M. S.; Tumuluru, J. S.; Jacobson, J. J.; Cafferty, K. G.; Hansen, J. K.; Kenney, K.; Teymouri, F.; Bals, B., Techno-economic analysis of decentralized biomass processing depots. *Bioresource Technology* 2015, *194*, 205-213.
- 73. Jacobson, J.; Lamers, P.; Roni, M.; Cafferty, K.; Kenney, K.; Heath, B.; Hansen, J. *Techno-economic analysis of a biomass depot*; INL/EXT-14-33225; Idaho National Laboratory: Idaho, 2014.
- 74. Kim, S.; Dale, B. E., Comparing alternative cellulosic biomass biorefining systems: Centralized versus distributed processing systems. *Biomass and Bioenergy* 2015, *74*, 135-147.
- 75. Crandall, M. S.; Adams, D. M.; Montgomery, C. A.; Smith, D., The potential rural development impacts of utilizing non-merchantable forest biomass. *Forest Policy and Economics* 2017, 74, 20-29.
- 76. Ng, R. T. L.; Maravelias, C. T., Design of biofuel supply chains with variable regional depot and biorefinery locations. *Renewable Energy* 2017, *100*, 90-102.
- 77. Martinkus, N.; Latta, G.; Brandt, K.; Wolcott, M., A Multi-Criteria Decision Analysis Approach to Facility Siting in a Wood-Based Depot-and-Biorefinery Supply Chain Model. *Frontiers in Energy Research* 2018, *6* (124).
- 78. Roni, M. S.; Eksioglu, S. D.; Searcy, E.; Jha, K., A supply chain network design model for biomass co-firing in coal-fired power plants. *Transportation Research Part E: Logistics and Transportation Review* 2014, *61*, 115-134.
- 79. Eranki, P. L.; Dale, B. E., Comparative life cycle assessment of centralized and distributed biomass processing systems combined with mixed feedstock landscapes. *GCB Bioenergy* 2011, *3* (6), 427-438.
- 80. Nguyen, L.; Cafferty, K. G.; Searcy, E. M.; Spatari, S., Uncertainties in Life Cycle Greenhouse Gas Emissions from Advanced Biomass Feedstock Logistics Supply Chains in Kansas. *Energies* 2014, *7* (11), 7125-7146.
- 81. Techno-Economic Analysis. https://abpdu.lbl.gov/capabilities/techno-economic-analysis/.
- 82. Tan, E. C. D.; Marker, T. L.; Roberts, M. J., Direct production of gasoline and diesel fuels from biomass via integrated hydropyrolysis and hydroconversion process—A technoeconomic analysis. *Environmental Progress & Sustainable Energy* 2014, *33* (2), 609-617.
- 83. Zhu, Y.; Jones, S. B. *Techno-economic Analysis for the Thermochemical Conversion of Lignocellulosic Biomass to Ethanol via Acetic Acid Synthesis*; PNNL-18483; Pacific Northwest National Lab (PNNL),: Richland, WA (United States), 2009.

- 84. Wright, M. M.; Daugaard, D. E.; Satrio, J. A.; Brown, R. C., Techno-economic analysis of biomass fast pyrolysis to transportation fuels. *Fuel* 2010, *89*, S2-S10.
- 85. Brown, T. R.; Thilakaratne, R.; Brown, R. C.; Hu, G., Techno-economic analysis of biomass to transportation fuels and electricity via fast pyrolysis and hydroprocessing. *Fuel* 2013, *106*, 463-469.
- 86. Sokhansanj, S.; Mani, S.; Tagore, S.; Turhollow, A. F., Techno-economic analysis of using corn stover to supply heat and power to a corn ethanol plant Part 1: Cost of feedstock supply logistics. *Biomass and Bioenergy* 2010, 34 (1), 75-81.
- 87. Peters, M.; Timmerhaus, K., *Plant design and economics for chemical engineers*. McGraw Hill: New York, 1980.
- 88. Pintarič, Z. N.; Kravanja, Z., The Importance of using Discounted Cash Flow Methodology in Techno-economic Analyses of Energy and Chemical Production Plants. *Journal of Sustainable Development of Energy, Water and Environment Systems* 2017, 5 (2), 163-176.
- 89. Cucchiella, F.; D'Adamo, I.; Gastaldi, M.; Miliacca, M., A profitability analysis of small-scale plants for biomethane injection into the gas grid. *Journal of Cleaner Production* 2018, *184*, 179-187.
- 90. Snowden-Swan, L. J.; Zhu, Y.; Jones, S. B.; Elliott, D. C.; Schmidt, A. J.; Hallen, R. T.; Billing, J. M.; Hart, T. R.; Fox, S. P.; Maupin, G. D. *Hydrothermal Liquefaction and Upgrading of Municipal Wastewater Treatment Plant Sludge: A Preliminary Techno-Economic Analysis, Rev. I*; PNNL-25464-Rev.1; Pacific Northwest National Lab (PNNL): Richland, WA (United States), 2016.
- 91. Shahabuddin, M.; Krishna, B. B.; Bhaskar, T.; Perkins, G., Advances in the thermochemical production of hydrogen from biomass and residual wastes: Summary of recent technoeconomic analyses. *Bioresource Technology* 2020, 299, 122557.
- 92. Patel, M.; Zhang, X.; Kumar, A., Techno-economic and life cycle assessment on lignocellulosic biomass thermochemical conversion technologies: A review. *Renewable and Sustainable Energy Reviews* 2016, *53*, 1486-1499.
- 93. Phillips, S. D.; Tarud, J. K.; Biddy, M. J.; Dutta, A., Gasoline from Woody Biomass via Thermochemical Gasification, Methanol Synthesis, and Methanol-to-Gasoline Technologies: A Technoeconomic Analysis. *Industrial & Engineering Chemistry Research* 2011, *50* (20), 11734-11745.
- 94. Swanson, R. M.; Platon, A.; Satrio, J. A.; Brown, R. C., Techno-economic analysis of biomass-to-liquids production based on gasification. *Fuel* 2010, *89*, S11-S19.
- 95. Anex, R. P.; Aden, A.; Kazi, F. K.; Fortman, J.; Swanson, R. M.; Wright, M. M.; Satrio, J. A.; Brown, R. C.; Daugaard, D. E.; Platon, A.; Kothandaraman, G.; Hsu, D. D.;

- Dutta, A., Techno-economic comparison of biomass-to-transportation fuels via pyrolysis, gasification, and biochemical pathways. *Fuel* 2010, *89*, S29-S35.
- 96. Thilakaratne, R.; Brown, T.; Li, Y.; Hu, G.; Brown, R., Mild catalytic pyrolysis of biomass for production of transportation fuels: a techno-economic analysis. *Green Chemistry* 2014, *16* (2), 627-636.
- 97. Sorunmu, Y.; Billen, P.; Spatari, S., A review of thermochemical upgrading of pyrolysis bio-oil: Techno-economic analysis, life cycle assessment, and technology readiness. *GCB Bioenergy* 2020, *12* (1), 4-18.
- 98. Shemfe, M. B.; Gu, S.; Ranganathan, P., Techno-economic performance analysis of biofuel production and miniature electric power generation from biomass fast pyrolysis and bio-oil upgrading. *Fuel* 2015, *143*, 361-372.
- 99. Silveira, J. L.; Gomes, L. a., Fuel cell cogeneration system: a case of technoeconomic analysis. *Renewable and Sustainable Energy Reviews* 1999, *3* (2), 233-242.
- 100. Rahimi, S.; Meratizaman, M.; Monadizadeh, S.; Amidpour, M., Techno-economic analysis of wind turbine–PEM (polymer electrolyte membrane) fuel cell hybrid system in standalone area. *Energy* 2014, *67*, 381-396.
- 101. Wang, J.; Wang, H.; Fan, Y., Techno-Economic Challenges of Fuel Cell Commercialization. *Engineering* 2018, *4* (3), 352-360.
- 102. Orella, M. J.; Brown, S. M.; Leonard, M. E.; Román-Leshkov, Y.; Brushett, F. R., A General Techno-Economic Model for Evaluating Emerging Electrolytic Processes. *Energy Technology* 2020.
- 103. Zhu, Y.; Biddy, M. J.; Jones, S. B.; Elliott, D. C.; Schmidt, A. J., Techno-economic analysis of liquid fuel production from woody biomass via hydrothermal liquefaction (HTL) and upgrading. *Applied Energy* 2014, *129*, 384-394.
- 104. Clausen, L. R.; Houbak, N.; Elmegaard, B., Technoeconomic analysis of a methanol plant based on gasification of biomass and electrolysis of water. *Energy* 2010, *35* (5), 2338-2347.
- 105. Trippe, F.; Fröhling, M.; Schultmann, F.; Stahl, R.; Henrich, E., Techno-Economic Analysis of Fast Pyrolysis as a Process Step Within Biomass-to-Liquid Fuel Production. *Waste and Biomass Valorization* 2010, *1* (4), 415-430.
- 106. Curran, M. A., Life Cycle Assessment: a review of the methodology and its application to sustainability. *Current Opinion in Chemical Engineering* 2013, *2* (3), 273-277.
- 107. Caro, D., Carbon Footprint. In *Encyclopedia of Ecology (Second Edition)*, Fath, B., Ed. Elsevier: Oxford, 2019; pp 252-257.

- 108. Nieuwlaar, E., Life Cycle Assessment and Energy Systems. In *Encyclopedia of Energy*, Cleveland, C. J., Ed. Elsevier: New York, 2004; pp 647-654.
- 109. Finnveden, G.; Hauschild, M. Z.; Ekvall, T.; Guinée, J.; Heijungs, R.; Hellweg, S.; Koehler, A.; Pennington, D.; Suh, S., Recent developments in Life Cycle Assessment. *Journal of Environmental Management* 2009, *91* (1), 1-21.
- 110. Guinée, J. B.; Heijungs, R.; Huppes, G.; Zamagni, A.; Masoni, P.; Buonamici, R.; Ekvall, T.; Rydberg, T., Life Cycle Assessment: Past, Present, and Future. *Environmental Science & Technology* 2011, 45 (1), 90-96.
- 111. Peters, J. F.; Iribarren, D.; Dufour, J., Life cycle assessment of pyrolysis oil applications. *Biomass Conversion and Biorefinery* 2015, *5* (1), 1-19.
- 112. Lan, K.; Ou, L.; Park, S.; Kelley, S. S.; Yao, Y., Life Cycle Analysis of Decentralized Preprocessing Systems for Fast Pyrolysis Biorefineries with Blended Feedstocks in the Southeastern United States. *Energy Technology* 2019, 1900850.
- 113. Iribarren, D.; Peters, J. F.; Dufour, J., Life cycle assessment of transportation fuels from biomass pyrolysis. *Fuel* 2012, *97*, 812-821.
- 114. Peters, J. F.; Iribarren, D.; Dufour, J., Biomass Pyrolysis for Biochar or Energy Applications? A Life Cycle Assessment. *Environmental Science & Technology* 2015, 49 (8), 5195-5202.
- 115. Righi, S.; Bandini, V.; Marazza, D.; Baioli, F.; Torri, C.; Contin, A., Life Cycle Assessment of high ligno-cellulosic biomass pyrolysis coupled with anaerobic digestion. *Bioresource Technology* 2016, *212*, 245-253.
- 116. Roberts, K. G.; Gloy, B. A.; Joseph, S.; Scott, N. R.; Lehmann, J., Life Cycle Assessment of Biochar Systems: Estimating the Energetic, Economic, and Climate Change Potential. *Environmental Science & Technology* 2010, 44 (2), 827-833.
- 117. Fan, J.; Kalnes, T. N.; Alward, M.; Klinger, J.; Sadehvandi, A.; Shonnard, D. R., Life cycle assessment of electricity generation using fast pyrolysis bio-oil. *Renewable Energy* 2011, *36* (2), 632-641.
- 118. Hsu, D. D., Life cycle assessment of gasoline and diesel produced via fast pyrolysis and hydroprocessing. *Biomass and Bioenergy* 2012, *45*, 41-47.
- 119. Dong, J.; Tang, Y.; Nzihou, A.; Chi, Y.; Weiss-Hortala, E.; Ni, M., Life cycle assessment of pyrolysis, gasification and incineration waste-to-energy technologies: Theoretical analysis and case study of commercial plants. *Science of The Total Environment* 2018, 626, 744-753.

- 120. Dang, Q.; Yu, C.; Luo, Z., Environmental life cycle assessment of bio-fuel production via fast pyrolysis of corn stover and hydroprocessing. *Fuel* 2014, *131*, 36-42.
- 121. Zhang, Y.; Hu, G.; Brown, R. C., Life cycle assessment of the production of hydrogen and transportation fuels from corn stover via fast pyrolysis. *Environmental Research Letters* 2013, 8 (2), 025001.
- 122. Peters, J. F.; Iribarren, D.; Dufour, J., Simulation and life cycle assessment of biofuel production via fast pyrolysis and hydroupgrading. *Fuel* 2015, *139*, 441-456.
- 123. Im-orb, K.; Arpornwichanop, A., Process and sustainability analyses of the integrated biomass pyrolysis, gasification, and methanol synthesis process for methanol production. *Energy* 2020, *193*, 116788.
- 124. Steele, P.; Puettmann, M. E.; Penmetsa, V. K.; Cooper, J. E., Life-Cycle Assessment of Pyrolysis Bio-Oil Production*. *Forest Products Journal* 2012, *62* (4), 326-334.
- 125. Zhong, Z. W.; Song, B.; Zaki, M. B. M., Life-cycle assessment of flash pyrolysis of wood waste. *Journal of Cleaner Production* 2010, *18* (12), 1177-1183.
- 126. Vienescu, D. N.; Wang, J.; Le Gresley, A.; Nixon, J. D., A life cycle assessment of options for producing synthetic fuel via pyrolysis. *Bioresource Technology* 2018, *249*, 626-634.
- 127. Chan, Y. H.; Tan, R. R.; Yusup, S.; Lam, H. L.; Quitain, A. T., Comparative life cycle assessment (LCA) of bio-oil production from fast pyrolysis and hydrothermal liquefaction of oil palm empty fruit bunch (EFB). *Clean Technologies and Environmental Policy* 2016, *18* (6), 1759-1768.
- 128. Kauffman, N.; Hayes, D.; Brown, R., A life cycle assessment of advanced biofuel production from a hectare of corn. *Fuel* 2011, *90* (11), 3306-3314.
- 129. Bridgwater, A.; Meier, D.; Radlein, D., An overview of fast pyrolysis of biomass. *Organic Geochemistry* 1999, *30* (12), 1479-1493.
- 130. Song, Y.; Gutiérrez, O. Y.; Herranz, J.; Lercher, J. A., Aqueous phase electrocatalysis and thermal catalysis for the hydrogenation of phenol at mild conditions. *Applied Catalysis B: Environmental* 2016, *182*, 236-246.
- 131. Lofrano, R. C. Z.; Madurro, J. M.; Abrantes, L. M.; Romero, J. R., Electrocatalytic hydrogenation of carbonylic compounds using an electrode with platinum particles dispersed in films of poly-[allyl ether p-(2-aminoethyl) phenol] co-polymerized with allyl phenyl ether. *Journal of Molecular Catalysis A: Chemical* 2004, *218* (1), 73-79.
- 132. Li, Z.; Kelkar, S.; Raycraft, L.; Garedew, M.; Jackson, J. E.; Miller, D. J.; Saffron, C. M., A mild approach for bio-oil stabilization and upgrading: electrocatalytic hydrogenation using ruthenium supported on activated carbon cloth. *Green Chemistry* 2014, *16* (2), 844-852.

- 133. Mondal, K.; Lalvani, S., Low temperature soybean oil hydrogenation by an electrochemical process. *Journal of Food Engineering* 2008, *84* (4), 526-533.
- 134. Cyr, A.; Chiltz, F.; Jeanson, P.; Martel, A.; Brossard, L.; Lessard, J.; Ménard, H., Electrocatalytic hydrogenation of lignin models at Raney nickel and palladium-based electrodes. *Canadian Journal of Chemistry* 2000, 78 (3), 307-315.
- 135. Laplante, F.; Brossard, L.; Ménard, H., Considerations about phenol electrohydrogenation on electrodes made with reticulated vitreous carbon cathode. *Canadian Journal of Chemistry* 2003, *81* (3), 258-264.
- 136. Garedew, M.; Young-Farhat, D.; Jackson, J. E.; Saffron, C. M., Electrocatalytic Upgrading of Phenolic Compounds Observed after Lignin Pyrolysis. *ACS Sustainable Chemistry & Engineering* 2019, 7 (9), 8375-8386.
- 137. Garedew, M.; Young-Farhat, D.; Bhatia, S.; Hao, P.; Jackson, J. E.; Saffron, C. M., Electrocatalytic cleavage of lignin model dimers using ruthenium supported on activated carbon cloth. *Sustainable energy & fuels* 2020.
- 138. Guerrero-Sánchez, C.; Saldívar, E.; Hernández, M.; Jiménez, A., A Practical, Systematic Approach for the Scaling-Up and Modeling of Industrial Copolymerization Reactors. *Polymer Reaction Engineering* 2003, *11* (3), 457-506.
- 139. Langer, S. H.; Sakellaropoulos, G. P., Kinetics of Electrogenerative Hydrogenation over Platinum Black Electrocatalyst. *Journal of the Electrochemical Society* 1975, *122*, 1619.
- 140. Sedighi, S.; Gardner, C. L., A kinetic study of the electrochemical hydrogenation of ethylene. *Electrochimica Acta* 2010, *55* (5), 1701-1708.
- 141. Bannari, A.; Proulx, P.; Ménard, H.; Cirtiu, C. M., Mathematical modeling of the kinetics of phenol electrocatalytic hydrogenation over supported Pd–alumina catalyst. *Applied Catalysis A: General* 2008, *345* (1), 28-42.
- 142. Song, Y.; Sanyal, U.; Pangotra, D.; Holladay, J. D.; Camaioni, D. M.; Gutiérrez, O. Y.; Lercher, J. A., Hydrogenation of benzaldehyde via electrocatalysis and thermal catalysis on carbon-supported metals. *Journal of Catalysis* 2018, *359*, 68-75.
- 143. Singh, N.; Song, Y.; Gutiérrez, O. Y.; Camaioni, D. M.; Campbell, C. T.; Lercher, J. A., Electrocatalytic Hydrogenation of Phenol over Platinum and Rhodium: Unexpected Temperature Effects Resolved. *ACS Catalysis* 2016, *6* (11), 7466-7470.
- 144. Sherbo, R. S.; Kurimoto, A.; Brown, C. M.; Berlinguette, C. P., Efficient Electrocatalytic Hydrogenation with a Palladium Membrane Reactor. *Journal of the American Chemical Society* 2019, *141* (19), 7815-7821.

- 145. Thomas, G. *Overview of storage development DOE hydrogen program*; Sandia National Laboratories: San Ramon, California, May 9-11, 2000, 2000.
- 146. Dunn, D. R. U.S. Energy Information Administration Monthly Energy Review, August 2016; August 2016, 2016; pp 27-47.
- 147. Lynes, M. International Energy Outlook 2016; DOE/EIA-0484(2016); 2016; p 128.
- 148. Perlack, R. D.; Eaton, L. M.; Turhollow Jr, A. F.; Langholtz, M. H.; Brandt, C. C.; Downing, M. E.; Graham, R. L.; Wright, L. L.; Kavkewitz, J. M.; Shamey, A. M., US billionton update: biomass supply for a bioenergy and bioproducts industry. 2011.
- 149. Langholtz, M.; Stokes, B.; Eaton, L. 2016 Billion-ton report: Advancing domestic resources for a thriving bioeconomy, Volume 1: Economic availability of feedstock; ORNL/TM-2016/160; U.S. Department of Energy: 2016.
- 150. Furimsky, E., Catalytic hydrodeoxygenation. *Applied Catalysis A: General* 2000, *199* (2), 147-190.
- 151. Czernik, S.; Bridgwater, A., Overview of applications of biomass fast pyrolysis oil. *Energy & fuels* 2004, *18* (2), 590-598.
- 152. Bui, V. N.; Laurenti, D.; Afanasiev, P.; Geantet, C., Hydrodeoxygenation of guaiacol with CoMo catalysts. Part I: Promoting effect of cobalt on HDO selectivity and activity. *Applied Catalysis B: Environmental* 2011, *101* (3), 239-245.
- 153. Baliban, R. C.; Elia, J. A.; Floudas, C. A., Biomass to liquid transportation fuels (BTL) systems: process synthesis and global optimization framework. *Energy & Environmental Science* 2013, 6 (1), 267-287.
- 154. Rinaldi, R.; Schüth, F., Design of solid catalysts for the conversion of biomass. *Energy & Environmental Science* 2009, *2* (6), 610-626.
- 155. Serrano-Ruiz, J. C.; Dumesic, J. A., Catalytic routes for the conversion of biomass into liquid hydrocarbon transportation fuels. *Energy & Environmental Science* 2011, 4 (1), 83-99.
- 156. Zhao, C.; Kou, Y.; Lemonidou, A. A.; Li, X.; Lercher, J. A., Highly Selective Catalytic Conversion of Phenolic Bio-Oil to Alkanes. *Angewandte Chemie* 2009, *121* (22), 4047-4050.
- 157. Choudhary, T.; Phillips, C., Renewable fuels via catalytic hydrodeoxygenation. *Applied Catalysis A: General* 2011, 397 (1), 1-12.
- 158. Elliott, D. C.; Hart, T. R., Catalytic hydroprocessing of chemical models for bio-oil. *Energy & Fuels* 2008, *23* (2), 631-637.

- 159. Ruddy, D. A.; Schaidle, J. A.; Ferrell III, J. R.; Wang, J.; Moens, L.; Hensley, J. E., Recent advances in heterogeneous catalysts for bio-oil upgrading via "ex situ catalytic fast pyrolysis": catalyst development through the study of model compounds. *Green Chemistry* 2014, *16* (2), 454-490.
- 160. Saidi, M.; Samimi, F.; Karimipourfard, D.; Nimmanwudipong, T.; Gates, B. C.; Rahimpour, M. R., Upgrading of lignin-derived bio-oils by catalytic hydrodeoxygenation. *Energy & Environmental Science* 2014, 7 (1), 103-129.
- 161. Diebold, J.; Thermalchemie, I., NRE Laboratory. *A review of the chemical and physical mechanisms of the storage stability of fast pyrolysis bio-oils* 2000.
- 162. Pootakham, T.; Kumar, A., Bio-oil transport by pipeline: A techno-economic assessment. *Bioresource technology* 2010, *101* (18), 7137-7143.
- 163. Blaikie, D. Most Efficient Solar Panels. http://sroeco.com/solar/most-efficient-solar-panels (accessed 11 Mar 2014).
- 164. Lantz, E.; Wiser, R.; Hand, M., The past and future cost of wind energy. *National Renewable Energy Laboratory, Golden, CO, Report No. NREL/TP-6A20-53510* 2012.
- 165. Clausen, L. R., Maximizing biofuel production in a thermochemical biorefinery by adding electrolytic hydrogen and by integrating torrefaction with entrained flow gasification. *Energy* 2015, *85*, 94-104.
- 166. Cherubini, F.; Jungmeier, G.; Wellisch, M.; Willke, T.; Skiadas, I.; Van Ree, R.; de Jong, E., Toward a common classification approach for biorefinery systems. *Biofuels, Bioproducts and Biorefining* 2009, *3* (5), 534-546.
- 167. McKendry, P., Energy production from biomass (part 1): overview of biomass. *Bioresource technology* 2002, *83* (1), 37-46.
- 168. Demirbaş, A., Calculation of higher heating values of biomass fuels. *Fuel* 1997, 76 (5), 431-434.
- 169. Sun, Z.-Y.; Tang, Y.-Q.; Iwanaga, T.; Sho, T.; Kida, K., Production of fuel ethanol from bamboo by concentrated sulfuric acid hydrolysis followed by continuous ethanol fermentation. *Bioresource technology* 2011, *102* (23), 10929-10935.
- 170. Laird, D. A., The charcoal vision: a win–win–win scenario for simultaneously producing bioenergy, permanently sequestering carbon, while improving soil and water quality. *Agronomy journal* 2008, *100* (1), 178-181.
- 171. Lehmann, J., A handful of carbon. *Nature* 2007, 447 (7141), 143-144.

- 172. Langholtz, M. 2016 Billion-Ton Report; ORNL (Oak Ridge National Laboratory (ORNL), Oak Ridge, TN (United States)): 2016.
- 173. Gaur, S.; Reed, T., Thermal Data for Natural and Synthetic Fuels, Marcel Deeker. *Inc.: New York, NY, USA* 1998.
- 174. Kolská, Z.; Kukal, J.; Zábranský, M.; Ruz`ic`ka, V., Estimation of the heat capacity of organic liquids as a function of temperature by a three-level group contribution method. *Industrial & Engineering Chemistry Research* 2008, 47 (6), 2075-2085.
- 175. Joback, K. G.; Reid, R. C., Estimation of pure-component properties from group-contributions. *Chem. Eng. Commun.* 1987, *57* (1-6), 233-243.
- 176. Marrero, J.; Gani, R., Group-contribution based estimation of pure component properties. *Fluid Phase Equilib.* 2001, *183*, 183-208.
- 177. Hukkerikar, A. S.; Sarup, B.; Ten Kate, A.; Abildskov, J.; Sin, G.; Gani, R., Group-contribution+ (GC+) based estimation of properties of pure components: Improved property estimation and uncertainty analysis. *Fluid Phase Equilib.* 2012, *321*, 25-43.
- 178. Goodman, B. T.; Wilding, W. V.; Oscarson, J. L.; Rowley, R. L., Use of the DIPPR Database for Development of Quantitative Structure—Property Relationship Correlations: Heat Capacity of Solid Organic Compounds. *Journal of Chemical & Engineering Data* 2004, *49* (1), 24-31.
- 179. Gil, M.; Gonzalez, A.; Gil, A. In *Evaluation of milling energy requirements of biomass residues in a semi-industrial pilot plant for co-firing*, Proceedings 16th European Biomass Conference and Exhibition, Valencia, Spain, 2008.
- 180. Kemp, I. C., Fundamentals of energy analysis of dryers. *Modern Drying Technology* 2011, *4*, 1-46.
- 181. Thoreson, C. P.; Darr, M. J.; Webster, K. E. In *Corn Stover Densification Methods and their Large-Scale Logistical Impacts—Preliminary Analysis*, 2010 Pittsburgh, Pennsylvania, June 20-June 23, 2010, American Society of Agricultural and Biological Engineers: 2010; p 1.
- 182. Nicolai, R.; Ollerich, J.; Kelley, J. In *Screw auger power and throughput analysis*, 2004 ASAE Annual Meeting, American Society of Agricultural and Biological Engineers: 2004; p 1.
- 183. Srivastava, A. K., *Engineering Principles of Agricultural Machines*. American Society of Agricultural Engineers: 2006.
- 184. Perry, R. H.; Green, D. W., *Perry's chemical engineers' handbook*. McGraw-Hill Professional: 1999.

- 185. Groundwater Temperature Map. http://www.enoscientific.com/groundwater-temp-map.htm.
- 186. Carmo, M.; Fritz, D. L.; Mergel, J.; Stolten, D., A comprehensive review on PEM water electrolysis. *Int. J. Hydrogen Energy* 2013, *38* (12), 4901-4934.
- 187. Zhou, Y.; Klinger, G. E.; Hegg, E. L.; Saffron, C. M.; Jackson, J. E., Multiple Mechanisms Mapped in Aryl Alkyl Ether Cleavage via Aqueous Electrocatalytic Hydrogenation over Skeletal Nickel. *Journal of the American Chemical Society* 2020.
- 188. Lam, C. H.; Lowe, C. B.; Li, Z.; Longe, K. N.; Rayburn, J. T.; Caldwell, M. A.; Houdek, C. E.; Maguire, J. B.; Saffron, C. M.; Miller, D. J., Electrocatalytic upgrading of model lignin monomers with earth abundant metal electrodes. *Green Chemistry* 2015, 17 (1), 601-609.
- 189. DOE Technical Targets for Hydrogen Production from Electrolysis. https://www.energy.gov/eere/fuelcells/doe-technical-targets-hydrogen-production-electrolysis#:~:text=The%202020%20target%20is%20based,year%20is%20set%20to%202025.
- 190. Ouammi, A.; Bersani, C.; Sacile, R.; Dagdougui, H., *Hydrogen Infrastructure for Energy Applications: Production, Storage, Distribution and Safety.* Elsevier Academic Press: 2018.
- 191. Campbell, R. M.; Anderson, N. M.; Daugaard, D. E.; Naughton, H. T., Financial viability of biofuel and biochar production from forest biomass in the face of market price volatility and uncertainty. *Applied Energy* 2018, *230*, 330-343.
- 192. Kocoloski, M.; Michael Griffin, W.; Scott Matthews, H., Impacts of facility size and location decisions on ethanol production cost. *Energy Policy* 2011, *39* (1), 47-56.
- 193. Thompson, J. L.; Tyner, W. E., Corn stover for bioenergy production: Cost estimates and farmer supply response. *Biomass and Bioenergy* 2014, *62*, 166-173.
- 194. Wakeley, H. L.; Hendrickson, C. T.; Griffin, W. M.; Matthews, H. S., Economic and Environmental Transportation Effects of Large-Scale Ethanol Production and Distribution in the United States. *Environmental Science & Technology* 2009, *43* (7), 2228-2233.
- 195. Hooper, A.; Murray, D. An Analysis of the Operational Costs of Trucking: 2018 Update; 2018.
- 196. Orella, M. J.; Román-Leshkov, Y.; Brushett, F. R., Emerging opportunities for electrochemical processing to enable sustainable chemical manufacturing. *Current Opinion in Chemical Engineering* 2018, *20*, 159-167.
- 197. Levelized Cost and Levelized Avoided Cost of New Generation Resources in the Annual Energy Outlook 2019; United States Energy Information Administration: 2019.

- 198. Pintauro, P. N.; Gil, M. P.; Warner, K.; List, G.; Neff, W., Electrochemical Hydrogenation of Soybean Oil with Hydrogen Gas. *Industrial & Engineering Chemistry Research* 2005, 44 (16), 6188-6195.
- 199. Ruthenium Price Chart. http://www.platinum.matthey.com/prices/price-charts#.
- 200. Peterson, D.; Vickers, J.; DeSantis, D. *Hydrogen Production Cost From PEM Electrolysis 2019*; February 03, 2020.
- 201. Peters, M. S.; Timmerhaus, K. D.; West, R. E. Equipment Costs-Plant Design and Economics for Chemical Engineers. http://www.mhhe.com/engcs/chemical/peters/data/.
- 202. Peters, M. S.; Timmerhaus, K. D.; West, R. E., *Plant Design and Economics for Chemical Engineers*. 5th Edition ed.; McGraw Hill.
- 203. Heat Exchanger Heat Transfer Coefficients. The Engineering Toolbox.
- 204. Xu, H.; Sieverding, H.; Kwon, H.; Clay, D.; Stewart, C.; Johnson, J. M. F.; Qin, Z.; Karlen, D. L.; Wang, M., A global meta-analysis of soil organic carbon response to corn stover removal. *GCB Bioenergy* 2019, *11* (10), 1215-1233.
- 205. An, W.; Hong, J. K.; Pintauro, P., Current efficiency for soybean oil hydrogenation in a solid polymer electrolyte reactor. *Journal of Applied Electrochemistry* 1998, *28*, 947-954.
- 206. Genovese, J.; Harg, K.; Paster, M.; Turner, J. Current (2009) State-of-the-Art Hydrogen Production Cost Estimate Using Water Electrolysis; NREL/BK-6A1-46676; NREL: 2009.
- 207. Colella, W. G.; James, B. D.; Moton, J. M.; Saur, G.; Ramsden, T. *Techno-economic Analysis of PEM Electrolysis for Hydrogen Production*; NREL, Strategic Analysis Inc.: Golden, Colorado, 2013.
- 208. Amos, W. A. *Costs of Storing and Transporting Hydrogen*; NREL/TP-570-25106; National Renewable Energy Laboratory (NREL): Golden, CO (US), 1999; p 6574.
- 209. Keiser, J.; Howell, M.; Lewis, S.; Connatser, R., Corrosion Studies Of Raw And Treated Biomass-Derived Pyrolysis Oils. 2012.
- 210. Lu, Q.; Zhang, J.; Zhu, X., Corrosion properties of bio-oil and its emulsions with diesel. *Chinese Science Bulletin* 2008, *53* (23), 3726-3734.
- 211. Loh, H. P.; Lyons, J.; White, C. W. *Process Equipment Cost Estimation Final Report*; DOE/NETL-2002/1169; National Energy Technology Laboratory (NETL): Morgantown, WV (United States), 2002; p 797810.

- 212. Saba, S. M.; Müller, M.; Robinius, M.; Stolten, D., The investment costs of electrolysis A comparison of cost studies from the past 30 years. *International Journal of Hydrogen Energy* 2018, 43 (3), 1209-1223.
- 213. Dutta, A.; Sahir, A.; Tan, E.; Humbird, D.; Snowden-Swan, L. J.; Meyer, P.; Ross, J.; Sexton, D.; Yap, R.; Lukas, J. *Process Design and Economics for the Conversion of Lignocellulosic Biomass to Hydrocarbon Fuels*; NREL/TP-5100-62455, PNNL-23823; NREL, PNNL: 2015.
- 214. Natural Gas Prices. U.S. Energy Information and Administration.
- 215. Campbell, R. M.; Anderson, N. M.; Daugaard, D. E.; Naughton, H. T., Technoeconomic and Policy Drivers of Project Performance for Bioenergy Alternatives Using Biomass from Beetle-Killed Trees. *Energies* 2018, *11* (2), 293.
- 216. Shabangu, S.; Woolf, D.; Fisher, E. M.; Angenent, L. T.; Lehmann, J., Technoeconomic assessment of biomass slow pyrolysis into different biochar and methanol concepts. *Fuel* 2014, *117*, 742-748.
- 217. Galinato, S. P.; Yoder, J. K.; Granatstein, D., The economic value of biochar in crop production and carbon sequestration. *Energy Policy* 2011, *39* (10), 6344-6350.
- 218. Kung, C.-C.; McCarl, B. A.; Cao, X., Economics of pyrolysis-based energy production and biochar utilization: A case study in Taiwan. *Energy Policy* 2013, *60*, 317-323.
- 219. Yoder, J.; Galinato, S.; Granatstein, D.; Garcia-Pérez, M., Economic tradeoff between biochar and bio-oil production via pyrolysis. *Biomass and Bioenergy* 2011, *35* (5), 1851-1862.
- 220. Dickinson, D.; Balduccio, L.; Buysse, J.; Ronsse, F.; van Huylenbroeck, G.; Prins, W., Cost-benefit analysis of using biochar to improve cereals agriculture. *GCB Bioenergy* 2015, 7 (4), 850-864.
- 221. Granatstein, C.; Kruger, C.; Collins, H.; Galinato, S.; Garcia-perez, M.; Yoder, J. *Use of biochar from the pyrolysis of waste organic material as a soil amendment*; 2009.
- 222. Kim, D.; Anderson, N. M.; Chung, W., Financial Performance of a Mobile Pyrolysis System Used to Produce Biochar from Sawmill Residues. *Forest Products Journal* 2015, *65* (5-6), 189-197.
- 223. Shackley, S.; Hammond, J.; Gaunt, J.; Ibarrola, R., The feasibility and costs of biochar deployment in the UK. *Carbon Management* 2011, *2* (3), 335-356.
- 224. Draper, K.; Groot, H.; Miles, T.; Twer, M. Survey and Analysis of the US Biochar Industry: Preliminary Report Draft (August 16, 2018); 2018.
- 225. Biomass Multi-Year Program Plan; U.S. Department of Energy: 2011.

- 226. Kreuter, W.; Hofmann, H., Electrolysis: The important energy transformer in a world of sustainable energy. *International Journal of Hydrogen Energy* 1998, *23* (8), 661-666.
- 227. Liu, L.; Chen, W.; Li, Y., An overview of the proton conductivity of nafion membranes through a statistical analysis. *Journal of Membrane Science* 2016, *504*, 1-9.
- 228. Singh, A.; Pant, D.; Korres, N. E.; Nizami, A.-S.; Prasad, S.; Murphy, J. D., Key issues in life cycle assessment of ethanol production from lignocellulosic biomass: Challenges and perspectives. *Bioresource Technology* 2010, *101* (13), 5003-5012.
- 229. Fu, G. Z.; Chan, A. W.; Minns, D. E., Life Cycle assessment of bio-ethanol derived from cellulose. *The International Journal of Life Cycle Assessment* 2003, 8 (3), 137-141.
- 230. Mu, D.; Seager, T.; Rao, P. S.; Zhao, F., Comparative Life Cycle Assessment of Lignocellulosic Ethanol Production: Biochemical Versus Thermochemical Conversion. *Environmental Management* 2010, 46 (4), 565-78.
- 231. Bai, Y.; Luo, L.; van der Voet, E., Life cycle assessment of switchgrass-derived ethanol as transport fuel. *The International Journal of Life Cycle Assessment* 2010, *15* (5), 468-477.
- 232. Dunn, J. B.; Mueller, S.; Kwon, H.-y.; Wang, M. Q., Land-use change and greenhouse gas emissions from corn and cellulosic ethanol. *Biotechnology for Biofuels* 2013, *6*, 51-51.
- 233. Wang, M.; Han, J.; Dunn, J. B.; Cai, H.; Elgowainy, A., Well-to-wheels energy use and greenhouse gas emissions of ethanol from corn, sugarcane and cellulosic biomass for US use. *Environmental Research Letters* 2012, 7 (4), 045905.
- 234. Kim, S.; Dale, B. E.; Jenkins, R., Life cycle assessment of corn grain and corn stover in the United States. *The International Journal of Life Cycle Assessment* 2009, *14* (2), 160-174.
- 235. Spatari, S.; Bagley, D. M.; MacLean, H. L., Life cycle evaluation of emerging lignocellulosic ethanol conversion technologies. *Bioresource Technology* 2010, *101* (2), 654-667.
- 236. Han, J.; Elgowainy, A.; Dunn, J. B.; Wang, M. Q., Life cycle analysis of fuel production from fast pyrolysis of biomass. *Bioresource Technology* 2013, *133*, 421-428.
- 237. Kim, S.; Zhang, X.; Reddy, A. D.; Dale, B. E.; Thelen, K. D.; Jones, C. D.; Izaurralde, R. C.; Runge, T.; Maravelias, C., Carbon-Negative Biofuel Production. *Environmental Science & Technology* 2020, *54* (17), 10797-10807.
- 238. Wang, M. *The Greenhouse Gases, Regulated Emissions, and Energy Use in Transportation Model*; Argonne National Laboratory: Argonne, Illinois, 1999.

- 239. Dunn, J. B.; Qin, Z.; Mueller, S.; Kwon, H. Y.; Wander, M.; Wang, M. *Carbon Calculator for Land Use Change from Biofuels Production (CCLUB)*; ANL/ESD/12-5 Rev. 2; Argonne National Laboratory: 2014.
- 240. Bare, J., TRACI 2.0: the tool for the reduction and assessment of chemical and other environmental impacts 2.0. *Clean Technologies and Environmental Policy* 2011, *13* (5), 687-696.
- 241. Bare, J. C. Tools for the Reduction and Assessment of Chemical and Other Environmental Impacts (TRACI), Version 2.1-User's Manual; United States Environment Protection Agency: 2012.
- 242. Bayart, J.-B.; Bulle, C.; Deschênes, L.; Margni, M.; Pfister, S.; Vince, F.; Koehler, A., A framework for assessing off-stream freshwater use in LCA. *The International Journal of Life Cycle Assessment* 2010, *15* (5), 439-453.
- 243. Boulay, A.-M.; Bare, J.; Benini, L.; Berger, M.; Lathuillière, M. J.; Manzardo, A.; Margni, M.; Motoshita, M.; Núñez, M.; Pastor, A. V.; Ridoutt, B.; Oki, T.; Worbe, S.; Pfister, S., The WULCA consensus characterization model for water scarcity footprints: assessing impacts of water consumption based on available water remaining (AWARE). *The International Journal of Life Cycle Assessment* 2018, 23 (2), 368-378.
- 244. Morelli, B.; Hawkins, T. R.; Niblick, B.; Henderson, A. D.; Golden, H. E.; Compton, J. E.; Cooter, E. J.; Bare, J. C., Critical Review of Eutrophication Models for Life Cycle Assessment. *Environmental Science & Technology* 2018, *52* (17), 9562-9578.
- 245. Norris, G. A., Impact Characterization in the Tool for the Reduction and Assessment of Chemical and Other Environmental Impacts: Methods for Acidification, Eutrophication, and Ozone Formation. *Journal of Industrial Ecology* 2002, 6 (3/4), 79.
- 246. Weidema, B. P.; Wesnæs, M. S., Data quality management for life cycle inventories—an example of using data quality indicators. *Journal of Cleaner Production* 1996, 4 (3), 167-174.
- 247. Toffel, M. W.; Horvath, A., Environmental Implications of Wireless Technologies: News Delivery and Business Meetings. *Environmental Science & Technology* 2004, *38* (11), 2961-2970.
- 248. Couillard, S.; Bage, G.; Trudel, J.-S. Comparative Life Cycle Assessment (LCA) of Artificial vs Natural Christmas Tree; 1043-RF3-09; 2009.
- 249. Kim, S.; Zhang, X.; Dale, B. E.; Reddy, A. D.; Jones, C. D.; Cronin, K.; Izaurralde, R. C.; Runge, T.; Sharara, M., Corn stover cannot simultaneously meet both the volume and GHG reduction requirements of the renewable fuel standard. *Biofuels, Bioproducts & Biorefining* 2018, *12*, 203-212.

- 250. Rees, J.; Schmer, M.; Wortmann, C. Corn Stover Removal: Nutrient Value of Stover and Impacts on Soil Properties. https://cropwatch.unl.edu/2017/corn-stover-removal-nutrient-value-stover-and-impacts-soil-properties.
- 251. Alvarez, R., A review of nitrogen fertilizer and conservation tillage effects on soil organic carbon storage. *Soil Use and Management* 2005, *21* (1), 38-52.
- 252. Baker, J. M.; Ochsner, T. E.; Venterea, R. T.; Griffis, T. J., Tillage and soil carbon sequestration—What do we really know? *Agriculture, Ecosystems & Environment* 2007, *118* (1), 1-5.
- 253. Minasny, B.; McBratney, A. B.; Bellon-Maurel, V.; Roger, J.-M.; Gobrecht, A.; Ferrand, L.; Joalland, S., Removing the effect of soil moisture from NIR diffuse reflectance spectra for the prediction of soil organic carbon. *Geoderma* 2011, *167-168*, 118-124.
- 254. West, T. O.; Post, W. M., Soil Organic Carbon Sequestration Rates by Tillage and Crop Rotation. *Soil Science Society of America Journal* 2002, *66* (6), 1930-1946.
- 255. Angers, D. A.; Eriksen-Hamel, N. S., Full-Inversion Tillage and Organic Carbon Distribution in Soil Profiles: A Meta-Analysis. *Soil Science Society of America Journal* 2008, 72 (5), 1370-1374.
- 256. Virto, I.; Barré, P.; Burlot, A.; Chenu, C., Carbon input differences as the main factor explaining the variability in soil organic C storage in no-tilled compared to inversion tilled agrosystems. *Biogeochemistry* 2012, *108* (1), 17-26.
- 257. Zhang, W.; Liu, K.; Wang, J.; Shao, X.; Xu, M.; Li, J.; Wang, X.; Murphy, D. V., Relative contribution of maize and external manure amendment to soil carbon sequestration in a long-term intensive maize cropping system. *Scientific Reports* 2015, 5 (1), 10791.
- 258. Lal, R.; Negassa, W.; Lorenz, K., Carbon sequestration in soil. *Current Opinion in Environmental Sustainability* 2015, *15*, 79-86.
- 259. Hoekstra, A. Y.; Chapagain, A. K.; Aldaya, M. M.; Mekonnen, M. M., *The Water Footprint Assessment Manual: Setting the Global Standard*. Earthscan: 2011.
- 260. Lampert, D. J.; Cai, H.; Elgowainy, A., Wells to wheels: water consumption for transportation fuels in the United States. *Energy & Environmental Science* 2016, 9 (3), 787-802.
- 261. Pfister, S.; Koehler, A.; Hellweg, S., Assessing the Environmental Impacts of Freshwater Consumption in LCA. *Environmental Science & Technology* 2009, *43* (11), 4098-4104.
- 262. Ridoutt, B. G.; Pfister, S., A revised approach to water footprinting to make transparent the impacts of consumption and production on global freshwater scarcity. *Global Environmental Change* 2010, 20 (1), 113-120.

- 263. Pfister, S.; Hellweg, S., The water "shoesize" vs. footprint of bioenergy. *Proceedings of the National Academy of Sciences* 2009, *106* (35), E93-E94.
- 264. Hoekstra, A. Y., A critique on the water-scarcity weighted water footprint in LCA. *Ecological Indicators* 2016, *66*, 564-573.
- 265. IPCC Revised 1996 IPCC Guidelines for National Greenhouse Gas Inventories; 1996.
- 266. Powers, S. E. Quantifying Cradle-to-Farm Gate Life-Cycle Impacts Associated with Fertilizer Used for Corn, Soybean, and Stover Production NREL: Golden, Colorado, 2005.
- 267. Smil, V., PHOSPHORUS IN THE ENVIRONMENT: Natural Flows and Human Interferences. *Annual Review of Energy and the Environment* 2000, *25* (1), 53-88.
- 268. Edwards, W. *Economics of Harvesting and Transporting Corn Stover* Iowa State University: 2014.
- 269. Hess, J. R.; Kenney, K. L.; Wright, C. T.; Perlack, R.; Turhollow, A., Corn stover availability for biomass conversion: situation analysis. *Cellulose* 2009, *16* (4), 599-619.
- 270. Sokhansanj, S.; Turhollow, A.; Wilkerson, E., Integrated Biomass Supply and Logistics: A Modeling Environment for Designing Feedstock Supply Systems for Biofuel Production. *Resource Magazine* 2008, *15* (6), 15-18.
- 271. Emery, I.; Mosier, N., Direct emission of methane and nitrous oxide from switchgrass and corn stover: implications for large-scale biomass storage. *GCB Bioenergy* 2015, 7 (4), 865-876.
- 272. Emery, I.; Dunn, J. B.; Han, J.; Wang, M., Biomass Storage Options Influence Net Energy and Emissions of Cellulosic Ethanol. *BioEnergy Research* 2015, 8 (2), 590-604.
- 273. Crombie, K.; Mašek, O.; Cross, A.; Sohi, S., Biochar synergies and trade-offs between soil enhancing properties and C sequestration potential. *GCB Bioenergy* 2015, 7 (5), 1161-1175.
- 274. Crombie, K.; Mašek, O., Investigating the potential for a self-sustaining slow pyrolysis system under varying operating conditions. *Bioresource Technology* 2014, *162*, 148-156.
- 275. Sun, K.; Jin, J.; Keiluweit, M.; Kleber, M.; Wang, Z.; Pan, Z.; Xing, B., Polar and aliphatic domains regulate sorption of phthalic acid esters (PAEs) to biochars. *Bioresource Technology* 2012, *118*, 120-127.
- 276. Panagopoulos, A.; Haralambous, K.-J.; Loizidou, M., Desalination brine disposal methods and treatment technologies A review. *Science of The Total Environment* 2019, *693*, 133545.

- 277. McGill, J.; Darr, M. *Transporting Biomass on Iowa Roadways* Iowa State University: 2014.
- 278. Kumar, D.; Murthy, G., Life cycle assessment of energy and GHG emissions during ethanol production from grass straws using various pretreatment processes. *The International Journal of Life Cycle Assessment* 2012, *17*, 388-401.
- 279. Dias Mayer, F.; Brondani, M.; Carrillo, M.; Hoffmann, R.; Lora, E., Revisiting Energy Efficiency, Renewability, And Sustainability Indicators In Biofuels Life Cycle: Analysis And Standardization Proposal. *Journal of Cleaner Production* 2019, 252, 119850.
- 280. Luo, L.; van der Voet, E.; Huppes, G.; Udo de Haes, H. A., Allocation issues in LCA methodology: a case study of corn stover-based fuel ethanol. *The International Journal of Life Cycle Assessment* 2009, *14* (6), 529-539.
- 281. Sheehan, J.; Aden, A.; Paustian, K.; Killian, K.; Brenner, J.; Walsh, M.; Nelson, R., Energy and Environmental Aspects of Using Corn Stover for Fuel Ethanol. *Journal of Industrial Ecology* 2003, 7 (3-4), 117-146.
- 282. Sokhansanj, S.; Turhollow, A.; Cushman, J.; Cundiff, J., Engineering aspects of collecting corn stover for bioenergy. *Biomass and Bioenergy* 2002, *23* (5), 347-355.
- 283. Follett, R. F.; Vogel, K. P.; Varvel, G. E.; Mitchell, R. B.; Kimble, J., Soil Carbon Sequestration by Switchgrass and no-Till Maize Grown for Bioenergy. *Bioenergy Research* 4 (3), 866-875.
- 284. Burnham, A.; Han, J.; Clark, C. E.; Wang, M.; Dunn, J. B.; Palou-Rivera, I., Life-Cycle Greenhouse Gas Emissions of Shale Gas, Natural Gas, Coal, and Petroleum. *Environmental Science & Technology* 2012, *46* (2), 619-627.
- 285. Bai, M.; Wilske, B.; Buegger, F.; Esperschütz, J.; Kammann, C. I.; Eckhardt, C.; Koestler, M.; Kraft, P.; Bach, M.; Frede, H.-G.; Breuer, L., Degradation kinetics of biochar from pyrolysis and hydrothermal carbonization in temperate soils. *Plant and Soil* 2013, *372* (1), 375-387.
- 286. Kuzyakov, Y.; Subbotina, I.; Chen, H.; Bogomolova, I.; Xu, X., Black carbon decomposition and incorporation into soil microbial biomass estimated by 14C labeling. *Soil Biology and Biochemistry* 2009, *41* (2), 210-219.
- 287. Brown, S.; Sathaye, J.; Cannell, M.; Kauppi, P. E., *Management of Forests for Mitigation of Greenhous Gas Emissions*. 1995.
- 288. Sundqvist, T.; Oasmaa, A.; Koskinen, A., Upgrading Fast Pyrolysis Bio-Oil Quality by Esterification and Azeotropic Water Removal. *Energy & Fuels* 2015, *29* (4), 2527-2534.

- 289. Oshchepkov, A. G.; Bonnefont, A.; Saveleva, V. A.; Papaefthimiou, V.; Zafeiratos, S.; Pronkin, S. N.; Parmon, V. N.; Savinova, E. R., Exploring the Influence of the Nickel Oxide Species on the Kinetics of Hydrogen Electrode Reactions in Alkaline Media. *Topics in Catalysis* 2016, 59 (15), 1319-1331.
- 290. Oshchepkov, A. G.; Bonnefont, A.; Parmon, V. N.; Savinova, E. R., On the effect of temperature and surface oxidation on the kinetics of hydrogen electrode reactions on nickel in alkaline media. *Electrochimica Acta* 2018, *269*, 111-118.
- 291. Tourwé, E.; Pintelon, R.; Hubin, A., Extraction of a quantitative reaction mechanism from linear sweep voltammograms obtained on a rotating disk electrode. Part I: Theory and validation. *Journal of Electroanalytical Chemistry* 2006, *594* (1), 50-58.
- 292. Singh, N.; Sanyal, U.; Ruehl, G.; Stoerzinger, K. A.; Gutiérrez, O. Y.; Camaioni, D. M.; Fulton, J. L.; Lercher, J. A.; Campbell, C. T., Aqueous phase catalytic and electrocatalytic hydrogenation of phenol and benzaldehyde over platinum group metals. *Journal of Catalysis* 2020, *382*, 372-384.
- 293. Barbir, F., PEM Fuel Cells. Imprint Academic Press: 2013.
- 294. Rolando, G.; Richard, G. C.; Juan, M. F.; Eliezer, G.; Jacek, L.; Wolfgang, S.; Sergio, T., Defining the transfer coefficient in electrochemistry: An assessment (IUPAC Technical Report). *Pure and Applied Chemistry* 2014, *86* (2), 245-258.
- 295. Prévoteau, A.; Geirnaert, A.; Arends, J. B. A.; Lannebère, S.; Van de Wiele, T.; Rabaey, K., Hydrodynamic chronoamperometry for probing kinetics of anaerobic microbial metabolism--case study of Faecalibacterium prausnitzii. *Scientific reports* 2015, 5, 11484-11484.